WHEEL-SHAPED POLYOXO AND POLYOXOTHIOMETALATES: FROM THE MOLECULAR LEVEL TO NANOSTRUCTURES

ANNE DOLBECQ and FRANCIS SÉCHERESSE

Institut Lavoisier, UMR 8637, Université de Versailles,
45 Avenue des Etats-Unis, 78035 Versailles, France

I. Introduction

The development of new concepts in inorganic chemistry such as host-guest based chemistry, supramolecularity, and the building block approach, together with improvements in structural characterization techniques, has stimulated the discovery and characterization of sophisticated chemical objects ranging from the molecular level (few angströms scale) to extended molecular arrangements (nanometer scale). Most of these compounds are prepared in aqueous solution or in inorganic solvents and are isolated by crystallization or precipitation. Soluble species adapt their size and shape in solution to minimize the

0898-8838/02 $35.00

interactions that could provoke their self-aggregation and precipitation but they can also tune their contact surface with the solvent to achieve the ideal entropy value of solvent-interaction. The molecular surface which is most complementary to these two propositions is that of a ring or a wheel. The most beautiful example we know of this is the soluble "big wheel" (see below), one of the key structures to enter mesoscopic coordination chemistry. Some of these wheel-shaped molecules are at the boundary of usual coordination chemistry and nanometric chemistry, and thus will allow us to explore the domain where the macroscopic properties arise from the microscopic level.

This review of the more recent wheels published in the literature covers both the molecular and nanometric domains. Our description will be limited to rings and disks with a minimum nuclearity of 5, the cavity of the wheel being empty or containing something inside, such as ions or templating groups. The review is organized in three parts: (i) rings of 3d-metals in moderate oxidation states (II, III) with O, N, and S-donor ligands; (ii) wheel-shaped polyoxo(thio)metalates containing metals in high oxidation states (IV, V, VI); and (iii) more sophisticated species based on Mo(VI), W(VI), and Mo(V) metal ions located at the boundary of molecular and solid-state chemistry. Not only do some of them have interesting magnetic properties, but in many cases they have been synthesized as "objects of beauty" as Professor Achim Müller first called them.

II. Wheels with 3*d* Metals in Oxidation States (II, III)

First of all, structures of wheels in which the metals are bridged by more than one atom are precluded from this section. In the latter category, heteroatoms, such as transition metals and nitrogen, substitute methylene carbon atoms in the ring of an organic crown ether and are thus often designated as metallacrown ethers. An example of a 12-metallacrown-4 structure, with four copper atoms bound by 3-amino-N-hydroxypropanamide ligands and an extra Cu atom at the center of the ring (*1*), is given in Fig. 1. These molecules have been the subject of a recent and extensive review (*2*).

We will thus consider in this section only metal wheels where the bridges between the M···M vectors are constituted by a single atom, either μ_2-bridging anions (OH^-, Cl^-, F^-, O^{2-}, S^{2-}) or μ_2-carbon, oxygen, nitrogen, or sulfur atoms from various organic ligands. The substitution of a transition metal atom for an ethane bridge atom (*3*) leads to

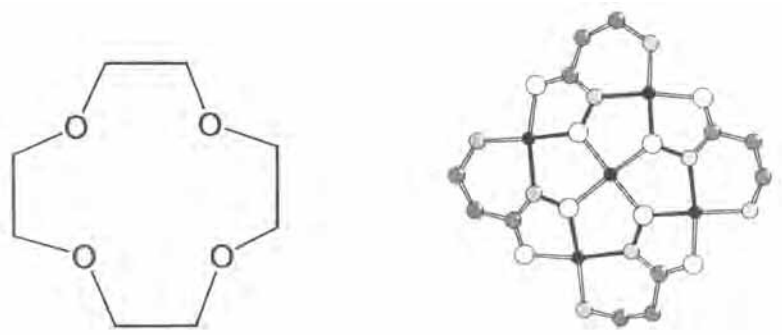

FIG. 1. Schematic diagram of 12-crown-4 (12-C-4) compared with the analogous core of the metallacrown: metal atoms, black spheres; C atoms, light gray spheres; N atoms: medium gray spheres.

a structural analogy with the organic crown ethers, which explains why these metal rings are sometimes also categorized as metallacrowns or metallacoronates. This structural analogy extends to comparable properties for the metallic rings and their organic counterparts. Indeed, like organic crown ethers, the metal wheels can complex small cations, such as alkaline cations or another metal atom, and their syntheses are often rationalized in terms of template effects although they often have been synthesized, by serendipity, from one-pot reactions. Rare examples of metal wheels in supramolecular interaction with anions are also described.

We will make a distinction between the metals with low coordination numbers (2, 4) and those which are surrounded by six ligands, defining an octahedral environment. In the first category, with the exception of the anecdotal mercury compound and the copper complex (see below), the ligands are thiolate or selenate groups; the size of the chalcogenide ion limits the coordination number of the metal to four while, in the second category, a variety of organic ligands is encountered.

A. METALS WITH LOW COORDINATION NUMBERS

The mercury wheel $\{[(CF_3)_2CHg]_5Cl_2\}^{2-}$ is a unique example of a metal ring with μ_2-C bridging atoms; the cyclic pentanuclear neutral ring $[(CF_3)_2CHg]_5$ contains five mercury atoms bridged by one carbon atom of a perfluoroisopropylidene ligand, in a planar ten-membered cycle (Fig. 2) (*4*). When this metal wheel is mixed with $[PPh_4]Cl$, $[PPh_4]Br$ or $[PPh_4]I$ in ethanol at room temperature, it forms halide complexes (*5*). In the solid state, two halides are located above and below

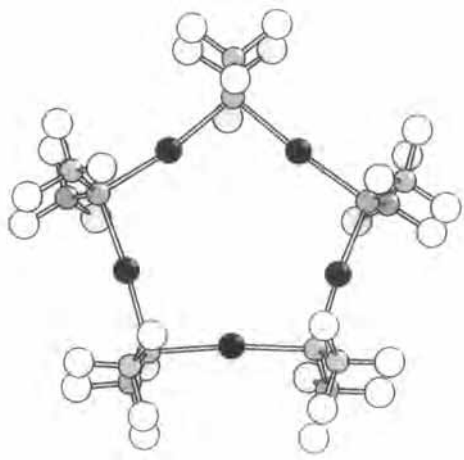

FIG. 2. Ball and stick representation of $\{[(CF_3)_2CHg]_5Cl_2\}^{2-}$.

the plane of the metallacycle with Hg–Cl distances (average 3.22 Å) significantly shorter than the sum of the Van der Waals radii of the Hg and Cl atoms (3.9 Å) and indicative of strong Hg $\cdots$ Cl interactions. This mercury compound is the only known example of a metallic wheel with a di-coordinated metal.

Metal atoms which are stable within an environment of four ligands, defining a building unit of formula MQ_4 (Q = S, Se), are more numerous. They can adopt either a tetrahedral coordination (M = Fe) or a square planar coordination (M = Ni, Pd, Cd, Pt); the connecting scheme between the M_2S_2 rhombic units in the two kinds of coordination is depicted in Fig. 3. Thiolate ligands QR (Q = S, Se; R = organic chain), bound to the ring via the chalcogenide atoms, dangle above and below the molecular plane. These compounds are often easily prepared by mixing the thiol ligand, base, and the metal salt and, according to the nature of R, are soluble in more or less polar solvents. The nuclearity of the ring varies from six to eighteen. The hexanuclear rings, of general formula $[M_6(QR)_{12}]$, contain six edge-sharing MQ_4 square coordination planes and display an hexagonal toroid shape, sometimes called the "tiara" structure. They are the most numerous, with 14 references found in the Cambridge structural database, with sulfur atoms and M = Ni, R = CH_3 (*6,7*), Et (*8,9*), Pr (*10*), CH_2CH_2OH (*11*), CH_2PhCl (*12*), $CH_2CH_2SiMe_3$ (*13*), $(CH_2)_3NH(CH_3)_2$ (*14*), $CON(CH_2)_3CH_3$ (*15*), $(CH_2)_3$ (*16*); M = Pd, R = Pr (*17*), CH_2COOCH_3 (*18*); M = Pt, R = Et or M = Cd, R = dimethylpyrimidine,2-thione (*19*). An example of an hexanuclear

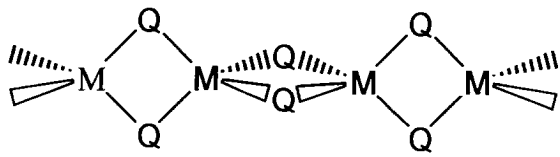

tetrahedral MQ_4

square planar MQ_4

FIG. 3. Connecting scheme between MQ_4 building units: M = Fe, Ni, Pd, Cd, Pt; Q = S, Se.

ring is depicted in Fig. 4 (*11*). The inner cavity is more or less accessible whether the organic group R is bulky or not.

There are fewer reported examples of structures containing $[M_8(QR)_{16}]$ rings, namely with Q = S, M = Ni, R = CH_2CO_2Et (*20*) and M = Pd, R = Pr (*21*). In these molecules, eight MS_4 rectangular coordination planes constitute an octagonal prism. The geometry of the wheel is analogous to the hexanuclear $[M_6(SR)_{12}]$ wheels with two extra metal atoms. A noteworthy octanuclear Cu_8 compound has eight Cu(II) ions in a square planar environment bridged by hydroxo groups and dimethylpyrazolato ligands (*22,23*). Its overall structure is reminiscent of the tiara geometry of the $[M_8(QR)_{16}]$ rings.

Fe ions adopt a tetrahedral coordination, which leads to a slightly different geometry of the ring. The nuclearity of the rings is either twelve with PhSe ligands or eighteen with sulfur ligands. In $[Fe_{12}(SePh)_{24}]$ (*24*), each Fe(II) is surrounded by four Se atoms of the ligand in a distorted tetrahedral fashion, and the edge-sharing FeS_4 tetrahedra connect to form a ring (Fig. 5). The phenyl groups are arranged in an alternating fashion above and below the plane of the Fe_{12} wheel, which has a diameter of about 12 Å. The synthesis of $[Fe_{12}(SePh)_{24}]$ is quite straightforward, from a suspension of $FeCl_3$ and PPh_3 in CH_2Cl_2 carefully covered with a layer of $PhSeSiMe_3$.

The $[Na_2Fe_{18}S_{30}]^{8-}$ ring (*25,26*) is distinctive at many levels. Sulfur ligands bridge iron atoms rather than thiolate ligands, as encountered in the previous examples. As the nuclearity of the ring increases, the complexity of the connecting scheme between the FeS_4 building units

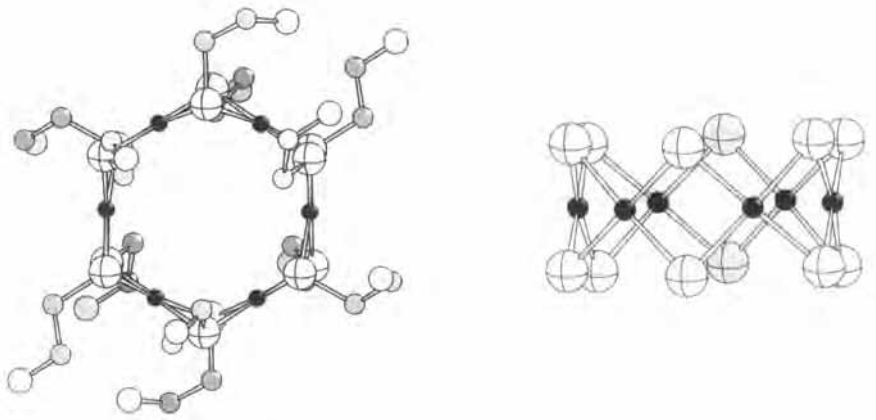

FIG. 4. Two views of $Ni_6(SCH_2CH_2OH)_{12}$: in the side-on view, the carbon and oxygen atoms of the organic ligand have been omitted for clarity; S atoms, white crossed spheres.

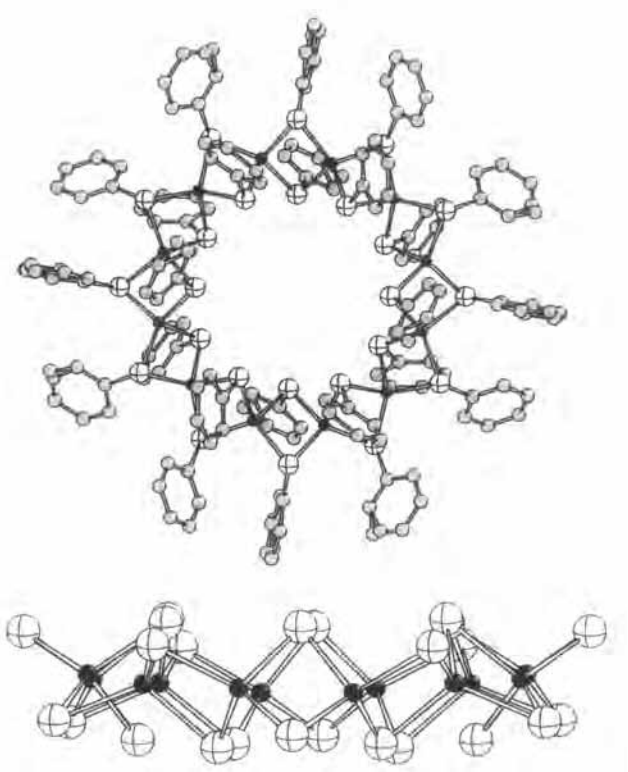

FIG. 5. Ball and stick representations of $[Fe_{12}(SePh)_{24}]$: in the side-on view, the carbon atoms of the phenyl rings have been omitted for clarity.

increases. Four Fe(II) and fourteen Fe(III) ions are in a tetrahedral environment; 22 Fe_2S_2 rhombs share edges and vertices to form the large wheel which can be described as a 14-membered ring with Fe(II) ions encapsulating four other $Fe^{III}S_4$ tetrahedra, although the electron repartition may not be as localized as suggested by this description. The anion of toroidal shape has two isomers, designated α and β, differing slightly by the atom connectivity. A view of the α isomer is depicted in Fig. 6. This view highlights the presence of two sodium atoms encapsulated within the ring, stabilizing the highly charged cluster. They may also play the role of template ion, inducing the formation of the cyclic structure.

B. Metals with an Octahedral Coordination

The number of metal wheels and, more generally, polynuclear cage complexes of the 3*d* metals has increased considerably in the last decade because of their magnetic properties, especially their behavior

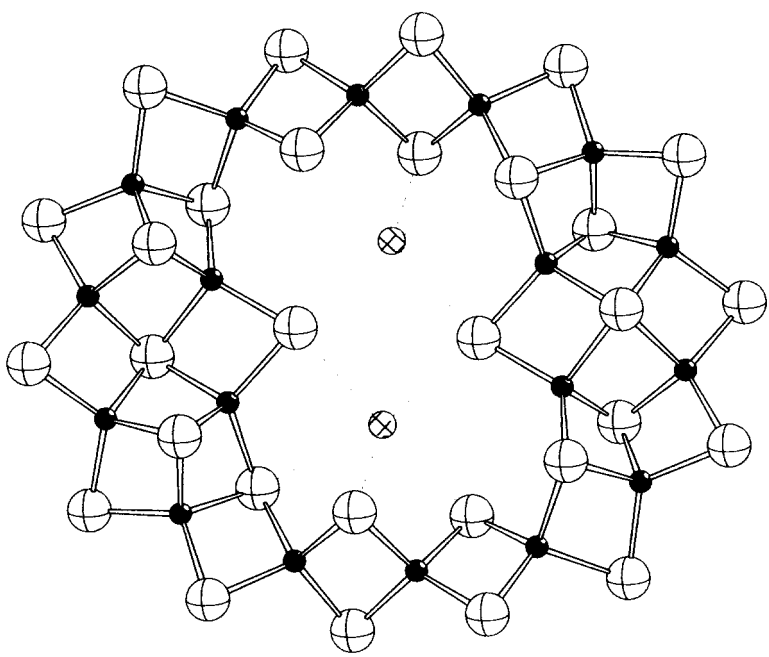

FIG. 6. Ball and stick representation of α-$[Na_2Fe_{18}S_{30}]^{8-}$: Na atoms, crosshatched spheres; the Na–S bonds are drawn as dotted lines.

as "single-molecule" magnets. This field of research started after the discovery in 1991 of the dodecanuclear manganese cage $[Mn_{12}O_{12}(O_2CMe)_{16}(H_2O)_4]$ (*27*) which has an $S = 10$ ground state. A large energy barrier between the $M = -10$ and $M = +10$ states leads to a slow relaxation of their magnetization below 10 K. Therefore, after the application of an external magnetic field, the molecule keeps its magnetization and behaves as a single-molecule magnet. However, so far, it is difficult to predict whether a molecule will have a high energy barrier or not. This explains the effort of synthetic chemists to design a large stock of compounds that will allow a systematic analysis of their properties and an understanding of the relationships between their composition and their magnetic properties. A review of the families of high nuclearity cages has been published recently (*28*). We will focus in this section on a specific class of cages, the metal wheels, known also as metallacoronates, from a structural point of view, including the molecules that do not necessarily have magnetic properties, starting with the smallest hexanuclear wheel and reaching the largest wheel known so far which contains 24 nickel atoms. We will give the most striking examples for each category of wheels, not necessarily trying to be exhaustive as this class of compound is very large.

1. Hexanuclear Wheels

The hexanuclear rings are regular, the six metal atoms being located at the corners of a hexagon. Formal replacement of the six metal atoms by ethane bridges leads to the topologically equivalent crown ether [12]crown-6, thus sometimes leading to the denomination of [12]metallacrown-6 for the metallic rings. The diameter of the hexanuclear rings, defined as the distance between two opposite metal atoms, is about 6.5 Å.

The manganese wheels and particularly the Mn(III) compounds attract much interest for single-molecule magnetism as the ferromagnetic coupling of Mn ions leads to ground states with high spin values. In $\{Mn \subset [Mn_6(OMe)_{12}(dbm)_6]\}$ (*29*) and $\{Na \subset [Mn_6(OMe)_{12}(dbm)_6]\}^+$ (*30*), where Hdbm is dibenzoylmethane, the six Mn ions of the wheel are bridged by μ_2-OMe and μ_3-OMe ligands and chelating dbm anions are found on the remaining coordination sites. In the heptanuclear complex, the metal wheel contains two Mn(II) and four Mn(III) ions whereas the central trapped Mn ion is a Mn(II) ion. In the sodium complex, all the Mn ions of the metal core are Mn(III) ions. In both manganese complexes, the Mn(III) ions are ferromagnetically coupled to give an $S = 12$ ground state.

The $\{Mn \subset [Mn_6(OH)_3Cl_3(hmp)_9]_6\}^{2+}$ (*31*) complex, where hmp is 2-hydroxymethylpyridine, is structurally very close to these two manganese rings. It is a mixed-valence manganese cluster with a central Mn^{2+} ion. A Cl^- counterion is hydrogen-bonded to the μ_3-OH^- groups which bridge the six Mn ions.

The Fe_6 rings have also been extensively studied. $[Fe_6(\mu_2\text{-}OMe)_{12}(dbm)_6]$ (*32,33*) is a neutral species but in the solid state it crystallizes with NaCl to give $[Na \subset Fe_6(\mu_2\text{-}OMe)_{12}(dbm)_6]^+$. The Na^+ ion is trapped in the center of the iron wheel, which acts like a crown ether complexing an alkaline ion.

Another example of a templated structure is given by $\{Na \subset Fe_6[N(CH_2CH_2O)_3]_6\}^+$ (*34*), where a sodium cation, in a distorted octahedral environment of six μ_3-oxygen atoms, is encapsulated in the center of the hexanuclear iron ring. Triethanolamine acts as a tetradentate ligand, linking three Fe(III) ions. The structure of $\{Na \subset Fe_6[N(CH_2CH_2O)_3]_6\}^+$ is depicted in Fig. 7 as a representative member of this family of hexanuclear rings.

The size of the sodium ion is perfectly adapted to the size of the cavity and probably sodium ions act as template ions for the synthesis of the six-membered cyclic structure. However, most of the metal rings have been discovered by serendipity and their syntheses rationalized *a posteriori*. The presence of a template agent does not seem necessary for all the compounds, as exemplified by the synthesis of $\{Fe_6[H_3C\text{—}N(CH_2CH_2O)_2]_6Cl_6\}$ (*34*). In this complex, one CH_3CH_2OH substituent of the ligand used for the synthesis of $\{Na \subset Fe_6[N(CH_2CH_2O)_3]_6\}^+$ has been replaced by a methyl group, leading to a tridentate ligand instead of a tetradentate one, and a μ_2-bridging chloride ion now completes the coordination sphere of the Fe(III) ions. The ring is empty.

Titanium wheels are rare but not uncommon. Two recent examples are $[Ti(\mu_2\text{-N-methyldiethoxoamine})(\mu_2\text{-O})]_6$ (*35*) and $[Ti(\mu\text{-}NMe_2)(NMe_2)(\mu\text{-F})(F)]_6$ (*36*). The latter compound is a unique example of a cyclic structure with bridging fluoride and amide groups. The hexanuclear structure is formed from distorted octahedrally coordinated titanium centers. The Ti octahedra are edge-sharing. This molecule was isolated as a by-product in the synthesis of titanium complexes with the pentamethylcyclopentadienide (Cp^*) ligand.

Finally, we also mention a cobalt ring (*37*), and the non-magnetic ring $\{Zn \subset [Zn(hmp)_2]_6\}^{2+}$ analogue (*38*), in which hmp is 2-hydroxymethylpyridine. A central octahedral Zn^{2+} ion is encapsulated in a hexanuclear ring.

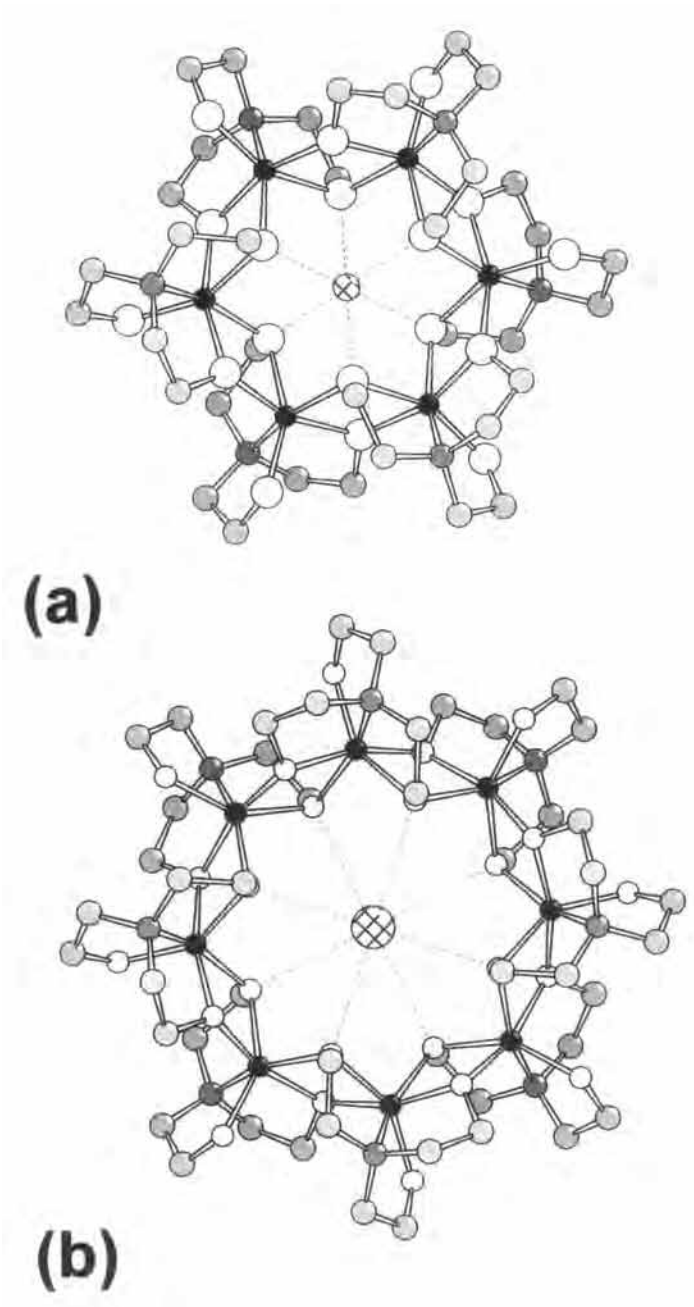

FIG. 7. Ball and stick representations of (a) $\{Na \subset Fe_6[N(CH_2CH_2O)_3]_6\}^+$ and (b) $\{Cs \subset Fe_8[N(CH_2CH_2O)_3]_8\}^+$, showing the template effect of the alkaline cation.

2. *Octanuclear Wheels*

A nice example of the self-assembly control of these supramolecular species (*39*) by the size of the template ion is given by the preparation of the octanuclear ring $\{Cs \subset Fe_8[N(CH_2CH_2O)_3]_8\}^+$ (*34*). When the synthesis of the metallic ring is performed in the presence of sodium ions, the hexanuclear ring $\{Na \subset Fe_6[N(CH_2CH_2O)_3]_6\}^+$ is obtained, whereas in similar conditions but in the presence of cesium ions, instead of sodium ions, the octanuclear complex is formed. In this octanuclear ring (Fig. 7) the eight iron atoms are located at the corners of a regular octagon with a diameter of about 8.2 Å. The cesium ion is surrounded by eight μ_3-O atoms in a quadratic antiprismatic coordination.

In $[V_8(\mu\text{-}OH)_4(\mu\text{-}OEt)_8(\mu\text{-}CH_3COO)_{12}]$ (*40*), the eight octahedral V(III) atoms, with six oxygen atoms coming from the bridging hydroxide, ethoxide and carboxylate ligands, are located in a crystallographic mirror plane. The molecule is neutral and the ring is empty. Interestingly, in the solid state, the cyclic compounds are stacked on top of each other to produce infinite channels.

We also mention the octanuclear chromic wheels $[CrF(O_2CCMe_3)_2]_8$ (*41*) and $[Cr_8(OH)_8(O_2CPh)_{16}]$ (*42*), which contain eight Cr(III) ions antiferromagnetically coupled.

3. *Decanuclear Wheels*

Probably the best known decanuclear ring is $[Fe(OMe)_2(O_2CCH_2Cl)]_{10}$ (*43,44*), known as the molecular "ferric wheel". In this molecule (Fig. 8), ten Fe(III) ions are linked by twenty bridging methoxide and ten bridging chloroacetate ligands in a similar way to the hexanuclear and octanuclear wheels previously described. The Fe(III) ions are antiferromagnetically coupled. The ring has a small inner diameter of 2–3 Å because of the presence of methoxy ligands restricting the cavity, thus no guest is observed. The $[Fe(OMe)_2(O_2CMe)]_{10}$ complex (*45*) is very similar to the "ferric wheel" reported by Lippard and coworkers.

While almost all the metallic wheels are synthesized in solution in one-pot reactions using standard conditions, the preparation of two chromic wheels $[Cr_{10}(\mu\text{-}O_2CMe)_{10}(\mu\text{-}OR)_{20}]$, R = Et or Me, by solvothermal reactions, on heating trinuclear chromium acetate in MeOH or EtOH, has recently been described (*46*). Interestingly, studies of magnetic susceptibilities revealed two different magnetic behaviors, namely a ferromagnetic Cr(III)$\cdots$Cr(III) exchange for R = Et and an antiferromagnetic exchange for R = Me.

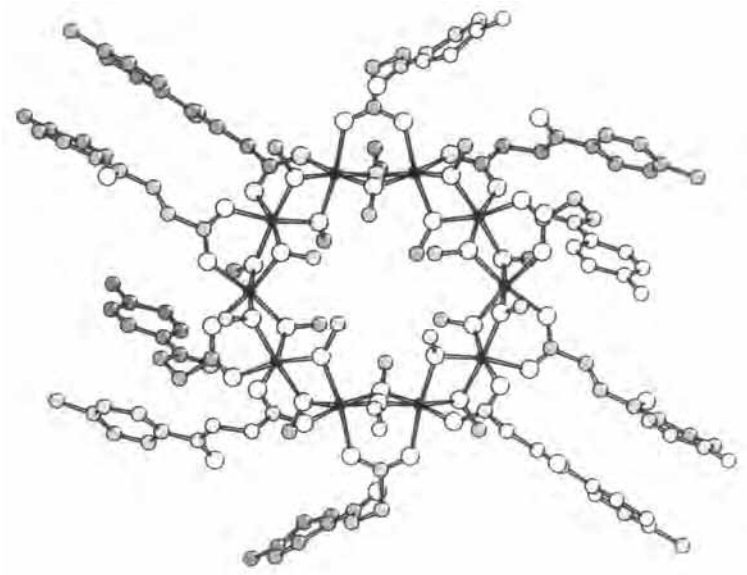

FIG. 8. Ball and stick representation of $[Fe(OMe)_2(O_2CCH_2Cl)]_{10}$.

4. *Dodecanuclear Wheels*

An example of a dodecanuclear ring is $[Ni_{12}(O_2CMe)_{12}(chp)_{12}(H_2O)_6(THF)_6]$ (*47*), where chp is the anion of 6-chloro-2-pyridone; magnetic studies indicate ferromagnetic coupling between the Ni(II) ions, leading to an $S = 12$ ground state. The isostructural cobalt wheel has also been synthesized (*48*).

5. *The Largest Wheels*

Wheels with nuclearities greater than twelve can no longer be described as formed from mononuclear fragments. In contrast, more than one type of bridging ligand is necessary to stabilize these large structures, and the building units are constituted of dinuclear or trinuclear fragments, as exemplified by $[Fe(OH)(XDK)Fe_2(OCH_3)_4(O_2CCH_3)_2]_6$ (*49*) where XDK is the dianion of *m*-xylylenediamine bis(Kemp's triacid imide). This complex is designated by the authors as the "molecular 18-wheeler" and is so far the largest cyclic iron(III) cluster. The Fe(III) centers are antiferromagnetically coupled. The inner diameter of the wheel is 4–5 Å, showing once more that the ring size does not necessarily determine the diameter of the inner cavity.

The search for high nuclearity cages has led recently to the striking complex $[Ni_{24}(OH)_8(mpo)_{16}(O_2CMe)_{24}(Hmpo)_{16}]$ (*50*), where mpo is 3-

methyl-3-pyrazolin-5-one; this ring (Fig. 9), owing to its size, is much less circular than smaller cyclic structures. The structure is stabilized by hydrogen bonding interactions between protons of the mpo ligands and oxygen atoms from acetate and mpo ligands. Magnetic measurements are consistent with the presence of 24 $S = 1$ centers, weakly antiferromagnetically coupled at low temperature.

III. Wheel-Shaped Polyoxo(thio)metalates with Metals in High Oxidation States (IV, V, VI)

Two types of compound are observed, the first one being composed of the Mo(VI) and W(VI) pentanuclear and hexanuclear rings as well as the cyclic V(IV) octanuclear ring. These rings can be described as oligomers of MO_6 octahedra with oxygen atoms coming from terminal oxo groups, bridging oxo or methoxy ligands and organic ligands. In these rings all the M···M distances are approximately equal. In the second class of compounds, the common building unit is the diamagnetic $M_2O_2E_2^{2+}$ (M = Mo(V), W(V); E = O, S) moiety. Short Mo–Mo distances (2.6 Å for E = O, 2.8 Å for E = S) are indicative of a metal–metal bond. Each metal atom bears one terminal oxo ligand and two μ_2-O or μ_2-S bridges. In the resulting polyoxo(thio)metalates short Mo–Mo distances, within the $M_2O_2E_2$ units, alternate with longer non-bonding Mo···Mo contacts (3.5 Å) between the building units. The various modes of connection of the organic or inorganic ligands to the metal atoms are gathered in Fig. 10.

A. Pentanuclear Wheels

In the pentanuclear rings $[(RPO_3)_2M_5O_{15}]^{14-}$ (M = Mo, W; R = O, alkyl or aryl groups), five M(VI) ($M\mu_2$ = Mo, W) atoms in an octahedral environment, bearing two terminal oxo ligands, are bridged by one oxo group and one μ_2-O and one μ_3-O from a phosphate or a phosphonate group, with types 2 and 3 connecting schemes. The RPO_3 groups lie above and below the plane defined by the metal atoms. Numerous examples of $[(RPO_3)_2M_5O_{15}]^{14-}$ polyoxoanions have been reported with M = Mo, R = O (*51,52,53*), R = CH_3 (*54,55*), R = $CH_2CH_2NH_3^+$ (*54*), R = *t*Bu (*55*), R = Ph (*56,57*), R = CH_2Ph (*55*), R = $C_5H_{11}NO$ (*58*), and R = $C_{10}H_{23}N_5O_4$ (*59*). An example is depicted in Fig. 11. The tungstate analogues are less stable in aqueous solutions; therefore fewer compounds are described in the literature (*60*).

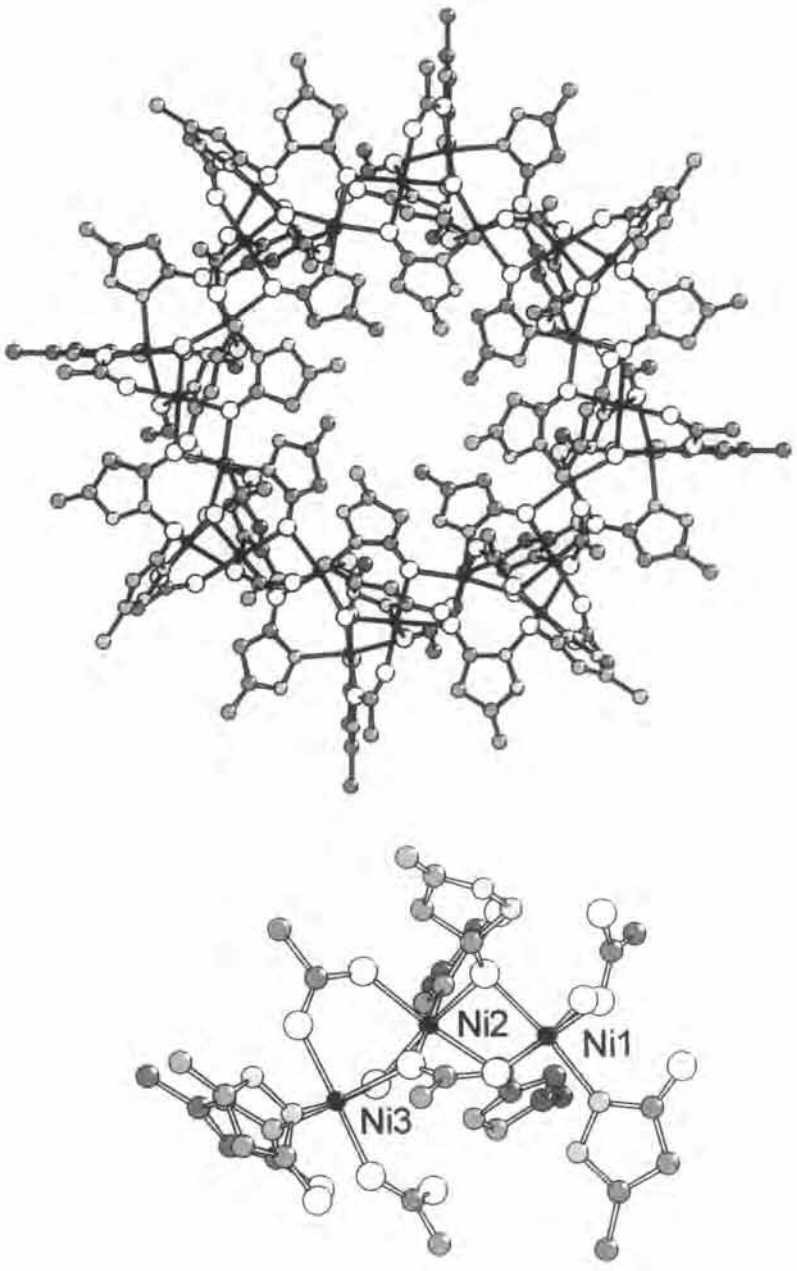

FIG. 9. Ball and stick representations of $[Ni_{24}(OH)_8(mpo)_{16}(O_2CMe)_{24}(Hmpo)_{16}]$ and its trinuclear oligomer.

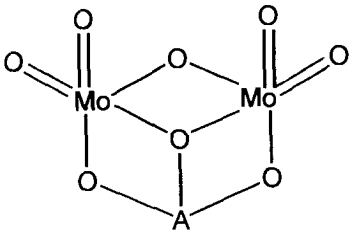

type 1

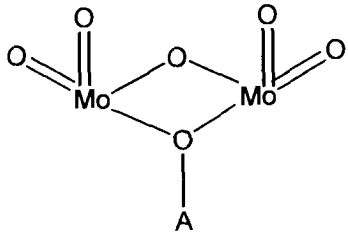

type 2

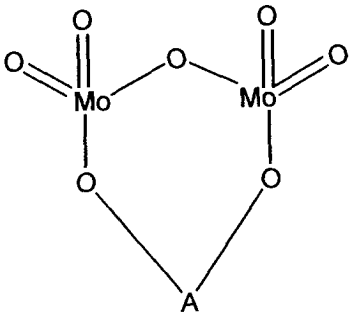

type 3

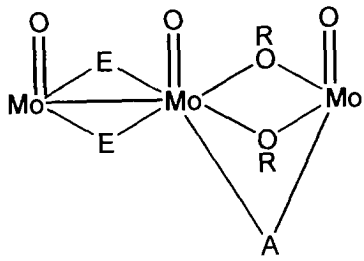

E = O, S

type 4

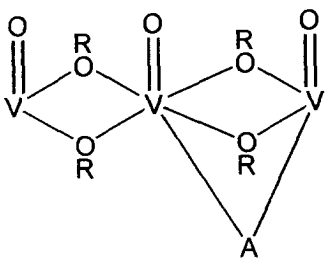

type 5

FIG. 10. Schematic diagrams showing the various connecting modes of a ligand A to the metal atoms.

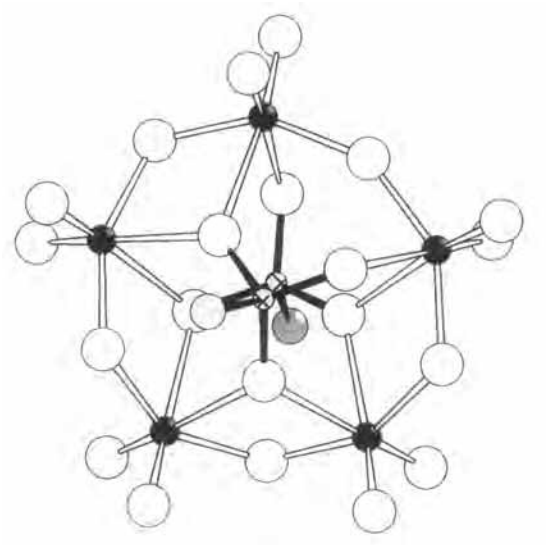

FIG. 11. Ball and stick representation of $[(CH_3PO_3)_2Mo_5O_{15}]^{14-}$.

B. HEXANUCLEAR WHEELS

Heteropolyanions with the Anderson structure have the general formula $[XM_6O_{24}]^{6-}$ (M = Mo, W). The six M(VI) atoms form a nearly perfect plane hexagon around the central XO_6 octahedron, with the connecting scheme of type 1 (Fig. 12). The average Mo · · · Mo distance is 3.3 Å. The six distorted MO_6 octahedra share edges within the hexanuclear ring. The Anderson structure has been described so far for X = Cr(III) (*61*), Mn(IV) (*62*), Co(III) (*63*), Cu(II) (*64*), Zn(II) (*65*), Te(VI) (*66,67*), I(I) (*68*), and Pt(IV) (*69*). In Anderson structures with central atoms having a +2 or +3 charge (Cr, Co, Cu, Zn), the six μ_3-O atoms of the XO_6 octahedra are protonated.

The structure of the $[(RAs)_2Mo_6O_{24}]^{4-}$ anions is similar to the Anderson structure except that the central XO_6 octahedron with six μ_3-O atoms has been replaced by two $RAsO_3$ tetrahedra sharing three μ_3-O atoms with the metal atoms of the ring, with types 2 and 3 connecting schemes (Fig. 13). It has been described for R = CH_3 (*70*), R = O, OH (*71*), R = $(CH_2)_2CH_3$ (*72*), and R = $PhNH_2$ (*73*). A structural analogy can be made between the polyoxoanion $[Mo_8O_{26}]^{4-}$ and the $[(RAs)_2Mo_6O_{24}]^{4-}$ anions. Indeed, $[Mo_8O_{26}]^{4-}$ (*74*) has a structure similar to that of the $[(RAs)_2Mo_6O_{24}]^{4-}$ anions, with two $\{MoO_4\}$ tetrahedra replacing the two $RAsO_3$ tetrahedra, as shown in Fig. 13.

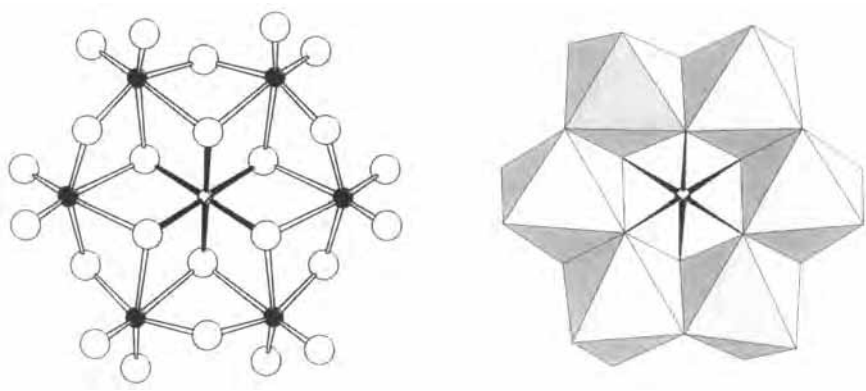

FIG. 12. Ball and stick (a) and polyhedral (b) representations of $[TeMo_6O_{24}]^{6-}$.

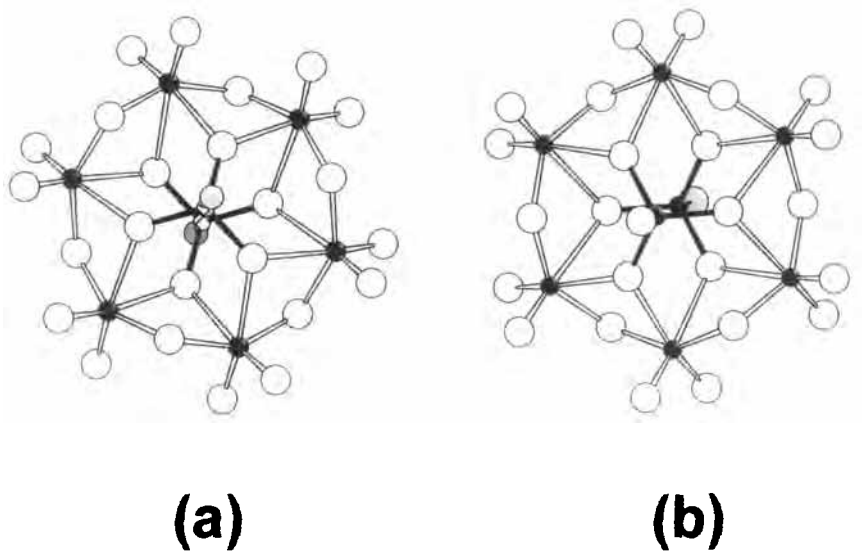

FIG. 13. Representation of (a) $[(CH_3As)_2Mo_6O_{24}]^{4-}$ compared to (b) $[Mo_8O_{26}]^{4-}$.

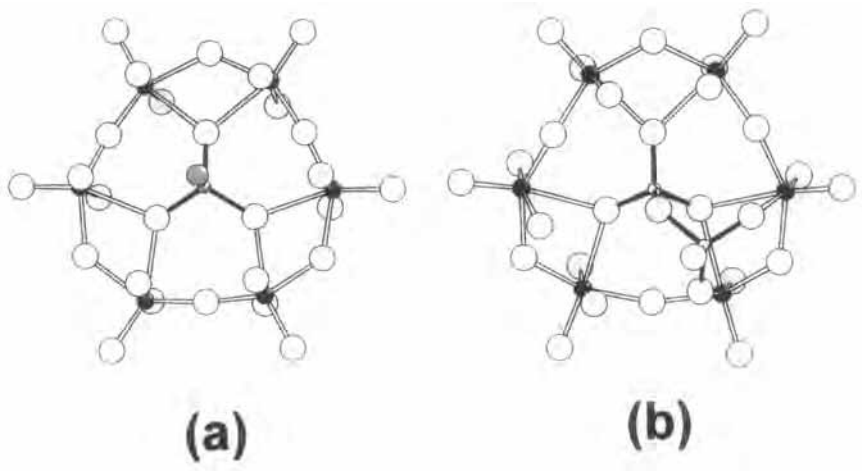

FIG. 14. Ball and stick representation of (a) $[CH_3AsMo_6O_{21}(H_2O)_6]^{2-}$ and (b) $[(P_2O_7)Mo_6O_{18}(H_2O)_4]^{2-}$.

Other examples of hexanuclear rings include $[CH_3AsMo_6O_{21}(H_2O)_6]^{2-}$. In this anion (*75*), each Mo atom has two terminal oxygen atoms in *cis* position and is coordinated by one water molecule. The MoO_6 octahedra form a ring by alternate corner- and edge-sharing around a central CH_3AsO_3 tetrahedron, with alternate types 2 and 3 connecting schemes (Fig. 14). The structures of $[(PRP)Mo_6O_{24}(H_2O)_4]^{2-}$ (R = O, CH_2) (*76,77*) present some similarities. In these anions, four Mo atoms are coordinated to terminal water molecules and one P atom of the central pyrophosphate or methylenediphosphonate group while the remaining two are connected to both ends of the inorganic ligand. A noteworthy feature of these two structures is that the metal ring loses its rigidity, owing to the presence of only one bridging atom, and is therefore much less circular than the hexanuclear rings previously described.

Slight variations on these anions are also encountered in the structures of $[(RAs)_2HMo_6O_{25}]^{5-}$, R = NO_2Ph (*78*) and $[(RAs)_2H_2Mo_6O_{25}]^{4-}$, R = Ph (*79*), and the phosphorous analogue $[(RP)_2Mo_6O_{24}]^{4-}$, R = *t*Bu (*80*).

C. Oxo and Oxothio P_4Mo_6 Anions

In the chemistry of Mo(V) and phosphates, the very stable anion $[P_4Mo_6E_6O_{22}(OH)_3]^{9-}$ (E = O, S), denoted $P_4Mo_6E_6$, is often encountered. The fully oxo compound $P_4Mo_6O_6$ has often been obtained by

hydrothermal synthesis, starting from MoO_4^{2-}, metallic Mo, as reducing agent, and phosphate ions. The degree of protonation varies from one structure to the other (*81*). Our group has recently described the synthesis of the analogous oxothioanion $[P_4Mo_6S_6O_{22}(OH)_3]^{9-}$ ($P_4Mo_6S_6$), easily prepared in solution under mild conditions starting from the $[Mo_2^VO_2(\mu\text{-}S)_2(H_2O)_6]^{2+}$ thiocation (*82*). A study of the O for S substitution of $P_4Mo_6S_6$, in solution, has led to the preparation of the half-substituted $[P_4Mo_6S_3O_{25}(OH)_3]^{9-}$ ($P_4Mo_6S_3O_3$) (*83*). We have shown by ^{31}P NMR that the substitution is regioselective. Indeed, in $P_4Mo_6S_6$, half of the sulfur bridging atoms, lying on the opposite side of the phosphate groups, are successively replaced by oxygen atoms. All three anions present the same overall structure depicted in Fig. 15.

In $P_4Mo_6E_6$ (E = O, S), three $\{Mo_2E_4\}$ units are mutually connected by a peripheral phosphato ligand and by a hydroxo group. The connections between each building unit are edge-sharing. The resulting hexanuclear ring is derived from the Anderson structure. A central phosphate group is encapsulated in the metal ring. The central and the three peripheral phosphate groups lie on the same side of the plane defined by the six molybdenum atoms. The connecting scheme is of type 5. The formation of dimeric species is often observed in this family of anions with an M^{2+} ion (M = Cr, Mn, Fe, Co, Ni, Zn, Cd) or a sodium cation, in a regular octahedral coordination, linking two $P_4Mo_6E_6$ anions via three (μ-O) atoms of the three $\{Mo_2E_4\}$ units (Fig. 15).

Related structures comprise the organophosphate ion $[Mo_6O_{15}(O_3PC_6H_5)(HO_3PC_6H_5)_3]^{5-}$ (*84*) and the $[AsMo_6O_{15}(OH)_3(SO_4)_3]^{6-}$ anion, the analogue of the $P_4Mo_6O_6$ anion with a central arsenite and three peripheral sulfate groups instead of phosphate groups (*85*). This latter compound is a rare example of a compound with $\{Mo_2^VO_2(\mu\text{-}O)_2\}$ building units prepared in solution, under mild conditions, by reduction of a Mo(VI) solution in the presence of arsenite and sulfate groups.

The structure of the hexanuclear oxovanadium(IV) anion $[(VO)_6(CO)_4(OH)_9]^{5-}$ (*86*) is highly reminiscent of the structure of the $P_4Mo_6E_6$ anions with four CO_3 groups replacing the four phosphato groups. The connecting scheme is of type 5. The nine oxo bridges are protonated.

D. Octanuclear Wheels

In $[Mo_8O_{16}(OCH_3)_8L_4]$ (L = pyridine, 3-methylpyridine, 3,5-lutidine) (*87,88*), the eight Mo(V) atoms are linked together alternatively by pairs of methoxy ligands and pairs of oxo groups with short Mo–Mo distances within the $\{Mo_2^VO_2(\mu\text{-}O)_2\}$ building units and longer Mo $\cdots$ Mo contacts

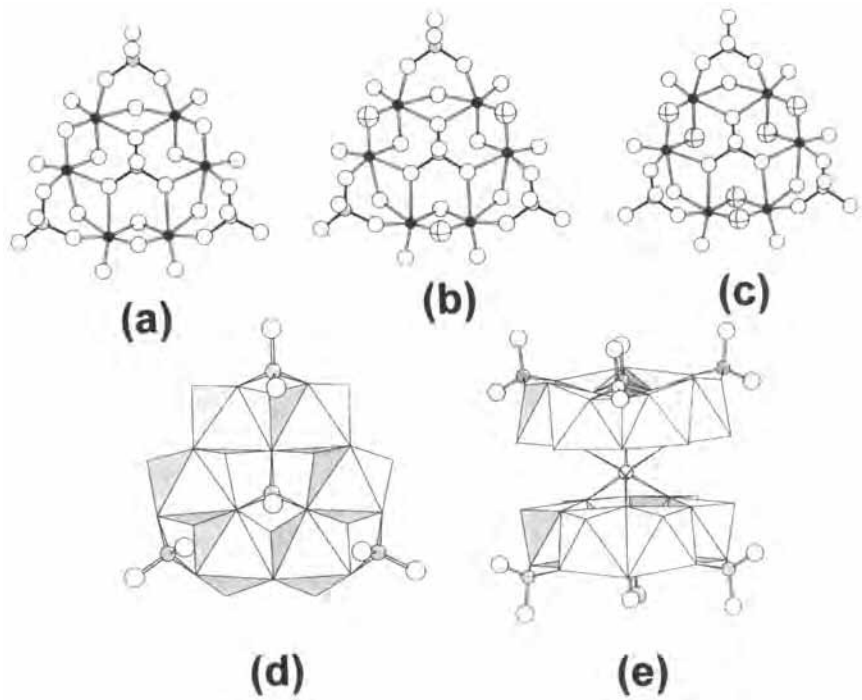

FIG. 15. Ball and stick representations of (a) $[P_4Mo_6O_{28}(OH)_3]^{9-}$ ($P_4Mo_6O_6$), (b) $[P_4Mo_6S_3O_{25}(OH)_3]^{9-}$ ($P_4Mo_6S_3O_3$), (c) $[P_4Mo_6S_6O_{22}(OH)_3]^{9-}$ ($P_4Mo_6S_6$); (d) their common polyhedral representation; (e) a view of the dimeric species formed by an M^{2+} ion (M = Cr, Mn, Fe, Co, Ni, Zn, Cd) or a sodium cation sandwiched by two $P_4Mo_6E_6$ units.

(3.5 Å) between each unit, producing a "tiara" framework (Fig. 16). One Mo atom of the dinuclear core is in a square pyramidal environment and the other one, to which the pyridine ligand is bound, is in a distorted octahedral environment. The polyhedra share edges within the ring. In the solid state, the rings stack on top of each other, forming channels.

The geometry of the $[Mo_8O_{16}(OCH_3)_8(PMe_3)_4]$ ring (*89*) is analogous to the structure of $[Mo_8O_{16}(OCH_3)_8L_4]$ (L = pyridine, 3-methylpyridine, 3,5-lutidine).

The geometry of the $[Mo_8O_{16}(OCH_3)_8(C_2O_4)]^{2-}$ ring (*90*) is also quite comparable to the other octanuclear rings, with Mo atoms alternately bridged by two methoxy groups and two oxo groups (Fig. 17). A remarkable feature of the structure of $[Mo_8O_{16}(OCH_3)_8(C_2O_4)]^{2-}$ is the presence of an oxalate ligand inside the cavity. Each oxygen atom of the oxalate moiety bridges two Mo centers with non-bonding Mo $\cdots$ Mo distances, thus completing the octahedral coordination sphere of each Mo atom.

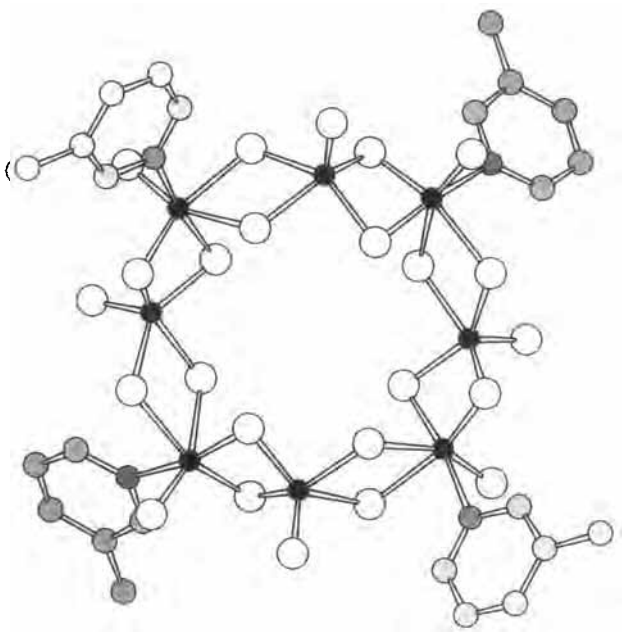

FIG. 16. Ball and stick representation of $[Mo_8O_{16}(OCH_3)_8L_4]$ (L = pyridine).

The Mo octahedra share edges within the ring. The molybdenum wheel $[Mo_8O_{16}(OCH_3)_8(C_2O_4)]^{2-}$ is the first example of a metal wheel incorporating organic ligands. This compound was synthesized from a mixture of rhodizonic acid $C_6H_2O_6$ and α-$[\eta$-$(C_4H_9)_4N][Mo_8O_{26}]$ in CH_3OH; a decomposition of the rhodizonic acid, concomitant with the reduction of Mo(VI) ions, leads to the octanuclear ring. We have recently developed a rational synthetic approach for the preparation of oxothiomolybdate rings incorporating various organic or inorganic ligands, based on the self-condensation of $\{Mo_2^{V}O_2(\mu\text{-}S)_2\}^{2+}$ structural units. On addition of hydroxide ions to a solution of $[Mo_2S_2O_2(H_2O)_6]^{2+}$, at pH below 3, a yellow solid precipitates (*91*) and affords, after recrystallization, the neutral cyclic derivative $[Mo_{12}S_{12}O_{12}(OH)_{12}(H_2O)_6]$ (*92*), the first member of this new family of oxothio compounds (see below). The crude product regenerates the thiocation in acid media and hydrolyzes in basic media to give the $[Mo_2S_2O_2(OH)_4(H_2O)_2]^{2-}$ anion, and is therefore a convenient precursor for further condensation reactions. The octanuclear ring $[Mo_8S_8O_8(OH)_8(C_2O_4)]^{2-}$ is synthesized in good yield by the reaction of the crude product and a stoichiometric amount of oxalate ions, in water, at pH around 5. The structure of

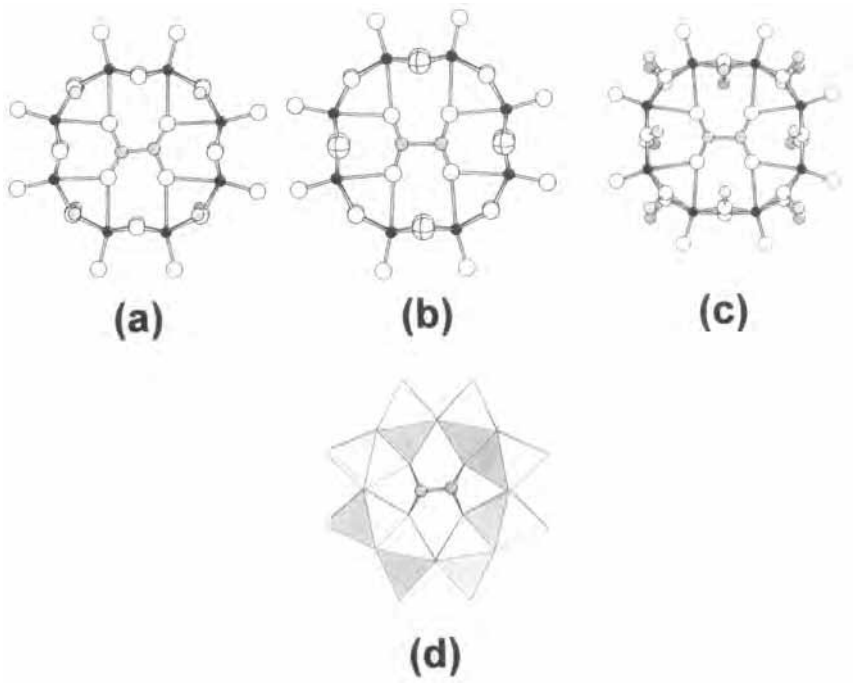

FIG. 17. Ball and stick representations of the octanuclear rings (a) $[Mo_8O_{16}(OCH_3)_8(C_2O_4)]^{2-}$, (b) $[Mo_8S_8O_{16}(OH)_3(C_2O_4)]^{2-}$, (c) $[V_8O_8(OCH_3)_{16}(C_2O_4)]^{2-}$; (d) their common polyhedral representation.

$[Mo_8S_8O_8(OH)_8(C_2O_4)]^{2-}$ (Fig. 17) is analogous to that of $[Mo_8O_{16}(OCH_3)_8(C_2O_4)]^{2-}$ with hydroxo bridges in place of methoxy groups and (μ_2-S) bridges instead of (μ_2-O) bridges.

The structure of the V(IV) ring $[V_8O_8(OCH_3)_{16}(C_2O_4)]^{2-}$ (*93*) is similar to that of $[Mo_8O_{16}(OCH_3)_8(C_2O_4)]^{2-}$ and $[Mo_8S_8O_8(OH)_8(C_2O_4)]^{2-}$, except that the vanadium analog exhibits methoxy bridges exclusively rather than alternating methoxy or hydroxo and oxo bridging pairs (Fig. 17). Consequently, the V $\cdots$ V distances are quite similar, while in the Mo(V) rings short and long Mo $\cdots$ Mo separations alternate within the ring. The V(IV) octanuclear ring is a unique example of a V cyclic compound. The polyhedral representation of the octanuclear rings (Fig. 17) shows the connecting schemes between the Mo_6 octahedra, alternately edge-sharing and face-sharing.

Octanuclear molybdenum wheels incorporating a Mo(VI) (*94*) or a W(VI) (*95*) octahedron can also be prepared from a basic solution of the oxothio precursor containing a stoichiometric amount of molybdate or

tungstate. The M(VI) (M = Mo, W) atoms of the central octahedron bear one terminal oxo group, one terminal aquo ligand, and are connected to the Mo(V) framework via four μ_3-O atoms (Fig. 18). The $[Mo_8S_8O_8(OH)_8\{HWO_5(H_2O)\}]^{3-}$ anion crystallizes as a lithium salt, exhibiting a remarkable three-dimensional structure with oxothioanions anchored to partially filled lithium columns interleaved by an intricate hydrogen-bonded network of water molecules which confer ionic conductivity properties (*95*).

E. Decanuclear and Dodecanuclear Wheels

In DMF, the self-condensation of the $\{Mo_2O_2(\mu\text{-}S)_2\}^{2+}$ precursor in the presence of iodide (*91*) or chloride (*96*) led to the decanuclear anionic ring $[X_2Mo_{10}O_{10}S_{10}(OH)_{10}(H_2O)_5]^{2-}$ (Fig. 19). Five units are connected to each other by double hydroxo bridges to form the neutral $[Mo_{10}O_{10}S_{10}(OH)_{10}(H_2O)_5]$ cyclic skeleton. Two halides are symmetrically located on both sides of the planar ring. The distance between the two halides and the five inner water molecules is short (3.570–3.622 Å for X = I, 3.201–3.376 Å for X = Cl), suggesting the stability of the bis-halide ring is related to strong hydrogen bonds within the cavity. The five X···H–OH···X interactions result in a shortening of the X···X distance, giving a value close to the sum of the halide ionic radii.

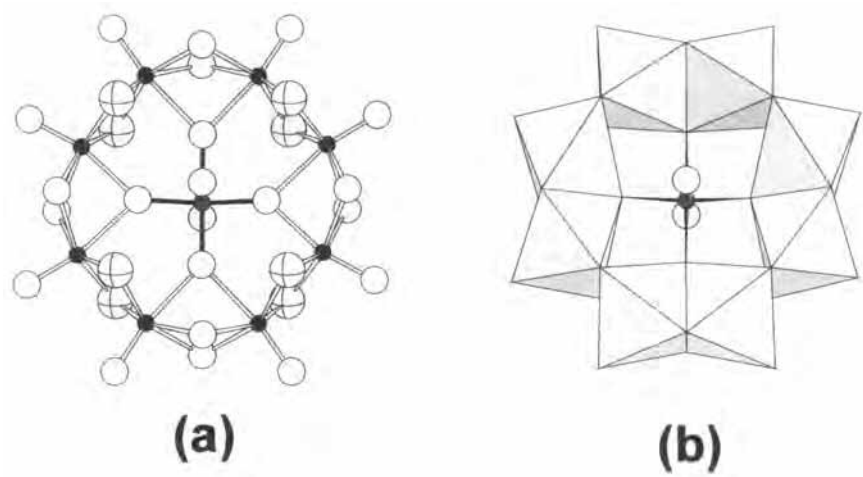

FIG. 18. (a) Ball and stick and (b) polyhedral representation of $[Mo_8S_8O_8(OH)_8\{HWO_5(H_2O)\}]^{3-}$.

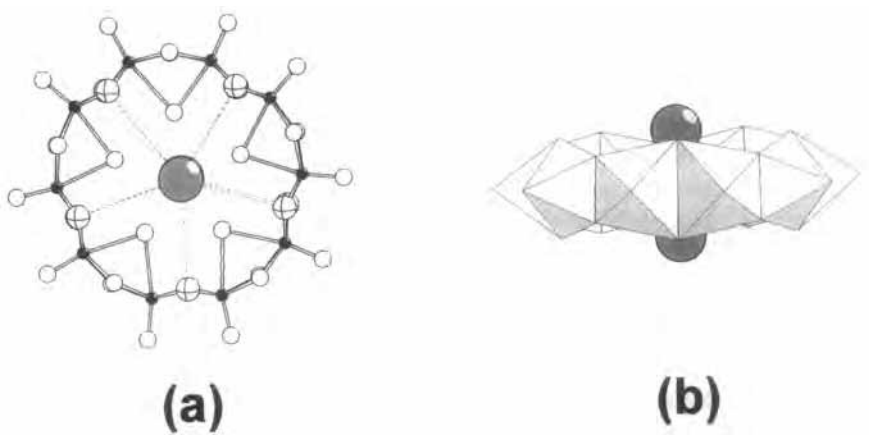

FIG. 19. Ball and stick (a) and polyhedral (b) representations of the decanuclear ring in $[X_2Mo_{10}S_{10}O_{10}(OH)_{10}(H_2O)_5]^{2-}$ (X = Cl, I) showing the two halide ions floating over the cavity of the Mo_{10} ring through hydrogen bonding interactions.

Another type of decameric ring, $[ClMo_{10}O_{10}S_{10}(OH)_{10}(H_2O)_3]^{3-}$, has been obtained by raising the pH of an aqueous solution of $\{Mo_2O_2(\mu\text{-}S)_2\}^{2+}$ to about pH = 6.2 in the presence of KCl (*96*). In contrast to the former decanuclear wheel, the cyclic skeleton is two times negatively charged and only a chlorine anion is located on a side of the planar Mo-ring which gives the −3 overall charge to the wheel. The increase of the negative charge is related to the loss of two protons by two inner water molecules of the cavity. In the solid state the anionic wheels arrange in a 3D framework through the three potassium ions balancing the charge. The resulting lattice is characteristic of a microporous solid, the pores being occupied only by free water molecules.

In acid medium, about pH = 2.5–3, mixtures containing the $\{Mo_2O_2(\mu\text{-}S)_2\}^{2+}$ dication and iodide ions led to a solid which, after recrystallization in pure water, gave crystals of the neutral dodecameric wheel $[Mo_{12}S_{12}O_{12}(OH)_{12}(H_2O)_6]$ (*92*). The cyclic arrangement of the neutral Mo_{12}-ring delimits a central cavity of 12 Å diameter lined by six water molecules as represented in Fig. 20. These inner water molecules are labile enough to be replaced by anionic groups stabilized by the cationic behavior of the cavity. Acidification of the molecular ring gives back the starting precursor $\{Mo_2O_2(\mu\text{-}S)_2\}^{2+}$, which illustrates the reversibility of the condensation process.

The dodecameric former wheel reacts with phosphates to give the two phosphato species, $[(HPO_4)_2Mo_{12}S_{12}O_{12}(OH)_{12}(H_2O)_2]^{4-}$ and $[(H_2PO_4)$-

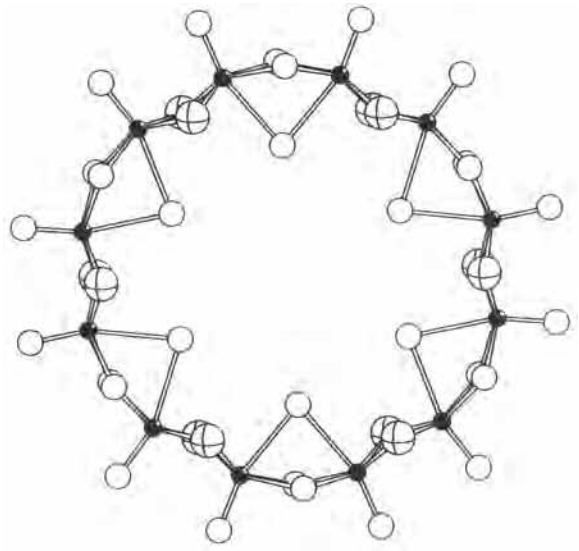

FIG. 20. Ball and stick representation of the neutral $[Mo_{12}S_{12}O_{12}(OH)_{12}(H_2O)_6]$.

$Mo_{10}S_{10}O_{10}(OH)_{11}(H_2O)_2]^{2-}$, in equilibrium in solution (*97*). A complete ^{31}P NMR study, including variable concentrations in phosphate and variable temperature and arsenate–phosphate exchanges, allowed one to characterize the different species in solution. The neutral cyclic backbones $[Mo_{2n}S_{2n}O_{2n}(OH)_{2n}]$, $n = 5$, 6, accommodate HPO_4^{2-} and $H_2PO_4^-$ ions respectively, resulting in the two structures given in Fig. 21. For $n = 6$, four inner water molecules have been replaced in the Mo_{12}-ring by two HPO_4^{2-} ions. The resulting wheel is strongly distorted from circular to elliptic due to the "pincer effect" of the chelating phosphates. Two Mo atoms close to the coordinated phosphates have lost their coordinated water, probably because of steric constraints, thus adopting a pyramidal geometry, see Fig. 21(a). In the solid state, the different wheels are mutually connected by sodium cations forming planes pillared by sodium columns. For $n = 5$, the decameric ring is circular, a Mo atom showing a pyramidal geometry, see Fig. 21(b).

The Mo_{12} wheel can fully encapsulate organic anions whether or not the size of the anion matches the ring dimension. Thus, $[C_6H_3(COO)_3]^{3-}$ exchanges with the five labile water molecules present in the cavity of Mo_{12} (*98*) to form $\{Mo_{12}S_{12}O_{12}(OH)_{12}[C_6H_3(COO)_3]\}^{3-}$. In this compound a good correspondence exists between the size of the guest and that of the host. Based on this observation, a series of interest-

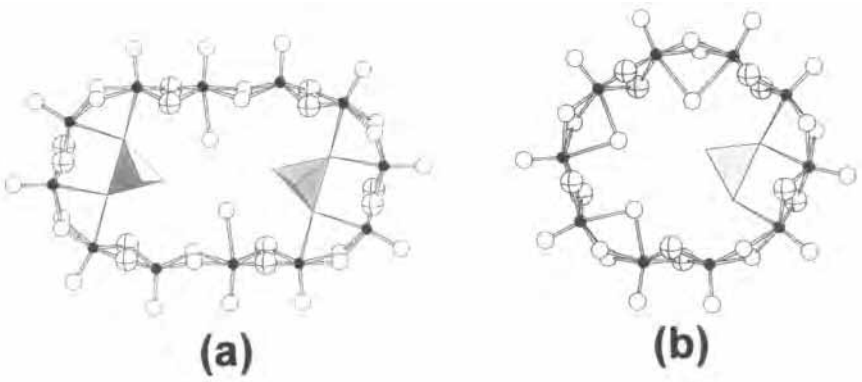

FIG. 21. View of the elliptical (a) $[(HPO_4)_2Mo_{12}S_{12}O_{12}(OH)_{12}(H_2O)_2]^{4-}$ and circular (b) $[(H_2PO_4)_2Mo_{10}S_{10}O_{10}(OH)_{11}(H_2O)_2]^{2-}$.

ing experiments has been performed by varying the size of the guest and showing that the host adapts its size to accommodate the anionic template (*99*). Fig. 22 presents the templating effect of the size of the alkyl chain of carboxylates on the size of the wheels. These wheels exhibit, in aqueous solution, striking dynamic effects observed by ^1H NMR at varying temperature, see Fig. 23. The variation of the spectra was interpreted by the motion, inside the cavity, of the carboxylate chain, a frozen conformation being obtained at low temperature.

With tungsten, the large pillared wheel $[W_{16}O_{16}S_{16}(OH)_{16}(H_2O)_4(C_5H_6O_4)_2]^{4-}$ was obtained by reacting $\{W_2O_2(\mu\text{-}S)_2\}^{2+}$ as precursor with glutarate in DMF (*100*). This big wheel is flexible and was obtained as single crystals under two different symmetries, D_{2h} (regular) and C_2 (distorted) (*100*) (Fig. 24).

IV. From the Molecular Level to Nanostructures

In this section, the constituting building units are no longer simple mononuclear or dinuclear fragments but more complex polyanionic-based fragments. The main common geometrical consequence is that the metal atoms, which were lying approximately in a plane in simple molecular architectures, are arranged in a torus geometry.

Predicted vacant polyoxometalates can be easily obtained by controlled hydrolyses, and are good reactive nucleophiles that can form a remarkable set of precursors for the design of large soluble molecules.

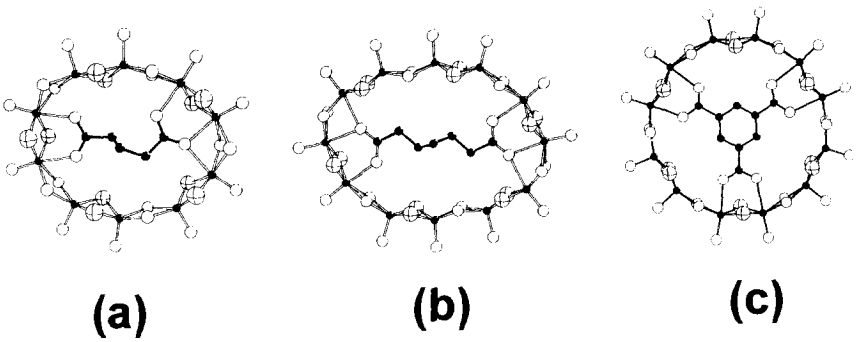

FIG. 22. Templating effect of carboxylates: the size of the wheels is tuned by the length of the alkyl chain of the carboxylate: (a) $\{Mo_{10}\}$-glutarate, (b) $\{Mo_{12}\}$-pimelate, (c) $\{Mo_{12}\}$-trimesate, $\{Mo_8\}$-oxalate (see Fig. 17).

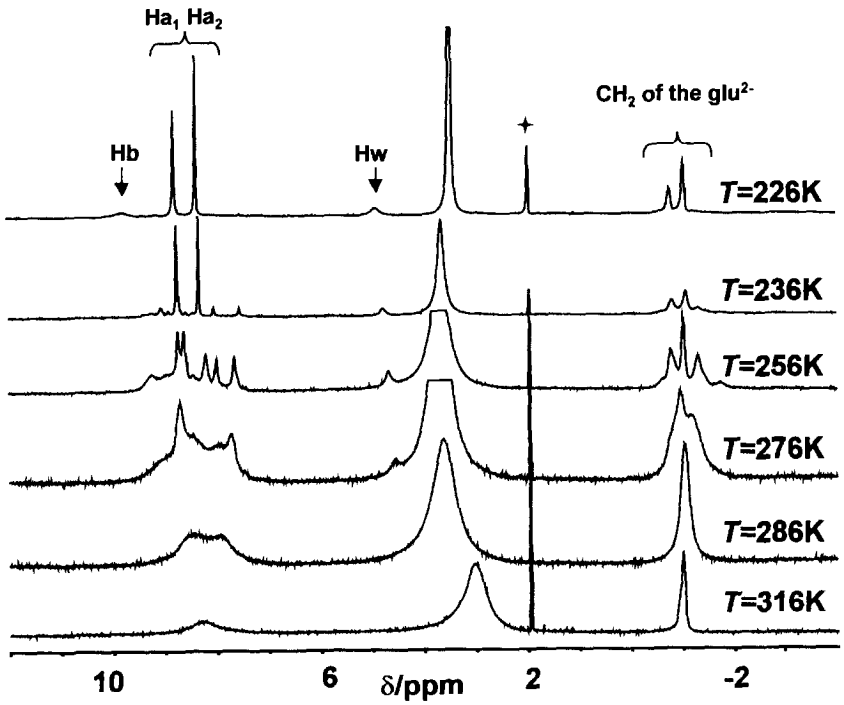

FIG. 23. Variable temperature ^1H NMR spectra for $Li_2[Mo_{10}$-glutarate] in CD_3CN (+: solvent feature). Ha, Hb are protons of OH-bridges; Hw are protons of water molecules.

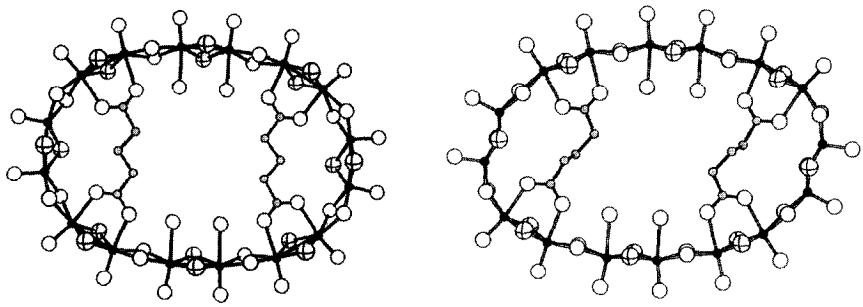

FIG. 24. Two glutarate anions acting as molecular pillars in the two conformations of $[W_{16}S_{16}O_{16}(OH)_{16}(H_2O)_4(C_5H_6O_4)_2]^{4-}$.

A. CROWN HETEROPOLYANIONS

The Preyssler anion $\{Na[P_5W_{30}O_{110}]\}^{14-}$, represented in Fig. 25, approximates to D_{5h} symmetry (*101,102*). It formally contains five PW_6O_{22} units, each derived from the archetypal Keggin anion $[PW_{12}O_{40}]^{3-}$ by removal of two sets of three-corner shared WO_6 octahedra. The ring contains a Na^+ ion statistically distributed on two sites located on the C_5 axis and separated by 2.5 Å. The presence of the inner cation reduces the symmetry from D_5 to C_5. The sodium is firmly encapsulated in the ring and cannot be directly exchanged by protons, which leads to the belief that sodium is required for the stability of the polyanion and probably acts as a templating agent in the formation process in solution. The sodium cation can be exchanged by calcium, a more polarizing cation having almost the same radius (1.26 Å) but a higher charge, on heating at 120°C for several hours (*101*).

The Dawson α-$[P_2W_{18}O_{62}]^{6-}$ was used as precursor since it hydrolyzes in a series of lacunary polyoxoanions by excision of octahedra (*103*) under controlled addition of a base. The heteropoly structure α-$[P_2W_{17}O_{62}]^{10-}$ is first formed in solution, then α-$[P_2W_{15}O_{56}]^{12-}$, following which stable α-$[H_2P_2W_{12}O_{48}]^{12-}$ is readily isolated in the solid state. After redissolving of the solid in a lithium acetate buffer and addition of exclusively potassium ions, $K_{28}Li_5[H_7P_8W_{48}O_{184}]$ crystallizes. The crown heteropolyanion (Fig. 26), with approximate D_{4h} symmetry, formally results from the condensation of four $P_2W_{12}O_{48}$ subunits derived from the α-$[P_2W_{18}O_{62}]^{6-}$ Dawson structure by abstraction of six adjacent octahedra. Eight potassium cations are distributed in the cavity at 2.74–3.1 Å from inner oxygen atoms. The presence of potassium decreases the repulsion between the negative charges on the inner cav-

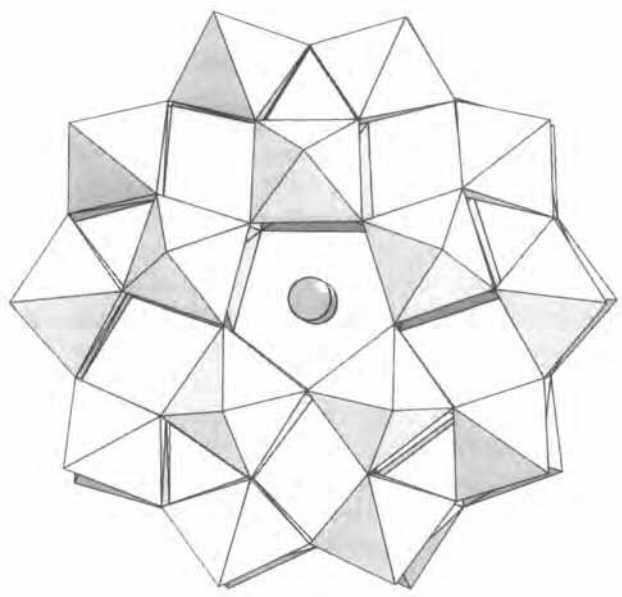

FIG. 25. Polyhedral view of $\{Na[P_5W_{30}O_{110}]\}^{14-}$.

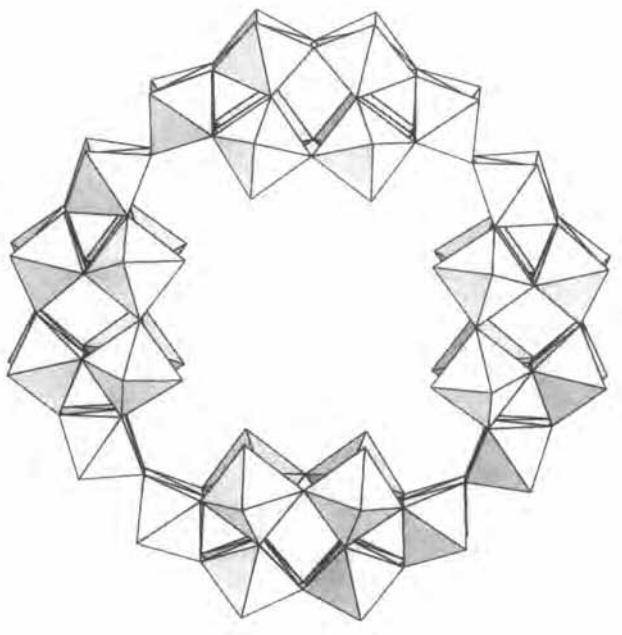

FIG. 26. Polyhedral representation of $[H_7P_8W_{48}O_{184}]^{33-}$.

ity surface and therefore has a key role in the stability of the $\{P_2W_{18}\}$ ring. The remaining cations (K^+ and Li^+) required to balance the charge are distributed in the lattice.

The molecular structure of $[NH_4Co_2As_4W_{40}O_{140}(H_2O)_2]^{23-}$, $\{Co_2As_4W_{40}\}$, represented in Fig. 27, consists of four AsW_9O_{33} subunits related through a pseudo (−4) axis (*104*) and linked through four extra additional WO_6 octahedra. Each AsW_9O_{33} fragment is a Keggin-type assemblage of three W_3O_{13} groups around the trigonal As(III). The lone pair is directed toward the outside of the AsW_9O_{33} group, referring the anion to the α-B type (*105,106*). Two AsW_9O_{33} units are linked to each extra tungsten atom by a corner-sharing process. The unshared oxygen atoms, and their symmetry-related positions, indicate a central cavity S1 occupied by an NH_4^+ cation, while two cobalt(II) ions are located in the S2 sites (see Fig. 27). In the S2 sites the two Co^{2+} can be replaced by four Ag^+ cations, although the two cations have quite different coordination geometry. Hervé and colleagues demonstrated the affinity of the central S1 site for alkali and rare earth and that of S2 for

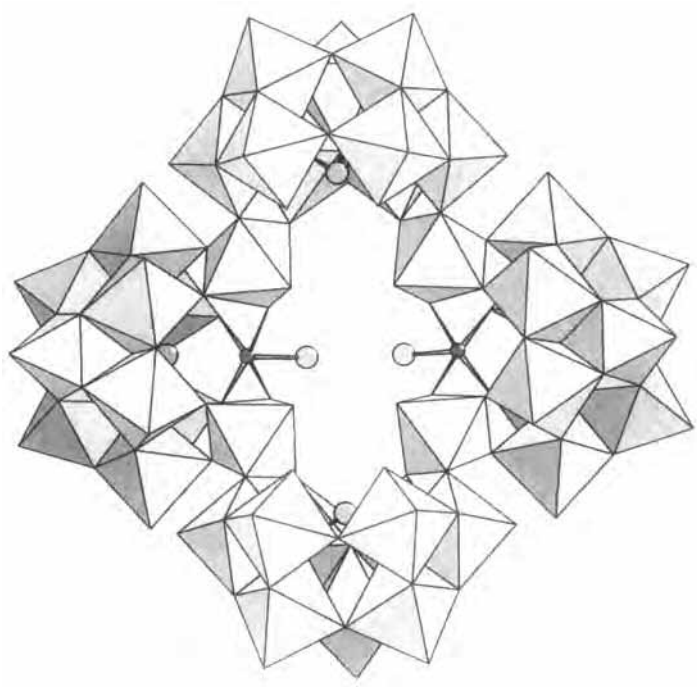

FIG. 27. Representation of the "As_4W_{40}" polyoxoanion.

transition metal ions (*107*). Recently, Pope *et al.* extended these experiments showing that the cyclic wheel is versatile enough to trap Ce^{3+} cations (*108*): $[Ce_4(H_2O)_{4-4x}(AsW_9O_{33})_4As(WO_3)_{2+x}(WO)_5]^{25-}$, $x < 0.5$, has a structure reminiscent of the previously described $\{Co_2As_4W_{40}\}$. In recent work, lanthanide cations have been systematically added to $\{As_4W_{40}\}$, resulting in the formation of the dimeric $\{[(H_2O)_{11}Ln(Ln_2OH)(B\text{-}\alpha\text{-}AsO_3W_9O_{30})_4(WO_2)_4]_2\}^{40-}$ (Ln = Ce, Nd, Sm, Gd), and discrete $[(H_2O)_{10}Ln(Ln_2OH)(B\text{-}\alpha\text{-}AsO_3W_9O_{30})_4(WO_2)_4]^{20-}$ (Ln = Ce, Sm, Gd). Other examples are given, illustrating the possibility for lanthanide cations to occupy S1 and/or S2 sites (*109*).

Thus, in the case of $[Ln_{16}As_{12}W_{148}O_{524}(H_2O)_{36}]^{76-}$ (Ln = La, Ce, Nd, Sm), the $As_{12}W_{148}$ unit is the largest discrete heteropolytungstate so far reported (*108*). The structure of the anion represented in Fig. 28 demonstrates that the limits of discrete, water-soluble polyoxometalate anions ($M = 40\ 000$) have probably not been reached and that various strategies of syntheses need to be developed to prepare chemical objects pertaining to the mesoscopic domain. The structure consists of an $AsW_{39}O_{33}$ group capped by two WO_6 octahedra and a CeO_8 square antiprism. This motif is 12 times repeated to generate the geometry of the

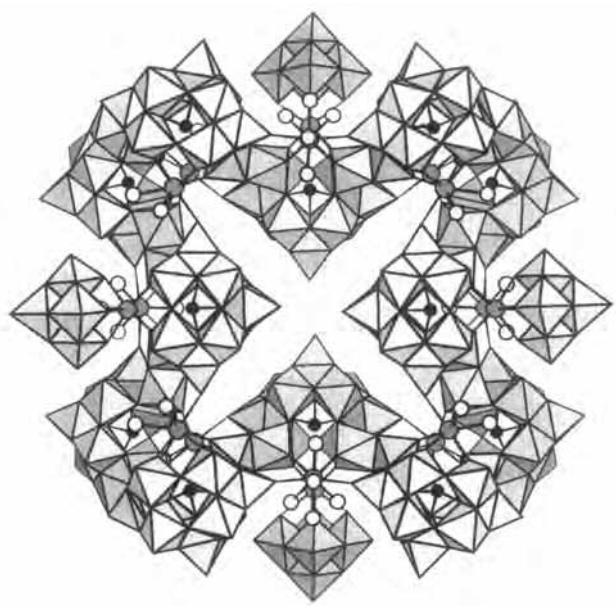

FIG. 28. Polyhedral representation of the giant $[Ln_{16}As_{12}W_{148}O_{524}(H_2O)_{36}]^{76-}$; Ln are lanthanides.

anion. The overall symmetry of the $As_{12}W_{148}$ ring is D_{2d}; the folding of the ring of linked AsW_9 groups means that there is no large central cavity, in contrast to the previously described cyclic polyoxometalates. The anion is stable in water, allowing ^{183}W NMR spectroscopy.

B. "Giant Wheels" and Derivatives

The reduction of acidified solutions of molybdates by various reducing agents leads to the well known molybdenum blue solutions (*110*). These solutions, and their derived amorphous solids, have been widely studied (*111*); however, the constitution of these compounds remained unclear until Müller and colleagues prepared and fully characterized $(NH_4)_{25\pm5}[Mo_{154}(NO)_{14}O_{420}(OH)_{28}(H_2O)_{70}].nH_2O$ (*112,113*), the so-called "big wheel". This beautiful chemistry has been largely developed by the Müller group, with some recent contributions from Chinese groups (*114–116*), and has been the subject of numerous publications and reviews (*117–119*). We have therefore chosen to limit our contribution to a summary of the topological features that allows an understanding of the shape of these sophisticated giant wheels (spheres are not considered here). Obviously these geometrical parameters have a chemical origin and result from factors such as the pH of the solution, reducing conditions, the presence of linking species (spacers), associated cations, and ionic strength (*120*).

1. *Description of the* {Mo_8}, {Mo_2} *and* {Mo} *Units*

The {Mo_8} group consists of a central MoO_7 or $Mo(NO)O_6$ in a bipyramidal arrangement with the five equatorial edges occupied by five MoO_6 octahedra. Two further MoO_6 octahedra occupy the axial positions to give the {Mo_8} unit. The {Mo_2} unit is made up of two edge-sharing $Mo(VI)O_6$ octahedra, and {Mo} is a single $Mo(VI)O_6$ octahedron.

The structures of $[Mo_{36}O_{112}(H_2O)_{16}]^{8-}$, $[Mo_{36}(NO)_4O_{108}(H_2O)_{16}]^{12-}$, $[Mo_{57}V_6O_{180}(NO)_6(H_2O)_{18}]^{21-}$, $[Mo_{57}Fe_6O_{164}(NO)_6(H_2O)_{30}]^{15-}$ (*121–125*) have been described recently (*117*) in terms of a combination of basic {Mo_8}, {Mo_2}, and {Mo} units. Two {Mo_8} units are connected to a {Mo} center to generate a {Mo_{17}} group which, self-assembled by two, gives the {Mo_{36}}-type clusters and, by three, gives the {Mo_{57}}-type cluster represented in Fig. 29. Three {Mo_8} groups are interlinked through three {Mo} octahedra and three V or Fe atoms. The dimensions of the cavity are 0.9×0.5 nm, perpendicular and parallel to the S_3 axis respectively. Three rather large openings are present in the crown, representing further coordination sites for electrophilic entering groups.

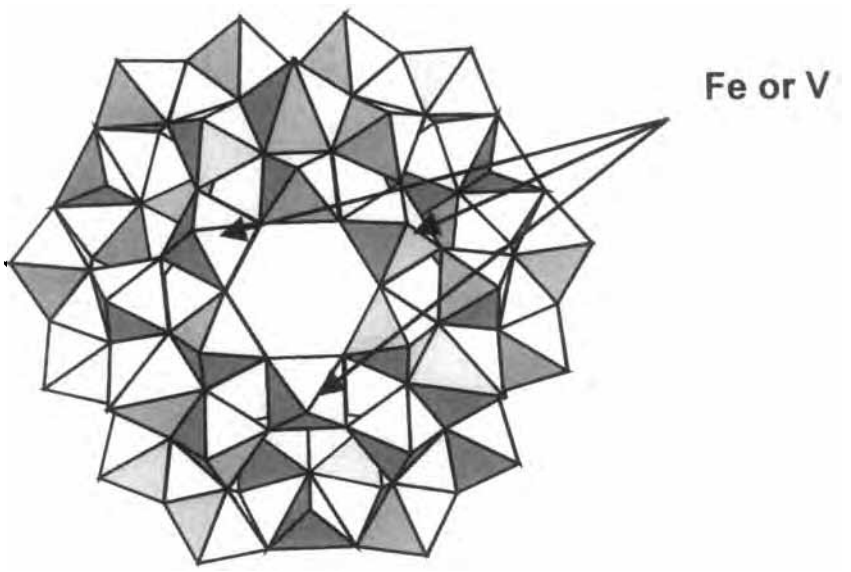

FIG. 29. $\{Mo_{57}\}$ wheel with central and side-located cavities.

2. The Big Wheels

The geometry of $[Mo_{154}O_{448}(NO)_{14}H_{14}(H_2O)_{70}]^{28-}$ (*112,113*), $\{Mo_{154}\}$, is represented in Fig. 30 and can be easily described in terms of $\{Mo_8\}$, $\{Mo_2\}$ and $\{Mo\}$ units in a combination of 14 of each. An alternative topological description has been published recently (*116*), based on the $\{Mo_{11}\}$ building unit obtained by connecting the central bipyramid to five MO_6 octahedra by edge sharing and to five other MO_6 octahedra by corner sharing, the $\{Mo_{11}\}$ thus obtained having C_5 symmetry. By changing the position of a MoO_6 octahedron in the former $\{Mo_{11}\}$ unit, another $\{Mo_{11}\}$ unit, is generated showing *C*s symmetry. The two possibilities are represented in Fig. 31. The $\{Mo_{11}\}$ unit of *C*s symmetry leads to a $\{Mo_{11}\}_n$ framework, $n = 14$ (Mo_{154}), $n = 16$ (Mo_{176}), while $\{Mo_{11}\}_n$ with C_5 symmetry leads to Kleperate type clusters ($n = 12$, $\{Mo_{132}\}$ sphere). The great interest of this novel description is that it allows preparation of either wheels or spheres if the chemist is able to find the chemical conditions which determine the symmetry of the $\{Mo_{11}\}$ unit. It is clear that the Müller group has managed to control this point in terms of the pH and initial reducing conditions (*119*).

The big wheel is structurally complete without any defect in the skeleton of the crown. The cavity measures about 20 Å in diameter,

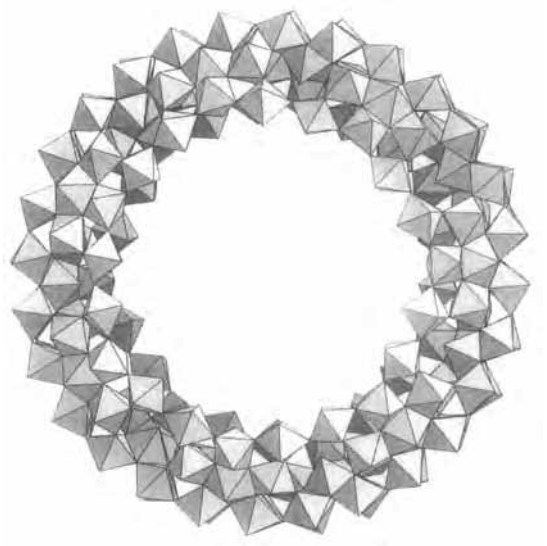

FIG. 30. $[Mo_{154}O_{448}(NO)_{14}(H_2O)_{70}]^{28-}$, the original "big wheel".

which places this molecule in the nanometer domain and led to the thought that new perspectives might exist for developing a host–guest chemistry in the cavity. As the Mo atoms of the fourteen $\{Mo_2\}$ units are reduced, the resulting excess of negative charge is partly balanced by a high degree of protonation. The cavity is lined by water molecules, which are also present at the surface of the crown. This large number of water molecules explains the high solubility of the wheel in water.

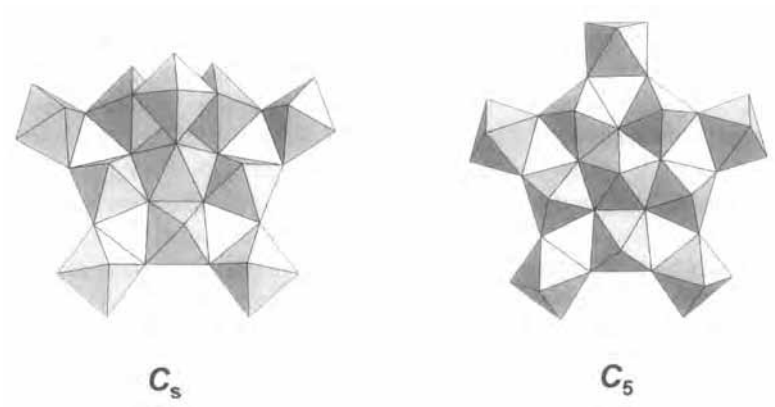

FIG. 31. Representations of the $\{Mo_{11}\}$ fragments.

Based on the same principle, $[Mo_{176}O_{528}(H_2O)_{80}]^{16-}$ (*126*) has a "saturated structure" and is made up of 16 $\{Mo_8\}$, 16 $\{Mo_2\}$, and 16 $\{Mo\}$ building units. Here the reduction of the $\{Mo_2\}$ units introduces 2×16 electrons into the cluster, where the charge is partly balanced by the protons in the ring. In the two wheels, the electrons are doubly located, (i) on the Mo(V) atoms through a metal–metal bond in the $\{Mo_2\}$ units, and (ii) in selected regions of the crown where the $\{Mo_2\}$ groups are situated.

The reactivity of these wheels is particularly interesting. They can be functionalized by ligand exchange (*127*) and also structurally modified by creating defects in the crown by abstraction of $\{Mo\}$ and $\{Mo_2\}$ units. In this case, the defects can be used as nucleophile regions to form chains or layer structures (*128–130*) in which wheels are covalently linked. For example, the replacement in $\{Mo_{154}\}$ of H_2O ligands located in the ring at the $\{Mo_2\}$ groups by terminal oxygen atoms of a $\{Mo_2\}$ group of another ring was successful. This reaction was made possible by increasing the nucleophile behavior of the $\{Mo_2\}$ unit by adding a donating ligand such as $H_2PO_4^-$ at appropriate neighboring sites. In another type of reaction, defects are also able to accommodate lanthanide cations (*131*).

V. Concluding Remarks

Although further structures may still be obtained in unexpected circumstances, efficient methods of synthesis have now been standardized, allowing the preparation of sophisticated "à la carte" wheels. Combination of hard σ-bonding systems with soft hydrogen-bonding interactions can lead to wheels containing more and more high-spin ground states to open the way to molecular magnets. In POM chemistry, the dimensions of the objects are still increasing and designs and tunings of cavities of predicted size and predicted reactivity are now possible. Applications of the resulting cryptate properties of these anions are being tested in the context of the separation process of nuclear waste in Europe and the United States. Replacement of oxo-atoms in polyoxoanions by sulfide groups was recently successful, thus modifying the electronic properties and the archetypal geometries to build a new family of polyoxothioanions.

Synthesis of the "big wheels", in addition to the intellectual satisfaction it produces, will serve in the future as a mini-reactor to perform hydrolysis reactions at the molecular level. Their colloidal solutions

could also serve to develop inorganic reactions in poly-phased medium. The wheel approach might also make it possible to obtain, at the molecular level, compounds with interesting bulk physical properties (magnets, electron reservoirs, catalysts).

References

1. Kurzak, B.; Farkas, E.; Glowiak, T.; Kozlowski, H. *J. Chem. Soc., Dalton Trans.* **1991**, 163.
2. Pecoraro, V. L.; Stemmler, A. J.; Gibney, B. R.; Bodwin, J. J.; Wang, H.; Kampf, J. W.; Barwin, A. *Prog. Inorg. Chem.* **1997**, *45*, 83.
3. Pecoraro, V. L.; Stemmler, A. J.; Gibney, B. R.; Bodwin, J. J.; Wang, H.; Kampf, J. W.; Barwinski, A. *Prog. Inorg. Chem.* **1997**, *45*, 83.
4. Antipin, M. Y.; Struchkov, Y. T.; Volkonvsky, A. Y.; Rokhlin, E. M. *Izv. Akad. Nauk. SSSR, Ser. Khim.* **1983**, 452.
5. Shur, V. B.; Tikhonova, I. A.; Dolgushin, F. M.; Yanovsky, A. I.; Struchkov, Y. T.; Volkonsky, A. Y.; Solodova, E. V.; Panov, S. Y.; Petrovskii, P. V.; Volpin, M. E. *J. Organomet. Chem.* **1993**, *443*, C19–C21.
6. Wark, T. A.; Stephan, D. W. *Organometallics* **1989**, *8*, 2836.
7. Schulbert, K.; Mattes, R. *Z. Naturforsch., Teil B* **1994**, *49*, 770.
8. Woodward, P.; Dahl, L. F.; Abel, E. W.; Crosse, B. C. *J. Am. Chem. Soc.* **1965**, *87*, 5251.
9. Miyamae, H.; Yamamura, T. *Acta Crystallogr., Sect. C* **1988**, *44*, 606.
10. Feld, H.; Leute, A.; Rading, D.; Benninghoven, A.; Henkel, G.; Kruger, T.; Krebs, B. *Z. Naturforsch., Teil B* **1992**, *47*, 929.
11. Gould, R. O.; Harding, M. M. *J. Chem. Soc. A* **1970**, 875.
12. Jin-Hua, C.; Bei-Sheng, K. *Chinese J. Struct. Chem.* **1993**, *12*, 397.
13. Mahmoudkhani, A. H.; Langer, V. *Polyhedron* **1999**, *18*, 3407.
14. Barrera, H.; Bayon, J. C.; Suades, J.; Germain, G.; Declerq, J. P. *Polyhedron* **1984**, *3*, 969.
15. Hoskins, B. F.; Pannan, C. D. *Inorg. Nucl. Chem. Lett.* **1974**, *10*, 229.
16. Sletten, J.; Kovacs, J. A. *Acta Chem. Scand.* **1994**, *48*, 929.
17. Kunchur, N. R. *Acta Crystallogr., Sect. B* **1968**, *24*, 1623.
18. Schneider, I.; Horner, M.; Olendzki, R. N.; Strahle, J. *Acta Crystallogr., Sect. C* **1993**, *49*, 2091.
19. Castro, R.; Garcia-Vazquez, J. A.; Romero, J.; Sousa, A.; Pritchard, R.; McAuliffe, C. A. *J. Chem. Soc., Dalton Trans.* **1994**, 1115.
20. Dance, I. G.; Scudder, M. L.; Secomb, R. *Inorg. Chem.* **1985**, *24*, 1201–1208.
21. Higgins III, J. D.; Suggs, J. W. *Inorg. Chim. Acta* **1988**, *145*, 247.
22. Ardizzoia, G. A.; Angaroni, M. A.; La Monica, G.; Cariati, F.; Moret, M.; Masciocchi, N. *Chem. Commun.* **1990**, 1021.
23. Ardizzoia, G. A.; Angaroni, M. A.; La Monica, G.; Cariati, F.; Cenini, S.; Moret, M.; Masciocchi, N. *Inorg. Chem.* **1991**, *30*, 4347.
24. Fenske, D.; Fischer, A. *Angew. Chem. Int. Ed. Engl.* **1995**, *34*, 307–309.
25. You, J.-F.; Snyder, B. S.; Papaefthymiou, G. C.; Holm, R. H. *J. Am. Chem. Soc.* **1990**, *112*, 1067–1076.
26. You, J.-F.; Papaefthymiou, G. C.; Holm, R. H. *J. Am. Chem. Soc.* **1992**, *114*, 2697–2710.

27. Caneschi, A.; Gatteschi, D.; Sessoli, R.; Barra, A. L.; Brunel, L. C.; Guillot, M. *J. Am. Chem. Soc.* **1991**, *113*, 5873.
28. Winpenny, R. E. P. *Comments Inorg. Chem.* **1999**, *20*, 233–262.
29. Abbati, G. L.; Cornia, A.; Fabretti, A. C.; Canesschi, A.; Gatteschi, D. *Inorg. Chem.* **1998**, *37*, 3759–3766.
30. Abbati, G. L.; Cornia, A.; Fabretti, A. C.; Canesschi, A.; Gatteschi, D. *Inorg. Chem.* **1998**, *37*, 1430–1431.
31. Bolcar, M. A.; Aubin, S. M. J.; Folting, K.; Hendrickson, D. N.; Christou, G. *Chem. Commun.* **1997**, 1485.
32. Gatteschi, D.; Caneschi, A., Sessoli, R.; Cornia, A. *Chem. Soc. Rev.* **1996**, 101.
33. Caneschi, A.; Cornia, A.; Lippard, S. J. *Angew. Chem. Int. Ed. Engl.* **1995**, *34*, 467–469.
34. Saalfrank, R. W.; Bernt, I.; Uller, E.; Hampel, F. *Angew. Chem.* **1997**, *109*, 2596; *Angew. Chem. Int. Ed. Engl.* **1997**, *36*, 2482.
35. Kemmit, T.; Al-Salim N. I.; Gainsford, G. J. *Eur. J. Inorg. Chem.* **1999**, 1847.
36. Santamaria, C.; Beckhaus, R.; Haase, D.; Saak, W.; Koch, R. *Chem. Eur. J.* **2001**, *7*, 622–625.
37. Schmid, R.; Beck, J.; Strahle, J. *Z. Naturforsch., Teil B* **1987**, *42*, 911.
38. Tesmer, M.; Müller, B.; Vahrenkamp, H. *Chem. Commun.* **1997**, 721.
39. Saalfrank, R. W.; Demleitner, B. "Transition Metals in Supramolecular Chemistry, Perspectives in Supramolecular Chemistry", vol. 5; J. P. Sauvage, Ed.; Wiley: New York, 1999, Chap. 1.
40. Kumagai, H.; Kitagawa, S. *Chem. Lett.* **1996**, 471-472.
41. Gerbeleu, N. V.; Struchkov, Y. T.; Timko, F. A.; Batsanov, A. S.; Indrichan, K. M.; Popovich, G. A. *Dokl. Akad. Nauk. SSSR.* **1990**, *313*, 1459.
42. Atkinson, I. M.; Benelli, C.; Murrie, M.; Parson, S.; Winpenny, R. E. P. *Chem. Commun.* **1999**, 285–286.
43. Taft, K. L.; Lippard, S. J. *J. Am. Chem. Soc.* **1990**, *112*, 9629–9630.
44. Taft, K. L.; Delfs, C. D.; Papaefthymiou, G. C.; Foner, S.; Gatteschi, D.; Lippard, S. J. *J. Am. Chem. Soc.* **1994**, *116*, 823–832.
45. Benelli, C.; Parsons, S.; Solan, G. A.; Winpenny, R. E. P. *Angew. Chem. Int. Ed. Engl.* **1996**, *35*, 1825–1828.
46. McInnes, E. J. L.; Anson, C.; Powell, A. K.; Thomson, A. J.; Poussereau, S.; Sessoli, R. *Chem. Commun.* **2001**, 89–90.
47. Blake, A. J.; Grant, C. M.; Parsons, S.; Rawson, J. M.; Winpenny, R. E. P. *J. Chem. Soc. Chem. Commun.* **1994**, 2363–2364.
48. Buhla, R.; Weatherburn, D. C. *Angew. Chem. Int. Ed. Engl.* **1991**, *30*, 688.
49. Watton, S. P.; Fuhrmann, P.; Pence, L. E.; Caneschi, A.; Cornia, A.; Abbati, G. L.; Lippard, S. J.; *Angew. Chem. Int. Ed. Engl.* **1997**, *36*, 2774–2777.
50. Dearden, A. L.; Parsons, S.; Winpenny, R. E. P. *Angew. Chem. Int. Ed. Engl.* **2001**, *40*, 151–154.
51. Aranzabe, A.; Wery, A. S. J.; Martin, S.; Guttierez-Zorrilla, J. M.; Luque, A.; Martinez-Ripoll, M.; Roman, P. *Inorg. Chim. Acta* **1997**, *255*, 35.
52. Lyxell, D.-G.; Strandberg, R.; Bostrom, D.; Petterson, L. *Acta Chem. Scand.* **1991**, *45*, 681.
53. Lu, J.; Xu, Y.; Goh, N. K.; Chia, L. S. *Chem. Commun.* **1998**, 2733.
54. Stalick, J. K.; Quicksall, C. O. *Inorg. Chem.* **1976**, *15*, 1577.
55. Chang, Y.-D.; Zubieta, J. *Inorg. Chim. Acta* **1996**, *245*, 177.
56. Lyxell, D.-G.; Strandberg, R. *Acta Crystallogr., Sect. C* **1988**, *44*, 1535.
57. Harrison, W. A. T.; Dussack, L. L.; Jacobson, A. J. *Acta Crystallogr., Sect. C* **1997**, *53*, 856.

58. Lowe, M. P.; Lockhart, J. C.; Clegg, W.; Fraser, K. A. *Angew. Chem., Int. Ed. Engl.* **1994**, *33*, 451.
59. Inoue, M.; Yamase, T. *Bull. Chem. Soc. Jpn.* **1996**, *69*, 2863.
60. Sethuraman, P. R.; Leparulo, M. A.; Pope, M. T.; Zonnevijlle, F. *J. Am. Chem. Soc.* **1981**, *103*, 7665–7666.
61. Gohlen, S.; Ouahab, L.; Grandjean, D.; Molinie, P. *Inorg. Chem.* **1998**, *37*, 1499.
62. Sergienko, V. S.; Molchanov, V. N.; Porai-Koshits, M. A.; Torchenkova, E. A. *Koord. Khim.* **1979**, *5*, 936.
63. He, Q.; Wang, E. *Inorg. Chim. Acta* **1999**, *295*, 244.
64. He, Q.; Wang, E. *Inorg. Chem. Commun.* **1999**, *2*, 399.
65. Allen, C. C.; Burns, R. C.; Lawrance, G. A.; Turner, P.; Hambley, T. W. *Acta Cryst.* **1997**, *C53*, 7.
66. Evans Jr, H. T. *Acta Cryst.* **1974**, *B30*, 2095–2100.
67. Lorenzo Luis, P. A.; Martin-Zarza, P.; Sanchez, A.; Ruiz-Perez, C.; Hernandez-Molina, M; Solans, X.; Gili, P. *Inorg. Chim. Acta* **1998**, *277*, 139.
68. Rosu, C.; Dickman, M. *Acta Cryst.* **1999**, *C55*, 11.
69. Lee, U.; Ichida, H.; Kobayashi, A.; Sasaki, Y. *Acta Cryst.* **1984**, *C40*, 5.
70. Kwak, W.; Rajkovic, L. M.; Stalick, J. K.; Pope, M. T.; Quicksall, C. O. *Inorg. Chem.* **1976**, *15*, 2778.
71. Hedman, B. *Acta Cryst.* **1980**, *B36*, 2241.
72. Liu, B.; Ku, Y.; Wang, M.; Zheng, P. *Inorg. Chem.* **1988**, *27*, 3868.
73. Ben-Yao, L.; Xin, W.; Gao-Yang, X.; Yie-Tong, K. *Chinese J. Struct. Chem.* **1990**, *9*, 211.
74. Hsieh, T.-C.; Shaikh, S. N.; Zubieta, J. *Inorg. Chem.* **1987**, *26*, 4072.
75. Matsumoto, K. Y. *Bull. Chem. Soc. Jpn* **1979**, *52*, 3284–3291.
76. Kortz, U.; Pope, M. T. *Inorg. Chem.* **1995**, *34*, 2160.
77. Kortz, U. *Inorg. Chem.* **2000**, *39*, 625.
78. Liu, B.; Xie, G.-Y.; Ku, Y.-T.; Wang, X. *Polyhedron* **1990**, *9*, 2023.
79. Matsumoto, K. Y. *Bull. Chem. Soc. Jpn.* **1978**, *51*, 492.
80. Chang, Y.-D.; Zubieta, J. *Inorg. Chim. Acta* **1996**, *245*, 177.
81. (a) Haushalter, R. C.; Lai, F. W. *Angew. Chem. Int. Ed. Engl.*, **1989**, *28*, 743; (b) Haushalter, R. C.; Lai, F. W. *Inorg. Chem.* **1989**, *28*, 2905; (c) Mundi, L. A.; Haushalter, R. C. *Inorg. Chem.*, **1992**, *31*, 3050; (d) Mundi, L. A.; Haushalter, R. C. *Inorg. Chem.* **1993**, *32*, 1579; (e) Lightfoot P.; Masson, D. *Acta Crystallogr.* **1996**, *C52*, 1077; (f) Xu, L.; Sun, Y.; Wang, E.; Shen, E.; Liu, Z.; Hu, C. *J. Solid State Chem.* **1999**, *146*, 533; (g) Xu, L.; Sun, Y.; Wang, E.; Shen, E.; Liu, Z.; Hu, C.; Xing, Y.; Lin, Y.; Jia, H. *New J. Chem.* **1999**, *23*, 1041; (h) Guesdon, A.; Borel, M. M.; Leclaire, A.; Raveau, B. *Chem. Eur. J.* **1997**, *3*, 1797; (i) Leclaire, A.; Guesdon, A.; Berrah, F.; Borel, M. M.; Raveau, B. *J. Solid State Chem.*, **1999**, *145*, 291.
82. Cadot, E.; Dolbecq, A.; Salignac, B.; Sécheresse, F. *Chem. Eur. J.* **1999**, *5*, 2396.
83. Dolbecq, A.; Cadot, E.; Eisner, D.; Sécheresse, F. *Inorg. Chim. Acta* **2000**, *300–302*, 151.
84. Cao, G.; Haushalter, R. C.; Strohmaier, K. G. *Inorg. Chem.* **1993**, *32*, 127.
85. Livage, C.; Dumas, E.; Marchal-Roch, C.; Hervé, G. *C. R. Acad. Sci., Ser. IIc* **2000**, *3*, 95.
86. Mak, T. C. W.; Li, P.-J.; Zheng, C.-M.; Huang, K.-Y. *J. Chem. Soc., Chem. Commun.* **1986**, 1597–1598.
87. Modec, B.; Brenčič, J. V.; Rotar, R.; Golič, L.; Prout, K. *Acta Cryst.* **1998**, *C54*, 1573–1575.
88. Modec, B.; Brenčič, J. V.; Golič, L. *Polyhedron* **2000**, *19*, 1219–1225.
89. Darensbourg, D. J.; Gray, R. L.; Delord, T. *Inorg. Chim. Acta* **1985**, *98*, L39–L42.
90. Chen, Q.; Liu, S.; Zubieta, J. *Angew. Chem. Int. Ed. Engl.* **1988**, *27*, 1724–1725.

91. Cadot, E.; Salignac, B.; Marrot, J.; Dolbecq, A.; Sécheresse, F. *Chem. Commun.* **2000**, 261.

92. Cadot, E.; Salignac, B.; Halut, S.; Sécheresse, F. *Angew. Chem., Int. Ed. Engl.* **1998**, *37*, 612.

93. Chen, Q.; Liu, S.; Zubieta, J. *Inorg. Chem.* **1989**, *28*, 4433–4434.

94. Dolbecq, A.; Cadot, E.; Sécheresse, F. *Chem. Commun.* **1998**, 2293.

95. Dolbecq, A.; du Peloux, C.; Auberty, A.-L.; Mason, S. A.; Barboux, P.; Marrot, J.; Cadot, E.; Sécheresse, F. *Chem. Eur. J.*, **2002**, *8*, 349–356.

96. Cadot, E.; Dolbecq, A.; Salignac, B.; Sécheresse, F. *J. Phys. Chem. Solids* **2001**, *62*, 1533,.

97. Cadot, E.; Salignac, B.; Loiseau, T.; Dolbecq, A.; Sécheresse, F. *Chem. Eur. J.* **1999**, *5*, 3390.

98. Dolbecq, A.; Cadot, E.; Sécheresse, F. *C. R. Acad. Sci. Paris, Série IIc*, **2000**, *3*, 193.

99. Salignac, B.; Riedel, S.; Dolbecq, A.; Sécheresse, F.; Cadot, E. *J. Am. Chem. Soc.* **2000**, *122*, 10381.

100. Cadot, E.; Marrot, J.; Sécheresse, F. *Angew. Chem. Int. Ed. Engl.* **2001**, *40*, 774.

101. Preyssler, C. *Bull. Soc. Chim. Fr.* **1970**, 30.

102. Alizadeh, M. H.; Harmalker, S. P.; Jeannin, Y.; Martin-Frère; J.; Pope, M. T. *J. Am. Chem. Soc.* **1985**, *107*, 2662–2669.

103. Contant, R.; Tézé, A. *Inorg. Chem.* **1985**, *24*, 4610–4614.

104. Robert, F.; Leyrie, M.; Hervé, G.; Tézé, A.; Jeannin, Y. *Inorg. Chem.* **1980**, *19*, 1746–1752.

105. Hervé, G.; Tézé, *A. Inorg. Chem.* **1977**, *16*, 2115.

106. Leyrie, M.; Hervé, G. *Nouv. J. Chim.* **1978**, *2*, *3*, 233.

107. Leyrie, M.; Thouvenot, R.; Tézé, A.; Hervé, G. *New J. Chem.* **1992**, *16*, 475–481.

108. Pope, M. T.; Wei, X.; Wassermann, K.; Dickman, M. H. *C. R. Acad. Sci. Paris, t1, Série IIc* **1998**, 297.

109. Wassermann, K.; Pope, M. T. *Inorg. Chem.* **2001**, *40*, 2763.

110. Berzelius, J. J. *Poggendorff's Ann. Phys. Chem.* **1825**, *6*, 385.

111. Müller, A.; Meyer, J.; Krickemeyer, E.; Diemann, E. *Angew. Chem. Int. Ed. Engl.* **1996**, *35*, 1206, and references therein.

112. Müller, A.; Krickemeyer, E.; Dillinger, S.; Bögge, H.; Plass, W.; Proust, A.; Dloczik, L.; Menke, J.; Rohfling, R. *Z. Anorg. Allg. Chem.* **1994**, *620*, 599.

113. Müller, A.; Plass, W.; Krickemeyer, E.; Dillinger, S; Bögge, H.; Armatage, A.; Proust, A.; Beugholt, C.; Bergmann, U. *Angew. Chem. Int. Ed. Engl.* **1994**, *33*, 849.

114. Jian, C. C.; Wei, Y. G.; Liu, Q.; Zhang, S. W.; Shao, M. C.; Tang, Y. Q. *J. Chem. Soc., Chem. Commun.* **1998**, 1937–1938.

115. Yang, W.; Lin, X.; Lu, C.; Zhuang, H.; Huang, J. *Inorg. Chem.* **2000**, *39*, 2706–2707.

116. Lu, C.; Lin, X.; Wang, S.; Zhuang, H. *Inorg. Chem. Commun.* **2001**, *4*, 245–247.

117. Müller, A.; Peters, F.; Pope, M. T.; Gateschi, D. *Chem. Rev.* **1998**, *98*, 239.

118. Pope, M. T.; Müller, A. (eds). "Polyoxometalates: From Platonic Solids to Anti-Retroviral Activity". Kluwer, Dordrecht, 1994.

119. Müller, A.; Kögerler, P.; Bögge, H. *Struct. Bond.* **2000**, *96*, 2203–2236.

120. Müller, A.; Serain, C. *Acc. Chem. Res.* **2000**, *33*, 2.

121. Krebs, B.; Paulat-Boschen, I. *Acta Crystallogr.* **1982**, *B38*, 1710.

122. Krebs, B.; Stiller, S.; Tytko, K. H.; Memke, J. *Eur. J. Solid State Chem.* **1991**, *28*, 883.

123. Tytko, K. H.; Glemser, O. *Adv. Inorg. Chem. Radiochem.* **1976**, *19*, 239.

124. Paulat-Boschen, I. *J. Chem. Soc., Chem. Commun.* **1979**, 780.

125. Pope, M. T. *Progr. Inorg. Chem.* **1991**, *39*, 181.

126. Müller, A.; Kögerler, P.; Kuhlmann, C. *Chem. Commun.* **1999**, 1347.

127. Müller, A.; Koop, M.; Schmidtmann, M.; Beugholt, C. *Chem. Commun.* **1998**, 1501.

128. Müller, A.; Krickemeyer, E.; Bögge, H.; Schmidtmann, C.; Beugholt, C.; Das, S. K.; Peters, F. *Chem. Eur. J.* **1999**, *5*, 2114.
129. Müller, A.; Krickemeyer, E.; Bögge, H.; Schmidtmann, C.; Peters, F.; Menke, C.; Meyer, J. *Angew. Chem., Int. Ed. Engl.* **1997**, *36*, 484.
130. Müller, A.; Das, S. E.; Bögge, H.; Beugholt, C.; Schmidtmann, C.; Peters, F. *Chem. Commun.* **1999**, 1035.
131. Müller, A.; Beugholt, C.; Bögge, H.; Schmidtmann, M. *Inorg. Chem.* **2000**, *39*, 3112.

REDOX CHEMISTRY AND FUNCTIONALITIES OF CONJUGATED FERROCENE SYSTEMS

HIROSHI NISHIHARA

Department of Chemistry, School of Science, The University of Tokyo, Hongo, Tokyo 113-0033, Japan

I. Introduction

The research field of transition metal organometallic chemistry was launched with the discovery of the compound ferrocene (**1**) just a half-century ago (*1–5*). Interest in ferrocene and the ferrocene family continues to increase, primarily because of the compound's inherent both organic and inorganic nature, including its high thermal stability, good solubility in organic media, versatility in the synthesis of derivatives using a reactivity similar to that of benzene, and its reversible redox ability, leading to easy electrochemical and chemical handling of the oxidation state due to its iron center (*6*). Because of these advantages, ferrocene has been employed as a molecular sensor (*7*), an electrochemical agent (*8,9*), a molecular ferromagnet (*10*), etc. Recently, the development of molecular-based devices has become a realistically attractive

0898-8838/02 $35.00

target of research (*11*). Ferrocene and its family are strong candidates for inclusion as components of molecular-based devices because of the merits noted above. In order to utilize the ferrocene family, it is important to understand how their electronic function can be regulated when combined with other molecular parts. In this sense, determining how to control the electronic conjugation of ferrocene moieties with each other or with other functional molecular moieties is essential for the design and construction of intelligent molecular systems.

The electronic structure of ferrocene includes the three metal-based, highest-filled levels derived from the d_{z2} orbital (a_{1g}) and the d_{xy}, d_{x2-y2} orbitals, which are degenerated to give e_{2g} in staggered D_{5d} geometry (Fig. 1) (*12*). The $1e^-$-oxidized form, the ferrocenium ion, has a similar electronic structure except for the energy levels of e_{2g} and a_{1g} being reversed, which leads to the singly occupied molecular orbital (SOMO) of the ferrocenium ion being e_{2g}. The e_{2g} orbitals have some character of δ-back-bonding through interaction with a combination of the cyclopentadienyl (Cp) anion lowest unoccupied molecular orbital (LUMOs), and the a_{1g} orbital involves some interaction of d_{z2} with the metal s orbital and with the Cp rings. The next highest orbitals, e_{1u}, of ferrocene are primarily ligand based, with some contribution from the metal p_x and p_y orbi-

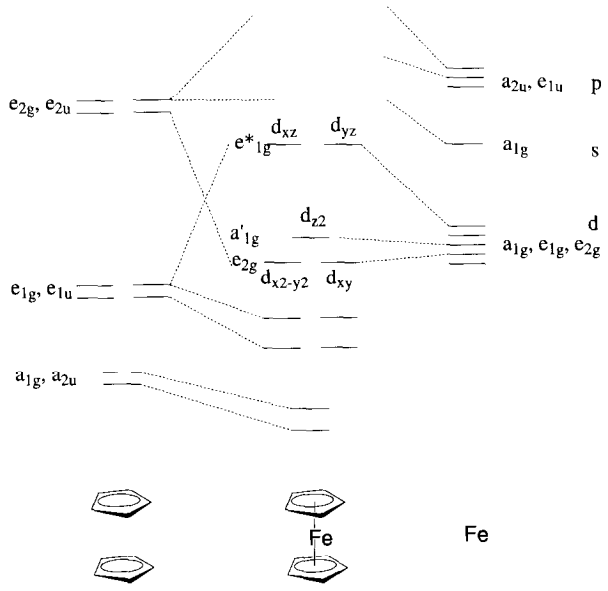

FIG. 1. Electronic structure of ferrocene (1).

tals. In contrast, the LUMO of ferrocene is derived from an out-of-phase π interaction between the d_{xz}/d_{yz} and Cp orbitals and has e_{1g} symmetry. Bonding of the electron-donating moieties to the Cp rings raises the energies of both the filled *d*-orbitals and the highest ligand-based orbitals, and the electron-withdrawing group does the opposite. However, due to the presence of the Cp rings, when a conjugated system is attached to ferrocene the most significant perturbation is not of the metal-based highest occupied molecular orbitals (HOMOs) but of the orbitals just below them. Actually, in a ferrocene derivative with a moderate electron-withdrawing conjugated substituent, the first ionization potential and electrochemical oxidation potential are similar to those of ferrocene (*13–15*).

Among the numerous known ferrocene derivatives, ferrocene oligomers in which the ferrocene units interact with each other electronically are part of a novel group exhibiting a formation of mixed-valence states where Fe(II) (ferrocene) and Fe(III) (ferrocenium ion) coexist within a molecule (*16–18*). In general, the study of intramolecular internuclear electron transfer in the mixed-valence complexes has provided insight into the factors that affect the rates of electron transfer in solution redox processes, solid-state materials, and biological electron-transport chains. The mechanism and kinetics of electron transfer reactions are generally considered in terms of the Marcus–Hush theory (*19*). Electrochemical and optical properties are the most convenient experimental means of measuring the magnitude of internuclear electronic interactions in the mixed-valence complexes in solution. Various other techniques such as Mössbauer, IR, Raman, NMR, and ESR as well as photoelectron spectroscopy and X-ray crystallography have been employed to measure the electron-exchange rate with different time windows from 10^{-5} to 10^{-13} s in the mixed-valence complexes, not only in solution but in the solid state.

In most cases of ferrocene dimers, the internuclear interaction is supported by conjugation through the Cp rings, as expected from the electronic structure of the ferrocene noted above. Biferrocene, **2**, is the most representative conjugated ferrocene dimer, and its monocationic form has been an unremitting target molecule for the study of mixed valency both in solution and in the solid state. In contrast, studies on oligoferrocenylenes higher than terferrocene, **3–5**, have been rather limited, probably because of growing difficulties in synthesis and handling due to a loss of solubility with increase in the number of ferrocene units. A variety of other ferrocene dimers and higher oligomers with conjugated spacer groups have also been synthesized. Their physical properties indicate that the chemical structure of the conjugated spacer group and its length dramatically affect the electronic interaction

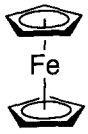

1

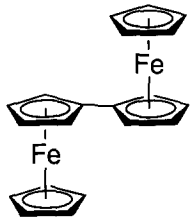

2

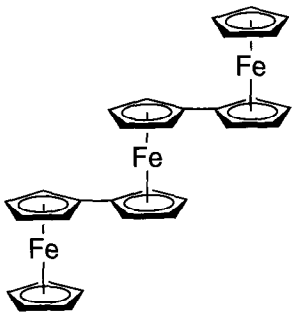

3

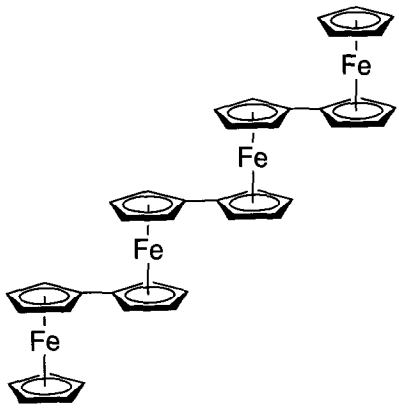

4

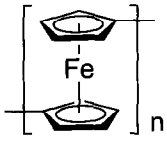

5

between the ferrocene moieties. Introduction of the proper bridging ligand between ferrocene moieties and modification of the Cp rings have brought about functionalities conferring unique physical and chemical properties.

Another category of the conjugated ferrocene system is constructed by a combination with electron-accepting molecular units. As the ferrocene moiety works as a good donor, these donor–acceptor conjugated compounds attract attention due to their fluctuating electronic structures, which are sensitive to outer fields, and exhibit novel behavior such as second-order non-linear optical (NLO) properties (*20*) and facile intramolecular electron transfer, causing drastic change in structure and physical properties.

In this chapter, an overview is given of recent reports concerning conjugated ferrocene systems in the following three categories: (1) oligo- and poly-ferrocenylenes, (2) ferrocene oligomers and polymers with conjugated spacers, and (3) ferrocene-acceptor conjugated compounds. Several reviews related to the above subjects and theoretical studies of mixed-valence complexes have been available (*21–28*); as a result, the redox properties and functionalities of the conjugated ferrocene systems are a primary focus in this chapter. In particular, analysis of the intramolecular electronic interaction based on the neighboring-site interaction model, isomerization behavior of azoferrocene, and proton-coupled intramolecular electron transfer in ferrocene–quinone complexes are described in each category.

II. Oligo- and Poly-Ferrocenylenes

A. Biferrocene Overview

Biferrocene, **2**, is the simplest conjugated ferrocene dimer formed by connecting two ferrocene moieties directly at the Cp rings (the fusion of two Cp rings forms the dianionic fulvalene ligand). The mixed-valence state formation of biferrocene by $1e^-$ oxidation attracted a great deal of interest in the 1970s (*29*), exhibiting various characteristic chemical and physical phenomena such as two-step one-electron oxidation of biferrocene corresponding to Fe(III)Fe(II)/Fe(II)Fe(II) and Fe(III)Fe(III)/Fe(III)Fe(II) couples and absorption in the near-IR region due to intervalence transfer (IT) (or metal-to-metal charge transfer (MMCT)). Analysis of the IT band has confirmed that the monocation belongs to Robin and Day class II mixed-valence complexes with med-

ium delocalization and a double potential minimum in the ground state (*30*). The energy of the IT band maximum (5000 cm^{-1}) and the strong electronic coupling between the two mixed-valence states, which respectively provide the small barrier (ca. 15 kJ mol^{-1}) and the relatively large transparence coefficient $\kappa = 1$ (*31,32*), suggest a large rate constant for intramolecular electron transfer between the Fe(II) and Fe(III) forms with $k_{et} > 10^{11}$ s^{-1} in solution. Quantitative measurement of the absolute k_{et} values in solution has been carried out using NMR spin-lattice relaxation by Masuda *et al.* (*33*). The k_{et} value of biferrocenium(1+) lies in the range of $(0.84–1.77) \times 10^{12}$ s^{-1} at 298 K, depending on the solvent.

Valence trapping and detrapping in the solid state has been an intriguing target of research for the monocationic form of biferrocene and its derivatives, **6–12** (*29,32,34–53*). Variable temperature ^{57}Fe Mössbauer spectroscopy, in which quadrupole splitting is large for ferrocene and small for ferrocenium, has been efficiently employed in analyzing valence detrapping, showing the coalescence of peaks, and in estimating an electron transfer rate on the order of 10^{-7} s in the solid state. IR spectra of the ring–metal stretch at 400–500 cm^{-1} and the C–H bending vibration at 800–900 cm^{-1} have provided information around a time scale of 10^{-11} s. EPR spectra and X-ray crystal structures have also been used to observe phase transitions by valence trapping. Some of the most thoroughly studied mixed-valence compounds are triiodide salts of biferrocenium(1+) derivatives with various substituents on Cp rings (**7–12**). It has been found that the environment surrounding a cation is the most important factor in determining the rate of intramolecular electron transfer. Recent studies of Dong *et al.* on biferrocenium salts, involving changes in the number and type of substituents, have shown that the cation–anion van der Waals interactions, the ring tilt between two Cp rings induced by the bulkiness of ligands, and the difference in crystal structures have marked effects on k_{et} (*34*). Nakashima *et al.* have discussed separately the effects of cation symmetry and packing, using racemic and chiral biferrocenium derivatives (*36*).

Electron transfer in the mixed-valence biferrocenium cation has been interpreted using PKS theory by Boukheddaden *et al.* (*54*). The HOMO of biferrocene is not easily estimated because the HOMO of ferrocene is a_{1g} and that of ferrocenium is e_{2g}, and biferrocenium is the mixture of both components (Fig. 2). The molecular-orbital calculation indicates that the d_{z2} HOMO should result in a dramatic increase in the quadrupole splitting of the ^{57}Fe Mössbauer spectra; thus far, however, no examples of a biferrocenium salt with quadrupole splitting larger than that of ferrocene in either the trapped or the detrapped state have been

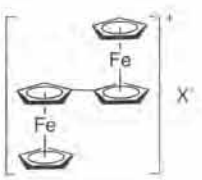

X⁻ = picrate, I_3^-

6

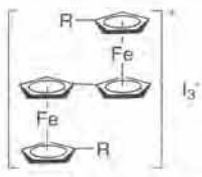

R = Cl, Br, I, Me, Et, Pr^n, Bu^n, n-C_9H_{19}, n-$C_{10}H_{21}CH_2Ph$, $CH_2CH_2CHPh_2$

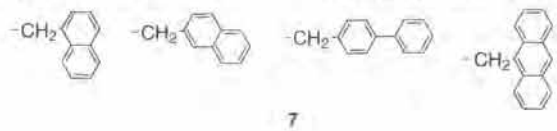

7

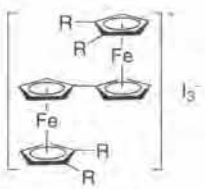

R = Et, Pr^n, CH_2Ph

8

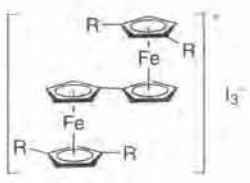

R = Et, Pr^n, CH_2Ph

9

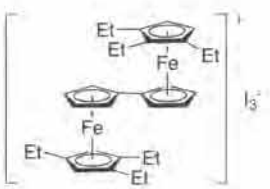

10

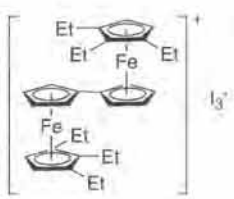

11

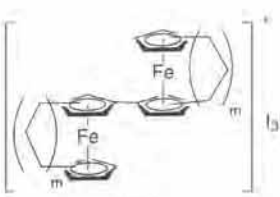

m = 1, 2

12

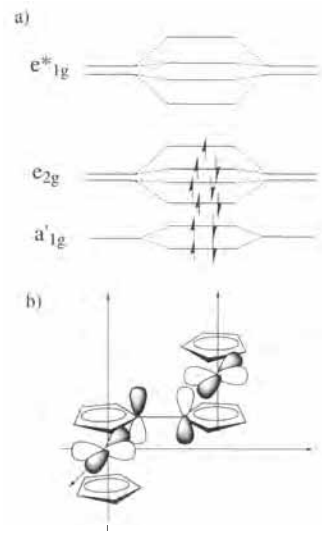

FIG. 2. Electronic structure of biferrocene (**2**): (a) energy diagram; (b) illustration of large electronic interaction between d_{x2-y2} orbitals (e_{2g}) of ferrocene units through p_z orbitals of Cp rings (*54*).

found. This rules out the possibility of a d_{z2}-based HOMO and indicates that d_{xy} and $d_{x2\text{-}y2}$ should generate the HOMO of biferrocenium(1+). The electronic interaction for d_{xy} is larger than for $d_{x2\text{-}y2}$, and the PKS model for intramolecular properties, considering both limiting cases, has been found to be fully consistent with available experimental data, the distortion parameter of the crystal structure, the transfer integral obtained from the IT band analysis, a specific heat Schottky anomaly (*55*), and the faster electron exchange compared with the Mössbauer time scale.

B. OLIGO- AND POLY-(1,1′-FERROCENYLENE) OVERVIEW

Synthesis of unsubstituted oligo- and poly-(1,1′-ferrocenylene) (**2–5**) has been carried out by various methods based on the established coupling reactions of benzene derivatives (*56*). The highest molecular weight of poly(1,1′-ferrocenylene) among those reported has reached 4–6 kDa (*57–59*). The limitation regarding molecular weight is primarily caused by a rapid decrease in solubility with increase in the degree of polymerization. Because of this low solubility of higher-order oligomers, study of their physical properties has been limited. Introduction of hexyl

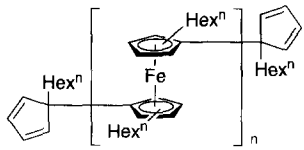

13_1 -13_7: n = 1 - 7

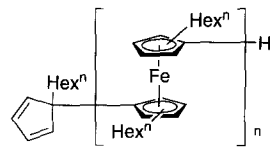

14_1 -14_5: n = 1 - 5

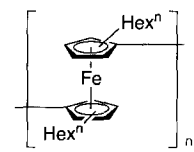

15

groups to the Cp ring gives oligomers and polymers, **13–15,** with good solubility in regular organic solvents (*60*).

The color of oligo- and poly-(1,1′-ferrocenylene) and their derivatives depends on the molecular weight, changing from orange to dark brown with increasing molecular mass (*56,60*). The polymer is air-stable, thermostable (m.p. $> 350°C$ when $M_n \geq 4700$ (*61*)), and insulating ($\sigma = 10^{-12}$ (*56*), $0.4–8 \times 10^{-10}$ S cm^{-1} (*57*) in the neutral state. An interesting question regarding the electronic structure of this polymer relates to how the *d*-electron delocalization occurs along the polymer chain. Experimental results concerning this question have been obtained by both UV–Vis and Mössbauer spectroscopy. Both the absorption maxima, λ_{max} and molar absorption coefficients ϵ of oligoferrocenylenes increase with the number of units n when $n < 4$, but remain almost constant when $n \geq 4$ (*60,62,63*), denoting the lack of significant electronic delocalization along the polymer chain. This increase is also supported by the Mössbauer spectroscopic parameters of ferrocene, biferrocene, and polyferrocenylene being relatively consistent, implying little or no *d*-electron interaction between adjacent ferrocene units (*56*).

Physical properties of **5** in the chemically oxidized (doped) form have been reported by several groups. The intervalence-transfer (IT) band of **5** oxidized with p-benzoquinone/HBr under argon appears at 1800–1850 nm, irrespective of the molecular weight and oxidation degree (*56*). These values are similar to those for the mixed valence states of oligoferrocenylenes, **2–4**, 1670–1990 nm (see below) (*56,64*). The electrical conductivity of **5** is increased dramatically by partial oxidation (*65,66*), affording at most 1×10^{-4} and 4×10^{-2} S cm^{-1} for I_2 and TCNQ doped forms, respectively, for polymer samples with $M_n = 5 \times 10^3$ (*57*). This result convincingly demonstrates that the through-bond electronic interaction in the mixed-valence state provides a better path for intrachain electronic conduction, resulting in higher bulk conductivity than would be found in a system composed simply of non-interacting ferrocene and ferrocenium units such as poly(vinylferrocene). However, the conductivity of poly(1,1′-ferrocenylene) is lower than that of π-conjugated organic conducting polymers such as polyacetylene, polypyr-

role, polythiophene, and polyaniline in the doped state, because the charge is very localized at the metal sites in the conjugated ferrocene polymers in which the ferrocene units are involved in the main chain. This finding is supported by the results of the crystal orbital calculation, as described below.

Although poly(ferrocenylene) in the partially oxidized valence state has an intrinsic semiconducting nature, as noted above, photoconductivity has been found for the complexes of oligo(1,1′-dihexylferrocenylene)s, **13_2**–**13_6**, and poly(dihexylferrocenylene) (**15**) with tetracyanoethylene (TCNE) (*60,67*). The complexes exhibit both charge-transfer (CT) and intervalence-transfer (IT) bands in the near-IR region. Mössbauer spectra of **13_3**-TCNE and **13_4**-TCNE at low temperatures (50–293 K) both give peaks due to Fe(III) of ferrocenium and Fe(II) of ferrocene, indicating that the charge is localized on the time scale of Mössbauer spectroscopy (10^{-7}s). The ratio of Fe(III) to total Fe estimated from the peak area and intensity of the spectra depends on the temperature, and is almost coincident with that theoretically determined from the formal potentials of **13_3**, **13_4**, and TCNE, and from the Nernst equation. Photoirradiation of the **15**-TCNE CT complex with near-IR light gives greater electronic conductivity than does irradiation with visible light. A positive dependence is observed between the near-IR photoconductivity and the number of ferrocene units in oligo- and poly-(dihexylferrocenylene)s. These results indicate that both IT and CT band excitation cause photoconductivity; more specifically, the CT band excitation alters the charge distribution on the poly(ferrocenylene) chain, and IT band excitation accelerates the intra-chain charge-transport rate.

A semiempirical crystal orbital calculation of **5** using the INDO method was carried out by Böhm (*68*). It is predicted that the highest filled band of polyferrocenylene is a ligand π-band and that Fe 3*d* bands are at lower energies. The calculated bandwidths for antisymmetric bands are narrow (< 0.6 eV) and those of symmetric bands broaden up to 2.6 eV as a result of the stronger intercell coupling. By avoiding crossing regions in the reciprocal k space region, a strong metal–ligand intermixing in some of the outer valence bands is observed. The conduction band is a ligand π-band with a narrow bandwidth, 0.04 eV, and the band gap is estimated to be 7.55 eV. These results are in agreement with experimental results showing that **5** in the neutral form is an insulator and that its electronic spectrum is somewhat dependent on the molecular mass (see above). It has also been shown that the hole states in the partially oxidized form of **5** are probably unstable against the formation of a state with trapped valencies, sug-

gesting that the conduction process of the partially oxidized polyferrocenylene derivative must be described as a hopping event between two iron sites in different oxidation states.

The electrochemistry of oligo- and poly-(ferrocenylene) is an intriguing subject of research because this system is an ideal model for demonstrating how the sequence of the redox site interaction dominates the redox properties of the whole system. Electrochemical properties have been reported on oligoferrocenylenes with $n \leq 4$ by Brown *et al.* (*64*). The oligomers give the same number of $1e^-$ oxidation waves as the ferrocene units, forming mixed-valence complexes before reaching the fully oxidized form with all Fe(III). In the mixed valence states of the oligomers with $n > 2$, there is more than one possibility for positioning the ferrocenium unit(s) in the chain, possibly resulting in oxidation-state isomerism. For example, two isomers, Fc^+–Fc'–Fc^+ and Fc^+–Fc'^+–Fc, where Fc and Fc′ are 1-ferrocenyl and 1,1′-ferrocenylene, respectively, exist as the dicationic form of terferrocenylene, and it has been estimated that the former is thermodynamically more stable by 11.5 kJ mol^{-1} on the basis of a method using a potential shift parameter of substituent effect. The negative shift of the first oxidation potential with increase in the number of ferrocene units has been explained as a result of the electron-withdrawing effects of the ferrocenyl group. Recently, Dong *et al.* (*69*) have prepared disubstituted terferrocenes (**16**) and tetraferrocenes (**17**) and have analyzed their redox properties by a method similar to that of Brown *et al.* ^{57}Fe-Mössbauer spectra of their mixed-valence cation indicates the presence of valence-trapping on a time scale of 10^{-7}s.

There is one report of the redox properties of poly(ferrocenylene) by Oyama *et al.* noting that the cyclic voltammetry of low molecular weight poly(ferrocenylene) ($M_w \simeq 900$) dissolved in CH_2Cl_2 or electrodeposited on Pt gives a broad redox wave with two (or three) peaks between 0.2 and 0.8 V *vs.* SSCE (*70*).

Contrary to the continuous advances in the study of poly(1,1′-ferrocenylene), investigation of other related polymetallocenylenes has been retarded. Oligo(1,2-ferrocenylene)s (**18**, $n = 3$–5) have been synthesized by the Ullmann coupling of iodoferrocene and 1,2-diiodoferrocene (*71,72*). A lesser amount of coplanarity between directly joined rings is inferred from NMR data for the sterically crowded 1,2-terferrocenylene. Mass spectra of 1,2-terferrocenylene and one of the 1,2-pentaferrocenylenes have suggested a highly probable elimination of two hydrogen atoms and a subsequent cyclization. Electrochemistry and physical data on the oxidized forms of the oligo(1,2-ferrocenylene)s have not yet been obtained.

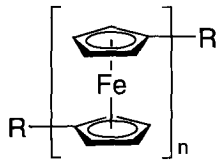

R = Et, Bu^n, CH_2OCH_3

16: n = 3
17: n = 4

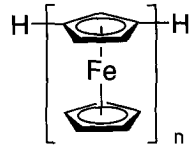

18

C. Neighboring-Site Interaction Model and Redox Properties of Oligo(ferrocenylene)

In general, thermodynamic stability of a mixed-valence dinuclear complex, which is denoted as a combination of reduced (Red) and oxidized (Ox) sites, Red–Ox, is exhibited as a difference in redox potentials $\Delta E^0 = E^0(\text{Ox–Ox/Red–Ox}) - E^0(\text{Red–Ox/Red–Red})$. This difference is related to the comproportionation constant, K_c, defined in Eq. (1):

$$K_c = \exp(\Delta E^0 F/RT) \tag{1}$$

The free energy of comproportionation, ΔG_c, involves several factors, as given in Eq. (2) by Sutton *et al.*:

$$\Delta G_c = \Delta G_s + \Delta G_e + \Delta G_i + \Delta G_r \tag{2}$$

where ΔG_s reflects the statistical distribution of the comproportionation equilibrium, ΔG_e accounts for the electrostatic repulsion of the two like-charged metal nuclei, ΔG_i is an inductive factor dealing with competitive coordination of the bridging ligand by the metal nuclei, and ΔG_r is the free energy of resonance exchange—the only component of ΔG_c that represents actual metal–metal coupling (*73*). A recent paper of Crutchley *et al.* noting the involvement of an extra parameter, ΔG_{ex}, which concerns the stabilization of one of the reactants in ΔG_c, has been presented by Sutin as a private communication (*74*). This approach has been employed for various mixed-valence complexes, but the analysis has been restricted to mostly dinuclear species.

An approach that provides a general theoretical insight into the redox properties of a linearly combined multi-redox system has been presented by Aoki and Chen (*75*). The theory is constructed on the basis of interaction energies between neighboring redox sites, u_{OR},

u_{OO}, and u_{RR}, where OR, OO, and RR denote combinations of Ox and Red, Ox and Ox, and Red and Red, respectively. Each interaction energy involves all the parameters given in Eq. (2), but we can assume that u_{OR} and u_{OO} consist primarily of resonance exchange energy (ΔG_r) and electrostatic repulsion energy (ΔG_e), respectively, when the internuclear electronic interaction is strong and the oxidized site is positively charged such as in conjugated ferrocene oligomers. More specifically, u_{OR} is negative, u_{OO} is positive, and u_{RR} is less important than the others. An interesting forecast of the theory is that a system with an odd number of redox nuclei, $n = 2m + 1$ ($m \geq 1$), gives three redox waves with m, 1, and m electrons, and a system with an even number of redox nuclei, $n = 2m + 2$ ($m \geq 1$), gives four redox waves with m, 1, 1, and m electrons. Consequently, it is predicted that the number of waves converges to two when m approaches infinity.

The first experimental recognition of the dependence on the number of redox nuclei in the linearly combined multi-redox system was obtained as a result of using oligo(dihexylferrocenylene)s up to a heptamer, $\mathbf{13_1}$–$\mathbf{13_7}$ and $\mathbf{14_1}$–$\mathbf{14_5}$ (*60,76*). Their redox behavior has been subjected to study based on the neighboring-site interaction model (*76,77*). The experimentally obtained redox potentials of the oligo(dihexylferrocenylene)s **13** and **14** are given in Fig. 3, where all the oligomers clearly exhibit one-electron oxidation processes. Simulation of the redox potentials of the oligoferrocenylenes by the theory based on the interaction between neighboring centers noted above has indicated that the redox-potential dependency of the oligomers up to the tetramer on the number of redox nuclei (i.e., ferrocene units) can be explained, but the separation of redox potentials for each one-electron oxidation step for pentamers, a hexamer, and a heptamer cannot be interpreted (see Fig. 3). The separation is reasonably interpreted by the introduction of an additional parameter, u_{OXR}, denoting the donor–acceptor interaction over three redox centers (Table I, Fig. 3). The simulation indicates that $u_1 = (u_{OO} + u_{RR})/2 - u_{OR} = 15\,\text{kJ mol}^{-1}$, $u_2 = (u_{OO} - u_{RR})/2 = 4.5\,\text{kJ mol}^{-1}$, and $u_{OXR} = -3.8\,\text{kJ mol}^{-1}$. Assuming $u_{RR} = 0$ because there is no electrostatic interaction or electron delocalization between Red and Red, it can be deduced that $u_{OO} = 9\,\text{kJ mol}^{-1}$ and $u_{OR} = -10.5\,\text{kJ mol}^{-1}$. With the magnitude of u_{OXR} only one-third that of u_{OR}, these results suggest that the positive charge in the molecule is primarily localized around the "Ox" sites. It should be noted that the free-energy difference between the isomers Ox–Red–Ox and Ox–Ox–Red is $u_{OO} - u_{OR} + u_{OXR} = 15.7\,\text{kJ mol}^{-1}$, larger than $11.5\,\text{kJ mol}^{-1}$ value reported previously that was estimated by a method using a substituent effect, as noted above (*64*).

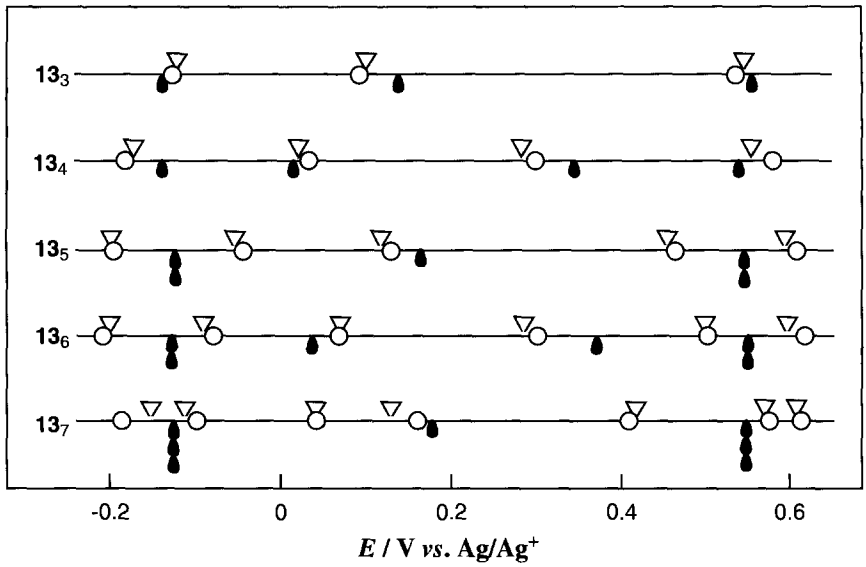

FIG. 3. Formal potentials of oligo(dihexylferrocenylene)s **13** (○) (*60,76*), those calculated from the first neighboring site interaction (▲) with $u_1 = 15\,\mathrm{kJ\,mol^{-1}}$ and $u_2 = 4.5\,\mathrm{kJ\,mol^{-1}}$, and those calculated from both first and second neighboring-site interaction (▽) with $u_1 = 15\,\mathrm{kJ\,mol^{-1}}$, $u_2 = 4.5\,\mathrm{kJ\,mol^{-1}}$, and $u_{\mathrm{OXR}} = -3.8\,\mathrm{kJ\,mol^{-1}}$ (*77*).

An attempt to determine the electronic structure of the favorable electronic isomers in the mixed-valence states of oligoferrocenylene, as noted above, has been made using IR spectroscopy of the ferrocene, biferrocene, and terferrocene derivatives $\mathbf{19_1}$–$\mathbf{19_3}$ involving an iron tricarbonyl moiety (*78*). In this structure, the infrared absorption of CO can sense the oxidation state of the terminal ferrocenyl group attached to the (η^4-cyclopentadiene)$Fe(CO)_3$ moiety, as the CO stretching vibration of metal carbonyls responds to even slight changes in the electronic state of the metal centers (*79–81*). In $\mathbf{19_1}$–$\mathbf{19_3}$, all oxidation of the ferrocene units occurs at potentials more negative than that of the iron carbonyl unit, so that changes in the electronic structures of ferrocene units are observed without oxidative decomposition of the iron carbonyl unit.

The infrared spectra of $\mathbf{19_1}$–$\mathbf{19_3}$ show two ν(CO) absorption peaks typical of (η^4-diene)$Fe(CO)_3$ complexes; one is strong and sharp at ca. $2040\,\mathrm{cm^{-1}}$ (A′(1)), and the other is medium and broad at ca. $1965\,\mathrm{cm^{-1}}$ (A′(2) and A″). Table II gives the wavenumbers of the ν(CO) peaks of $\mathbf{19_1}$–$\mathbf{19_3}$ in each oxidation state generated electrochemically with $\Delta\nu_{\mathrm{CO}}$,

TABLE I

REDOX POTENTIALS $E_{N,i}$ OF A LINEARLY COMBINED MULTI-REDOX SYSTEM BASED ON THE NEIGHBORING-SITE INTERACTION MODEL

Species	μ^0	$E_{Ni} - (\mu_O^0 - \mu_R^0)$	$(E_{Ni} - E_{Ni-1})e$
(dimer)			
RR	$2\mu_R^0 + u_{RR}$	$-u_{RR} + u_{OR}$	
RO	$\mu_R^0 + \mu_O^0 + u_{OR}$	$u_{OO} - u_{OR}$	$2u_1$ [a]
OO	$2\mu_O^0 + u_{OO}$		
(trimer)			
RRR	$3\mu_R^0 + 2u_{RR}$	$-2u_{RR} + 2u_{OR}$	
ROR	$2\mu_R^0 + \mu_O^0 + 2u_{OR}$	0	$2u_1 - 2u_2$
ORO	$\mu_R^0 + 2\mu_O^0 + 2u_{OR}$	$2u_{OO} - 2u_{OR}$	$2u_1 + 2u_2$
OOO	$3\mu_O^0 + 2u_{OO}$		
(tetramer)			
RRRR	$4\mu_R^0 + 3u_{RR}$	$-2u_{RR} + 2u_{OR} + u_{OXR}$	
RORR	$3\mu_R^0 + \mu_O^0 u_{RR} + 2u_{OR} + u_{OXR}$	$-u_{RR} + u_{OR} - u_{OXR}$	$u_1 - u_1 - 2u_3$
RORO	$2\mu_R^0 + 2\mu_O^0 + 3u_{OR}$	$-u_{OR} + u_{OO} + u_{OXR}$	$2u_1 + 2u_3$
OROO	$\mu_R^0 + 3\mu_O^0 + 2u_{OR} + u_{OO} + u_{OXR}$	$-2u_{OR} + 2u_{OO} - u_{OXR}$	$u_1 + u_2 - 2u_3$
OOOO	$4\mu_O^0 + 3u_{OO}$		
(pentamer)			
RRRRR	$5\mu_R^0 + 4u_{RR}$	$-2u_{RR} + 2u_{OR} + 2u_{OXR}$	
RRORR	$4\mu_R^0 + \mu_O^0 + 2u_{RR} + 2u_{OR} + 2u_{OXR}$	$-2u_{RR} + 2u_{OR} - 2u_{OXR}$	$-4u_3$
ROROR	$3\mu_R^0 + 2\mu_O^0 + 4u_{OR}$	0	$2u_1 - 2u_2 + 2u_3$
ORORO	$2\mu_R^0 + 3\mu_O^0 + 4u_{OR}$	$2u_{OO} - 2u_{OR} + 2u_{OXR}$	$2u_1 + 2u_2 + 2u_3$
OOROO	$\mu_R^0 + 4\mu_O^0 + 2u_{OR} + 2u_{OO} + 2u_{OXR}$	$2u_{OO} - 2u_{OR} - 2u_{OXR}$	
OOOOO	$5\mu_O^0 + 4u_{OO}$		
(hexamer)			
RRRRRR	$6\mu_R^0 + 5u_{RR}$	$-2u_{RR} + 2u_{OR} + 2u_{OXR}$	
RRRORR	$5\mu_R^0 + \mu_O^0 + 3u_{RR} + 2u_{OR} + 2u_{OXR}$	$-2u_{RR} + 2u_{OR}$	$-2u_3$
RORROR	$4\mu_R^0 + 2\mu_O^0 + u_{RR} + 4u_{OR} + 2u_{OXR}$	$-u_{RR} + u_{OR} - 2u_{OXR}$	$u_1 - u_2 - 2u_3$
RORORO	$3\mu_R^0 + 3\mu_O^0 + 5u_{OR}$	$u_{OO} - u_{OR} + 2u_{OXR}$	$2u_1 + 4u_3$
ORROORO	$2\mu_R^0 + 4\mu_O^0 + u_{OO} + 4u_{OR} + 2u_{OXR}$	$2u_{OO} - 2u_{OR}$	$u_1 + u_2 - 2u_3$
OOOROO	$\mu_R^0 + 5\mu_O^0 + 3u_{OO} + 2u_{OR} + 2u_{OXR}$	$2u_{OO} - 2u_{OR} - 2u_{OXR}$	$-2u_3$
OOOOOO	$6\mu_O^0 + 5u_{OO}$		
(heptamer)			
RRRRRRR	$7\mu_R^0 + 6u_{RR}$	$-2u_{RR} + 2u_{OR} + u_{OXR}$	
RRRORRR	$6\mu_R^0 + \mu_O^0 + 4u_{RR} + 2u_{OR} + 2u_{OXR}$	$-2u_{RR} + 2u_{OR} + 2u_{OXR}$	$-u_3$
RORRORR	$5\mu_R^0 + 2\mu_O^0 + 2u_{RR} + 4u_{OR} + 3u_{OXR}$	$-2u_{RR} + 2u_{OR} - 3u_{OXR}$	$-4u_3$
ROROROR	$4\mu_R^0 + 3\mu_O^0 + 6u_{OR}$	0	$2u_1 - 2u_2 + 3u_3$
ORORORO	$3\mu_R^0 + 4\mu_O^0 + 6u_{OR}$	$2u_{OO} - 2u_{OR} + 3u_{OXR}$	$2u_1 + 2u_2 + 3u_3$
OROOROO	$2\mu_R^0 + 5\mu_O^0 + 2u_{OO} + 4u_{OR} + 3u_{OXR}$	$2u_{OO} - 2u_{OR} - u_{OXR}$	$-4u_3$
OOOROOO	$\mu_R^0 + 6\mu_O^0 + 4u_{OO} + 2u_{OR} + 2u_{OXR}$	$2u_{OO} - 2u_{OR} - 2u_{OXR}$	$-u_3$
OOOOOOO	$7\mu_O^0 + 6u_{OO}$		

[a] $u_1 = (u_{OO} + u_{RR})/2 - u_{OR}$, $u_2 = (u_{OO} - u_{RR})/2$

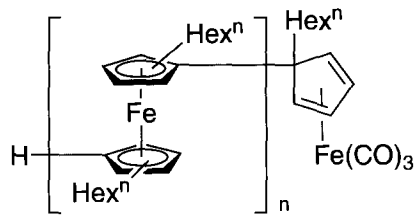

19_1 -19_3: n = 1 - 3

which is the shift of ν_{CO} from the neutral form to a given oxidized form, and $\theta(\Delta\nu_{CO})$, which denotes the ratio of $\Delta\nu_{CO}$ for a given oxidation state to $\Delta\nu_{CO}$ for a fully oxidized state. The wavenumber shift of the CO stretching mode to higher wavenumbers by 12–18 cm^{-1} is observed, corresponding to the $1e^-$ oxidation. The direction of the wavenumber shift from the fully reduced form to the fully oxidized form is reasonable because the positively charged ferrocenium site withdraws electrons from Fe(II) in the (cyclopentadiene)$Fe(CO)_3$ moiety and, consequently, the back-donation from Fe to CO must be lessened.

The monocationic form of the dimer **19_2** gives peaks at wavenumbers between those for the neutral and dicationic forms, and the peak width is broadened, which can be attributed to the rate of electron exchange between two electronic isomers, Red–Ox–$Fe(CO)_3$ and Ox–Red–$Fe(CO)_3$, where $Fe(CO)_3$ refers to an [(η^4-cyclopentadiene)$Fe(CO)_3$]

TABLE II

ν_{CO} AT DIFFERENT OXIDATION STATES OF 19_1–19_3

Complex	Wavenumber(cm^{-1})		$\Delta\nu_{CO}$ (cm^{-1})		$\theta(\Delta\nu_{CO})$
$\mathbf{19}_1^0$	2039	1965	—	—	0
$\mathbf{19}_1^{1+}$	2051	1980	12	15	1
$\mathbf{19}_2^0$	2038	1965	—	—	0
$\mathbf{19}_2^{1+}$	2047	1976	9	11	0.6–0.7
$\mathbf{19}_2^{2+}$	2051	1982	4	6	1
$\mathbf{19}_3^0$	2038	1964	—	—	0
$\mathbf{19}_3^{1+}$	2041	1970	3	6	0.2–0.3
$\mathbf{19}_3^{2+}$	2050	1979	9	9	0.8–0.9
$\mathbf{19}_3^{3+}$	2052	1982	2	3	1

moiety, being comparable to the time scale of IR (10^{11}–10^{13} s^{-1}) (*80,81*). These findings are in accordance with the value of k_{et} obtained by Masuda *et al.* (*33*), assuming that the (cyclopentadiene)$Fe(CO)_3$-attached ferrocene unit can be either Red or Ox if the attached and non-attached ferrocenes are electronically similar.

In the case of the trimer **19**$_3$, the consideration based on neighboring-site interactions indicates that the three-step oxidation pathway is composed of Red–Red–Red–$Fe(CO)_3$ → Red–Ox–Red–$Fe(CO)_3$ → Ox–Red–Ox–$Fe(CO)_3$ → Ox–Ox–Ox–$Fe(CO)_3$. The (cyclopentadiene)$Fe(CO)_3$-attached ferrocene site should change from Red to Ox at the second oxidation step from monocation to dication. This prediction is roughly correct, as it can be seen in the IR spectra that the most significant wavenumber shift occurs in the second step, although small wavenumber shifts can be observed even for the first and third oxidation steps. A simple interpretation is that the shifts at the first and third steps correspond to approximately 20% and 80% oxidation of the (cyclopentadiene)$Fe(CO)_3$-attached ferrocene site if the total wavenumber shift (14–18 cm^{-1}) corresponds to the full change in charge density of the ferrocene site from 0 to 1. The values of partial charge density can be regarded as the degree of electron delocalization.

D. Intervalence-Transfer Bands for Mixed-Valence Oligo(ferrocenylene)s

Ever since the appearance of the pioneering theoretical work by Hush in the 1950s, theoretical investigation of the intervalence-transfer (IT) band (or MMCT band) in mixed-valence complexes has been of continuing interest (*22,26*). The regular method of analyzing IT bands is to converge their parameters into the mixing coefficient α and resonance energy H_{AB} according to Eqs. (3) and (4), respectively:

$$\alpha^2 = (4.2 \times 10^{-4}/m_d m_a)\epsilon_{max}\nu_{1/2}\Delta\nu_{max}^{-1}r^{-2} \tag{3}$$

$$H_{AB} = \nu_{max}\alpha \tag{4}$$

where m_d, m_a, and r are the number of donor sites, the number of acceptor sites, and the donor–acceptor distance, respectively. The value of $\Delta\nu_{1/2}$ for a homonuclear mixed-valence dimer at 300 K is given as Eq. (5):

$$\Delta\nu_{1/2} = (2310\nu_{max})^{1/2} \tag{5}$$

One more recent advance is the theory of Creutz, Newton, and Sutin (CNS) on the relation of metal–ligand and metal–metal coupling ele-

ments (*26*). The role of the bridging ligand between the metal nuclei on the electron exchange process is specifically addressed in this model. Experimental support for the CNS model has been presented for some mixed-valence complexes other than ferrocene oligomers (*74,82*).

Morrison and Hendrickson have reported that the IT band of biferrocenium monocation has two peaks at 77 K (*50*), whereas the analysis of IT bands of biferrocene derivatives observed at room temperature is carried out assuming one broad peak, and it has been reported that Eq. (5) is applicable to biferrocene (*41*). As for the IT bands of higher unsubstituted oligo(ferrocene-1,1′-diyl)s in the mixed-valence states, only one report by Brown *et al.* on the IT bands of the monocation and dication of terferrocene and the dication of quaterferrocene (tetramer) has been published (*64*).

The first systematic study of the effects of IT bands on the number of nuclei and the oxidation number was carried out for oligo(dihexylferrocenylene)s, $\mathbf{13_2}$–$\mathbf{13_6}$ (*83,84*). All the oxidation states of $\mathbf{13_2}$–$\mathbf{13_6}$ were generated by a quantitative chemical oxidation method. Table III shows the dependence of ν_{max}, ϵ_{max}, and $\Delta\nu_{1/2}$ values of the IT band on the oxidation state and the number of ferrocene units. The $\Delta\nu_{1/2}$ values

TABLE III

PARAMETERS OF IT BANDS FOR OLIGO(DIHEXYLFERROCENYLENE)S, **13**

Substrate	ν_{max} (cm^{-1})	ϵ_{max} ($M^{-1}\,cm^{-1}$)	$\Delta\nu_{1/2}$ (cm^{-1})	Total extra energy	ν_{max}(calc.) (cm^{-1})
$\mathbf{13}^{+}$	4870	1060	3740	0	
$\mathbf{13_3}^{+}$	4830	1490	3850	0	4830
$\mathbf{13_3}^{2+}$	6140	990	3910	u_{ex}	6140
$\mathbf{13_4}^{+}$	4700	1730	4000	0	4700
$\mathbf{13_4}^{2+}$	5280	1500	3880	$\{(1+\sqrt{2})/(1+2\sqrt{2})\}u_{ex}$	5530
$\mathbf{13_4}^{3+}$	5680	1250	3570	u_{ex}	6010
$\mathbf{13_5}^{+}$	4550	1500	3750	0	4550
$\mathbf{13_5}^{2+}$	4860	1400	3550	$\{\sqrt{2}/(1+\sqrt{2})\}u_{ex}$	5320
$\mathbf{13_5}^{3+}$	5860	1430	3550	u_{ex}	5860
$\mathbf{13_5}^{4+}$	5860	1010	3340	u_{ex}	5860
$\mathbf{13_6}^{+}$	4410	1890	3800	0	4410
$\mathbf{13_6}^{2+}$	4580	1680	3940	0	4410
$\mathbf{13_6}^{3+}$	5140	1680	4010	$\{(3+\sqrt{2})/(3+2\sqrt{2})\}u_{ex}$	5480
$\mathbf{13_6}^{4+}$	5600	1630	3820	u_{ex}	5720
$\mathbf{13_6}^{5+}$	5680	1400	3570	u_{ex}	5720

obtained for the oligo(ferrocenylene)s are in the range of 3100–4000 cm^{-1}, which is similar to the range of values calculated by Eq. (5), 3200–3800 cm^{-1}. A characteristic feature that can be seen in the table is a higher energy shift in ν_{max} as the oxidation number for each oligomer increases, and a lower energy shift in ν_{max} for the monocationic form of the oligomers as the number of ferrocene units increases.

The shift in ν_{max} of IT bands was analyzed on the basis of a model assuming that the mixed-valence states are a linear combination of Red and Ox, as follows. In the case of the biferrocenium cation, $\mathbf{13}_2^+$, photoexcitation of Red–Ox yields Ox-Red, and thus no alteration in the internuclear distance is necessary during the relaxation process. In contrast, the terferrocenium monocation, $\mathbf{13}_3^+$, for which the ground and electron-transferred excited states are Red–Ox–Red and Ox–Red–Red, respectively, needs a change in the internuclear distance in the relaxation process, since the appropriate distance for Red–Ox is different to that for Red–Red. A similar internuclear distance alteration occurs for the terferrocenium dication,$\mathbf{13}_3^{2+}$, for which the ground and excited states are Ox–Red–Ox and Red–Ox–Ox, respectively. In this case, the combination Red–Ox changes to Ox–Ox, resulting in the largest distance alteration, as the Red–Ox distance is the shortest due to the attractive interaction resulting from electronic delocalization and the Ox–Ox distance is the longest due to electrostatic repulsion. Consequently, the photochemical intervalence transfer of Red–Ox–Red (or Ox–Red–Ox) requires more energy than that of biferrocene, not only because of the energetic difference between unequal ground states before and after photo-electron transfer but also because of strain derived from the difference in internuclear distance between Red–Ox and Red–Red (or Ox–Ox) combinations. As it can be deduced that the extra energy for the change from Red–Ox to Ox–Ox is the largest, this energy, u_{ex}, is employed as the factor for rationalization of the ν_{max} shift due to the change in oxidation number of the higher oligomers. The estimation of the ν_{max} shift based on u_{ex} (= 13 kJ mol^{-1}) and the transition probability ratio qualitatively rationalizes the dependency of ν_{max} on the number of ferrocene units and the oxidation states, as given in Table III.

E. Hybridized Redox Functions of Oligoferrocenylene

Several systems have been reported regarding the connection between oligoferrocenylene multistep redox reactions and the functions of other molecular units. Colbert *et al.* have reported Mn and Ru complex-conjugated biferrocene derivatives, **20**, showing large electron

delocalization between the iron atoms of the biferrocene moiety and the metal centers in the one-electron oxidized forms (*85*). In this complex, Mn and Ru centers donate electron density through the acetylene linkage to the biferrocene ligand.

Dong *et al.* have reported on crown ether-bound biferrocene, **21**, in which the redox potentials are shifted by the capture of metal ions within the crown ether (*35*). For example, the electrochemical behavior observed for the biferrocene derivative with Ba^{2+} ion is fundamentally different, as new redox couples are observed for **9** with Ba^{2+} concentrations within the range $0 < [Ba^{2+}] < 2$ eq. The peak currents for the two new redox couples increase with concentrations of the Ba^{2+} ion until a full equivalent is added: at this point, the original redox couples disappear and the new redox couples reach full development.

Another example is metal clusters modified with biferrocene-terminated alkanethiol. Gold clusters stabilized with alkanethiols were prepared, and resulted in the development of a new research area at the metal–molecule interface (*86*). The redox properties of biferrocene and terferrocene-attached Au clusters (2.2 ± 0.3 nm in diameter), **22,** have been investigated (*87,88*). The modified Au clusters with biferrocene and terferrocene attached undergo quasi-reversible two-step and three-step $1e^-$ oxidation reactions, respectively, in Bu_4NClO_4–CH_2Cl_2, while the consecutive potential scans in the same potential range cause electrodeposition to give redox-active Au cluster films on the electrode surface. The λ_{max} value of the surface plasmon band for the Au cluster film is strongly dependent on the potential. The self-assembled monolayer of the biferrocene derivative on a bulk Au electrode has also been investigated (*89*).

III. Ferrocene Oligomers and Polymers with Conjugated Spacers

A. Dependence of Redox Properties on the Spacers in Conjugated Ferrocene Oligomers

Effects of spacer groups on the formation and properties of the mixed-valence states of conjugated ferrocene dimers have been extensively studied by both electrochemical and spectroscopic methods. It should be noted that a characteristic feature in the electronic spectra of ferrocene dimers with conjugated spacer groups is the appearance of metal-to-ligand charge transfer (MLCT) bands in the neutral form as well as IT bands in the mixed-valence state. The dimer Fc—CH=CH—**Fc**

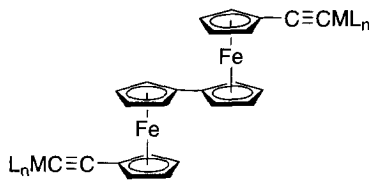

20a: $ML_n = Mn(CO)_3(dppm)$
20b: $ML_n = Ru(dppm)_2Cl$
(dppm = diphenylphosphinomethane)

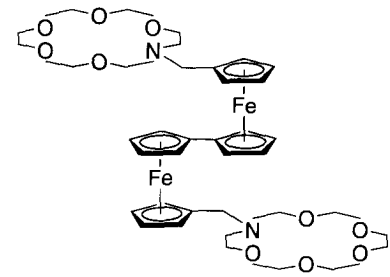

21

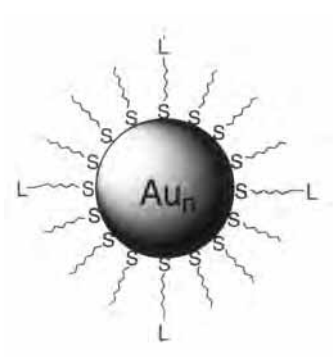

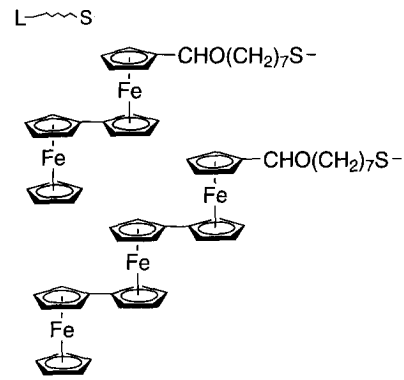

22

(**23$_1$**) has an MLCT band at 458 nm with $\epsilon = 1450\,M^{-1}\,cm^{-1}$ in CH_2Cl_2 (*90*), and Fc—C≡C—Fc (**24**) has a band at 453 nm with $\epsilon = 820\,M^{-1}\,cm^{-1}$ in $CHCl_3$ (*91*). In the case of Fc—N=N—Fc (**25**) a band at 533 nm with $\epsilon = 4170\,M^{-1}\,cm^{-1}$ in CH_2Cl_2 is obtained (*92*). In this section, only the redox properties of conjugated ferrocene dimers are appraised.

Table IV lists the redox potentials of conjugated ferrocene oligomers (mainly dimers with a single bridge). Potential values are denoted against different reference electrodes as given in the references. The values can be primarily compared using the relationship mentioned in the footnote of the table, although care should be taken with some errors derived from junction potentials which depend on experimental conditions. There have been several reports on the quantitative estimation of structural factors affecting internuclear electron delocalization.

TABLE IV

REDOX POTENTIALS OF CONJUGATED FERROCENE OLIGOMERS

Compound	$E^{0'}$ of ferrocene moieties	$\Delta E^{0'}$	Electrolyte	Reference electrode[m]	Ref.
1	0.31, 0.65	0.34	a	SSCE	*64*
2	0.22, 0.44, 0.82	0.22, 0.38	a	SSCE	*64*
3	0.16, 0.36, 0.61, 0.89	0.20, 0.25, 0.28	a	SSCE	*64*
16a	0.19, 0.35, 0.80	0.16, 0.45	a	SCE	*69*
16b	0.19, 0.35, 0.80	0.16, 0.45	a	SCE	*69*
16c	0.25, 0.45, 0.80	0.20, 0.35	a	SCE	*69*
17a	0.19, 0.31, 0.58, 0.86	0.12, 0.27, 0.28	a	SCE	*69*
17b	0.20, 0.32, 0.60, 0.87	0.12, 0.28, 0.27	a	SCE	*69*
17c	0.20, 0.38, 0.60, 0.83	0.16, 0.22, 0.23	a	SCE	*69*
20a	−0.20, 0.05	0.25	b	k	*85*
20b	−0.37, −0.21	0.16	b	k	*85*
23_1	0.290, 0.460	0.170	b	SCE	*90*
23_2	0.294, 0.423	0.129	b	SCE	*90*
23_3	0.366, 0.460	0.094	b	SCE	*90*
23_4	0.405($2e^-$)	0	b	SCE	*90*
24_1	0.625. 0.755	0.130	c	SCE	*93*
24_2	0.58, 0.68	0.10	c	SCE	*93*
25	0.106, 0.316	0.210	d	k	*92*
26	−0.11, 0.03	0.14	e	k	*97*
27	−0.15, −0.06, 0.05(2e)	0.09, 0.11, 0	e	k	*97*
28	0.40, 0.55	0.15	c	Ag/AgCl	*98*
29	0.61, 0.76	0.15	c	Ag/AgCl	*98*
30	0.47, 0.56	0.09	d	SCE	*99*
31	0.463, 0.539	0.076	f	SCE	*100*
32a	0.35, 0.47	0.12	g	SCE	*101*
32b	0.34, 0.53	0.19	g	SCE	*101*
33	0.55, 0.74	0.19	g	SCE	*101*
34a	0.08, 0.37	0.29	c	k	*103*
34b	0.01, 0.33	0.32	c	k	*103*
35	0.04, 0.26	0.22	c	SCE	*105*
36a	1.480, 1.545	0.065	h	l	*106*
36b	1.475($2e^-$)	0	h	l	*106*
37a	0.765, 0.809	0.044	d	Ag/AgCl	*107*
37b	0.665($2e^-$)	0	d	Ag/AgCl	*107*
38a	0.19, 0.20	0.29	d	Ag/Ag^+	*108*
38b	−0.321, 0.152	0.473	d	Ag/Ag^+	*109*
39	0.22, 0.44	0.22	d	Ag/Ag^+	*110*
40	0.38, 0.44	0.06	c	SCE	*112*
41a	−0.27, −0.08	0.19	g	k	*113*
41b	−0.24, 0.17	0.41	g	k	*113*
42a	0.70, 0.82	0.12	d	SCE	*114*
42b	0.61, 0.75	0.14	d	SCE	*114*

Table IV *continued*

Compound	$E^{0'}$ of ferrocene moieties	$\Delta E^{0'}$	Electrolyte	Reference electrode[m]	Ref.
42c	0.72, 0.90	0.18	d	SCE	*114*
43a	0.59, 0.86	0.27	d	SCE	*115*
43b	0.40, 0.91	0.51	d	SCE	*115*
43c	0.30, 0.86	0.56	d	SCE	*115*
44	−0.14, 0.00, 0.20	0.14, 0.20	i	k	*126*
46a	−0.04, 0.05, 0.44	0.09, 0.39	c	k	*127*
46b	−0.01, 0.09, 0.51	0.10, 0.42	c	k	*127*
47$_2$	0.09, 0.26, 0.41, 0.63	0.17, 0.15, 0.22	c	SCE	*128*
47$_3$	0.32, 0.42, 0.52(2e$^-$)	0.10, 0.10, 0	c	SCE	*129*
47$_4$	0.25, 0.41, ~ 0.7(2e$^-$)	0.16, 0.3, 0	c	SCE	*130*
47$_5$	0.45, (2e$^-$), 0.54(2e$^-$)	0, 0.09, 0	c	SCE	*131*
47$_6$	0.23(4e$^-$)	0, 0, 0	c	SCE	*132*
48	−0.03, 0.15, 0.29, 0.39	0.18, 0.14, 0.10	e	k	*133*
49	0.00, 0.22, 0.45	0.22, 0.23	g	k	*134*
50a$_2$	0.546, 0.795	0.249	j	Ag/AgCl	
50a$_3$	0.548, 0.703, 0.876	0.165, 0.163	j	Ag/AgCl	*135*
50a$_4$	0.550, 0.674, 0.797, 0.889	0.124, 0.123, 0.092	j	Ag/AgCl	*135*
50b$_2$	0.529, 0.772	0.243	j	Ag/AgCl	*135*
50a$_3$	0.551, 0.703, 0.869	0.152, 0.166	j	Ag/AgCl	*135*
50a$_4$	0.553, 0.674, 0.790, 0.878	0.121, 0.116, 0.082	j	Ag/AgCl	*135*
54	0.13, 0.42	0.29	f	Ag/Ag$^+$	*138*
55a	−0.24, −0.07	0.17	c	—	*139*
55b	−0.20, −0.01	0.19	c	—	*139*
63	0.136(2e$^-$), 0.526	0, 0.390	d	k	*92*
64	−0.054, 0.156, 0.476	0.210, 0.370	d	k	*92*

[a] Bu_4NPF_6–CH_2Cl_2 + MeCN (1:1 v/v).
[b] Bu_4NBF_4–CH_2Cl_2.
[c] Bu_4NPF_6–CH_2Cl_2.
[d] Bu_4NClO_4–CH_2Cl_2.
[e] Bu_4NClO_4–PhCN.
[f] Bu_4NClO_4–CH_2Cl_2 + MeCN (1:1 v/v).
[g] CH_2Cl_2 (electrolyte salt was not specified).
[h] Bu_4NPF_6–EtCN.
[i] Bu_4NPF_6–PhCN.
[j] Bu_4NPF_6–MeCN.
[k] Ferrocenium/ferrocene.
[l] Cobaltocenium/cobaltocene.
[m] $E^{0'}$ (ferrocenium/ferrocene) = 0.312 V *vs.* SSCE (*176*), 0.307 V *vs.* SCE (*176*), 0.351 V *vs.* Ag/AgCl (*177*), 1.345 V *vs.* cobaltocenium/cobaltocene (*106*), and 0.21 V *vs.* Ag/Ag$^+$ (10 mM in MeCN) (*84*).

The dependence of internuclear electron transfer on the metal–metal distance for $Fc(CH{=}CH)_nFc$ (**23**, $n = 1$–6) indicates that $\Delta E^{0'}$ decreases with increasing n, becoming almost zero when $n = 4$ (*90*). The $\Delta E^{0'}$ values of acetylene-bridged dimers, $Fc(C{\equiv}C)_nFc$ (**24**, $n = 1,2$) indicate the similar electronic bridging ability of the triple bond to the double bond (*93,94*). The IT band observation suggests that the selective encapsulation of $[FcC{\equiv}CFc]^+$ into β-cyclodextrin causes a decrease in the self-exchange rate by increasing the thermal activation barrier (*95*). The topological effects of *m*-phenylene-bridged ferrocene dimers have shown that *m*-phenylene-bridged dimers exhibit smaller $\Delta E^{0'}$, that is, a weak internuclear interaction, compared with *o*- and *p*-phenylene-bridged dimers (*96*). By introducing the electron-withdrawing substituents on the 5-position of *m*-phenylene (1,3-phenylene), both $E_1^{0'}$ and $E_2^{0'}$ shift in a positive direction but the $\Delta E^{0'}$ values remain constant in the range of 80–100 mV. Face-to-face fixed diferrocenyl and tetraferrocenyl-1,6-methano[10]annulenes, **26** and **27**, show two and three redox waves, respectively, reflecting not only the through-bond but also the through-space interactions of the ferrocene nuclei (*97*). The [3]- and [4]-dendrarens, **28** and **29**, provide good links for electronic communication (*98*). Ferrocene dimers with N-containing bridges, **30** and **31**, show moderate internuclear interactions (*99,100*).

The electrochemistry of some single-atom bridged ferrocene dimers gives a separation of two $1e^-$ waves. The carbon atoms in CROH and C=O can communicate between ferrocene units in **32** and **33** (*101*). Diferrocenyl sulfide, **34**, shows significant $\Delta E^{0'}$ values, 0.29–0.33 V, indicating the presence of strong internuclear interactions (*102,103*).

Recently, a number of systems where a transition metal is involved in the spacer have been reported. A Ru bis(acetylide) complex-bridged ferrocene dimer, **35**, shows a separation of redox potentials of two ferrocene units at 0.22 V (*104,105*). Mixed-valence complexes of relating acetylene-bridged Fe(III)–Ru(II) dimers indicate strong donor–acceptor interactions between the two metal sites. In the trinuclear metallocenes that are η^5-cyclopentadienyl-bridged by two adjacent Me_2Si groups, **36** $\Delta E^{0'} = 65$ and ca. 0 mV when the incorporated metals are Cr and Co, respectively (*106*). A Ni complex of S-benzyl-3-(1-ferrocenylethylidene)-dithiocabazate, **37a**, shows a redox potential separation of 44 mV, but no separation occurs for the Cu complex, **37b** (*107*). These results indicate the important role of the *d*-orbitals of the metals involved in the spacer group. Ferrocene dimers with conjugated metallacyclic spacers such as cobaltacyclopentadiene (**38**) and ruthenacyclopentatriene (**39**) exhibit quite strong internuclear interactions (*108–110*). The $\Delta E^{0'}$ value is 0.39–0.47 V, larger than the separation of biferrocene, 0.35 V,

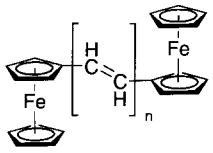

23_1 -23_6: n = 1 - 6

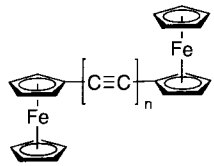

24_1, 24_2: n = 1, 2

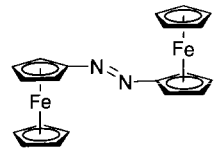

25

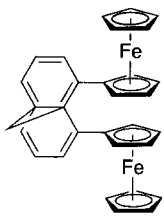

26

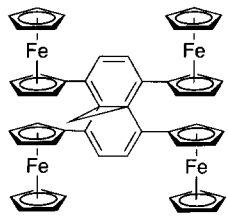

27

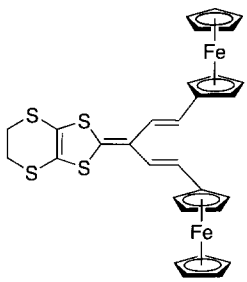

28

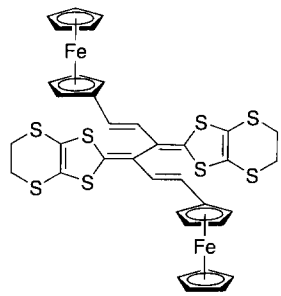

29

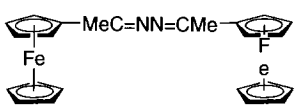

30

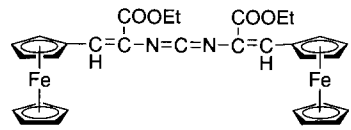

31

when cobaltacyclopentadienylene is inserted; this can be attributed to the strong assistance of the electron exchange between ferrocene nuclei via cobalt, since the cobaltacyclopentadiene unit has an aromatic nature and the energy level of the HOMO of cobaltacyclopentadiene is similar to that of ferrocene (*111*). The cobalt dinuclear complex assists in the communication between the ferrocenes in **40** (*112*). In bis(ferrocenyl)porphyrins, **41a** and **41b**, the internuclear interaction increases when Ni(II) is bound to the porphyrin (*113*). The $\Delta E^{0'}$ values are 0.19 and 0.41 V, and λ_{max} of IT is 1080 and 946 nm for free porphyrin and Ni porphyrin. The small bandwidth of the IT band for Ni porphyrin ($\nu_{1/2} = 1400\,cm^{-1}$) suggests that it is a class III complex, while the free porphyrin shows class II complex behavior ($\Delta\nu_{1/2} = 2600\,cm^{-1}$. Ferrocenyldiazabutadiene metal carbonyl complexes (M = Cr, Mo, W), **42**, exhibit an electronic interaction between the peripheral ferrocenyl substituents that increases upon complexation to the metal tetracarbonyl moieties (*114*). The diferrocenyltriphosphines undergo a single $2e^-$ oxidation, whereas their Ru complexes, **43**, exhibit two separated $1e^-$ oxidations with $\Delta E^{0'} = 0.27$–0.56 V, classified as class II and class III complexes (*115*).

Weak or no internuclear interaction of ferrocene dimers via a metal complex bridge has also been reported for Cu(I), Ag(I), and Pd(II) complexes with Schiff base ligands (*116,117*), Cu(I), Ag(I), Pd(II), and Pt(II) tetrathiaferrocenophane complexes (*118*), bis(ferrocenylvinyl)terpyridine complexes of Fe(II) and Co(II) (in this case, electropolymerization takes place) (*119*), an (arene)$Cr(CO)_3$-inserted ferrocene dimer (*120*), ferrocenylpyridine complexes of Au(III) and Ag(I) (*121*), 1-ferrocenyl-1,3-butanedionate complexes (*122*), Fe, Co, and Ni complexes of ferrocenyltris((methylthio)methyl)borate) (*123*), 1,1′-bis(diphenylphosphino)-ferrocene derivatives of $R_2C_2Co_2(CO)_6$ (R = MeO_2C, CF_3) (124), and bis(ferrocenylhydrazone)$PdCl_2$ (*125*).

Redox potential data are limited for the ferrocene oligomers higher than dimers with strong electronic communication, while their redox properties are important in estimating the neighboring-site interaction energy by Aoki's model (*75*). Reported examples are as follows. A single carbon-bridged ferrocene trimer, **44**, exhibits three-step $1e^-$ oxidation at $E^{0'} = -0.14$, 0.00, and 0.20 V *vs.* ferrocenium/ferrocene (*126*). This affords $u_{OR} = -7\,kJ\,mol^{-1}$ and $u_{OO} = 3\,kJ\,mol^{-1}$, assuming $u_{RR} = 0$, indicating a stronger delocalization in the mixed-valence state than that of the isostructural single silicon-bridged oligomers, oligo(ferrocenyldimethylsilane)s, **45**, as noted below. Bis(ferrocenylthio)ferrocene gives $\Delta E_1^{0'} = 0.01$ and 0.10 V and $\Delta E_2^{0'} = 0.49$ and 0.42 V for unsubstituted and di(trimethylsilyl)-substituted derivatives, **46**, respectively (*127*).

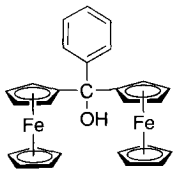

32a: R = H
32b: R = Ph

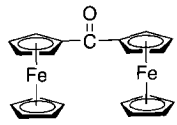

33

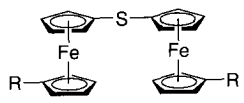

34a: R = H
34b: R = $SiMe_3$

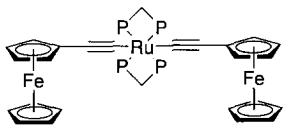

35

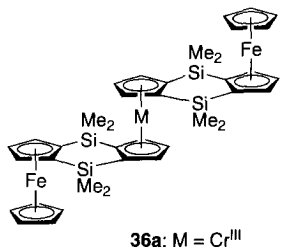

36a: M = Cr^{III}
36b: M = Co^{III}

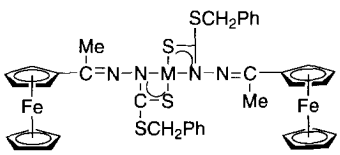

37a: M = Ni
37b: M = Cu

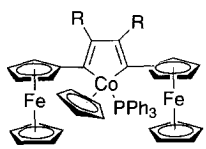

38a: R = H
38b: R = Me

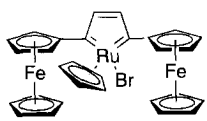

39

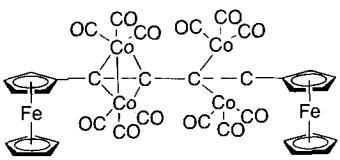

40

These small $\Delta E_1^{0'}$ values give $u_{OR} = -0.25$ and $-2.5\,kJ\,mol^{-1}$ and $u_{OO} = 12$ and $8\,kJ\,mol^{-1}$, assuming $u_{RR} = 0$.

A series of cumulene-bound ferrocene tetramers, **47**, have been synthesized and their electrochemical properties examined by

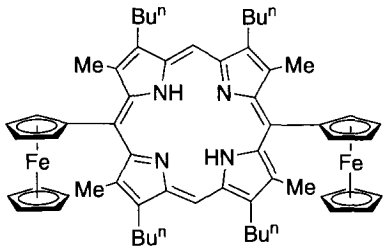

41a

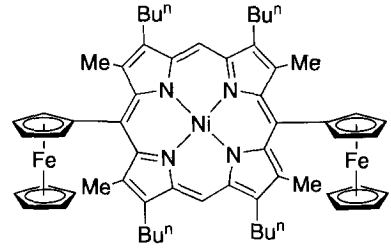

41b

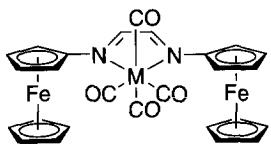

42a: M = Cr
42b: M = Mo
42c: M = W

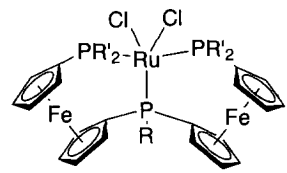

43a: R = R' = Ph
43b: R = Ph, R' = Pr^i
43c: R = R' = Pr^i

Bildstein *et al.* (*128–132*). The redox properties are as follows: $n = 2$, four separate $1e^-$ oxidations; $n = 3$, two separate $1e^-$ oxidations followed by a further $2e^-$ oxidation; $n = 4$, two $2e^-$ oxidations separated by $\Delta E^{0'} = 0.16$ V; $n = 5$, two $2e^-$ oxidations separated by $\Delta E^{0'} = 0.09$ V; and $n = 6$; one $4e^-$ oxidation. Another tetramer, $SiFc_4$ (**48**) is oxidized with $1e^-$ stepwise at -0.03, 0.15, 0.29, and 0.39 V *vs.* ferrocenium/ferrocene (*133*). Trimetallic [1]silaferrocenophene, **49**, showed three oxidation waves at 0, 0.22, and 0.45 V *vs.* ferrocenium/ferrocene (*134*). Acetylene-bridged ferrocene oligomers, **50,** and polymers, **51**, where the main chain consists of 1,3-cyclopentadienylene moieties so that iron is not involved in the main chain, were prepared, and their redox properties and the optical properties of their mixed valence states have been reported by Plenio *et al.* (*135*). The dimers to tetramers undergo separated $1e^-$ oxidations, and the polymer affords two redox waves roughly coinciding with the prediction of the neighboring-site interaction model (*75*). The IT bands of the monocationic forms of the dimer and the trimer appear at 1330/1540 nm and 1203 nm, respectively, and then $H_{AB} = 427/525$ and 552 cm^{-1}.

Synthesis of oligomeric or low-molecular weight polymeric metallocenes (M = Fe or Ru) in which the separate metallocene units are held

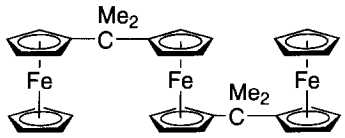

44

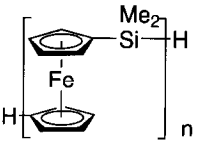

45$_n$: n = 2 - 9

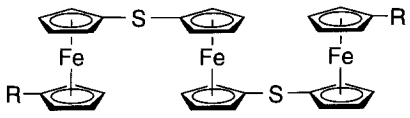

46a: R = H
46b: R = $SiMe_3$

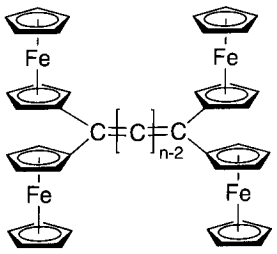

47$_n$: n = 2 - 6

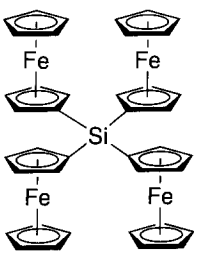

48

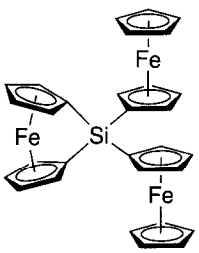

49

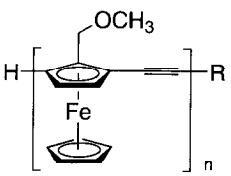

50a$_2$-50a$_4$: R = H, n = 2 - 4
50b$_2$-50b$_4$: R = $SiMe_3$, n = 2 - 4

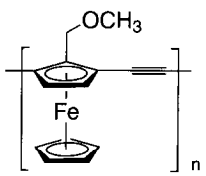

51

proximate and face-to-face by the bridging peri-substituted naphthalene rings, **52**, has been reported by Arnold *et al.* (*136*). Cyclic voltammetry of the ferrocene oligomers gives more than one oxidation wave, indicating some degree of electronic interaction and charge delocalization between the metal centers of the partially oxidized species, either by direct interaction of the cofacial π-orbitals of the metallocene units or by through-bond interactions. Polymers containing the 1,1′-ferrocenylene and 1′,1‴-biferrocenylene units in a π-conjugated main chain, **53** and **54**, show broadened cyclic voltammograms, suggesting an exchange of electrons between the Fc units along the π-conjugated main chain (*137,138*). The polymers themselves are insulating; they are, however, converted into semiconducting materials with a conductivity of 10^{-7} to $10^{-4}\,S\,cm^{-1}$ by formation of adducts with iodine. Another series of ferrocenylene-containing polymers with arylene bridges, **55**, shows two redox waves of ferrocene units, indicating a moderate internuclear interaction (*139*). Electropolymerized film of poly(oligothiophene-ferrocene), **56**, on the electrode shows redox behavior of ferrocene coupled with that of the oligothiophene moiety (*140*).

Dendrimers with multiple ferrocene moieties at the surface usually show one-step multielectron redox reactions due to little internuclear interaction (*141–143*), while those with locally communicating ferrocenyl groups have also been reported (*141*).

Ring-opening polymerization (ROP) of [1]metallocenophanes, in which a heteroatom such as Si, Ge, P, or S bridges two cyclopentadienyl rings, gives various series of conjugated metallocene polymers. Manners and his coworkers have been developing this system since their first discovery of ROP for silicon-bridged [1]ferrocenophane, in 1992 (*144,145*). Electrochemical properties have been reported for polymers and oligomers **57** (*144–146*), **58** (*148*), **59** (*147*), **60** (*149*), **61** (*103*), and **62** (*150*). Cyclic voltammetry of Si-, Ge-, P-, and S-bridged polymers with high molecular weights shows two quasi-reversible oxidation waves at $E_1^{0'} = -0.07$–$0.07\,V$ and $E_2^{0'} = 0.12$–$0.31\,V$ *vs.* ferrocenium/ferrocene. The separation of the two redox potentials, which denotes the quantity of interaction between ferrocene sites through bonds, lies at 0.19–0.29 V. Cyclic voltammograms of the oligomers **62** ($n = 2$–9) depend significantly on whether n is odd or even (*150*). The trimer (**62**$_3$), pentamer (**62**$_5$), heptamer (**62**$_7$), and nonamer (**62**$_9$) give two reversible oxidation waves of relative intensity 2:1, 3:2, 4:3, and 5:4, respectively. It is expected that the first wave involves the oxidation of two ferrocenyl end groups for $n = 3$, two end groups plus the middle repeat unit for $n = 5$, and two end groups plus two repeat units at the third and fifth positions for $n = 7$. In contrast, cyclic voltammetry of the dimer (**62**$_2$),

tetramer (**62**$_4$), hexamer (**62**$_6$), and octamer (**62**$_8$) shows two or three oxidation waves of relative intensity 1:1, 2:1:1, 3:1:2, and 4:1:3, respectively. These results may be explained by the first oxidation being due to alternating iron units, the second one to the other end group, and the third one to the remaining groups (e.g., the first, third, fifth, and seventh units at the first oxidation, the eighth unit at the second oxidation, and the second, fourth, and sixth units at the third oxidation when $n = 8$) (*150*). The results and this interpretation are closely related to the neighboring-site interaction model (*75–77*). Analysis of the redox potentials of **62** in the reference based on the neighboring-site interaction model gives $u_1 = 7\,\mathrm{kJ\,mol^{-1}}$, $u_2 = 3\,\mathrm{kJ\,mol^{-1}}$, and u_{OXR}, which can be neglected as shown in Fig. 4. These results indicate that $u_{\mathrm{OO}} = 6\,\mathrm{kJ\,mol^{-1}}$ and $u_{\mathrm{OR}} = -4\,\mathrm{kJ\,mol^{-1}}$ when we assume $u_{\mathrm{RR}} = 0$. The difference in u_{OO} between **13** and **62**, $3\,\mathrm{kJ\,mol^{-1}}$, can be ascribed to the stronger electrostatic repulsion of the smaller internuclear distance in **13** compared with that in **62**. The significantly higher u_{OR} value of **13** compared with that of **62** indicates the decrease in charge delocalization by the insertion of dimethylsilylene between ferrocene nuclei.

B. Redox, Optical, and Photoisomerization Properties of Azo-Bridged Ferrocene Oligomers

Azoferrocene, **25**, is one of the π-conjugated ferrocene dimers discussed in the previous section and also one of the simplest analogs of azobenzene, with two redox-active metal complex units. Its synthesis was first reported by Nesmeyanov *et al.* in 1961 (*151,152*). Although **25** is an intriguing complex, since the azo group has been known as the representative photoisomerizable unit, only a few studies have been reported on azoferrocene in the more than forty years since its discovery. Recently, X-ray crystallography of an azoferrocene crystal obtained under ambient conditions has determined that the azo moiety is in the *trans* form, and that the two cyclopentadienyl rings of the two ferrocene units and the azo moiety are almost on the plane best for π-conjugation (Fig. 5) (*92*). The ferrocene moieties are on the opposite side of the plane, and the Fe–Fe distance is 6.80 Å, indicating that there are few through-space interactions between the ferrocene nuclei. Higher azo-bridged ferrocene oligomers such as trimers, **63** and **64**, and a polymer, **65**, have also recently been prepared (*92*).

The *trans*-azo bridge acts as a spacer assisting in the electron exchange between ferrocene moieties, similar to the vinylene bridge, as given for $\Delta E^{0'}$ of azoferrocene (**25**) in Table IV and its IT band feature (*92,153*). The mixed-valence cation of **25** formed in benzonitrile by $1e^-$

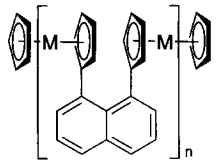

M = Fe, Ru

52

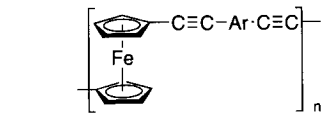

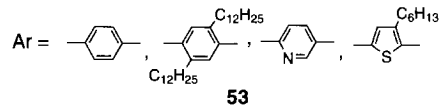

53

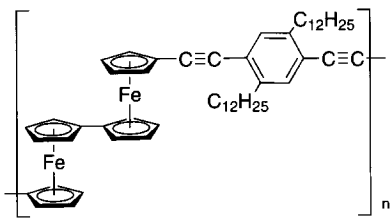

54

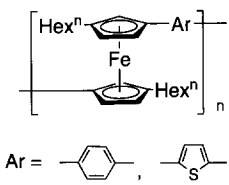

55

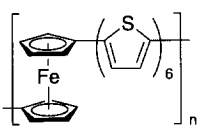

56

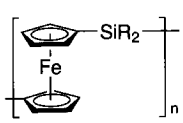

57

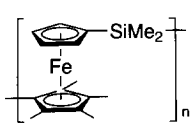

58

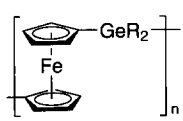

59

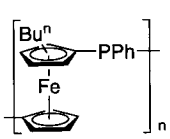

60

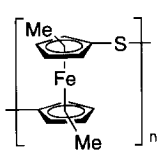

61

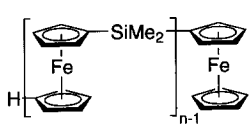

62$_2$ - 62$_9$: n = 2 - 9

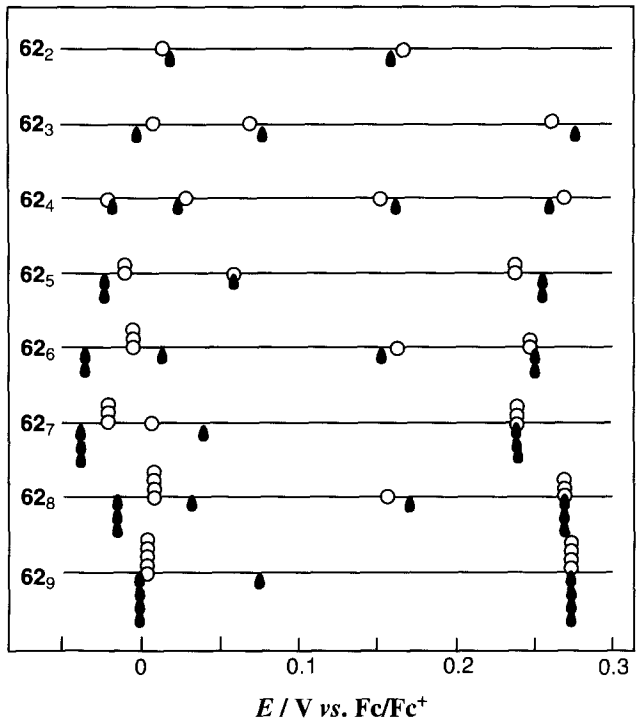

FIG. 4. Formal potentials of oligo(ferrocenyldimethylsilane)s **62** (○) measured in Bu_4NPF_6–CH_2Cl_2 + CH_3CN(1:1 v/v) (*150*), and those calculated from the first neighboring site interaction energies (▲) with $u_1 = 7\,kJ\,mol^{-1}$ and $u_2 = 3\,kJ\,mol^{-1}$.

chemical oxidation exhibits an ESR spectrum characterized by the superposition of narrow signals ($g = 1.9$) and a broad signal ($g_{\|} = 3.0$, $g_{\perp} = 1.9$) due to a ferrocenium Fe(III) cation at 7.6 K (*153*), similar to the spectrum of a solid sample of $[Fe_2(C_5H_4)_4]I_3$ at 77 K (*50*), indicating exchange narrowing and some weak hyperfine structures due to coupling with the ring protons. The trimer, **63,** in aprotic solvents such as CH_2Cl_2 or THF exhibits a cyclic voltammogram showing reversible $2e^-$ and $1e^-$ oxidation waves, contrary to the behavior of terferrocene (three $1e^-$ waves), as noted above. This behavior can be rationalized by the assumption that the positive charge in the monocation is localized primarily around the terminal ferrocene unit (correspondingly, Fc^+–N_2–Fc'–N_2–Fc) due to a strong electron-withdrawing effect of the azo group (*92*). This charge distribution in the mixed-valence states of **63** is supported by the characteristics of the IT

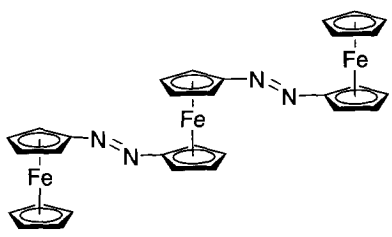

63

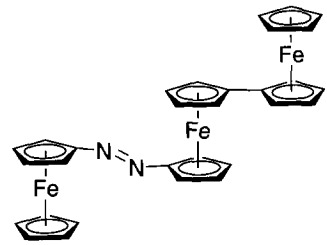

64

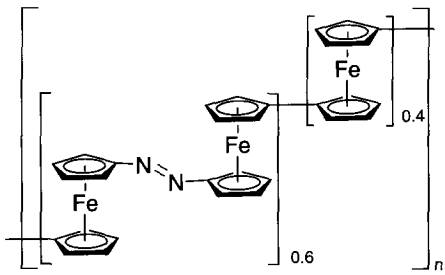

65

bands. An asymmetrical complex, **64**, undergoes a three-step $1e^-$ oxidation, and the two mixed-valence forms can be roughly expressed as Fc^+–Fc′–N_2–Fc and Fc^+–Fc′–N_2–Fc^+.

Azo-bridged ferrocene oligomers also show a marked dependence on the redox potentials and IT-band characteristics of the solvent, as is usual for class II mixed valence complexes (*21,22*). As for the conjugated ferrocene dimers, **2** and $\mathbf{24_1}$, the effects of solvents on the electron-exchange rates were analyzed on the basis of the Marcus–Hush theory, in which the ν_{max} of the IT band depends on $(1/D_{op} - 1/D_s)$, where D_{op} and D_s are the solvent's optical and static dielectric constants, respectively (*155–157*). However, a detailed analysis of the solvent effect on ν_{max} of the IT band of the azo-bridged ferrocene oligomers, $\mathbf{25_2^+}$, $\mathbf{64^+}$, and $\mathbf{64^{2+}}$, indicates that the ν_{max} shift is dependent not only on the parameters in the Marcus–Hush theory but also on the nature of the solvent as donor or acceptor (**92**).

Strong MLCT bands appear in the neutral form of azo-bridged ferrocene oligomers, as noted above. The absorption of the MLCT band at 534 nm diminishes, and a new band appears and increases at 672 nm with the oxidation to $\mathbf{25^+}$. The new band can be assigned to a ligand-to-

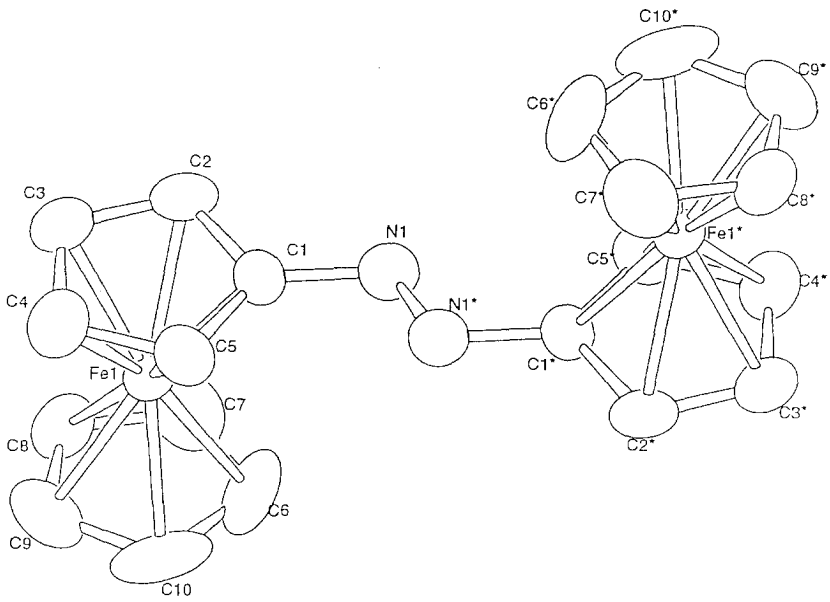

FIG. 5. ORTEP drawing of azoferrocene (**25**) with a probability level of 50%. Selected bond length (Å) and angles (°): Fe1–Cl 2.039(8), Fe1–C2 2.059(8), Fe1–C3 2.072(10), Fe1–C4 2.06(1), Fe1–C5 2.050(8), Fe1–C6 2.05(1), Fe1–C7 2.06(1), Fe1–C8 2.041(9), Fe1–C9 2.031(10), Fe1–C10 2.025(10), C1–N1 1.43(1), N1–N1* 1.27(1), C2–C1–N1 120.8(7), C5–C1–N1 129.8(8), C1–N1–N1* 111.4(9). Fe–Fe distance is 6.8 Å. (Reprinted with permission from Ref. *92.*)

metal charge transfer (LMCT) band with an electron transfer from the π orbital of the azo group to an Fe(III) *d* orbital. Similar LMCT bands appear in the mixed valence state of trimers **63** and **64**. A more donating solvent affords the higher IT and LMCT energies of **25**, **63**, and **64** in the mixed-valence states, indicating a hole-transfer mechanism (*26*).

Recently, a photoisomerization reaction of azoferrocene was found to proceed in polar solvents such as benzonitrile and DMSO through both a π–π^* transition of the azo-group with a UV light (365 nm) and the MLCT transition with a green light (546 nm) (Fig. 6) (Scheme 1) (*153*). The quantum yields of the photo-isomerization reaction at 365 nm and 546 nm were estimated to be 0.002 and 0.03, respectively. The transformation into the *cis* form causes the higher field shift of Cp protons in the ^{1}H-NMR spectrum and an appearance of ν(N=N) at 1552 cm^{-1}. The *cis* form is greatly stabilized in polar media, and dilution of the polar solution of *cis*-**25** with less polar solvents resulted in a prompt recovery of the *trans* form.

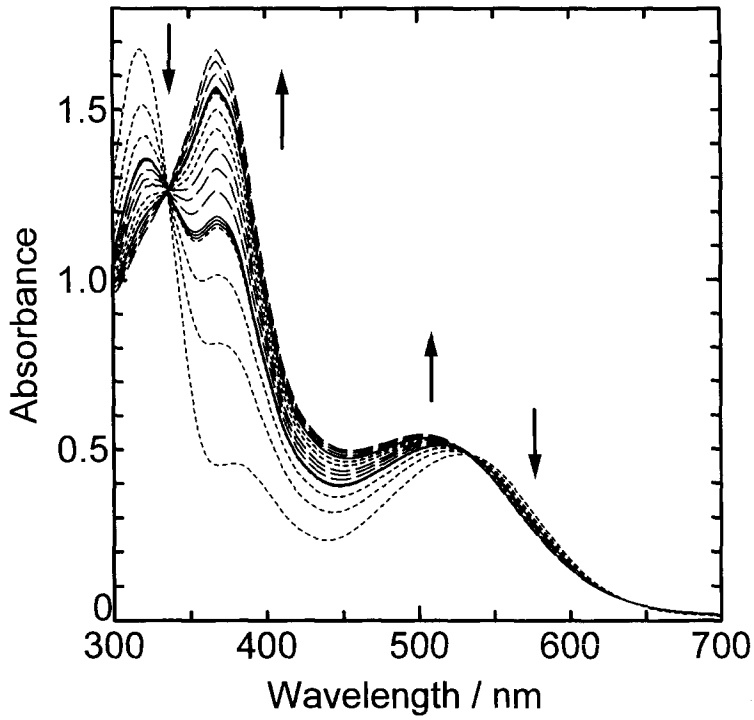

FIG. 6. UV–Vis absorption spectral change of *trans*-**25** (0.126 mM) in acetonitrile under a nitrogen atmosphere upon photoirradiation with three bright lines (λ_{max} = 365, 436, and 546, nm) of a super-high-pressure Hg lamp. The spectra are depicted at 10 min intervals of photoirradiation. The irradiation with each bright line was continued for 30 min in ascending order of wavelength. (Reprinted with permission from Ref. *153*.)

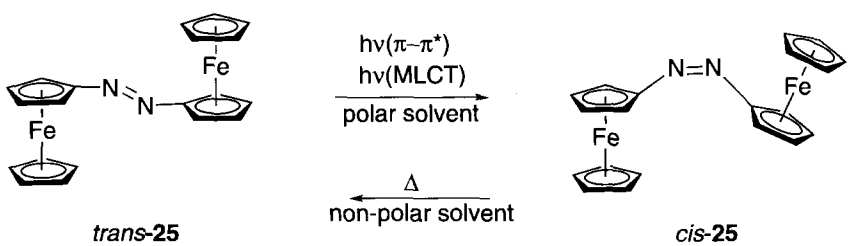

trans-**25** *cis*-**25**

SCHEME 1

Contrary to *trans*-azoferrocene, the *cis* form exhibits one-step $2e^-$ oxidation waves, and its oxidation potential, $E^{0'} = 0.03$ V in Bu_4NClO_4–benzonitrile, is more negative than that of the *trans* form ($E^{0'} = 0.29$ and 0.50 V *vs.* Ag/Ag^+) by 0.3 V. These data imply that the π-conjugation ability and electron-withdrawing nature of the azo group is retarded in the *cis* form.

IV. Ferrocene-Acceptor Conjugated Compounds

One of the interesting properties of ferrocene derivatives involving electron-accepting moieties is their second-order optical nonlinearity (*20*). Most of the accepting moieties in such ferrocene complexes investigated for their microscopic nonlinearity are organic moieties such as NO_2-, CN-, CHO-, or CO_2Me-substituted benzene, stilbene, or azobenzene derivatives (*158–161*), and there are only a few recent reports describing metal complexes acting both as acceptors and donors (*160–164*). Here the ferrocene-acceptor complexes for which redox properties have been reported are discussed.

Cationic ferrocene complexes with one, two, and four cationic [B(R)bpy] (bpy = 2, 2′-bipyridine) acceptors such as **66** show absorption at $\lambda_{max} = 496$–540 nm with the contribution of charge transfer between the ferrocene unit and the B(R)bpy substituent(s) (*165*). This is confirmed by the EPR spectrum of the monoreduced neutral species, which features a line shape indicating a considerable admixture of the ligand and metal orbitals. Preparation and physical properties of the related polymer, **67**, have also been reported (*166*).

The effects of metal-to-metal electronic coupling are observed for several complexes where a ferrocene moiety is bound to transition-metal complexes with a π-conjugated chain, **68** (*167*), **69** (*168*), and **70** (*169*). Tertiary amine–ferrocene conjugated molecules, **71**, show two-step $1e^-$ oxidation, and their monocationic forms exhibit strong LMCT bands at 600–700 nm (*170*).

Proton-coupled intramolecular electron transfer has been investigated for the quinonoid compounds linked to the ferrocene moiety by a π-conjugated spacer, **72** (*171*) and **75** (*172*). The complex **72** undergoes $2e^-$ oxidation in methanol to afford **74**, which consists of an unusual allene and a quinonoid structure, with the loss of two hydrogen atoms from **72** (Scheme 2). The addition of CF_3SO_3H to an acetonitrile solution of **74** results in two intense bands around 450 nm, characteristic of a semiquinone radical, and a weak broad band at 1000 nm in the electronic

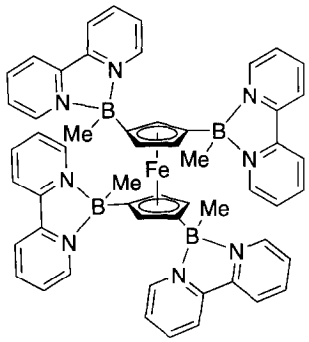

66

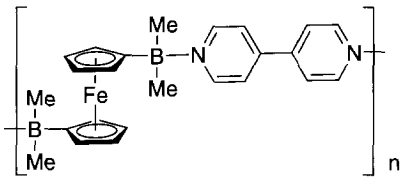

67

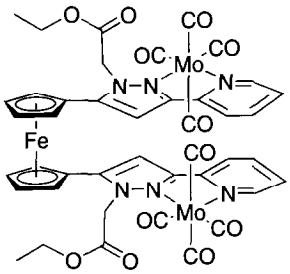

68

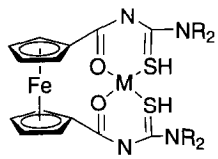

M = Ni(II), Cu(II), Co(II), Mn(II), Pt(II). Pd(II)

69

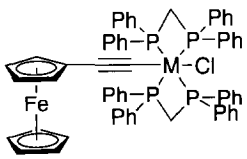

M = Ru, Os

70

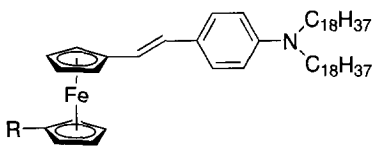

R = CH_2OH, CHO, $C{=}C(CN)_2$

71

spectrum and a well-resolved signal ($g_{\|} = 3.97, g_{\perp} = 1.64$) due to a ferrocenium cation, including paramagnetic Fe(III) nuclei in the EPR spectrum at 6.4 K. The structure of the protonated form is assignable to an ethylene-bridged ferrocenium cation-semiquinone, **73-1**, implying that the diamagnetic complex **74** can be converted into the paramagnetic

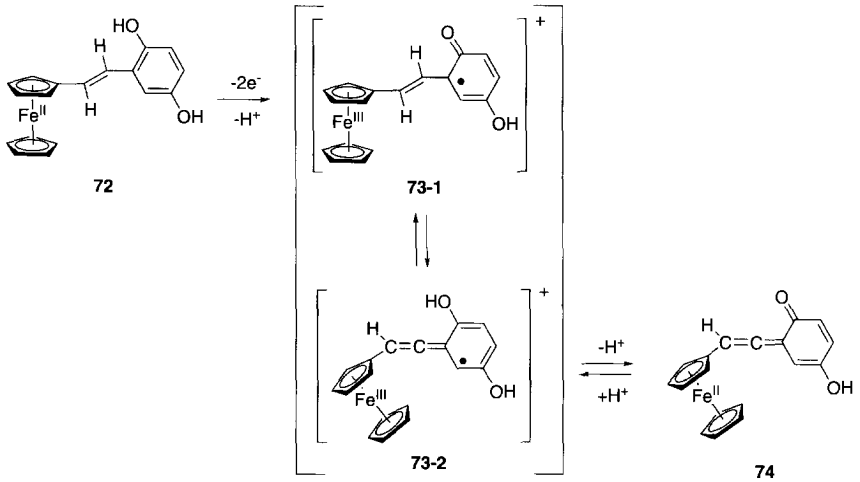

SCHEME 2

complex **73-1** by proton-coupled intramolecular electron transfer from the Fe(II) center in ferrocenyl sites to the quinonoid site of **74**.

Another ferrocene–quinone conjugated compound, **75**, undergoes a drastic structural rearrangement into the fulvene–cumulene structure by the proton-coupled intramolecular electron transfer from the ferrocene to the anthraquinone moiety (Scheme 3) (*172*). The X-ray crystallography of **75** shows that the cyclopentadienyl rings of the ferrocene moiety are perpendicular to the plane of the anthraquinone moiety, and the UV–Vis absorption spectrum in benzonitrile exhibits a specific absorption band at 510 nm assignable to the MLCT transition from the Fe(II) to the ethynyl–anthraquinone moiety. Addition of a stoichiometric amount of CF_3SO_3H to a benzonitrile solution of 1-FcAq causes a spectral change in which the MLCT band increases in intensity, and in which a new broad band with a half-width $\Delta\nu_{1/2} = 5.2 \times 10^3\ cm^{-1}$ appears in visible and near-IR regions ($\lambda_{max} = 939$ nm). The protonated complex of **75** is a diamagnetic complex involving a cumulene moiety, **76**. The deprotonated form, **75**, shows reversible two-step $1e^-$ reduction at $E^{0'} = -1.26$ and -1.71 V *vs.* ferrocene/ferrocenium derived from the anthraquinone moiety and reversible $1e^-$ oxidation at $E^{0'} = 0.22$ V due to the ferrocene moiety in Bu_4NClO_4–CH_2Cl_2. The first reduction potential shifts dramatically in the positive direction to $E^{0'} = -0.06$ V, and the oxidation potential shifts moderately in the positive direction to $E^{0'} = 0.33$ V in the protonation product, **76,** whereas the second reduction potential is little changed. These results correspond to the struc-

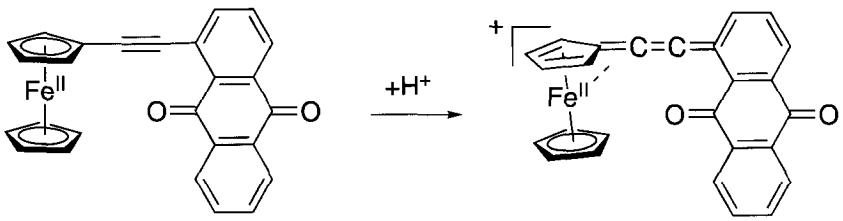

75 **76**

SCHEME 3

tural changes in both ferrocene and anthraquinone moieties by protonation.

The ferrocenyldiphynylpropargyl cation, **77**, has an intrinsic delocalization nature exhibiting a valence tautomerization band at 856 nm, and its nucleophilic trapping reactions give rise to the formation of ferrocenyldiphyenylallenes (*173*). The bis(acetylide) mixed-valence complexes of ferrocene and the Ru complex moiety, **78,** also behave as a fulvene–cumulene structure, **79,** showing a ν(M=C=C=C) band at 1985 cm^{-1} (*174*). Related alleylidene and cumulenylidene complexes of transition metals have been reviewed by Bruce (*175*).

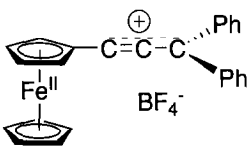

77

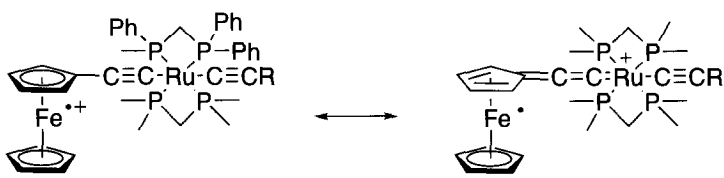

R = Ph, C_6H_4-4, $C_6H_4Me^{-4}$, $C_6H_4NO_2$-4, C_6H_3Me-3-NO_{2-4}, $C_6H_4NO_2^{-2}$

78 **79**

V. Concluding Remarks

In this review, recent studies on the fundamental properties, and especially redox behavior, of conjugated ferrocene systems have been surveyed. Various kinds of ferrocene dinuclear mixed-valence complexes have been synthesized and their physical properties investigated. To understand the intramolecular electron-transfer mechanism and dynamics in such complexes is important in elucidating fundamental concepts regarding the development of redox-based molecular devices. The next stage of research on the conjugated ferrocene systems should be to identify the intramolecular electronic events between multiple redox nuclei, to control internuclear electron transfer using external stimuli, and to combine the redox abilities of ferrocene. The studies of many researchers are advancing in these directions, as has been described in this review.

References

1. Kealy, T. J.; Pauson, P. L. *Nature* **1951**, *168*, 1039.
2. Miller, S. A.; Tebboth, J. A.; Tremaine, J. F. *J. Chem. Soc.* **1952**, 632.
3. Woodward, R. B.; Rosenblum, M.; Whiting, M. C. *J. Am. Chem. Soc.* **1952**, *74*, 3458.
4. Wilkinson, G. *J. Am. Chem. Soc.* **1952**, *74*, 6148.
5. Fisher, E. O.; Hafner, W. *Z. Naturforsch.* **1954**, *96*, 3.
6. Togni, A.; Hayashi, T. Eds.; "Ferrocenes," VCH Publishers, New York, **1995**.
7. Beer, P. D.; Cadman, J. *Coord. Chem. Rev.* **2000**, *205*, 131.
8. Butler, I. R. In "Organometallic Chemistry"; Abel, E.W., Ed.; Vol. 21, p. 338. Royal Society of Chemistry, Specialist Periodic Reports, **1992**.
9. Connelly, N. G.; Geiger, W. E. *Chem. Rev.* **1996**, *96*, 877.
10. Miller, J. S.; Epstein, A. J.; Reiff, W. M. *Chem. Rev.* **1988**, *88*, 201.
11. Joachim, C.; Gimzewski, J. K.; Aviram, A. *Nature* **2000**, *408*, 541.
12. Lauher, J. W.; Hoffmann, R. *J. Am. Chem. Soc.* **1976**, *98*, 1729.
13. Barlow, S.; Bunting, H. E.; Ringham, C.; Green, J. C.; Bublitz, G. U.; Boxer, S. G.; Perry, J. W.; Marder, S. R. *J. Am. Chem. Soc.* **1999**, *121*, 3715.
14. Coe, B. J.; Jones, C. J.; McCleverty, J. A.; Bloor, D.; Cross, G. H. *J. Organomet. Chem.* **1994**, *464*, 225.
15. Coe, B. J.; Foulon, J.-D.; Hamor, T. A.; Jones, C. J.; McCleverty, J. A.; Bloor, D.; Cross, G. H.; Axon, T. L. *J. Chem. Soc., Dalton Trans.* **1994**, 3427.
16. Neuse, E. W. *J. Macromol. Sci.-Chem.* **1981**, *A16*, 3.
17. Nishihara, H. In "Handbook of Organic Conductive Molecules and Polymers"; Nalwa, H.S., Ed.; Wiley, Chichester, **1997**; Vol. 2, pp. 799–832, and references therein.
18. Nguyen, P.; Gómez-Elipe, P.; Manners, I. *Chem. Rev.* **1999**, *99*, 1515, and references therein.
19. Hush, N. S. *Coord. Chem. Rev.* **1985**, *64*, 135, and references therein.
20. Barlow, S.; Marder, S. R. *Chem. Commun.* **2000**, 1555.
21. Omberg, K. M.; Chen, P. Y.; Meyer, T. J. *Adv. Chem. Phys.* **1999**, *106*, 553.

22. Brunschwig, B. S.; Creutz, C.; Sutin, N. *Coord. Chem. Rev.* **1998**, *177*, 61.
23. Vance, F. W.; Williams, R. D.; Hupp, J. T. *Int. Rev. Phys. Chem.* **1998**, *17*, 307.
24. Chen, P.; Meyer, T. J. *Chem. Rev.* **1998**, *98*, 1439.
25. Myers, A. B. *Chem. Rev.* **1996**, *96*, 911.
26. Creutz, C.; Newton, M. D.; Sutin, N. *J. Photochem. Photobiol. A: Chem.* **1994**, *82*, 47.
27. Hendrickson, D. N. In "Mixed Valence Systems: Applications in Chemistry, Physics and Biology"; Prassides, K., Ed.; NATO ASI Series, Kluwer, Dordrecht, **1991**; pp. 67–90.
28. Nishihara, H. *Bull. Chem. Soc. Jpn.* **2001**, *74*, 19.
29. Kaufman, F.; Cowan, D. O. *J. Am. Chem. Soc.* **1970**, *92*, 6197.
30. Robin, M. B.; Day, P. *Adv. Inorg. Chem. Radiochem.* **1967**, *10*, 247.
31. McManis, G. E.; Gochev, A.; Nielson, R. M.; Weaver, M. J. *J. Phys. Chem.* **1989**, *93*, 7733.
32. Lowey, M. D.; Hammack, W. S.; Drickamer, H. G.; Hendrickson, D. N. *J. Am. Chem. Soc.* **1987**, *109*, 8019.
33. Masuda, A.; Masuda, Y.; Fukuda, Y. *J. Phys. Chem. A* **1997**, *101*, 2245.
34. Dong, T.-Y.; Ho, P.-H.; Lai, X.-Q.; Lin; Z.-W.; Lin, K.-J. *Organometallics* **2000**, *10*, 1096.
35. Dong, T.-Y.; Chang, C.-K.; Cheng, C.-H.; Lin, K.-J. *Organometallics* **1999**, *18*, 1911.
36. Nakashima, S.; Kai, M.; Watanabe, M. *Inorg. Chem. Commun.* **1999**, *2*, 341.
37. Nakashima, S.; Oda, T.; Okuda, T.; Watanabe, M. *Inorg. Chem.* **1999**, *38*, 4005.
38. Nakashima, S.; Hori, A.; Sakai, H.; Watanabe, M.; Motoyama, I. *J. Organomet. Chem.* **1997**, *542*, 271.
39. Dong, T.-Y.; Lee, S.-H.; Lee, T.-Y. *Organometallics* **1996**, *15*, 2354, and references therein.
40. Nakashima, S.; Ueki, Y.; Sakai, H.; Maeda, Y. *J. Chem. Soc., Dalton Trans.* **1996**, 139.
41. Dong, T.-Y.; Huang, C.-H.; Chang, C.-K.; Hsieh, H.-C.; Peng, S.-M.; Lee, G.-H. *Organometallics* **1995**, **14**, 1776.
42. Dong, T.-Y.; Lee, S.-H.; Chang, C.-K.; Lin, K.-J. *J. Chem. Soc., Chem. Commun.* **1995**, 2453.
43. Dong, T.-Y.; Lee, T.-Y.; Lee, S.-H.; Lee, G.-H.; Peng, S.-M. *Organometallics*, **1994**, *13*, 2337.
44. Nakashima, S.; Masuda, Y.; Motoyama, I.; Sano, H. *Bull. Chem. Soc. Jpn.* **1987**, *60*, 1673.
45. Dong, T. Y.; Kambara, T.; Hendrickson, D. N. *J. Am. Chem. Soc.* **1986**, *108*, 5857.
46. Dong, T. Y.; Kambara, T.; Hendrickson, D. N. *J. Am. Chem. Soc.* **1986**, *108*, 4423.
47. Dong, T. Y.; Hendrickson, D. N.; Pierpoint, C. G.; Moore, M. F. *J. Am. Chem. Soc.* **1985**, *107*, 4777.
48. Kramer, J. A.; Hendrickson, D. N. *Inorg. Chem.* **1980**, *19*, 3330.
49. LeVanda, C.; Bechgaard, K.; Cowan, D. O.; Mueller-Westerhoff, U. T.; Elbracht, P.; Candela, G. A.; Collins, R. L. *J. Am. Chem. Soc.* **1976**, *98*, 3181.
50. Morrison W. H.; Hendrickson, D. N. *Inorg. Chem.* **1975**, *14*, 2331.
51. Morrison, W. H.; Hendrickson, D. N. *J. Chem. Phys.* **1974**, *59*, 380.
52. Cowan, D. O.; Collins, R. L.; Kaufman, F. *J. Phys. Chem.* **1971**, *75*, 2025.
53. Cowan, D. O.; Candela, G. A.; Kaufman, F. *J. Am. Chem. Soc.* **1971**, *93*, 3889.
54. Boukheddaden, K.; Linares, J.; Bousseksou, A.; Nasser, J.; Rabah, H.; Varret, F. *Chem. Phys.* **1993**, *170*, 47.
55. Nakano, M.; Sorai, M.; Hagen, P. M.; Hendrickson, D. *Chem. Phys. Lett.* **1992**, *196*, 486.
56. Neuse, E. W. *J. Macromol. Sci.-Chem.* **1981**, *A16*, 3.
57. Sanechika, K.; Yamamoto, T.; Yamamoto, A. *Polym. J.* **1981**, *13*, 255.

58. Neuse, E. W.; Bednarik, L. *Transition Metal Chem.* **1979**, *4*, 87.
59. Neuse, E. W.; Bednarik, L. *Macromolecules* **1979**, *12*, 187.
60. Hirao, T.; Kurashina, M.; Aramaki, K.; Nishihara, H. *J. Chem. Soc., Dalton Trans.* **1996**, 2929.
61. Clough, R. L.; Mison, P.; Roberts, J. D. *J. Org. Chem.* **1976**, *41*, 2252.
62. Kretchmer, R. A.; Glowinski, R. *J. Org. Chem.* **1976**, *41*, 2661.
63. Clough, R. L.; Mison, P.; Roberts, J. D. *J. Org. Chem.* **1976**, *41*, 2252.
64. Brown, G. M.; Meyer, T. J.; Cowan, D. O.; LeVanda, C.; Kaufman, F.; Roling, P. V.; Rausch, M. D. *Inorg. Chem.* **1975**, *14*, 506.
65. Cowan, D. O.; Park, J.; Pittman, Jr, C. U.; Sasaki, Y.; Mukherjee, T. K.; Diamond, N. A. *J. Am. Chem. Soc.* **1972**, *94*, 5110.
66. Pittman, Jr, C. U.; Sasaki, Y. *Chem. Lett.* **1975**, 383.
67. Nishihara, H.; Kurashina, M.; Aramaki, K.; Kubo, K. *Synth. Metals* **1999**, *101*, 457.
68. Böhm, M. C. *J. Chem. Phys.* **1984**, *80*, 2704.
69. Dong, T.-Y.; Lee, W.-Y.; Su, P.-T.; Chang, L.-S.; Lin, K.-J. *Organometallics* **1998**, *17*, 3323.
70. Oyama, N.; Takizawa, Y.; Matsuda, H.; Yamamoto, T.; Sanechika, K. *Denki Kagaku* **1988**, *56*, 781.
71. Rausch, M. D. *Pure Appl. Chem.* **1972**, *30*, 523.
72. Rolling, P. V.; Rausch, M. D. *J. Organomet. Chem.* **1977**, *141*, 195.
73. Sutton, J. E.; Sutton, P. M.; Taube, H. *Inorg. Chem.* **1979**, *18*, 1017.
74. Evans, C. E. B.; Naklicki, M. L.; Rezvani, A. R.; White, C. A.; Kondratiev, V. V.; Crutchley, R. J. *J. Am. Chem. Soc.* **1998**, *120*, 13096.
75. Aoki, K.; Chen, J. *J. Electroanal. Chem.* **1995**, *380*, 35.
76. Nishihara, H.; Hirao, T.; Aramaki, K.; Aoki, K. *Synth. Metals* **1997**, *84*, 935.
77. Aoki, K.; Chen, J.; Nishihara, H.; Hirao, T. *J. Electroanal. Chem.* **1996**, *416*, 151.
78. Hirao, T.; Aramaki K.; Nishihara, H. *Bull. Chem. Soc. Jpn.* **1998**, *71*, 1817.
79. Wolf, M. O.; Wrighton, M. S. *Chem. Mater.* **1994**, *6*, 1526.
80. Ito, T.; Hamaguchi, T.; Nagino, H.; Yamaguchi, T.; Washington, J.; Kubiak, C. P. *Science* **1997**, *277*, 660.
81. Ito, T.; Hamaguchi, T.; Nagino, H.; Yamaguchi, T.; Kido, H.; Zavarine, I. S.; Richmond, T.; Washington, J.; Kubiak, C. P. *J. Am. Chem. Soc.* **1999**, *121*, 4625.
82. Rezvani, A. R.; Bensimon, C.; Cromp, B.; Reber, C.; Greedan, J. E.; Kondratiev, V. V.; Crutchley, R. J. *Inorg. Chem.* **1997**, *36*, 3322.
83. Nishihara, H.; Horikoshi, T. *Synth. Metals* **1999**, *102*, 1523.
84. Horikoshi, T.; Kubo, K.; Nishihara, H. *J. Chem. Soc., Dalton Trans.* **1999**, 3355.
85. Colbert, M. C. B.; Hodgson, D.; Lews, J.; Raithby, P. R.; Long, N. J. *Polyhedron* **1995**, *14*, 2759.
86. Templeton, A. C.; Wuelfing, W. P.; Murray, R. W. *Acc. Chem. Res.* **2000**, *33*, 27, and references therein.
87. Horikoshi, T.; Itoh, M.; Kurihara, M.; Kubo, K.; Nishihara, H. *J. Electroanal. Chem.* **1999**, *473*, 113.
88. Kurihara, M.; Kubo, K.; Horikoshi, T.; Kurosawa, M.; Nankawa, T.; Matsuda, T.; Nishihara, H. *Macromol. Symp.* **2000**, *156*, 21.
89. Kubo, K.; Kondow H.; Nishihara, H. *Electrochemistry* **1999**, *67*, 1129.
90. Ribou, A.-C.; Launay, J.-P.; Sachtleben, M. L.; Li, H.; Spangler, C. W. *Inorg. Chem.* **1996**, *35*, 3735.
91. Rosenblum, M.; Brown, N.; Papenmeier, J.; Applebaum, M. *J. Organomet. Chem.* **1966**, *6*, 173.

92. Kurosawa, M.; Nankawa, T.; Matsuda, T.; Kubo, K.; Kurihara, M.; Nishihara, H. *Inorg. Chem.* **1999**, *38*, 5113.
93. Levanda, C.; Bechgaard, K.; Cowan, D. O. *J. Org. Chem.* **1976**, *41*, 2700.
94. Jutzi, P.; Kleinebekel, B. *J. Organomet. Chem.* **1997**, *545–546*, 573.
95. Nielson, R. M.; Lyon, L. A.; Hupp, J. T. *Inorg. Chem.* **1996**, *35*, 970.
96. Patoux, C.; Coudret, C.; Launay, J. P.; Joachim, C.; Gourdon, A. *Inorg. Chem.* **1997**, *36*, 5037.
97. Iyoda, M.; Okabe, T.; Katada, M.; Kuwatan, Y. *J. Organomet. Chem.* **1998**, *569*, 225.
98. Bryce, M. R.; Coffin, M. A.; Skabara, P. J.; Moore, A. J.; Batsanov, A. S.; Howard, J. A. K. *Chem. Eur. J.* **2000**, *6*, 1955.
99. Osborne, A. G.; da Silva, M. W.; Hursthouse, M. B.; Malik, K. M. A.; Opromolla, G.; Zanello, P. *J. Organomet. Chem.* **1996**, *516*, 167.
100. Molina, P.; Pastor, A.; Vilaplana, M. J.; Velasco, M. D.; de Arellano, M. C. R. *Organometallics* **1997**, *16*, 5836.
101. Ferguson, G.; Glidewell, C.; Opromolla, G.; Zakaria, C. M.; Zanello, P. *J. Organomet. Chem.* **1996**, *517*, 183.
102. Salazar, D.C.O.; Cowan, D. O. *J. Organomet. Chem.* **1991**, *408*, 227.
103. Rulkens, R.; Gates, D. P.; Balaishis, D.; Pudelski, J. K.; McIntosh, D. F.; Lough, A. J.; Manners, I. *J. Am. Chem. Soc.* **1997**, *119*, 10976.
104. Colbert, M. C. B.; Lewis, J.; Long, N. J.; Raithby, P. R.; White, A. J. P.; Williams, D. J. *J. Chem. Soc., Dalton Trans.* **1997**, 99.
105. Jones, N. D.; Wolf, M. O.; Giaquinta, D. M. *Organometallics* **1997**, *16*, 1352.
106. Atzkern, H.; Bergerat, P.; Beruda, H.; Fritz, M.; Hiermeier, J.; Hudeczek, P.; Kahn, O.; Köhler, F. H.; Paul, M.; Weber, B. *J. Am. Chem. Soc.* **1995**, *117*, 997.
107. Yu, Z.; Zhou, Y.; Yang, W.; Tian, Y.; Duan, C.; Liu, R.; You, X. *Chem. Lett.* **1996**, 957.
108. Ohkubo, A.; Fujita, T.; Ohba, S.; Aramaki, K.; Nishihara, H. *J. Chem. Soc., Chem. Commun.* **1992**, 1553.
109. Shimada, H. MS thesis, Keio University, Japan, **1997**.
110. Yamada, Y.; Muzutani, J.; Masato, K.; Nishihara, H.; *J. Organomet. Chem.*, **2001**, *637–639*, 80.
111. Shimura, T.; Ohkubo, A.; Matsuda, N.; Matsuoka, I.; Aramaki, K.; Nishihara, H. *Chem. Mater.* **1996**, *8*, 1307, and references therein.
112. McAdam, C. J.; Duffy, N. W.; Robinson, B. H.; Simpson, J. *Organometallics* **1996**, *15*, 3935.
113. Boyd, P. D. W.; Burrell, A. K.; Campbell, W. M.; Cocks, P. A.; Gordon, K. C.; Jameson, G. B.; Officer, D. L.; Zhao, Z. *Chem. Commun.* **1999**, 637.
114. Bildstein, B.; Malaun, M.; Kopacka, H.; Fontani, M.; Zanello, P. *Inorg. Chim. Acta* **2000**, *300–302*, 16.
115. Butler, I. R.; Griesbach, U.; Zanello, P.; Fontani, M.; Hibbs, D.; Hursthouse, M. B.; Malik, K. L. M. A. *J. Organomet. Chem.* **1998**, *565*, 243.
116. Duan, C.-Y.; Tian, Y.-P.; Liu, Z. H.; You, X.-Z.; Mak, T. C. W. *J. Organomet. Chem.* **1998**, *570*, 155.
117. Hall, C. D.; Sachsinger, N.; Nyburg, S. C.; Steed, J. W. *J. Organomet. Chem.* **1998**, *561*, 209
118. Sato M.; Anano, H. *J. Organomet. Chem.* **1998**, *555*, 167.
119. Padilla-Tosta, M. E.; Martínez-Máñez, R.; Soto, J.; Lioris, J. M. *Tetrahedron* **1998**, *54*, 12039.
120. Müller, T. J. J. *J. Organomet. Chem.* **1999**, *578*, 95.
121. Barranco, E. M.; Crespo, O.; Gimeno, M. C.; Jones, P. G.; Laguna, A.; Villacampa, M. D. *J. Organomet. Chem.* **1999**, *592*, 258.

122. Zanello, P.; de Biani, F. F.; Glidewell, C.; Koenig, J.; Marsh, S. J. *Polyhedron* **1998**, *17*, 11.
123. Schebler, P. J.; Riordan, C. G.; Liable-Sands, L.; Rheingold, A. L. *Inorg. Chim. Acta* **1998**, *270*, 543.
124. McAdam, C. J.; Duffy, N. W.; Robinson, B. H.; Simpson, J. *J. Organomet. Chem.* **1997**, *527*, 179.
125. López, C.; Bosque, R.; Solans, X.; Font-Bardía, M. *J. Organomet. Chem.* **1997**, *535*, 99.
126. Barlow, S.; Murphy, V. J.; Evans, J. S. O.; O'Hare, D. *Organometallics* **1995**, *14*, 3461.
127. Zanello, P.; Opromolla, G.; Herberhold, M.; Brendel, H.-D. *J. Organomet. Chem.* **1994**, *484*, 67.
128. Bildstein, B.; Denifl, P.; Wurst, K.; André M.; Baumgarten, M.; Friedrich, J.; Ellmerer-Müller, E. *Organometallics* **1995**, *14*, 4334.
129. Bildstein, B.; Kopacka, H.; Schweiger, M.; Ellmerer-Müller, E.; Ongaina, K.-H.; Wurst, K. *Organometallics* **1996**, *15*, 4398.
130. Bildstein, B.; Schweiger, M.; Kopacka, H.; Wurst, K. *J. Organomet. Chem.* **1998**, *553*, 73.
131. Bildstein, B.; Schweiger, M.; Kopacka, H.; Ongaina, K.-H.; Wurst, K. *Organometallics* **1998**, *17*, 2414.
132. Bildstein, B.; Schweiger, M.; Angleitner, H.; Kopacka, H.; Wurst, K.; Ongaina, K.-H.; Fontani, M.; Zanello, P. *Organometallics* **1999**, *18*, 4286.
133. MacLachlan, M. J.; Lough, A. J.; Geiger, W. E.; Manners, I. *Organometallics* **1998**, *17*, 1873.
134. MacLachlan, M. J.; Zheng, J.; Thieme, K.; Lough, A. J;. Manners, I.; Mordas, C.; LeSuer, R.; Geiger, W. E.; Liable-Sands, L. M.; Rheingold, A. L. *Polyhedron* **2000**, *19*, 275.
135. Plenio, H.; Hermann, J.; Sehring, A. *Chem. Eur. J.* **2000**, *6*, 1820.
136. Arnold, R.; Matchett, S. A.; Rosenblum, M. *Organometallics* **1988**, *7*, 2261.
137. Morikita, T.; Maruyama, T.; Yamamoto, T.; Kubota, K.; Katada, M. *Inorg. Chim. Acta* **1998**, *269*, 310.
138. Yamamoto, T.; Morikata, T.; Maruyama, T.; Kubota, K.; Katada, M. *Macromolecules* **1997**, *30*, 5390.
139. Southard, G. E.; Curtis, M. D. *Organometallics* **1997**, *16*, 5618.
140. Higgins, S. J.; Jones, C. L.; Francis, S. M. *Synth. Metals* **1999**, *98*, 211.
141. Casado, C. M.; Cuadrado, I.; Morán, M.; Alonso, G.; García, B.; González, B.; Losada, J. *Coord. Chem. Rev.* **1999**, *185–186*, 53, and references therein.
142. Nlate, S.; Ruiz, J.; Blais, J.-C.; Astruc, D. *Chem. Commun.* **2000**, 417.
143. Shu, C.-F.; Shen, H.-M. *J. Mater. Chem.* **1997**, *7*, 47.
144. Foucher, D. A.; Tang, B.-Z.; Manners, I. *J. Am. Chem. Soc.* **1992**, *114*, 6246.
145. Manners, I. *Chem. Commun.* **1999**, 857, and references therein.
146. Foucher, D. A.; Ziembinski, R.; Peterson, R.; Pudelski, J.; Edwards, M.; Ni, Y.; Massey, J.; Jaeger, C. R.; Vancso, G. J.; Manners, I. *Macromolecules* **1994**, *27*, 3992.
147. Foucher, D. A.; Honeyman, C. H.; Nelson, J. M.; Tang, B. Z.; Manners, I. *Angew. Chem. Int. Ed. Engl.* **1993**, *32*, 1709.
148. Pudelski, J. K.; Manners, I. *J. Am. Chem. Soc.* **1995**, *117*, 7265.
149. Withers, Jr, H. P.; Seyferth, D.; Fellmann, J. E.; Garrou, P. E.; Martin, S. *Organometallics* **1982**, *1*, 1283.
150. Rulkens, R.; Lough, A. L.; Manners, I.; Lovelace, S. R.; Grant, C.; Geiger, W. E. *J. Am. Chem. Soc.* **1996**, *118*, 12683.
151. Nesmeyanov, A. N.; Perevalova, E. G.; Nikitina, T. V. *Dokl. Adad. Nauk SSSR* **1961**, *138*, 118.

152. Nesmeyanov, A. N.; Sazonova, V. A.; Romanenko, V. I. *Dokl. Adad. Nauk SSSR* **1961**, *157*, 922.
153. Kurihara, M.; Matsuda, T.; Hirooka, A.; Yutaka, T.; Nishihara, H. *J. Am. Chem. Soc.* **2000**, *122*, 12373.
154. Delgado-Pena, F.; Talham, D. R.; Cowan, D. O. *J. Organomet. Chem.* **1983**, *253*, C43.
155. Powers, M. J.; Meyer, T. J. *J. Am. Chem. Soc.* **1978**, *100*, 4393.
156. McManis, G. E.; Gochev, A.; Nielson, R. M.; Weaver, M. J. *J. Phys. Chem.* **1989**, *93*, 7733.
157. Blackbourn, R. L.; Hupp, J. T. *J. Phys. Chem.* **1990**, *94*, 1788.
158. Green, M. L.; Marder, S. R.; Thomson, M. E.; Bandy, J. E.; Bloor, D.; Kolinsy, P. V.; Jones, R. J. *Nature* **1987**, *330*, 360.
159. Blanchard-Desce, M.; Runser, C.; Fort, A.; Barzoukas, M.; Lehn, J. M.; Bloy, V.; Alain, V. *Chem. Phys.* **1995**, *199*, 253.
160. Balavoine, G. G. A.; Daran, J. C.; Iftime, G.; Lacroix, P. G.; Manoury, E.; Delaire, J. A.; Maltey-Fanton, I.; Nakatani, K.; Di Bella, S. *Organometallics* **1999**, *18*, 21.
161. Lee, I. S.; Seo, H.; Chunk, Y. K. *Organometallics* **1999**, *18*, 1091.
162. Calabrese, C. J.; Cheng, L. T.; Green, J. C.; Marder, S. R.; Tam, W. *J. Am. Chem. Soc.* **1991**, *113*, 7227.
163. Coe, B. J.; Houbrechts, S.; Asselberghs, I.; Persoons, A. *Angew. Chem. Int. Ed. Engl.* **1999**, *38*, 366.
164. Jayaprakash, K. N.; Ray, P. C.; Matsuoka, I.; Bhadbhade, M. M.; Puranik, V. G.; Das, P. K.; Nishihara, H.; Sarkar, A. *Organometallics*, **1999**, *18*, 3851.
165. de Biani, F. F.; Gmeinwieser, T.; Herdtweck, E.; Jäkle, F.; Laschi, F.; Wagner, M.; Zanello, P. *Organometallics* **1997**, *16*, 4776.
166. Fontiani, M.; Peters, F.; Scherer, W.; Wachter, W.; Wagner, M.; Zanello, P. *Eur. J. Inorg. Chem.* **1998**, 1453.
167. Thiel, W. R.; Priermeier, T.; Fiedler, D. A.; Bond, A. M.; Mattner, M. R. *J. Organomet. Chem.* **1996**, *514*, 137.
168. Seidelmann, O.; Beyer, L. *Polyhedron* **1998**, *17*, 1601.
169. Colbert, M. C. B.; Ingham, S. L.; Lews, J.; Long, N. J.; Raithby, P. R. *J. Chem. Soc., Dalton Trans.* **1994**, 2215.
170. Chai, X. D.; Jang, W. S.; Yang, W. S.; Zhang, D.; Lu, R.; Lu, N.; Cao, Y. W.; Li, T. J. *Supramol. Sci.* **1998**, *5*, 479.
171. Kurihara, M.; Sano, H.; Murata, M.; Nishihara, H. *Inorg. Chem.* **2001**, *40*, 4.
172. Murata, M.; Fujita, T.; Yamada, M.; Kurihara, M.; Nishihara, H. *Chem. Lett.* **2000**, 1328.
173. Ansorge, M.; Polborn, K.; Müller, T. J. J. *Eur. J. Inorg. Chem.* **2000**, 2003.
174. Colbert, M. C. B.; Lewis, J.; Long, N. J.; Raithby, P. R.; White, A. J. P.; Williams, D. J. *J. Chem. Soc., Dalton Trans.* **1997**, 99.
175. Bruce, M. I. *Chem. Rev.* **1998**, *98*, 2797.
176. Bard, A. J.; Faulkner, L. R. "Electrochemical Methods, Fundamentals and Applications"; Wiley, New York, **1980**.

NEW ASPECTS OF METAL–NUCLEOBASE CHEMISTRY

ANDREW HOULTON

Department of Chemistry, University of Newcastle upon Tyne,
Newcastle upon Tyne, NE1 7RU, United Kingdom

I. Introduction

It is now almost 50 years since the structure of DNA was elucidated by Watson and Crick (*1*) (Fig. 1). Since then the double helix has become an icon for modern scientific achievement. With the rapid growth of molecular biology and the consequent success of the human genome project (*2*) we are now firmly in a post-genomic era. However, in spite of, or perhaps because of this, efforts to understand fundamental aspects of metal–ion interactions with DNA continue to be vigorously pursued.

At present the best understood metal-ion interactions with DNA are those involving the platinum drugs, e.g., *cis*-$[PtCl_2(NH_3)_2]$ (*3–5*). In such cases the metal–ion binding generates 1,2-intrastrand adducts which are formed predominantly at the N7 site of guanine in GG sequences (Fig. 2) (*3,6,7*). Research into metal-containing anti-tumor drugs is extremely active (*8*), with the synthesis of new lead compounds (*9–11*), investigations into the molecular mode of action (*12–16*), and

0898-8838/02 $35.00

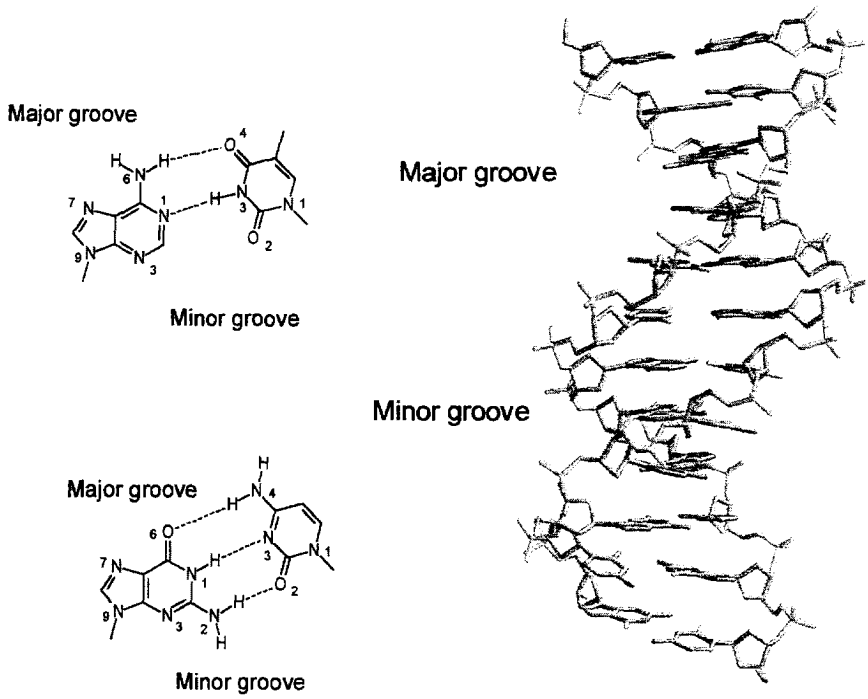

FIG. 1. Duplex DNA indicating the locations of the major and minor grooves and their relationship to the Watson–Crick base pairs.

new strategies for drug development such as high throughput screening of libraries are all being explored (*17,18*). The synthesis of new complexes including, e.g., polynuclear platinum drugs $[(trans\text{-}PtCl(NH_3)_2)_2\{\mu\text{-}trans\text{-}Pt(NH_3)_2(NH_2(CH_2)_6NH_2)_2\}]^{4+}$, is another expanding area (*19–22*). The complexes of other metals such as ruthenium (*10,11*) and titanium (*23*) are also being considered as alternatives to platinum, and the first of these, as $[RuCl_4(dmso)(Imidazole)][ImidazoleH]$, has now entered clinical trials (*24*). However, since metallo-drug DNA chemistry is frequently reviewed and often dominated by G–N7 interactions, only a few selected examples from this field are included here.

Instead, this review seeks to cover less well-known and newly emerging aspects of metal–nucleobase chemistry. In addition to biomedical relevancies, nucleic acid chemistry offers a paradigm for organizing molecules via base pairing. Combining the hydrogen bonding

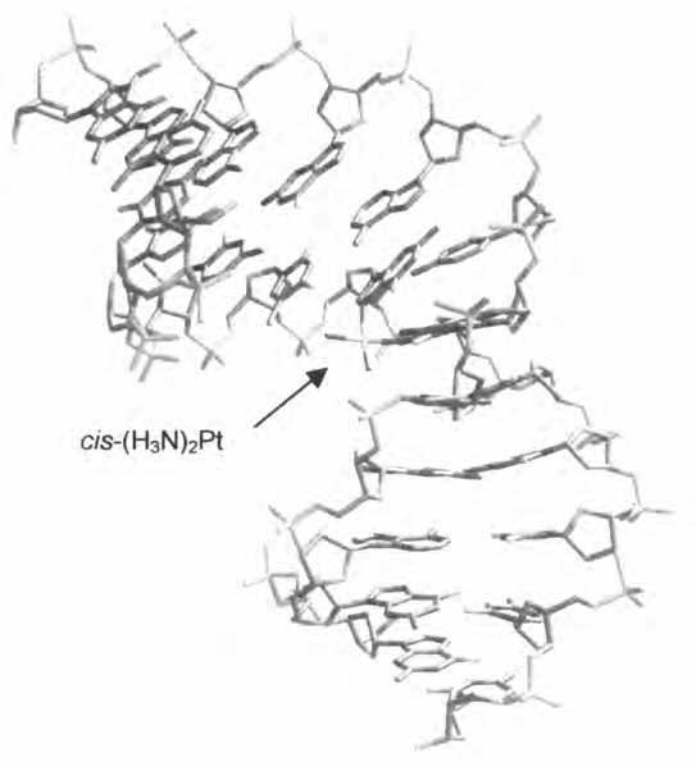

FIG. 2. Molecular structure of the major *cis*-platin–DNA adduct (*6*).

capabilities of nucleobases with their ability for metal–ion binding is increasingly exploited as a basis for building varied molecular architectures. The plethora of binding modes for these nitrogenous heterocycles, adenine (A), guanine (G), thymine/uracil (T/U), and cytosine (C), gives rise to an extensive variety of complexes, including metal–metal bonded species, and discrete macromolecules and polymers. Metal ions, in the form of appended complexes, have been used to introduce site-specific redox- and photo-active centers in DNA and address questions concerning charge transport (*25*). The possibility for DNA nanotechnology, including DNA-based molecular electronics, is frequently advocated and different strategies have emerged to take advantage of the molecules' unique properties (*26,27*). In this area, too, the involvement of metal ions is important.

II. Metal–Nucleobase Binding

A. Metal–Nucleobase N– and O– Interactions

Very recently the *trans*-$[Pt(NH_3)_2Cl_2]$ isomer has been shown to promote the formation of some highly unusual multiple strand nucleic acid structures (*28*). A parallel-stranded DNA duplex, psPtDNA, has been prepared which incorporates a *trans*-$Pt(NH_3)_2^{2+}$ crosslink. The platinated strands were synthesized through the series of reactions illustrated in Fig. 3. The initial mono-functional G–N7 adduct is formed at pH 3.5 by addition of *trans*-$[Pt(NH_3)_2(H_2O)Cl]^+$ to the pyrimidine-rich sequence 5′-d(T_4CT_4G). After the pH is increased, normal anti-parallel duplex formation occurs upon addition of the complementary purine-rich strand, 5′-d(A_4GA_4G). This intermediate anti-parallel stranded

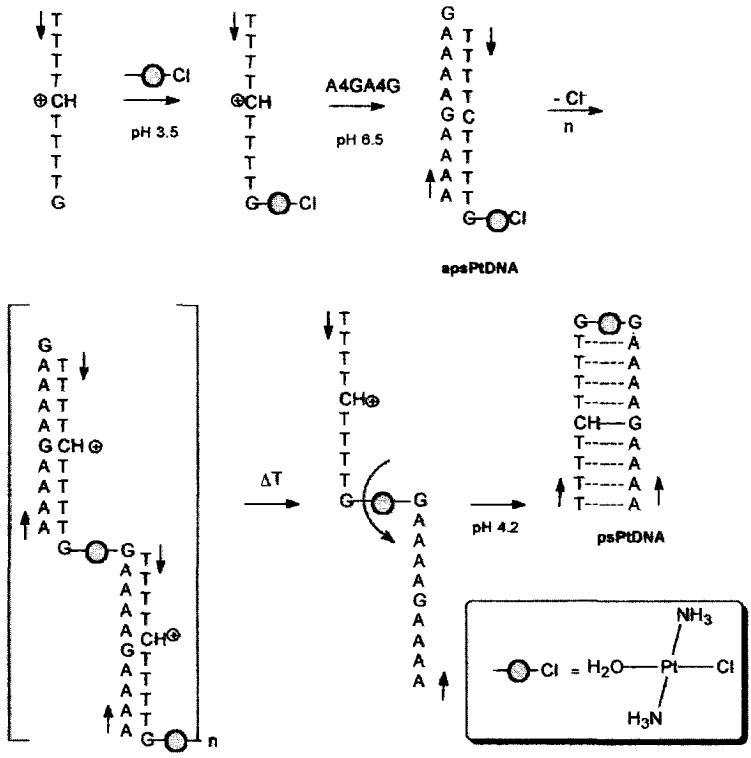

FIG. 3. Reaction scheme for the preparation of platinated parallel DNA (psPtDNA). Adapted from Ref. (*28*).

DNA, apsPtDNA, contains an overhanging G-residue that undergoes preferential inter-duplex crosslinking (4°C over a period of 2 months) to form 3′-crosslinked complementary strands. Duplex melting and intramolecular hybridization at pH 4.2 leads to the formation of parallel stranded DNA, psPtDNA.

CD spectroscopy of the psPtDNA duplex at pH 4.2 indicates the formation of Hoogsteen base pairs. For the GC pair this requires protonation of C–N3, which is consistent with the low pH conditions required. At higher pH (6.5) a range of different conformations is suggested. The parallel stranded duplex, psPtDNA, is more stable than the anti-parallel analogue ($T_m = 21°C$ *vs.* 35°C). The Hoogsteen-paired psPtDNA duplex undergoes hybridization to form a triplex structure that exhibits unusual reversed melting behavior, with the Watson–Crick (WC) duplex melting before the Hoogsteen. This effect can be explained by the stabilizing effect of the Pt-crosslink on the latter. A further interesting property of psPtDNA is the observed concentration dependence that indicates the formation of a homodimer at higher concentrations (dimer:monomer ratios 60:40, 40:60, and 0:100% at 2.0, 0.5, and 0.05 μM, respectively). While several structural possibilities for a homodimer exist (Fig. 4), the most probable is a quadruple helix. Hydrogen bonding patterns that are compatible with quadruplex formation are available and are shown in Fig. 5.

The use of metallo-based crosslinking of DNA strands is increasingly considered for enhancing antisense and antigene strategies whereby an irreversible interaction is formed following hybridization (Fig. 6) (*29*). This is aimed to address the significant problem that adducts of DNA probe oligomers and the target DNA or RNA do not survive replication and transcription events. *Trans*-$(NH_3)_2Pt^{II}$-modified DNA oligomers have been shown to be capable of forming such crosslinked DNA duplex with target strands (*30*). The platinated-labeled antisense strand was prepared by reaction with a pyrimidine-rich 12-mer containing a single terminal G residue, 5′-d($GT_2C_2T_2C_2T_2C$). Hybridization reactions with the d($GA_2G_2A_2G_2A_2G$) oligomer analyzed by HPLC, ESMS, and ^{1}H NMR indicated three major species, all of which contained G–Pt–G interstrand crosslinks. From these studies some general principles for the design of Pt-based antisense molecules emerge: (i) the need for a minimum length of sequence for recognition; (ii) the terminal-Pt group seems to be superior for crosslinking; (iii) for post-synthetic platination of the antisense strand a sequence containing a single G-residue facilitates preparation.

The design of site-specific reagents has obvious benefits in the preparation of platinum-modified strands. The sterically crowded mono-

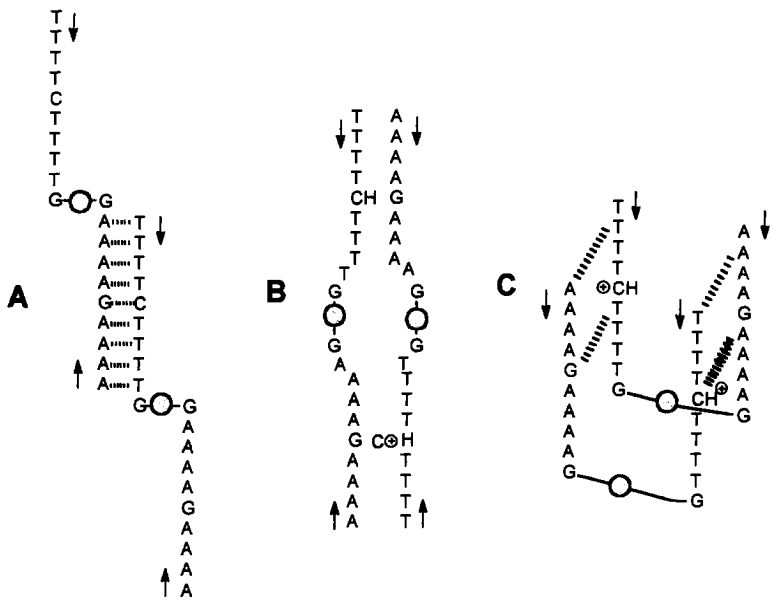

FIG. 4. Possible homo-dimers of psPtDNA: (**A**) antiparallel duplex, (**B**) parallel duplex, (**C**) quadruplex. Adapted from Ref. (*28*).

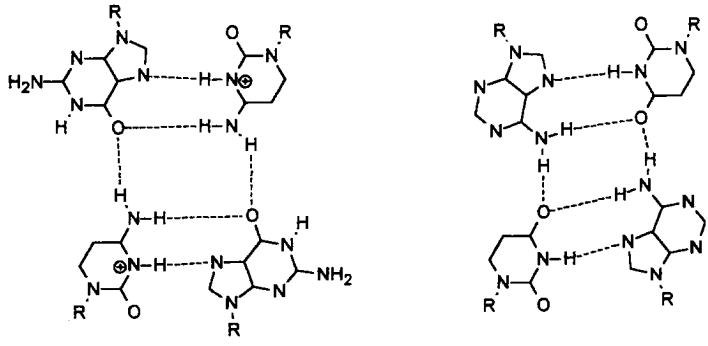

FIG. 5. Possible base-pairing interactions for the quadruplex homodimer. Hoogsteen pairings of the parallel stranded PtDNA duplex requires protonation of the GC pair. Adapted from Ref. (*28*).

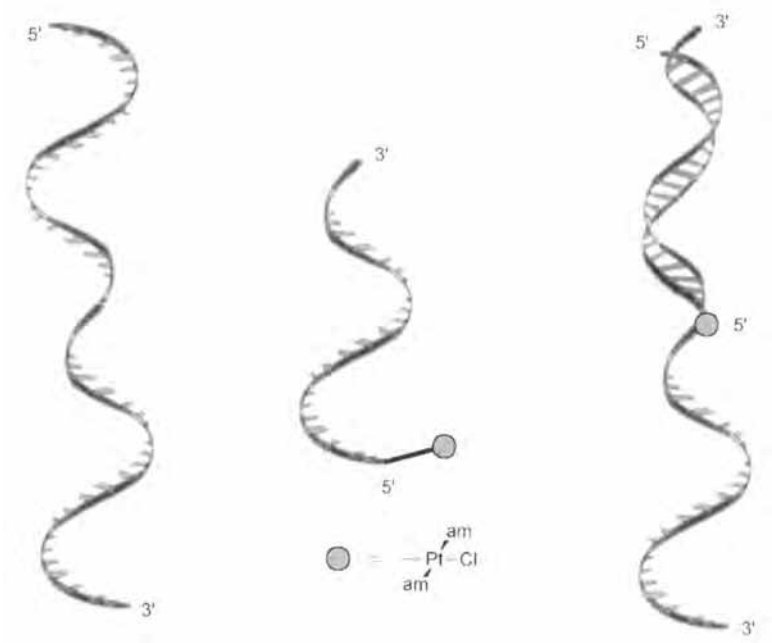

FIG. 6. Metal-crosslinking in antisense and antigene technology. The recognition of the target (sense) strand by the antisense strand is rapid and is followed by a slower irreversible metal crosslinking.

functional complex [Pt(1-MeC–N_3)$_3$(H_2O)], **1**, has been shown to bind to N7 of *terminal*-G nucleotides in duplex DNA with high selectivity (*31*). This is in contrast to $[Pt(dien)X]^{n+}$, which binds at the same site on G-bases but does so randomly in a sequence. Though **1** lacks the necessary reactivity for antisense applications it does illustrate that complexes can have specific reactivity for a particular DNA feature. Efforts to develop alternative methods for synthesizing DNA oligomers bearing reactive Pt-groups have been explored (see below).

While the critical role of intrastrand 1,2-crosslinks in the mechanism of action of the anti-tumor drug *cis*-[$PtCl_2(NH_3)_2$] is well established, much less is known about the few *trans*-analogs that exhibit similar efficacy. A series of 1,3-adducts has been characterized with 3-mers generally involving purine–N7 coordination (*32–34*), and either monofunctional or interstrand adducts are formed with duplex DNA (*35*). However, one of the most active compounds, *trans*-[$PtCl_2${(*E*)–HN=C(OMe)Me}$_2$], (**2**), has been shown to form a 1,2-adduct with 2-mer ribonucleotide sequence r(AG) (*36*). Though the formation of the

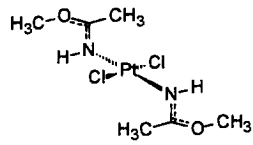

2

adduct chelate ring is slow, the resulting compound is stable. ^{1}H NMR and molecular modeling indicate that binding involves G–N7 and, unusually, A–N3. In duplex DNA these sites are located in the major and minor grooves, respectively. The importance, or otherwise, of this new type of adduct in the molecular mode of Pt-based drug action will undoubtedly be the subject of further studies.

There has been an increasing number of reports of metal ions binding at less common sites on nucleobases in DNA and in model systems. Another site on duplex DNA to emerge as a target for binding metal complexes is N3 of pyrimidines, thymidine and uridine (*37*). This site is located in the center of the double helix and hence coordination must involve an opening up of the helical structure. Kimura and co-workers have established that Zn^{2+}-cyclen, **3**, and its derivatives are highly specific in coordinating these bases (Fig. 7).

Using DNA footprinting, it has been shown that $[Zn(cyclen)]^{2+}$ derivatives bearing aryl–methyl substituents selectively bind to duplex DNA at AT-rich regions in the minor groove (*37*). The stacking ability and number of aryl rings affect the affinity and selectivity of binding. It appears that Zn^{2+} is essential for DNA binding; cyclen derivatives alone, or as Cu^{2+} or Ni^{2+} complexes, are ineffective. It was shown that the DNA binding is inhibited by the thiolate ligand captopril, suggesting the mode of interaction involves coordinate bond formation. Footprinting experiments using the micrococcal nuclease enzyme indicated that, in comparison with typical groove binding molecules such as distamycin A, the Zn^{2+}-cyclen derivatives bind to thymidine of A–T base pairs (Fig. 8). The Zn^{2+}-(4-quinolyl–methyl)-cyclen is competitive with Distamycin A for AT-rich regions supporting the minor groove as the site through which interaction occurs (Fig. 8).

N3-coordination by monomeric and dimeric Zn^{2+}-cyclen derivatives has also been shown to both inhibit the photo[2+2]cycloaddition of thymidilyl(3′-5′)thymidine, d(TpT), and to accelerate the photosplitting process of the [T-*cis*,*syn*-T] dimer (78% after 1 h of UV exposure) (*38*).

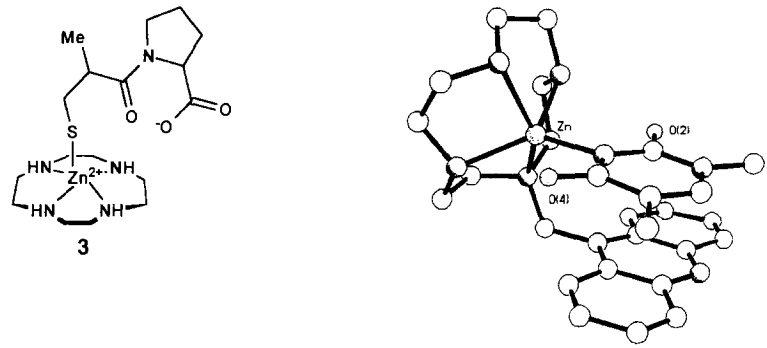

FIG. 7. A Zn^{2+}-cyclen derivative (**3**) with coordinated captopril, and molecular structure of a Zn^{II}(cyclen)–N3 bound 1–MeT.

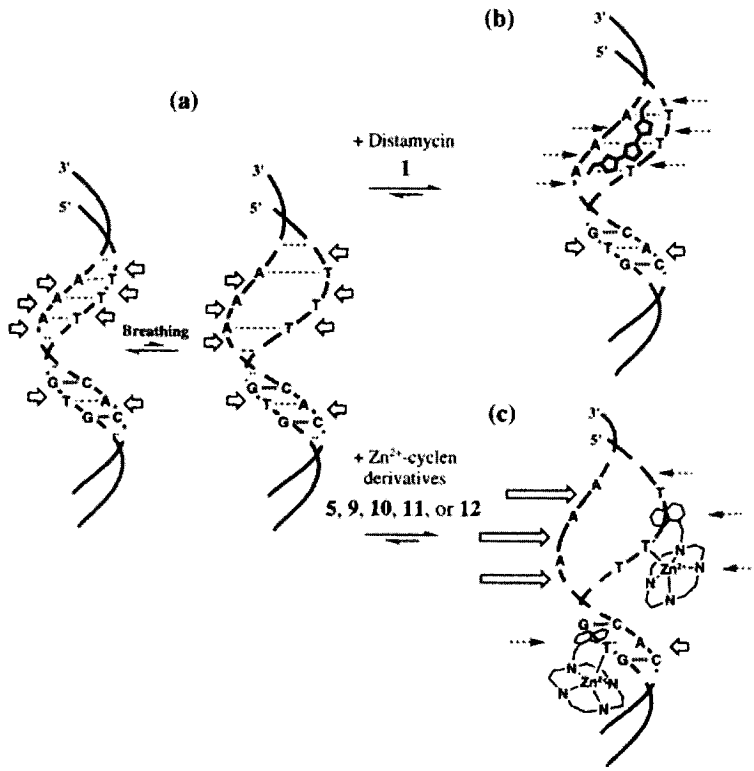

FIG. 8. Schematic for the micrococcal nuclease attack to (**a**) breathing ds-DNA, (**b**) distamycin-bound DNA, and (**c**) Zn^{2+}-cyclen derivative-bound DNA. Arrows and dashed arrows, respectively, indicate successful and failed enzyme hydrolysis. Reproduced with permission from Ref. (*37*). Copyright 1999, American Chemical Society.

The $Zn–N3_{imide}$ interaction has been used to selectively extract imide-containing nucleosides and nucleotides into lipophilic media (*39*). Hexadecyl-derivatized Zn^{2+}-cyclen was shown to extract dT from an aqueous solution containing a mixture of C, A, and G nucleobases. The antiviral agent AZT (3′azido–3′deoxythymidine) could also be extracted into $CHCl_3$ from neutral aqueous solutions. Transport across a lipophilic layer was also shown, using acidic conditions, to promote the release of dT and AZT (Fig. 9).

The T–N3 imido-site is also preferred for Hg^{II} binding to hairpin 12-mer DNA oligomers (*40*). The nature of the adduct was found to be dependent on the number of T nucleotides in the loop. For sequences with runs of 2 and 3 thymidines, d(ATGGGTTCCCAT) and d(GCGCTTTGCGC), interstrand TN3–Hg–TN3 crosslinking was found. In contrast, for d(GCGCTTTTGCGC) with a T_4-run, the hairpin was stabilized by an intramolecular crosslinking (Fig. 10).

While often somewhat ignored by coordination chemists, the interaction of Group I ions has recently received increased attention, particularly with regard to duplex DNA. To a large extent these ions are involved in charge neutralization of the anionic backbone of (deoxy)-ribonucleotide polymers. However, more specific effects have been

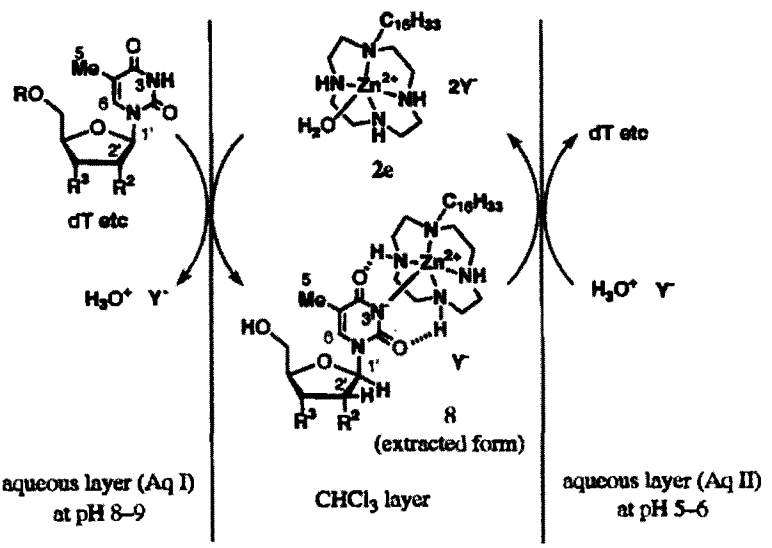

FIG. 9. Transport of dT and AZT through a liquid membrane: released pyrimidine; dT (100%); AZT (~ 21%). Reproduced with permission from Ref. (*39*). Copyright 1998, American Chemical Society.

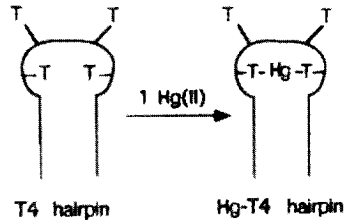

FIG. 10. Intrastrand Hg^{II}-crosslink in T_4-hairpin structures. Reproduced with permission from Ref. (*40*). Copyright 1996, American Chemical Society.

suggested, as for example in the minor groove of B-DNA. Here the so-called "spine of hydration" identified in the Dickerson–Drew duplex $d(CGCGAATTCGCG)_2$ has been reinterpreted as containing metal ions (*41*). Molecular dynamics simulations have located a Na^+ ion localized at the ApT step interacting with T–O2 atoms on opposite strands of the duplex. Analysis of the electrostatic potential of the possible combination of base pair steps reveals the ApA, TpA, and ApT combinations to possess the most negative electrostatic potential which may possibly bind otherwise mobile cations (Fig. 11). On this basis it has been suggested that metal ion$\cdots$DNA minor groove interactions may be a source of sequence-dependent effects, such as groove narrowing at A-tracts (*42*). In testing this with MD simulations, both inner- and outer-sphere interactions with the DNA bases were observed (Fig. 12) and a correlation between groove width and ion penetration was noted.

Crystallographic data for the same $d(CGCGAATTCGCG)_2$ dodecamer duplex containing Rb^+ showed partial occupancy of the metal ion at the site of the water molecule which hydrogen-bonds the T–O2 atoms on opposite strands (*43*). The difficulty in locating alkali metal ions, especially Na^+, in single-crystal X-ray structure determinations has been addressed by single-wavelength anomalous diffraction (*44*).

Line-broadening effects have been observed in ^1H NMR studies of the interaction of Mn^{II} ions with DNA oligomers $d(GCA_4T_4GC)$ and $d(CGT_4A_4CG)$ (*45*). Most affected were the A–H2 resonances of bases located centrally in the dodecamer sequences. These so-called A-tracts (runs of 4–6 dA bases) act to bend DNA in the direction of the minor groove. The authors suggested T–O2 as the site for interaction, based on the electronegativity of oxygen.

A dramatic illustration of the effect of metal ions on DNA structure is seen in the STM images of DNA circles in the presence of either $MgCl_2$ or $ZnBr_2$ (*46*). The shape of the DNA circles of 168-base-pair (bp) length

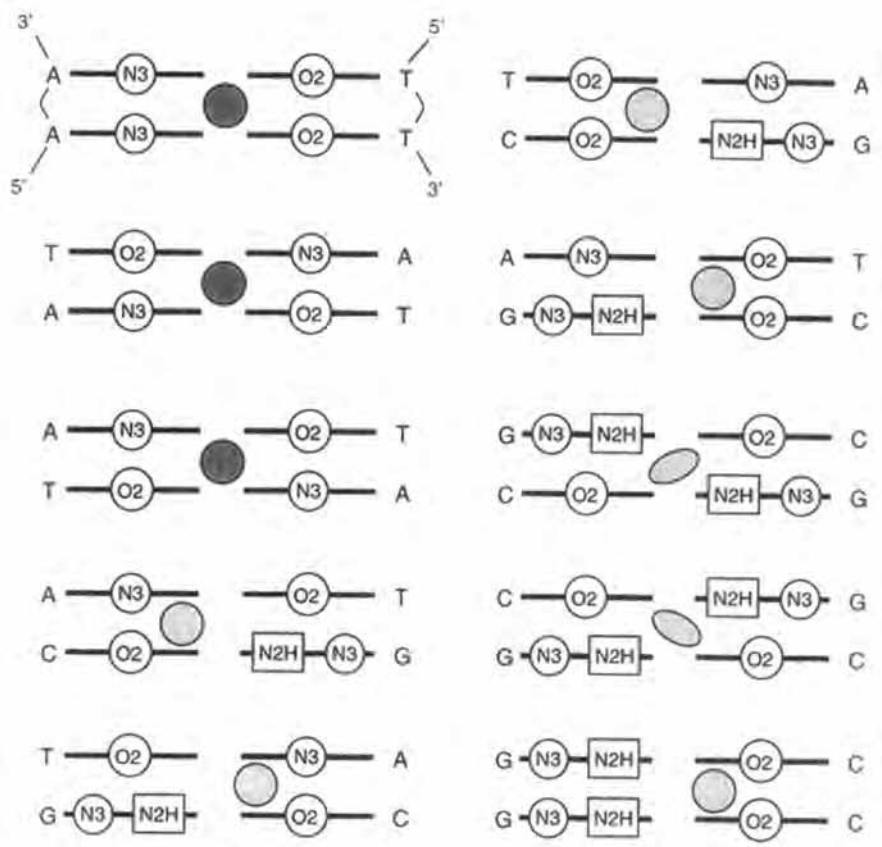

FIG. 11. Schematic of DNA bp steps in the minor groove, indicating possible locations of electrostatic pockets (shaded regions). Shading is proportional to the putative efficacy of the binding. Electronegative atoms are indicated by circles and hydrogen atoms by squares. Reproduced with permission from Ref. (*41*). Copyright 1997, American Chemical Society.

in the presence of Mg^{2+} ions is smoothly curved (Fig. 13). Replacing the Mg^{2+} ions with Zn^{2+} induces almost linear sections joined by abrupt kinks. These effects were not seen in smaller circles (126-bp), which suggests that axial strain in the DNA is required for the ion-induced transformation.

The lack of structural detail for interactions involving labile metals, particularly the Group I ions, is problematic and here model compounds are proving useful. A range of binding modes for Na^+ and K^+ ions involving both T–O2 and T–O4 have been realized with N1-alkylated thymi-

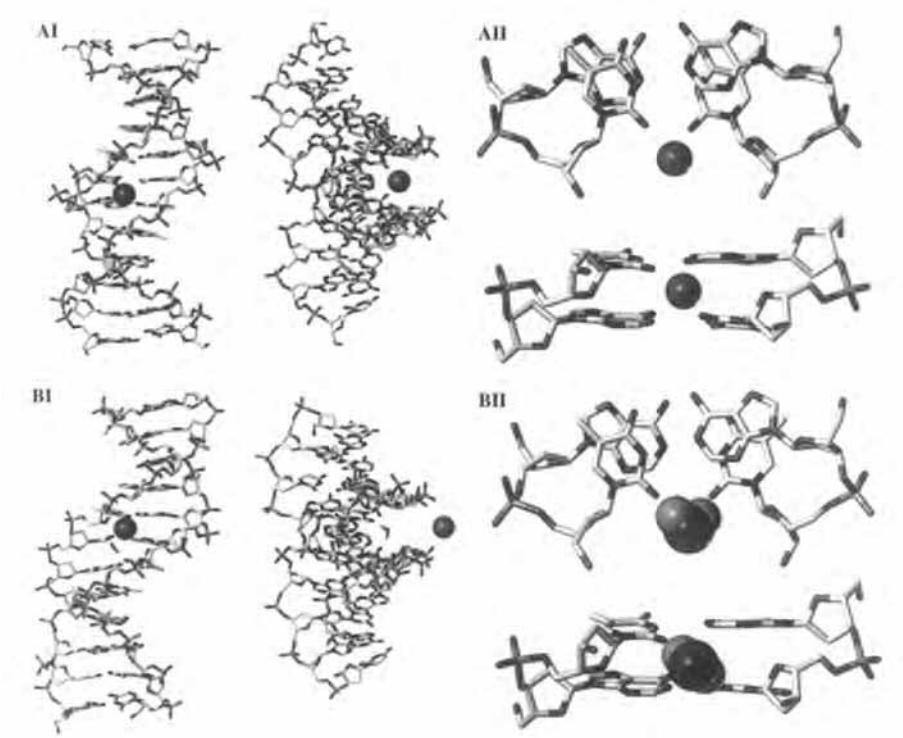

FIG. 12 (**A**) The d(CGCGAATTCGCG)$_2$ duplex with a narrow groove and a sodium ion coordinated at the ApT step. (I) The DNA is shown in stick representation and the ion in space-filling size. Left view is directly into the central minor groove. Right view: left view rotated 90° counterclockwise and tilted 30° to show the ion in the minor groove. (II) The base pair views are of the central ApT step. Top view is down the helix axis, bottom view is directly into the minor groove. (**B**) The DNA duplex with a phosphate-oxygen pair–sodium ion interaction and a water molecule coordinated at the ApT step. (II) Views as in Fig. 12A for the phosphate-ion–water-base complex at the AT site. Reproduced with permission from Ref. (*42*). Copyright 2000, American Chemical Society.

dine (*47*). Such interactions are also seen in metalated nucleobases (*48,49*), such as *trans*-[{Pt(NH$_3$)$_2$(1-MeU)$_2$}$_2$AgNa(H$_2$O)$_4$]$^{2+}$, which features Na–O4 binding.

One approach, pursued by two groups in particular, is to use model nucleobases that feature an additional metal–ion binding group. Gokel and co-workers have used this strategy with aza-crown derivatives (*50,51*). X-ray crystallography of *bis*-(3-(1-thyminyl)propyl)-4,13-diaza-18-crown-6, **4**, reveals the Na$^+$ is coordinated by T–O2 [Na–O distances 2.488 and 2.468 Å] (*51*). Aza-crown derivatives with multiple base substi-

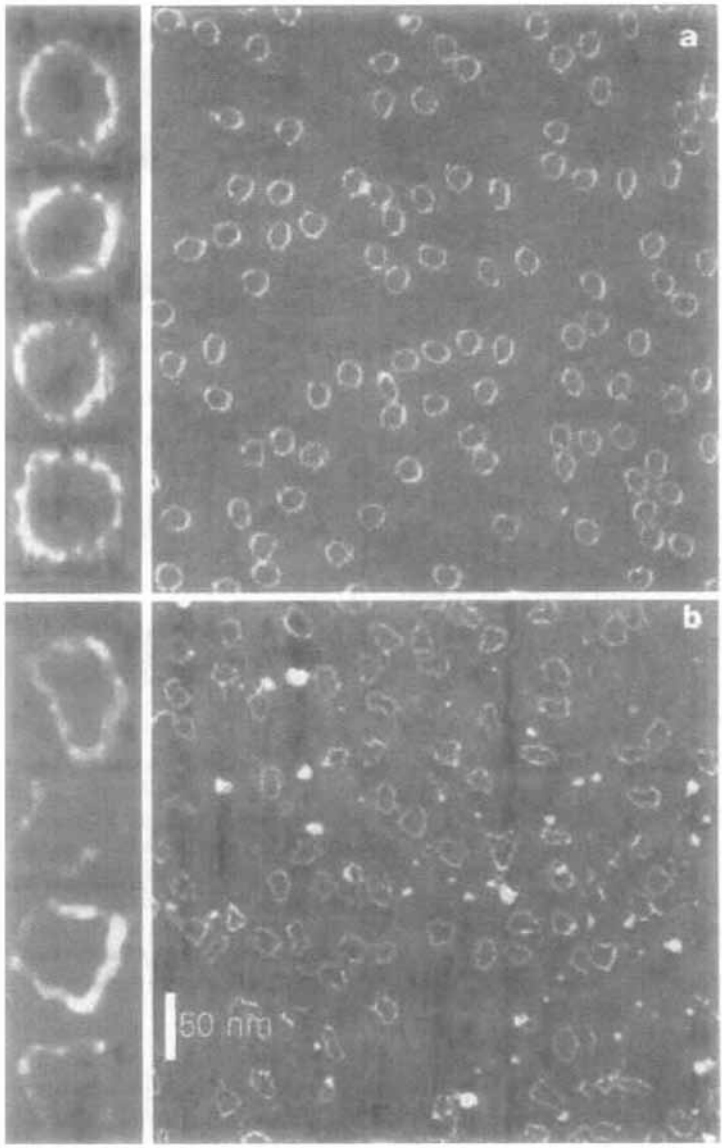

FIG. 13. Images of 168-base-pair DNA minicircles in 1 mM $MgCl_2$ (a) and 1 mM $ZnBr_2$ (b), showing a factor of 4 increase in kink density inZn^{2+}. Reproduced with permission from Ref. (*46*). Copyright 1997, *Nature* (London).

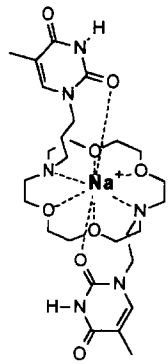

4

tuents have also been described. Metal–ion binding here disrupts inter-nucleobase hydrogen bonding due to the induced conformational change of the macrocycle, **5**.

In the case of the Na^+ and K^+ complexes of N9-ethyladenine-aza-18-crown-6, the metal ions exhibit different types of interaction at the minor groove site N3 (Fig. 14) (*52*). The Na^+ complex, **6**, shows a second-sphere interaction involving the coordinated H_2O hydrogen bonding to N3 [Na–OH_2 2.327, $H_O \cdots$ N3 2.836 Å]. In contrast, the K^+ complex, **7**,

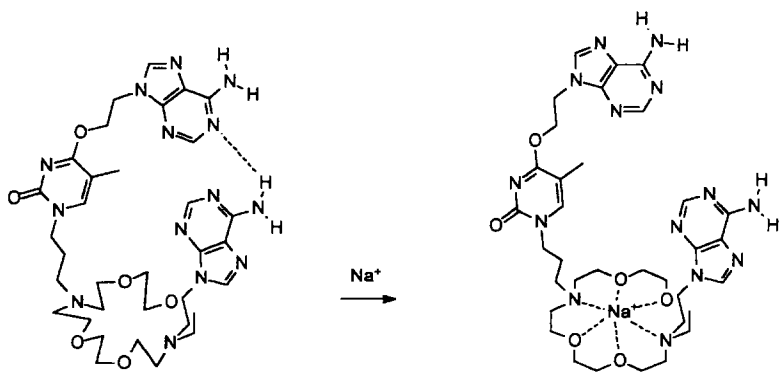

5 Na^+ (**5**)

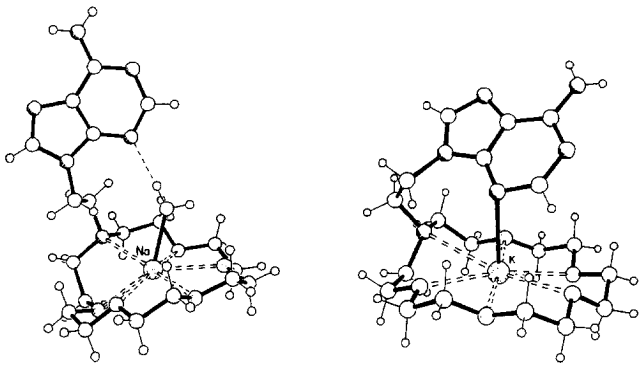

6 7

FIG. 14. Structures of (**6**), illustrating the second-sphere interaction with A–N3, and (**7**), showing the K^+–A–N3 binding. Reproduced with permission from Ref. (*52*). Copyright 2001, Royal Society of Chemistry.

has a direct K^+–N3 interaction [K^+–N3 2.939 Å], though here the metal ion lies significantly out of the nucleobase plane, suggesting the interaction has a highly ionic character. A similar interaction is seen in the few other X-ray structures containing K–$N3_A$ interactions (*53,54*).

A series of amine-tethered nucleobases such as **8** has also been developed. These ligand systems have allowed the interaction of d-block metal ions with the $N3_{purine}$ site to be probed and an indication of base-specific metal–ion binding has begun to emerge (*55–58*).

Titrations of Zn^{II} ions with ethylenediamine-N,9-ethyladenine, **8**, followed by ^1H NMR, show line broadening for H2, indicative of a ligand exchange at N3 (*58*). However, this behavior is anion dependent. Thus line broadening is seen with NO_3^- and ClO_4^- (Fig. 15), but not with Cl^- ions. Structural data obtained on compounds isolated from these reac-

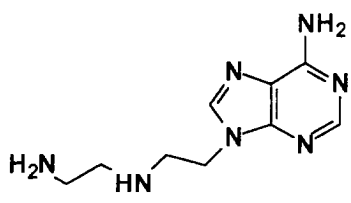

8

tion mixtures support these observations. With $Zn(ClO_4)_2$ the complex $[Zn(Cl)(en–Et–A–N3)H_2O]^+$ (**9**) contains a trigonal bipyramidal Zn^{II} which is coordinated by adenine N3 [Zn–N3 2.070 Å] (Fig. 16). On addition of $ZnCl_2$ the trinuclear complex $[Zn_3Cl_6(en–Et–A–N7)_2(H_2O)_2]$ is isolated whereby each adenine coordinates a $[ZnCl_3]^-$ group at N7. Reaction between the guanine analog, en–Et–G, and $Zn(NO_3)_2$ yielded the dimer **10** in which each ligand strand bridges the two metal ions by

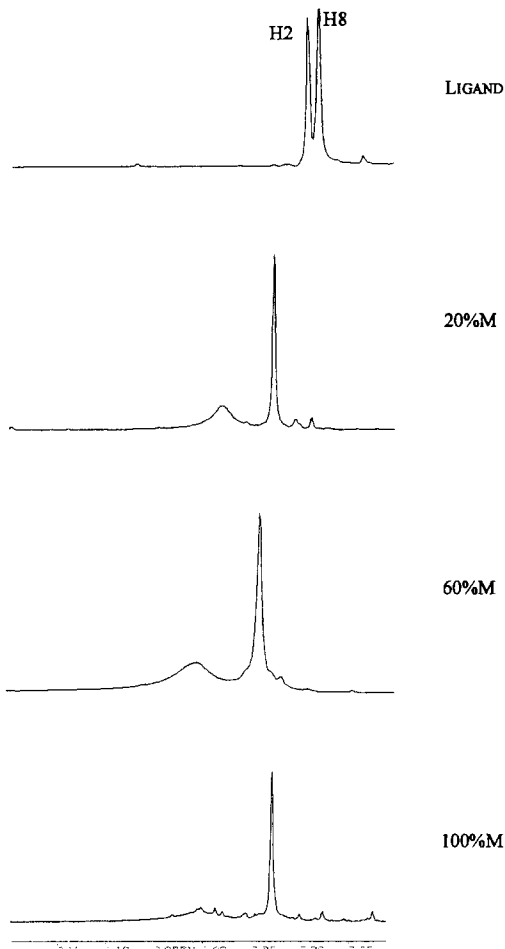

FIG. 15. Aromatic region of the ^1H NMR spectrum for $Zn(ClO_4)_2$ and ethylenediamine–*N*,9-ethyladenine hydrochloride, A–Et–enH^+,Cl^-, in D_2O, illustrating the broadening of the H2 resonance of the adenine moiety. Reproduced with permission from Ref. (*58*). Copyright 2000, Wiley–VCH.

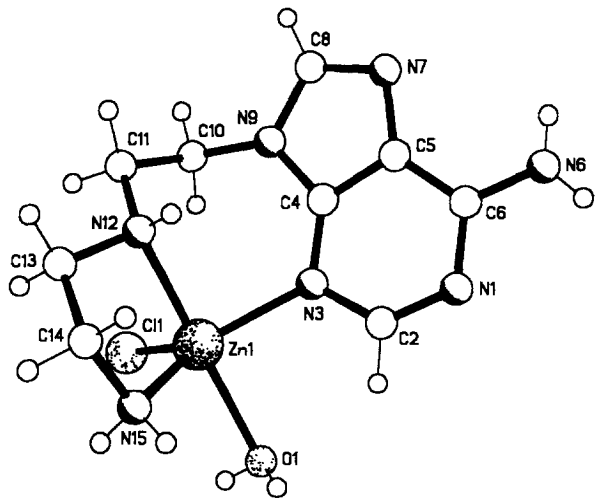

9

FIG. 16. Molecular structure of the Zn^{II}–A–*N3* complex (**9**). Reproduced with permission from Ref. (*58*). Copyright 2000, Wiley–VCH.

a coordinating one at N7, and chelating the second at the diamine [Zn–N7 2.002 Å; Zn–N_{en} 2.079 Å, Zn–N_{en} 2.005 Å] (Fig. 17).

Reactions of aqua Cu^{II} ions and either G–Et–en,HCl or A–Et–en,HCl generate helical coordination polymers (*57*) (Fig. 18). In both cases the metal ions adopt square pyramidal coordination; however, the polymer topologies are quite different. In the case of [Cu(Et–*N7*–G–en)$(H_2O)_2$]NO_3,Cl hydrate, **11**, the extended structure contains stacked guanine bases [Cu–N7 1.99 Å; G···G separation 3.2 Å] which are rotated by 90° and inclined at 9.6° with respect to the nearest neighbor. In contrast, in the analogous adenine complex, [CuCl(Et–*N7*, *N3*–en)]NO_3, H_2O, **12**, the bases make an angle of 74.4° with neighbors. This difference is due to the involvement of N3 in metal–ion binding in the case of adenine [Cu–N3 2.019 Å; Cu–N7 2.064 Å]. The same [A–N3 + diamine] binding mode is observed in a Cd-coordination polymer. The greater tendency for coordination at A–N3 than at G–N3 is a prevalent feature in the chemistry of these chelate-tethered nucleobase systems.

Another helical coordination polymer to contain binding at A–N3 is the product isolated from the reaction between *trans*-[$(NH_3)_2$Pt(9-MeA–*N7*)(9-MeH–*N7*)]$^{2+}$ (*H* = 9-methylhypoxanthine) and an excess of $AgNO_3$, **13** (*59*). Unusually, in this material the 9–MeA is bound by metal ions at N1, N3, and N7 simultaneously. The chain polymer is

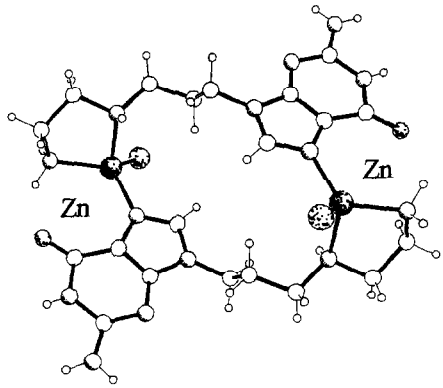

FIG. 17. Molecular structure of the Zn^{II}–guanine dimer (**10**). Reproduced with permission from Ref. (*58*). Copyright 2000, Wiley–VCH.

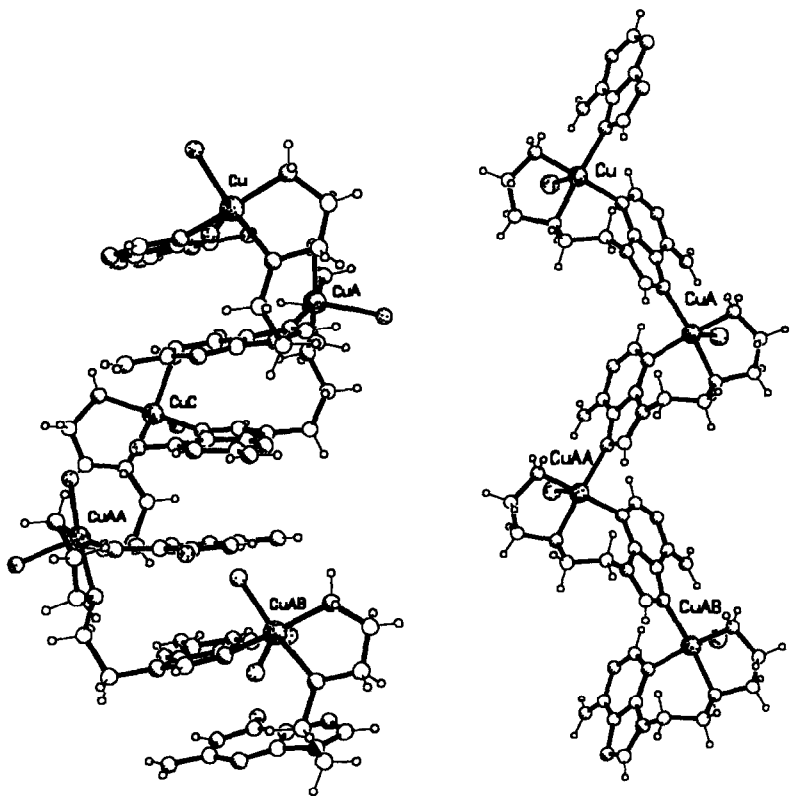

FIG. 18. Molecular structures of the polymeric chains in (left) (**11**) and (right) (**12**). Reproduced with permission from Ref. (*57*). Copyright 2000, Wiley–VCH.

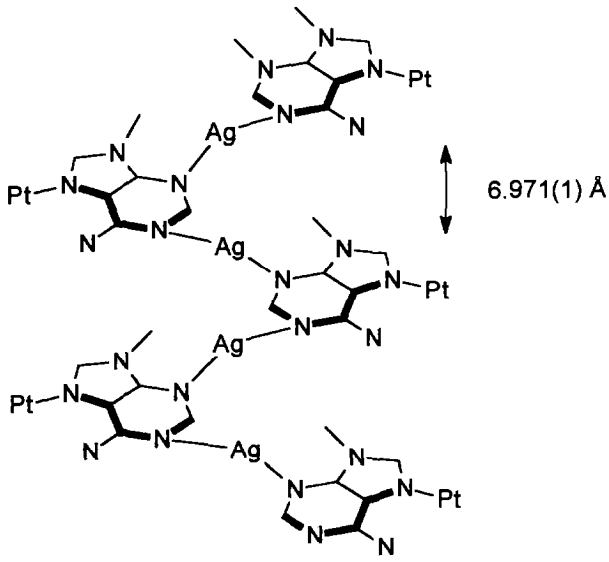

13

extended through Ag–N1 and Ag–N3 binding and the resulting Ag · · · Ag separation is 6.971 Å, which also describes the helical pitch.

N3-coordinated complexes containing platinum group metal ions have also been synthesized and studied (*56,60,61*). Steric hindrance has been used to direct binding to N3 in a series of Pd- and Pt-containing complexes of 6,6,9-trimethyladenine (*60*). Platinum modification was found to have a pronounced effect on the basicity of the adenine moiety. The protonation constants (log K_H values) for the twofold protonation of 6,6,9-trimethyladenine are 4.15 and −0.75, with the initial protonation occurring at N1 followed by N7. The equivalent values for the formation of [Pt(dien)TMA–*N3*)H]$^{3+}$ and [Pt(dien)TMA–*N3*)H_2]$^{4+}$ are 0.3 and −1.2, respectively. Moreover, the site of initial protonation was found to be N7 (Fig. 19). These observations are supported by theoretical studies (*62*).

Reaction of 6,6-dialkyladenine (alkyl = R = Me or Et) with the Re^{III} complex [$ReCl_3$(MeCN)(PPh_3)$_2$] also yields an N3-coordinated complex, *mer,cis*-[$ReCl_3$(6,6-Me_2AH–*N3*)$_2$(PPh_3)] (Re–N distances 2.391, 2.392 Å), which can be oxidized with HCl to the Re^{IV} species [$ReCl_4$(6,6-Me_2AH–*N3*)(PPh_3)] (Re–N distance 2.339 Å) (*63*). Both of these contain an intramolecular Re–Cl · · · HN9A hydrogen bond. A similar type of interaction has been observed earlier in the Rh^I complex [(cod)Rh(Me_2AH–*N3*)Cl]

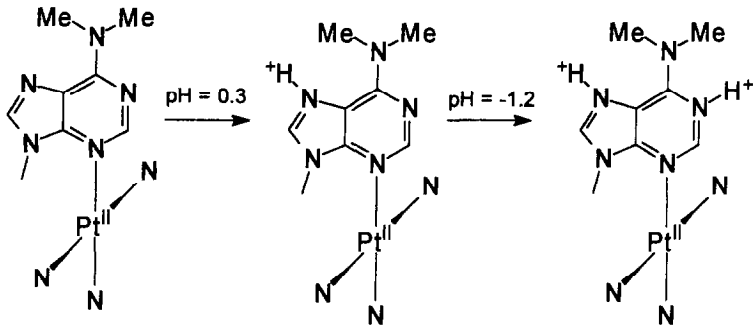

FIG. 19. Stepwise protonation of N3-platinated 6,6,9-trimethyladenine.

(*64*). A product, **14**, was also isolated from the reaction between 6,6-Me_2AH and *cis*-$[ReCl_4(MeCN)_2]$. X-ray crystallography identified this as **14** resulting from insertion of the C≡N group into the adenine N9–H bond [Re–N3 2.351 Å]. Formation of **14** is explained by activation of the coordinated MeCN towards intramolecular nucleophilic attack by the deprotonated adeninyl N9.

The presence of a chelating tether, such as ethylenediamine or dithioethane, has allowed the rational synthesis of N3-bound Pd, Pt, and Rh complexes with N9-alkylated adenine itself (*56,65*). Bond lengths to the nucleobase are typical for the respective metal ions (e.g., Pd–N3 range 2.031 to 2.047 Å) (*56*). The molecular structure of $[PdCl(A–N7–Et-en)]^+$, **15**, is shown in Fig. 20. A key spectroscopic feature of N3-bound metal complexes is the downfield shift of C–H resonances attached to N9 due to the close proximity of the metal ion (Fig. 21) (the Pd · · · H distance in **15** is 2.851 Å) (*56,60*). This spectroscopic signature has assisted in the assignment of the [G–*N7*–Pt–A–*N3*] adduct formed by *trans*-$[PtCl_2\{(E)–HN{=}C(OMe)Me\}_2]$, **2**, and may become increasingly useful in the assignment of this binding mode in more complex systems.

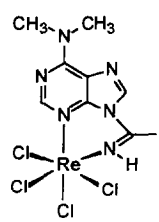

14

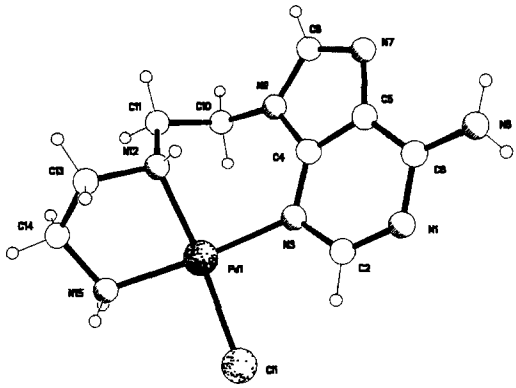

FIG. 20. Molecular structure of the AN3–Pd complex **15**. Reproduced with permission from Ref. (*56*). Copyright 2001, Wiley–VCH.

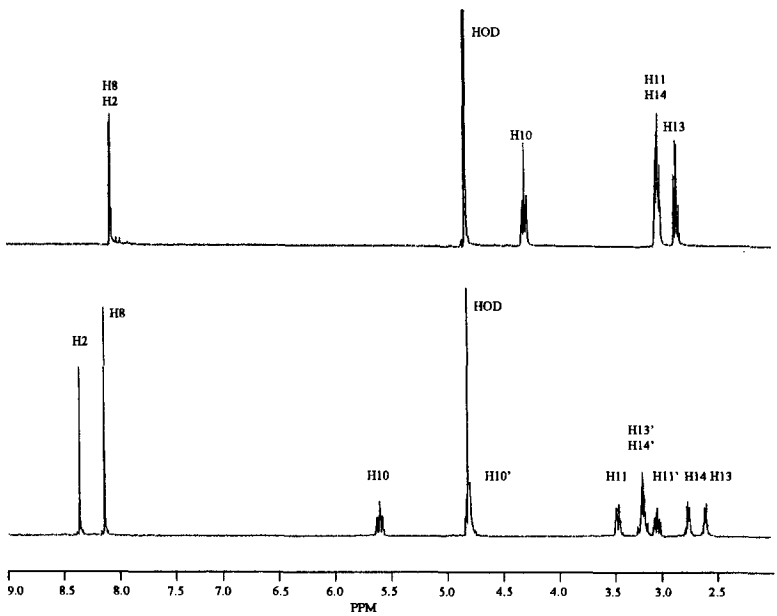

FIG. 21. ^{1}H NMR spectrum of (top) **8** and (bottom) **15**, highlighting the downfield shift for resonances of the methylene group attached to N9. Reproduced with permission from Ref. (*56*). Copyright 2001, Wiley–VCH.

Of all the known sites for metal–ion binding to the heteroatoms of DNA bases, G–N3 is the most elusive. The adjacent 2-amino group is often considered to offer steric hindrance to binding at this site. However, while this undoubtedly influences the chemistry it does not *preclude* binding. The tri-metalated $[\{Pt(NR_3)_3\}_3(9\text{-EtG}\text{–}N1,N3,N7)]^{5+}$ compound has for many years been the only structurally characterized example of an N3-coordinated guanine (*66*). A second example has now been reported, the tetranuclear octacation **16** (*56*). In this complex both the N7 and N3 atoms are bound to Pd^{2+} (Fig. 22). The molecule presents an interesting new architecture for a guanine-tetramer. Such structures are well known in DNA chemistry and are almost inevitably metal–ion stabilized (*67,68*).

It is interesting to speculate as to what types of DNA structure might be prone to coordination at G–N3. G-quartets, **17**, as seen in telomeres, are assembled through a combination of hydrogen bonding involving WC → H face interactions (*67,68*). This arrangement presents four G–N3 sites pointing outwards toward potentially reactive electrophiles. Whether G-quartets are susceptible to coordination at N3 has not yet been established, but as such structural motifs are increasingly tar-

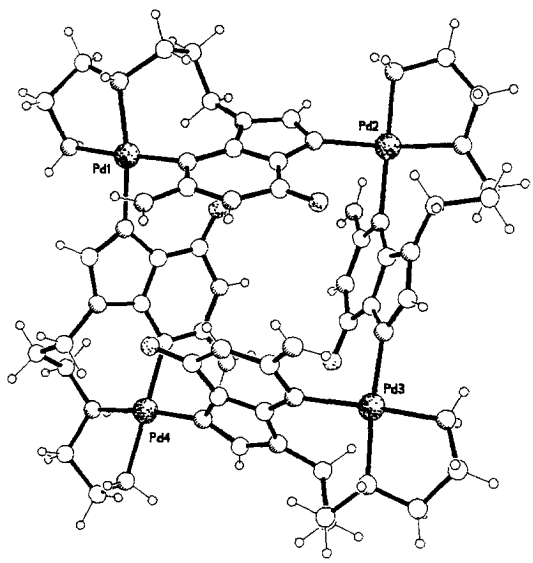

16

FIG. 22. Molecular structure of the tetrameric octacation **16**. Reproduced with permission from Ref. (*56*). Copyright 2001, Wiley–VCH.

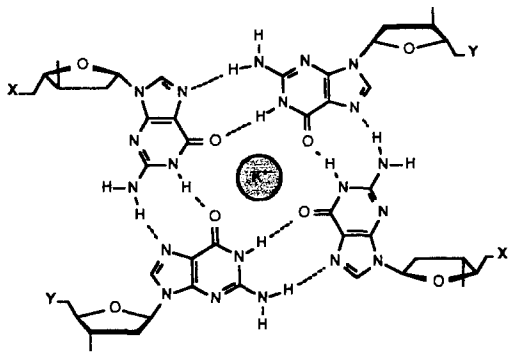

17

geted in, e.g., drug action (*69–71*), this aspect of DNA coordination chemistry may become important.

Interestingly, the G–N3 site has been shown to be involved in G–C base pairing should N7 and N1 be unavailable (*72*). This type of hydrogen-bonding interaction is also frequently observed in the packing of guanine derivatives in the solid state, including metal derivatives (*56,73*).

Recently, Switzer and co-workers have further extended the multistranded motifs for nucleic acids with the formation of a quintet assembly with oligonucleotides containing 2′deoxy-iso-guanosine (*74*). To support the quintet, metal ions larger than those appropriate for quartet stabilization were required, and Cs^+ ions were found to best meet this requirement. From modeling studies, a structure in which a central Cs^+ interacts with ten O2–iG atoms at a distance of ~ 3.5 Å was proposed.

B. Metal–Metal Interactions

There is an extensive number of nucleobase complexes that contain multiple metal ions (*75*). In some cases the binding sites are in close proximity and there is the possibility for metal–metal interactions. Figures 23 and 24 illustrate various binding modes involving the N,O-donor sites which can potentially give rise to such phenomena.

For the purines, only in the case of adenine has the [N3 + N9] bridging mode been observed (*76–78*). This further highlights the difference in binding patterns between the N3 of A and G. A recent example is seen in the Pd_2–adenine complex, **18**, formed in reactions of **19** with

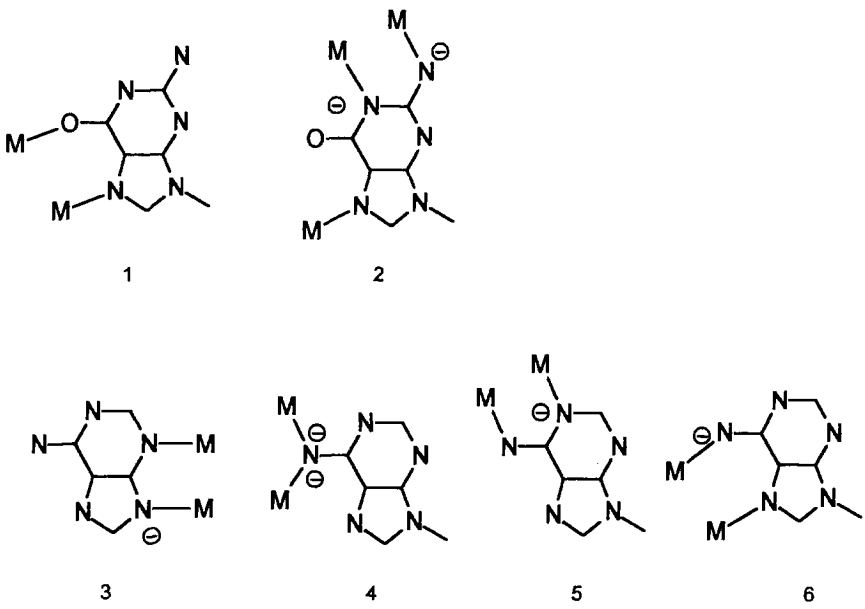

FIG. 23. Metal–ion binding modes for A and G that may give rise to metal · · · metal interactions. Adapted from Ref. (*75*).

DNA (*78*). The proposed mechanism of formation involves an initial non-covalent binding in the minor groove of duplex DNA by complex **19**. Metal–nucleobase bond formation involving the A–N3 activates the base towards cleavage of the glycosidic bond (depurination). A second complex then reacts at A–N9 to give the product, **18**. However, this reaction was performed at low pH and high temperature for a prolonged period (reaction conditions: HCl, 3 days at 95°C). Under such harsh conditions a more likely explanation is that acid-catalyzed depurination of the DNA liberated free adenine that subsequently reacted with **19**.

For the pyrimidines a range of the binding modes offers the possibility for metal–metal interactions (Fig. 24). Many of these combinations have been confirmed by X-ray crystallography, and a discussion of metal–metal interactions has been presented (*79*). The extent of interaction appears to be dependent on both the electronic configuration and the geometry of the metal. Short intermetallic separations (Pt–Pd = 2.49 Å) are observed for *trans*-Pt(amine)$_2$ derivatives, particularly those in which the filled Pt d_{z2} orbital can donate electron density into the heterometal d_{x2-y2} orbital (Fig. 25) (*80*).

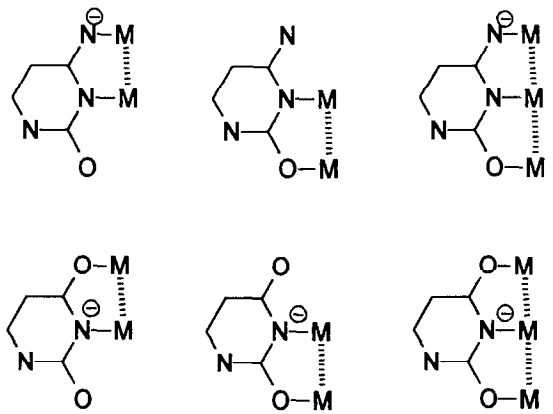

FIG. 24. Metal–ion binding modes for C and T/U that may give rise to metal···metal interactions. Adapted from Ref. (*75*).

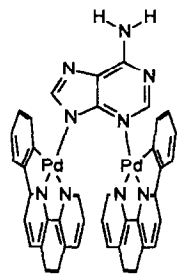

18

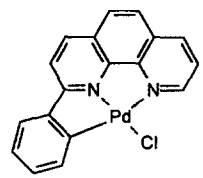

19

An interesting recent example of a polymetallic complex is the trimetallic Cu_2Pt complex, **20**, prepared by reacting $[Pt(1\text{-MeC}\text{–}N3)_4]^{2+}$ with $CuCl_2$ under relatively basic conditions (pH = 8–12) (*81*). The resulting compound $[Pt(1\text{-MeC}^-\text{–}N3,N4,O2)_4Cu_2Cl_2]$ undergoes substitution reactions with H_2O, SCN^-, or N_3^-, with displacement of Cl^-. X-ray crystallographic studies of the Cl^- and aqua derivatives reveal short Cu–Pt distances (range 2.519–2.531 Å). Both of these compounds are diamagnetic owing to unusually strong antiferromagnetic coupling between the Cu centers ($J = 980 \pm 30\,cm^{-1}$, Cu···Cu distances ~ 5 Å). The results suggest that novel magnetic materials based on metal–nucleobase complexes may be developed in this way.

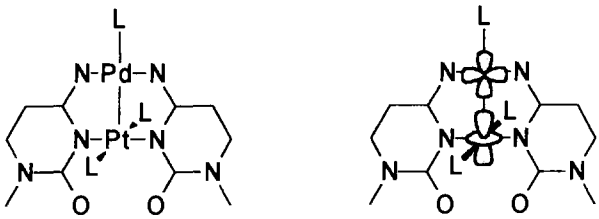

FIG. 25. Heterometallic complex of 1-methylcytosine, highlighting the nature of the metal–metal interaction involving the filled Pt^{II} d_{z2} with the Pd^{II} d_{x2-y2}.

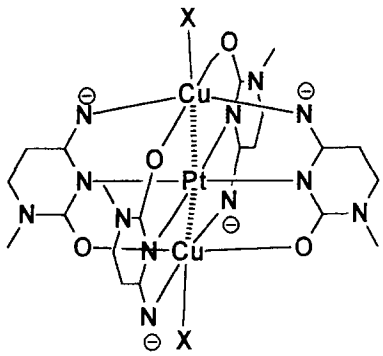

20

C. METAL–NUCLEOBASE CARBON BONDS

While metal–nitrogen and metal–oxygen bonded compounds dominate nucleobase coordination chemistry, examples in which metal–carbon bonds are formed have been identified. Early studies on the synthesis of metal-labeled DNA demonstrated that nucleotide–triphosphates, UTP, CTP, dUTP, and dCTP, can undergo mercury modification at C5 (*82,83*). The UTP derivative was also shown to act as a substrate for RNA polymerase in the presence of mercaptans (*83*). Later, guanosine was shown to undergo mercury modification at C8 though, in this case, the purine was multiply substituted, **21** (*84*).

The most common site for metalation of the carbon framework is C5 of the pyrimidines, C and U. For these reactions to occur, basic reaction conditions are generally required to assist in a deprotonation step. The first structurally characterized species was the di-Pt^{III} complex of 1-methyluracil, which also featured N3- and O4-binding (Pt–C5 distance 1.90–2.01 Å) (*85*).

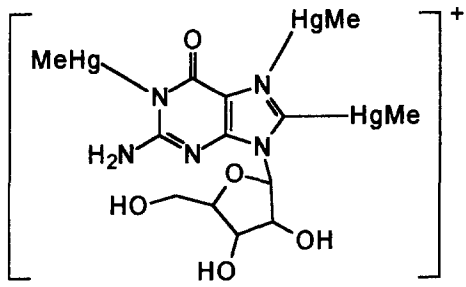

21

Reactions of either *trans*-$[Pt(MeNH_2)_2(H_2O)_2]^{2+}$ or $[Pt(dien)(H_2O)]^{2+}$ with 1,3-Me_2U yield the corresponding C5-bound complexes over a period of several days (Pt–C5 bond lengths 1.90–2.01 Å] (*86*). Reactions with $Hg(CH_3COO)_2$ to give Hg(1,3-Me_2U–*C5*)(CH_3COO) are somewhat faster, ~ 16 h (Hg–C5 bond lengths 2.07 Å). Homo- and hetero-metallic N3,C5-derivatives have been prepared by initial coordination of $[Pt(dien)]^{2+}$ at the N3-site of 1-methyluracil. Subsequent reaction with either $[Pt(dien)]^{2+}$or $Hg(CH_3COO)_2$ gives the corresponding N3,C5-bonded species (*86*). More recently the 1-methylcytosine dianion (1-MeC^{2-}) has been reported with an Hg–C5 bond. In this unusual cyclic compound six Hg and two Pt centers are bonded to four 1MeC dianions, **22** (*87*). This structure contains the six Hg^{II} in a plane with separations ranging from 3.540 to 5.231 Å. Reactions of some of these C5-substituted complexes have been explored, including the reaction of (1,3-dimethyluracil–*C5*)HgOAc with 9-MeA. This gives the mixed nucleobase complex [Hg(1,3-dimethyluracil–*C5*)(9-MeA–*N6*)]$^+$ in which the adenine is in the N1-protonated imino tautomer form (*88*).

The binding of Au^{III} to C5 has been confirmed crystallographically for the 1,3-dimethyluracil anion, though the reaction is rather slow (*89*). The Au–C5 bond lengths range from 2.082 to 2.358 Å for *trans*-$[Au(CN)_2Cl$(1,3-DiMeU–*C5*)$]^-$ and *trans*-$[Au(CN)_3$(1,3-DiMeU–*C5*)$]^-$ with various counterions. Such species have been proposed as possible intermediates in the dimerization of uracil derivatives in aqueous solution (*90*). Reaction of 1-MeU or 1,3-Me_2U with $AuCl_4^-$ in D_2O (22°C) over a period of hours to days gives the 5,5′diuracilyl dimer **23** as the major product (Fig. 26). Also characterized during the course of the reaction were a variety of soluble species which included [Au Cl_3 (1MeU–*N3*)], [Au Cl_3 (1MeU–*C5*)]$^-$, $[(AuCl_3)_2$-1MeU–*C5,N3*$)]^{2-}$, and 5-Cl,1-MeUH. Compound **23** does not form if 1-MeU is replaced by the 5-chloro analog. Reductive elimination of two *cis*-oriented uracil moieties bonded to Au^{III} is suggested as a route to formation.

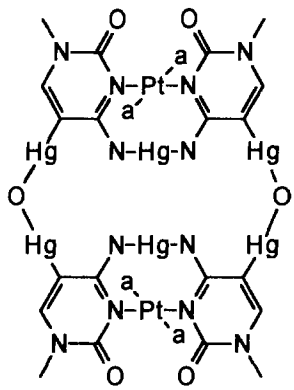

22

These studies may be relevant to the proposed photosensitization of DNA by Au^{III}. Of particular interest here, oxidative degradation of the 9-MeG of the trivalent gold complex $AuCl_3$(9-MeG–*N7*) has been observed, though the process is slow (2 months) (*91*). The fragmentation of the purine gives rise to a mixture of compounds. *N*-methylparabanic acid is the major product if the reaction is performed under aerobic conditions (Fig. 27). In the absence of air the formation is minimal and guanidinium appears to be the predominant product.

There have been few reports of purine derivatives[1] that contain metal–carbon nucleobase binding (*75*), and those that have been described are often polymetalated (*84*). Quite recently mononuclear complexes of adenine and guanine have been prepared that contain

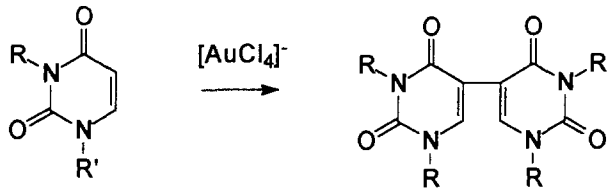

23

FIG. 26. Au-promoted dimerization of uracil derivatives. (R = H, R′ = Me; R = Me, R′ = Me; R = H, R′ = ribose). Adapted from Ref. (*90*).

[1]There are a few reports of C8-metalated purine derivatives that are not nucleobases (*92–94*).

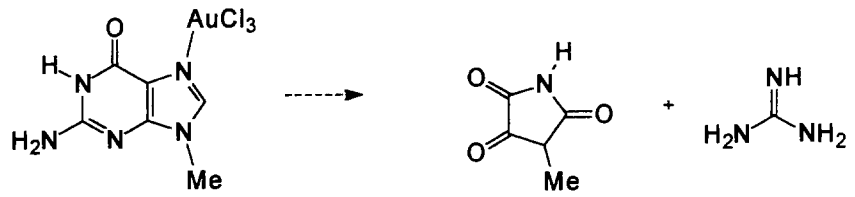

FIG. 27. Degradation of the 9-MeG complex of $AuCl_3$(9-MeG–*N7*). Adapted from Ref. (*91*).

metal–C8 bonds (*56,95*). Reaction of the diamine-tethered adenine **8** with $[RuCl_4(dmso)_2]^-$ gives the C8-metalated derivative **25** (Ru–C8 bond length 1.989 Å), Fig. 28. In this case the formation of **25** is stepwise, as is confirmed by the isolation and structural characterization of **24** (*95*). This intermediate compound contains a pendant adenine moiety with binding of the diamine function alone occurring. Conversion of **24** to the cyclometalated **25** derivative is achieved on refluxing in MeOH, when loss of dmso and C8H → N7H proton transfer is observed. The interconversion can be judged by UV–visible spectroscopy as a new band is formed at $\lambda = 332$ nm. The analogous guanine compound **26** has also been described (Ru–C8 bond length 1.994 Å) (*56*). In the latter, the importance of a chelating reaction was confirmed by studies on the control reaction with 9EtG, where the N7-coordinated species $[RuCl_3(N7\text{–}9EtG)(H_2O)(dmso)]$, **27**, is formed (*96*). Electron-counting in both **25** and **26** requires the nucleobase to act as a two-electron donor for the products to be diamagnetic 18-electron compounds. In contrast, in **28** the guaninyl group acts as a one-electron donor for the compound to be 16-electron.

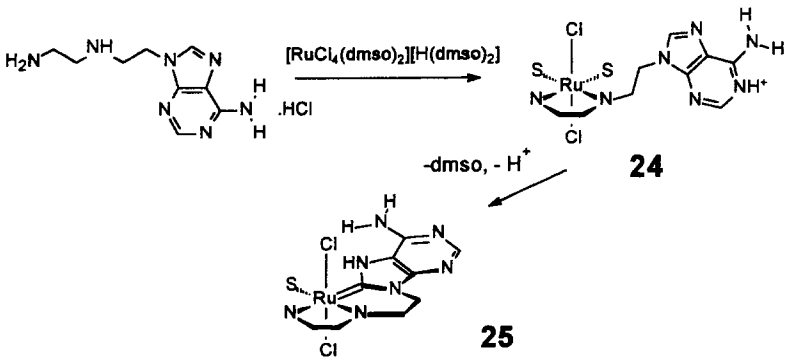

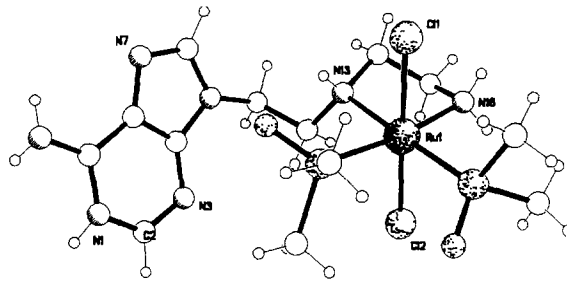

24

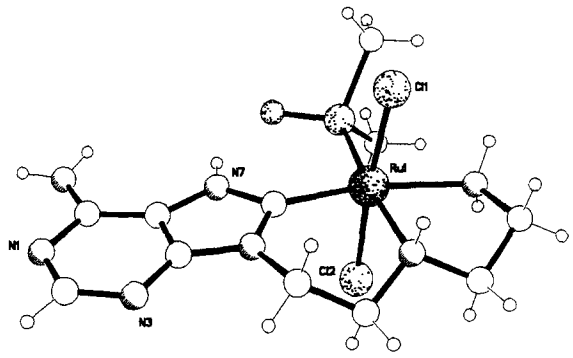

25

FIG. 28. Molecular structures of **24** and **25**. Reproduced with permission from Ref. (*95*). Copyright 1997, Wiley–VCH.

The reaction between $[PdCl_2(MeCN)_2]$ and ethylenediamine–*N,9*-ethylguanine yields the analogous C8-cyclometalated compound $[PdCl(en\text{–}Et\text{–}A\text{–}C8)]^+$ **28** (Pd–C bond length 1.974 Å) (*56*) (Fig. 29). Again, proton transfer to the adjacent N7 accompanies C8-metalation and this is observed downfield in the ^1H NMR spectrum (δN7H = 11.57 ppm). While these reactions are rather unusual with regard to metal–nucleobase chemistry, they are in fact examples of classical cyclometalation (*97*). Such reactions often involve a pre-coordination step, as observed in the formation of **25**.

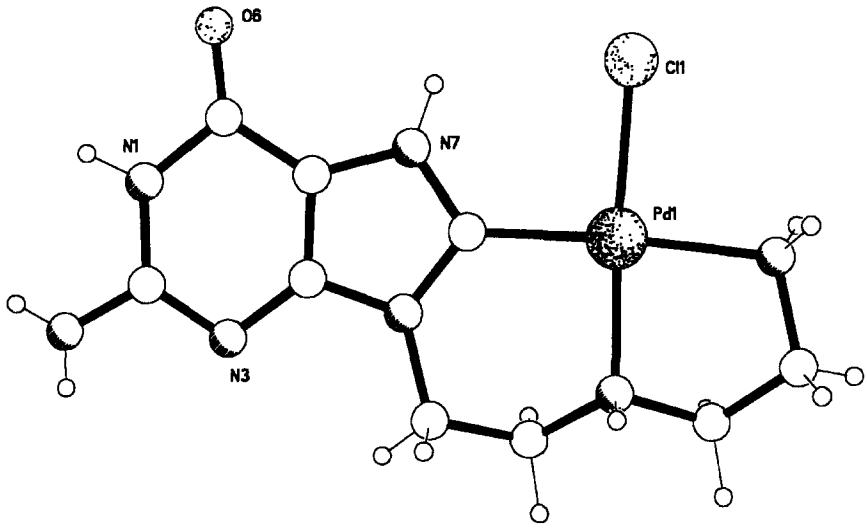

28

FIG. 29. Molecular structure of the C8-palladated guanine complex, **28**. Reproduced with permission from Ref. (*56*). Copyright 2001, Wiley–VCH.

D. RARE TAUTOMERS

Metal–ion binding has been shown to stabilize rare tautomeric forms of nucleobases (*88,98–102*). This may be a contributing factor in the mutagenic effect of metal ions since changes in base-pair hydrogen-bonding patterns can arise (*103*). With Pt^{II}, Hg^{II}, and Ru^{III}, reagents binding to the exocyclic amino group of either adenine and cytosine stabilize an *exo* → *endo* proton shift to the N1 and N3 atoms respectively (*88,98–100*). The effect of possible mispairings of the imino tautomer of A on genetic information transfer has been illustrated (Figs. 30 and 31) (*88*).

Quantum calculations on metal-assisted tautomerization indicate a substantial stabilization to protonation of the endocyclic nitrogen atoms (*99*). In the case of $HgCH_3^+$, adducts are formed by binding at either A–N6 or C–N4, which increases the stability of the respective $N1H^+$ or $N3H^+$ protonated species by 10–14 kcal/mol. For Pt^{II} binding at C–N4 the effect is much greater at ~ 30–34 kcal/mol.

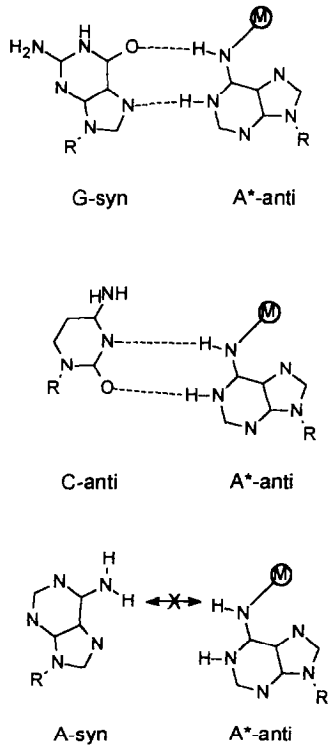

FIG. 30. Possible mispairing schemes for adenine N6–metallo imino tautomer. Adapted from Ref. (*88*).

III. Supramolecular Aspects of Metallo-Nucleobase Chemistry

Controlling molecular assembly is a significant challenge for synthetic chemistry, and numerous approaches have been considered (*104*). Frequently, the methods are informed by biology, and DNA-type assembly, more than any other, has been used to organize synthetic compounds. The hydrogen-bonding base-pair paradigm has been increasingly exploited in coordination chemistry. Numerous examples of metal complexes exist which use pendant nucleobases as substituents to bring about intermolecular interaction. These include, for example, metalloporphyrins (*105–108*), ferrocenylnucleobases (*109–111*), and pyridyl–metal chelates (*112,113*). Here the focus will be primarily on

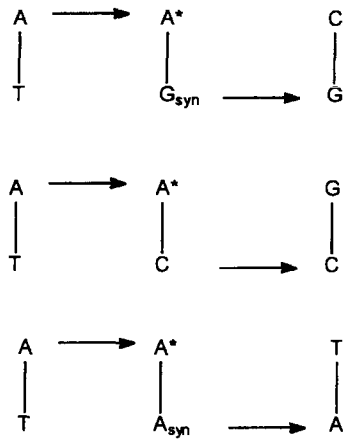

FIG. 31. Effects of mispairing in genetic information transfer (Fig. 30). Top, transversion of an AT → CG via A*G pair. Middle, transition AT → GC. Bottom, AT → TA transversion. Adapted from Ref. (*88*).

examples that exploit both the metal–ion binding and the hydrogen-bonding properties of nucleobases.

Lippert, in particular, has outlined the extensive possibilities of structure building using this bond-forming bifunctionality (*114*). Many of the geometric architectures that can be designed arise from the orthogonality of the principal purine binding sites N1 and N7 (see A. below). With *trans*-substituted metal ions a plethora of networks can be constructed and many of these have been realized. The area has been reviewed quite extensively (*114*), and no attempt is made here to provide an exhaustive coverage of systems so far reported.

Significantly, it has been shown that coordination of nucleobases *can enhance base pairing interactions* (*115*). These findings confirm previous theoretical calculations (*116*). The association constant for Watson–Crick interactions between 9-EtG and 1-MeC was 6.9 M^{-1}, determined

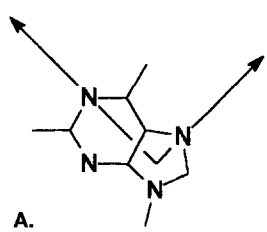

A.

by concentration-dependent NMR studies. In comparison, pairings between 1-MeC and the series of complexes [Pt(dien)(*N7*-EtG)], **29**, and **30**, are $K = 13.2, 22$, and $16.4\,M^{-1}$, respectively (Fig. 32).

A similar enhancement has been noted for the coordination of N1 cytosine (*73,117*). The order of stability for GC base pairs was found to be in the order III ~ II > I (Fig. 33) (*117*). X-ray studies on co-crystals of *trans*-[Pt(*N1*–C)$_2$(CH$_3$NH$_2$)$_2$] with 9-ethylguanine confirm WC base pairings. The stability constant for the *trans*-[Pt(C–*N1*)$_2$(CH$_3$NH$_2$)$_2$]/9-EtG base pairing was calculated as $K = 10.0\,M^{-1}$, compared to a value $K = 6.9\,M^{-1}$ for 9-EtG/1-MeC in the same solvent (d_6-DMSO). These observations are important and show that base-pair hydrogen bonding can be realistically considered a design principle for assembling nucleobase–metal complexes. They also suggest the feasibility of molecular recognition of natural DNA targets by artificial metal-analogs.

Multiple stranded DNA structures, such as quartets (*67,68,118*), that are observed in biological systems are increasingly matched by synthetic analogs. Figure 34 illustrates possible methods of quartet assembly based on a combination of metal–ligand and/or hydrogen-bonding interactions. The structures involve either 4, 6, or 8 metal–ligand interactions.

Metal-modified base pairs have been reported some time ago for identical (*119*), complementary (*120*), and non-complementary bases (*59,121–126*). These may assemble into a type I quartet through dimerization, as seen for *trans*-[(NH$_3$)$_2$Pt–(9-EtG–*N7*)(1-MeC–*N3*)]$^+$ which has an association constant of $59.1\,M^{-1}$ in d_6-DMSO (*123*). Rather unusual is the involvement of the aromatic C–H5 proton in the hydrogen bond-

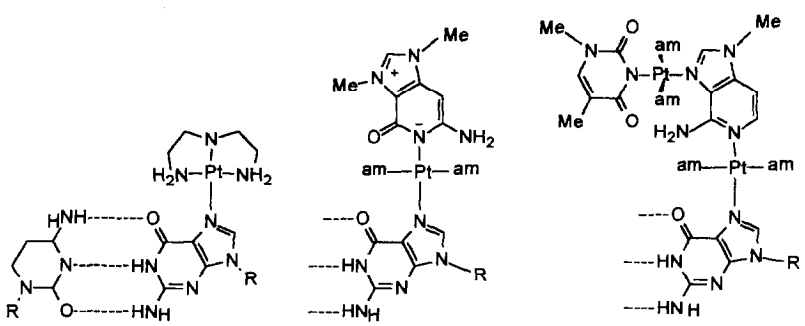

FIG. 32. CG base pairing for N7-platinated guanine derivatives [Pt(dien)(9-EtG–*N7*)]$^{2+}$, **29**, and **30**. Adapted from Ref. (*115*).

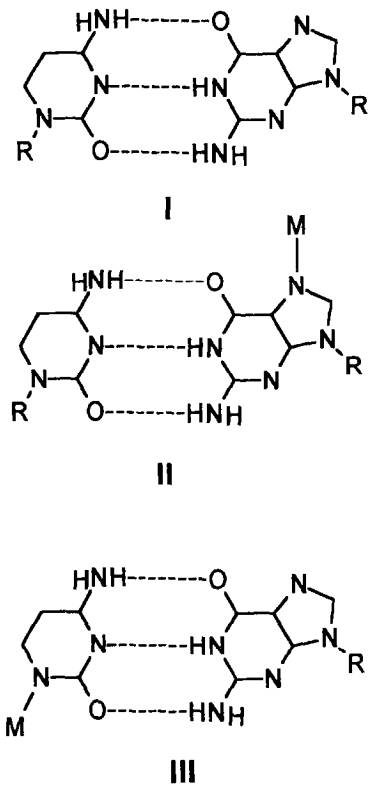

FIG. 33. Watson–Crick base pairs [C–G], [C–G–$N7_{metal}$], [C-$N1_{metal}$–G]. Adapted from Ref. (*117*).

ing, which was proposed initially on the basis of ^{1}H NMR data (*123*) and subsequently confirmed by X-ray diffraction (*124*).

An alternative form of quartet involves a single base binding to a tri-base structure by hydrogen bonding alone (Type II, Fig. 34). Such an assembly can be considered to involve a di-metal–tri-nucleobase receptor binding a fourth base via non-covalent recognition. All four nucleobases have been incorporated into such a single compound by co-crystallizing 1-MeC with the diplatinum complex *trans*-[$(NH_3)_2$Pt(1-MeU–*N3*)(9-EtA–*N7,N1*)Pt$(MeNH_2)_2$(9-EtG–*N7*)]$^{3+}$, **31** (*127*) (Fig. 35). The GC pair interact in a Watson–Crick manner. Subsequently, the involvement of the coordinated pyrimidine in the recognition process has been investigated and found to be considerable (*128*). Association constants for 1-MeC with *trans*-[$(NH_3)_2$Pt(9-EtA–*N7*)(9-MeG–*N7*)]$^{2+}$

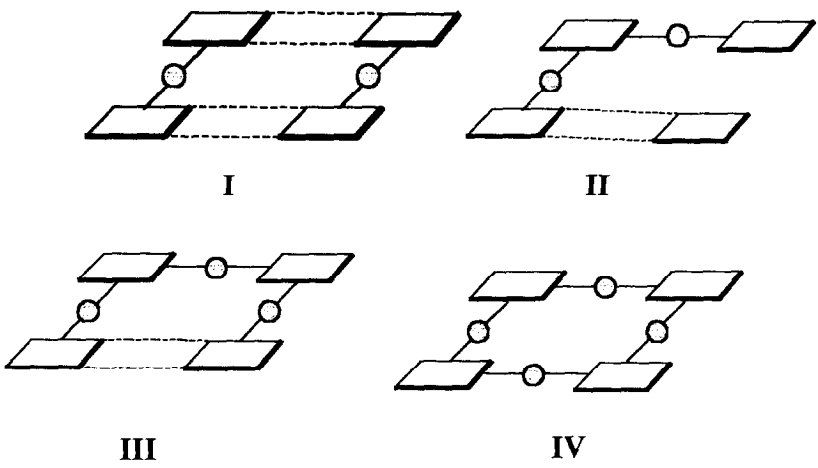

FIG. 34. Schematic representation of metal-containing nucleobase quartets.

and *trans*-$[(NH_3)_2Pt(1\text{-MeU}–N3)(9\text{-EtA}–N7,N1)Pt(MeNH_2)_2(9\text{-EtG}–N7)]^{3+}$ are $K = 11.1 \pm 3.2\,M^{-1}$ and $K = 24.2 \pm 12.4\,M^{-1}$ respectively, where in the latter a large error is observed. It was found that C5–H of 1-MeC is also involved in hydrogen-bond interactions, as is indicated by a downfield shift in the ^1H NMR with increased concentration.

This same di-platinum complex **31** has generated perhaps the largest discrete metal–nucleobase assembly characterized to date: a sextet

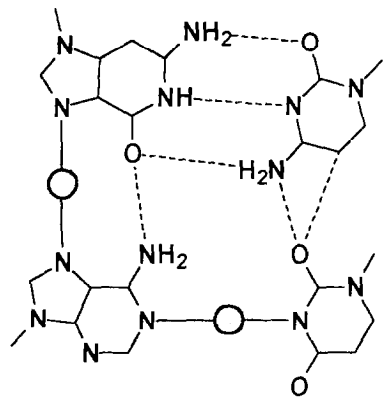

31

FIG. 35. Schematic of **31**, highlighting the hydrogen bonding interactions. Adapted from Ref. (*127*).

formed by self-association (*129*). Semi-deprotonation at G–N1 allows dimerization via a complementary hydrogen-bonding interaction, involving the Watson–Crick face of guanine, to form the sextet. The six-base assembly is highly co-planar, involving multiple hydrogen bonds, and has an exceptional stability in solution ($K = 500\,M^{-1}$ in dmso).

A type III quartet has been synthesized by crosslinking *trans*-$[(NH_3)_2Pt(9\text{-MeA-}N7)(9\text{-MeG-}N7)]^{2+}$ units with *trans*-$(NH_2CH_3)_2PtCl_2$ via the N1 position of the adenine, **32** (*130*). The resulting trimetallic quartet features hydrogen bonding between crosslinked A···G pairs [A–N6···G–O6 range 2.77–2.90]. The separation between the non-crosslinked 9-MeG is too large to allow such interactions. Reaction with $Hg(NO_3)_2$ generates [A-N6–Hg–N6–A], [G–N1–Hg–N1–G], and [G–N2–Hg–N2–G] crosslinks.

A variety of fully crosslinked quartets has been reported (type IV), including that derived from the uracilate anion (*131–134*). This complex may be considered a calix[4]arene analog. The compound is prepared by dehydration of $[enPt(U\text{-}N1)H_2O]^+$ (en = ethylenediamine) to give the cyclic tetranuclear $[(en)Pt(uracilate)]_4^{4+}$ species. While in the solid state the molecular cation adopts a 1,3-alternate conformation **33a** in solution, following deprotonation, a second, cone-conformer, **33b** dominates (*133*). The two conformations exhibit different metal–ion binding modes involving the uracilate oxygen atoms. The 1,3-alternate arrangement binds four additional metal ions whereas the cone-conformer has been shown to bind either one or four. Examples of this last type of complex are with the incorporation of Cu^{II} or Zn^{II} (M) and feature Pt–M interactions consistent with a weak σ-donation by the Pt-ion (*134*). In addition to metal ions, these metallocycles also bind small molecules such as *p*-toluenesulfonate and 3-(trismethylsilyl)–1-propanesulfonate (*133*).

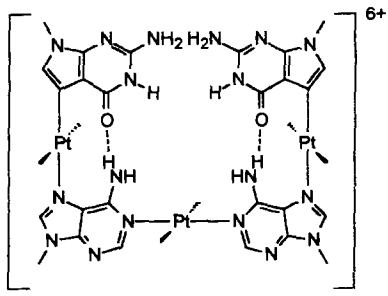

32

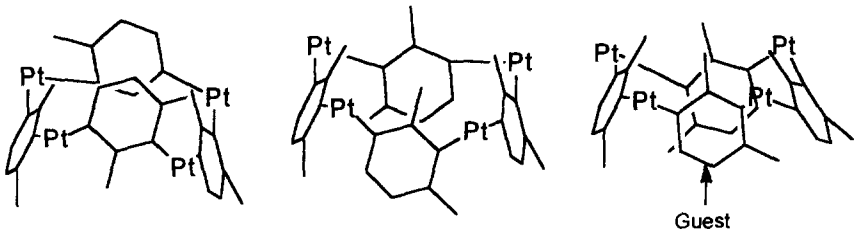

33a **33b**

The presence of a chelating flexible tether at the N9 position of guanine has given rise to some unique quartet structures (*56,58*). For example, the reaction of $CdSO_4$ with en–Et–G yields the G-quartet structure **34**, shown in Fig. 36. The G_4–Cd_4 squares are bridged through SO_4^{2-} ions, generating intramolecular G···G columns with a separation of 6.9 Å. Regular stacking distances of 3.5 Å are formed through intermolecular interactions (*58*). Such stacking is absent in the Pd-based G-quartet **16** due to the non-planar arrangement of the nucleobases (*56*). An earlier Pd-tetramer, **35**, was proposed on the basis of ^{1}H NMR studies for the species formed in equimolar solutions of [Pd–ethylenediamine)$(NO_3)_2$] and 5′GMP or 5′-IMP. In this case the binding sites are N1 and N7 (*135*).

A unique aspect of the G-quartets **34** and **16** is that their assembly involves only metal–ligand bond formation. Since the sites on the nucleobase involved in coordination are either N7 or [N7 + N3] this

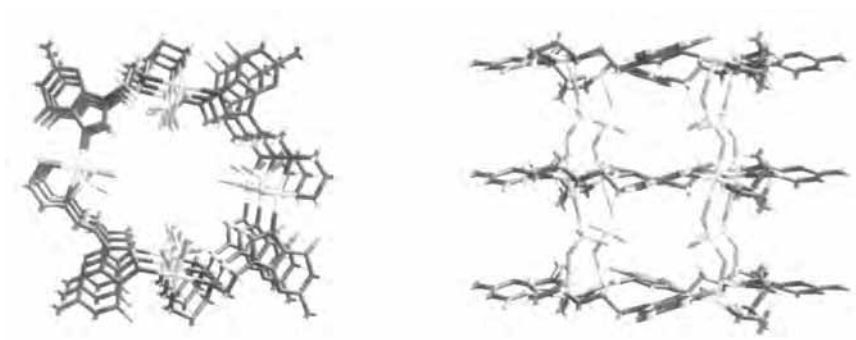

FIG. 36. Molecular structure of **34** viewed down the channel axis of the Cd_4–G_4 square. Right, view of the sulfate bridging of individual Cd_4–G_4 squares. Reproduced with permission from Ref. (*58*). Copyright 2000, Wiley–VCH.

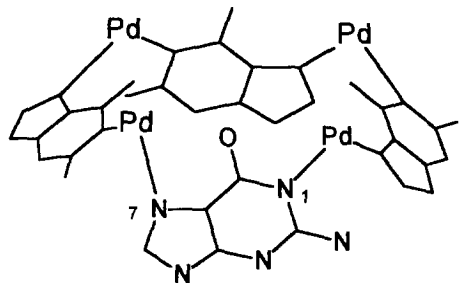

leaves the WC face available for base pairing. This feature presents numerous opportunities for preparing macromolecular metal–DNA hybrid structures, such as that shown in Fig. 37, assembled via complementary H-bonding interactions.

Base-pairing interactions have been realized in metal complexes by extending ligand functionalization to include two complementary nucleobases (*136*). Sequential alkylation of 1,2-dithioethane using 2-chloroethyl-9-adenine and 3-chloropropyl-1-thymine yields the AT-

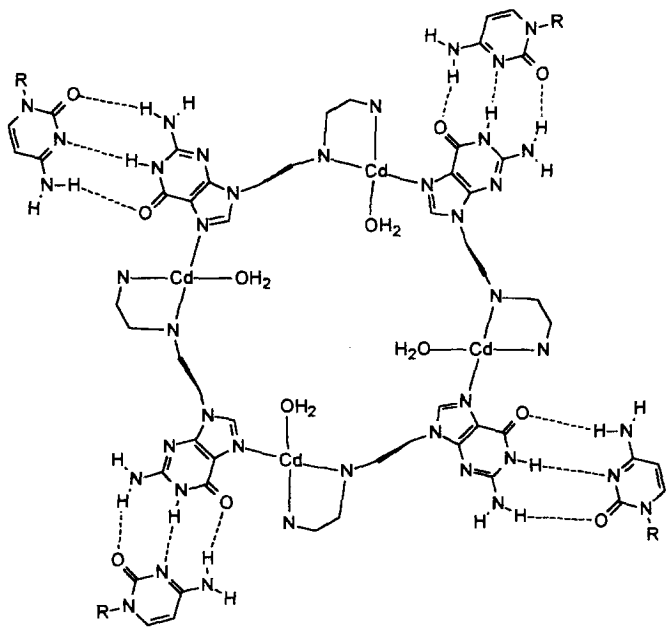

FIG. 37. Possible base-pairing scheme for **34** and four cytosine-containing derivatives. Reproduced with permission from Ref. (*58*). Copyright 2000, Wiley–VCH.

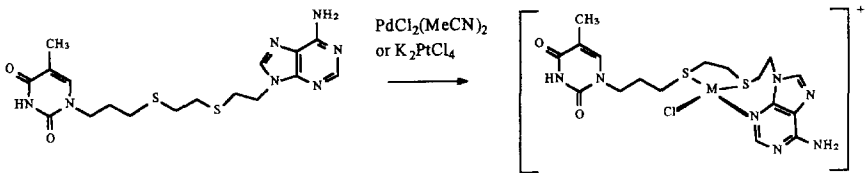

36 **37**

containing dithioether, **36**. Refluxing **36** with either $[PdCl_2(MeCN)_2]$ or $K_2[PtCl_4]$ gives the isostructural complex cations $(\mathbf{37})^+$ (M = Pd^{II} or Pt^{II}), in which the dithioether strand is coordinated through S-atoms and A–N3. In the solid state the complex cations form infinite chains of Hoogsteen base-pairs (T–N3 · · · A–N7 separation 2.886 Å), Fig. 38.

Loeb and co-workers have reported metallo-macrocycles, e.g., **38** and derivatives thereof, based on organopalladium chemistry (*61,137*). These complexes can recognize nucleobases via a combination of inner- and outer-sphere coordination. Sonication of a solution of the metallo-receptor with a 10-fold excess of solid nucleobase (A, C, G, or T) in deutero-acetone or deutero-acetonitrile highlighted the relative affinities of the various receptors for the four nucleobases (Fig. 39). None of the receptors extract T to any appreciable extent, while C is bound by all receptors in acetone. Crystal structure data confirm the inner- and outer-sphere binding involved. Cytosine binds through N3 to the metal ion (Pd–N3 bond length 2.171 Å) and forms a hydrogen bond between $N4H_2$ and an ether oxygen of the macrocycle (*137*). Examples containing guanine feature Pd–N7 coordination, π–π aromatic stacking, and hydrogen bonding involving the N2 amino group and the polyether chain. The two adenine-bound derivatives characterized to date involve N3-coordination of the nucleobase (Pd–N3 bond lengths 2.129 and 2.128 Å, respectively). As all the potential binding sites, N1, N3, N7, and, after deprotonation, N9, are available, this is a

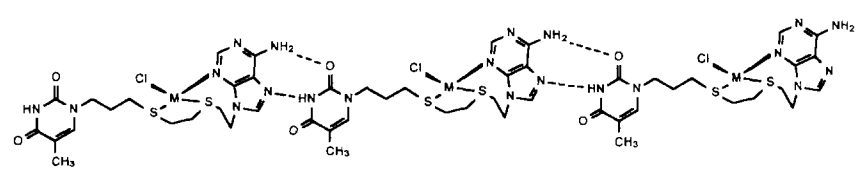

FIG. 38. Solid-state interactions of **37** involving Hoogsteen base-pairing of the coordinated adenine and the pendant thymine.

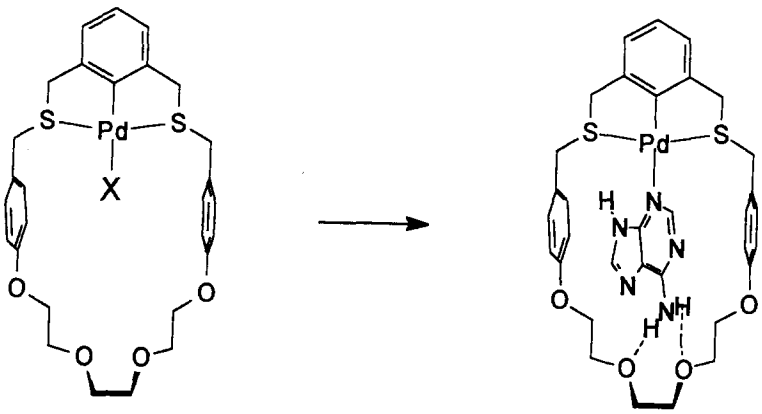

38 **38 + A**

surprising result. *It suggests that the hydrogen bonding between the nucleobase and the organic framework has a considerable influence, and directs the metal–nucleobase interaction (61).*

A series of adenine-derived cyclic trimers has been prepared and the ability to bind guest molecules explored (*138*). The trimer motif **39** is prepared by reaction of $[Cp^*RhCl_2]_2$ (Cp^* = pentamethylcyclopentadienyl) with an adenine derivative (9-methyladenine, adenosine, 2′deoxyadenosine, 2′,3′-dideoxyadenosine, 5-adenosine-monophosphate) after initial metathesis with AgOTf (Fig. 40). The resulting trimers contain Cp^*Rh^{III} fragments coordinated by bridging adenines. The binding involves a monodentate interaction with N1 and a chelating interaction involving N7 and the singly deprotonated N6. An X-ray structure of one of the enantiomers of the adenine trimer shows that the molecule has a C_3 axis, and that the cavity for binding guest molecules is about 7.5 Å wide and 4 Å deep (Fig. 40). Perhaps of most interest is the ability of these molecules to preferentially bind small biomolecules, such as amino acids, in aqueous solution at neutral pH. For comparison, the association constants for L–Trp and L–Phe binding to [Cp^*Rh-(2′deoxyadenosine)]$_3$(OTf)$_3$ are 607 and $< 10\,M^{-1}$, respectively.

A series of ferrocenylmethyl nucleobases has been synthesized and the interactions with DNA in aqueous solution have been studied by electrochemistry (*109,110*). The neutral $(\eta^5-C_5H_5)Fe(\eta^5-C_5H_4CH_2-)$ derivatives were prepared by alkylation of the corresponding base with $(\eta^5-C_5H_5)Fe(\eta^5-C_5H_4CH_2N(CH_3)_3^+$ (*110*). For thymine and cyto-

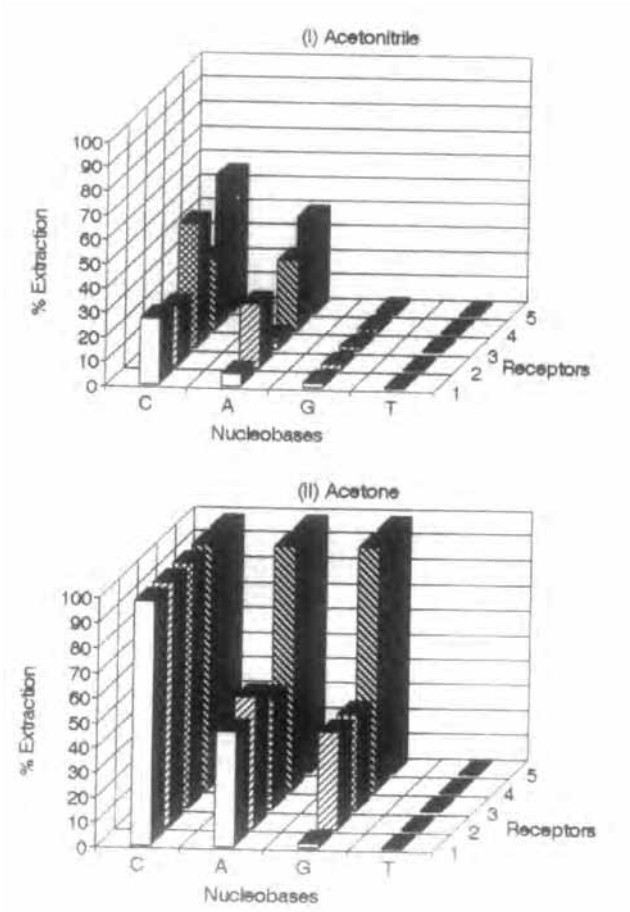

FIG. 39. Plot of the amount extracted (%) of solid nucleobase (C, A, G, T) into solutions of receptors of type **38** in (I) CD_3CN and (II) $(CD_3)_2CO$. Reproduced with permission from Ref. (*136*). Copyright 1993, American Chemical Society.

sine alkylation at N1 was preferential while for uracil the major product was the N3-isomer. Guanine is too insoluble to use directly; however, 2-acetylguanine gave the N7 and N9 isomers in approximately 3:1 ratio. Multiple alkylation involving N9 and the exocyclic amino group is observed with both adenine and 6-chloro-2-amino-purine (*110,139*). The electrode potentials of the compounds lie in the range +135 to −8 mV (vs. the ferrocenium–ferrocene couple). Electrochemical studies of the interaction of **40** (Fig. 41) with ds-DNA showed that the incorporation of the single T enhances the binding compared to the similarly charged $[FcCH_2N(CH_3)_3]^+$ control.

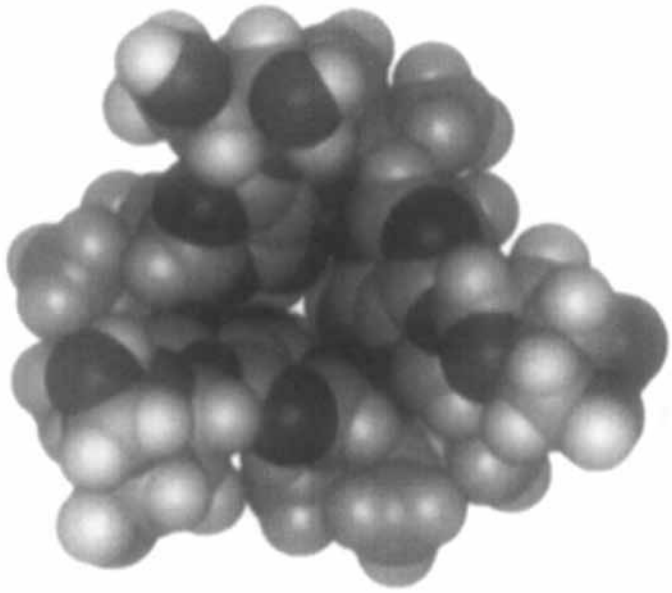

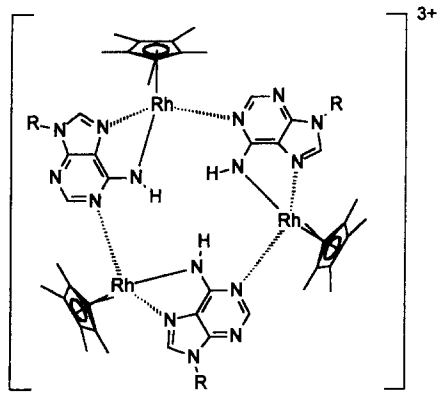

39

FIG. 40. Schematic and CPK model of the host compound **39.**

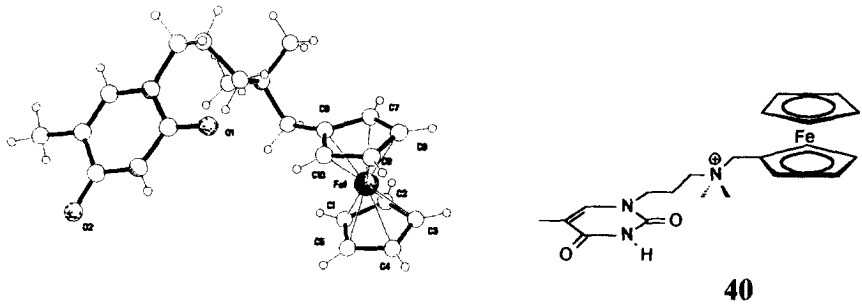

40

FIG. 41. Schematic and molecular structure of **40**. Adapted from Ref. (*109*).

IV. Metal-Modified DNA Using Solid-Phase Methods

Metal–ion complexes linked to DNA strands are of interest as artificial nucleases (*140–143*), hybridization probes (*144,145*), and for investigating DNA-mediated charge transport processes (*25*). Typically, the synthesis of such molecules has relied upon either post-synthetic conjugation of a preformed complex at the terminal position of an oligonucleotide (*25,146-150*), or addition of metal ions to oligonucleotides containing a multidentate ligand (*141,142,151,152*). In some cases, advantage has been taken of the phosphoramidite chemistry used in automated solid-phase oligonucleotide synthesis to prepare 5′-terminal labeled strands (*146,147,149,150,153*). More recently, this approach has been extended to metallo-crosslinking reagents (*154–156*), and to *base-modified* derivatives (*157–164*). The approach is well developed in organic chemistry but has been little considered for metal-modified nucleosides. The chemistry for automated solid-phase DNA synthesis is shown in Fig. 42.

The critical chain-extension reaction involves the nucleophilic attack at the P^{III} phosphoramidite by the 5′-hydroxyl group to form a phosphite. This is subsequently oxidized to the more stable phosphate. Removal of the base-protecting groups and cleavage from the solid support generally involves treatment in strong base, such as aqueous NH_3. Clearly, to use this approach for incorporating metal-containing groups the complexes must be sufficiently stable to repeated cycles of oxidation and strong base. This presents a considerable challenge for reactive metal groups, such as Pt-reagents, designed to undergo subsequent ligand substitution with DNA itself. However, the synthesis of Pt-labelled oligonucleotides for *in vitro* studies of metal–DNA

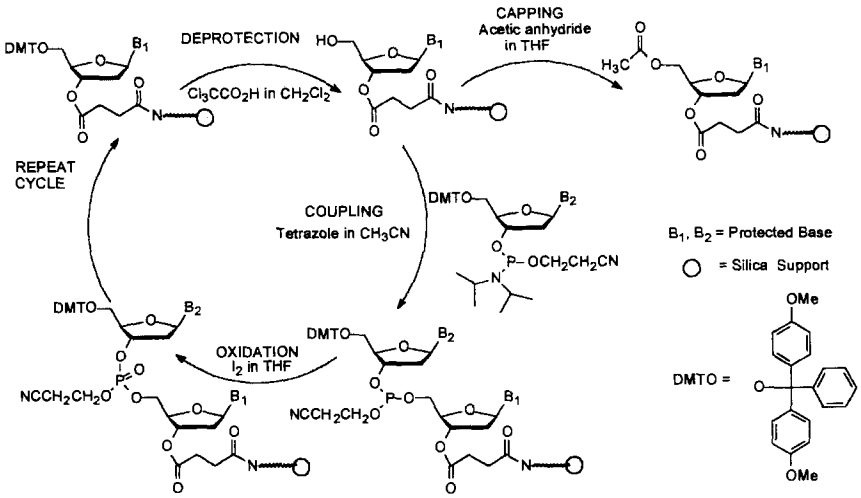

FIG. 42. Solid-phase synthesis of DNA oligomers, using phosphoramidites.

adducts has been realized (*154*). The N7-monofunctional complex *cis*-[Pt(NH_3)$_2$(5′DMT–deoxyguanosine–*N*7–3′phosphoramidite)Cl]$^+$ is unstable under the reaction conditions; however, the fully protected deoxyguanosine 3′-H-phosphonate proved suitable (Fig. 43). This reagent was used to form the 1,2-intrastrand crosslinked 20-mer oligonucleotide 5′-T_1 C_2 A_3 G_4 G_5 T_6 A_7 G_8^* G_9^* A_{10} C_{11} T_{12} T_{13} G_{14} G_{15} T_{16} G_{17} T_{18} C_{19} T_{20}-3′ (where * denotes the site of platinum attachment). The synthetic protocol involved standard automated oligonucleotide synthesis to the point in the sequence prior to the 3′-target dG base. The platinum-modified H-phosphonate was then introduced manually and the automated synthesis continued. The monofunctional adduct was converted to the 1,2-intrastrand dGdG crosslink oligomer by incubation in deionized water at 37°C prior to cleavage from the solid support.

Current limitations in antisense and antigene technology have also inspired interest in Pt-based reagents compatible with solid-phase DNA synthesis (*155,156*). Studies on nucleobase models have for some time indicated that *trans*-metal-complexes may act as effective crosslinking agents. However, the development of reagents for these applications has been non-trivial. Initial attempts to develop reactive *trans*-(amine)$_2$Pt-labeled oligonucleotides were only partially successful owing to problems of ligand substitution (*155*). More recently, these problems have been overcome and a short homo-pyrimidine oligonucleotide bearing a tethered *trans*-Pt–Cl unit has been prepared (*156*).

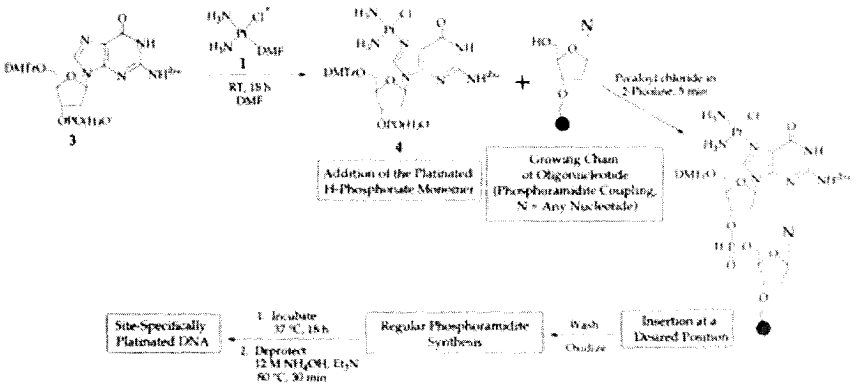

FIG 43. Site-specific platination of oligonucleotides. Reproduced with permission from Ref. (*152*). Copyright 1996, American Chemical Society.

Critical to the success of this procedure was the development of a suitable temporary ligand that is sufficiently inert to conditions of oligonucleotide deprotection (typically aqueous ammonia, 6 h at 50°C) and can subsequently be replaced by chloride. The nucleobase derivative 1-cyclohexamethyl-thymine **41** was found to satisfy these criteria and can be converted to the *trans*–Pt-Cl species by treatment with dilute HCl (pH 2.3, 40°C, 48 h). This last step restricts the range of possible oligonucleotide sequences to those that are not susceptible to depurination, but clearly establishes a prototype system for future development.

Substitution-inert complexes have also recently been introduced into DNA as modified-base phosphoramidites. Interest here is generally focused on photo- and redox-active metal species for use as probes for sensing applications (*165*) and in studies on DNA-mediated electron

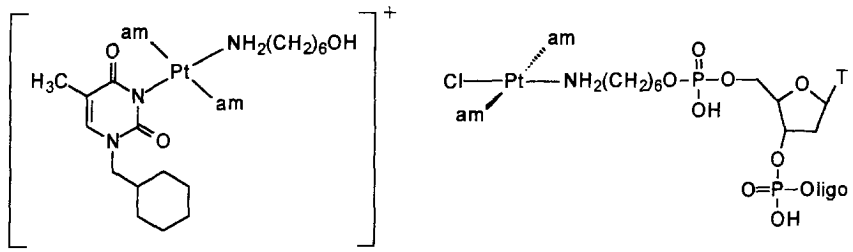

41

transfer (*25*). The generally preferred sites for nucleobase modification are C5–pyrimidine and C7-deaza-purine, as used in the fluorescent-labeled derivatives for sequencing, or the C8–purine site (Fig. 44). To date, metal-modified examples have been derived predominantly from uridine.

Hurley and Tor (*157*) have used Pd(0) cross-coupling reactions to prepare $[M(phen)(bipy)_2]^{2+}$ (M = Os, Ru), a C5–uridine derivative (Fig. 45a), which can be incorporated into 20-mer oligomers. Extended coupling times were required to optimize the incorporation (5 min > 90% efficiency), which was presumed to be due to the steric bulk of the metal complex. Thermal denaturation curves indicated that the metal-modified oligonucleotides had little effect on the stability of duplex structures, with a reduction of ~ 3°C for duplex structures containing the modified base in the middle of the sequence. In the case of 20-mer duplexes containing both Ru^{II} and Os^{II} attached complex separated by one natural AT base pair, a large (70–85%) reduction in the intensity of the Ru-centered 630 nm emission is observed compared to a duplex containing Ru alone (Fig. 45b). The quenching was dependent on distance and reduced to 40% for a 7-base-pair separation between two modified base pairs, suggesting intramolecular quenching of the excited state of the Ru by the Os.

An interesting alternative strategy for preparing base-modified oligonucleotides has been reported by Grinstaff (*159,161*). Alkynyl-derivatized metal complexes, based on $Ru(bipy)_3$–**42** and ferrocenyl–**43**, were attached to oligonucleotides containing a 2′deoxy-5-iodouridine using the Sonogashira Pd(0) cross-coupling reaction (Fig. 46). Regular automated solid-phase synthesis was interrupted after incorporation of the reactive iodo-nucleoside and the protected, supported, growing oligonucleotide was reacted with the alkynyl-derivatized metal complex under conditions to effect C–C coupling, $Pd(PPh_3)_4$, CuI, DMF:Et_3N,

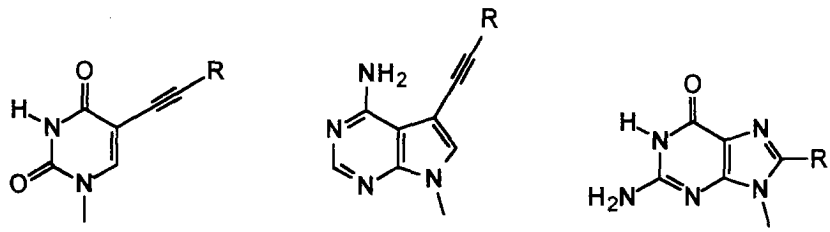

FIG. 44. Common sites for attaching redox- and photo-active groups to nucleosides C5–pyrimidine, C7–deaza-purine, and C8–purine.

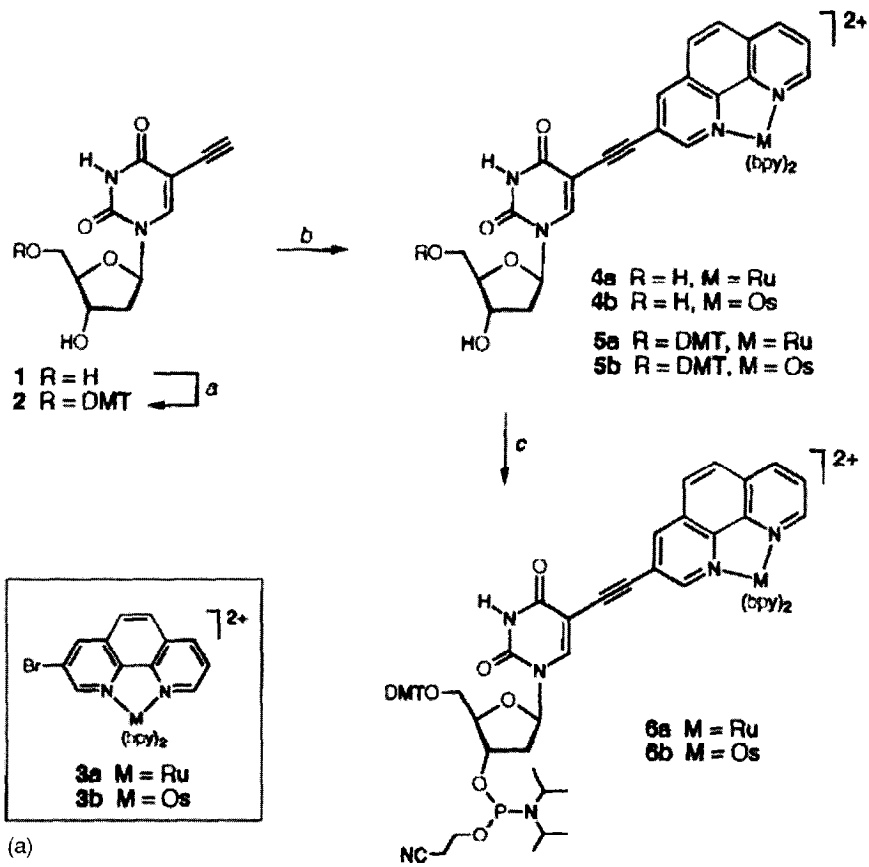

FIG. 45. (a) Introduction of $M(phen)_3^{2+}$ complex into DNA oligomers. (b). Steady-state emission spectra of modified oligonucleotides in 0.01 M sodium phosphate buffer, pH 7.0, 0.1 NaCl. Top: $Ru(phen)_3^{2+}$-modified 20-mer duplex (solid line), a 1:1 mixture of non-complementary $Ru(phen)_3^{2+}$- and $Os(phen)_3^{2+}$-modified 20-mers (· · ·) and a 20-mer duplex containing $Ru(phen)_3^{2+}$ and $Ps(phen)_3^{2+}$groups on different strands separated by one base pair (- - -). Bottom: 20-mer duplex with 5′-terminal $Ru(phen)_3^{2+}$ (solid line), and $Ru(phen)_3^{2+}/Os(phen)_3^{2+}$-containing analog (- - -). Reproduced with permission from Ref. (*157*). Copyright 1998, American Chemical Society.

reaction time 3 h. Normal synthesis was then resumed. Performing the coupling reaction immediately following the incorporation of the 2′deoxy-5-iodouridine significantly improved the yield compared to reactions with the completed oligonucleotide (50%, cf. 8%) (*161*). Such an on-column method has several advantages, including a reduction in the number of synthetic steps involved, and makes possible the introduction of a wide range of functional groups.

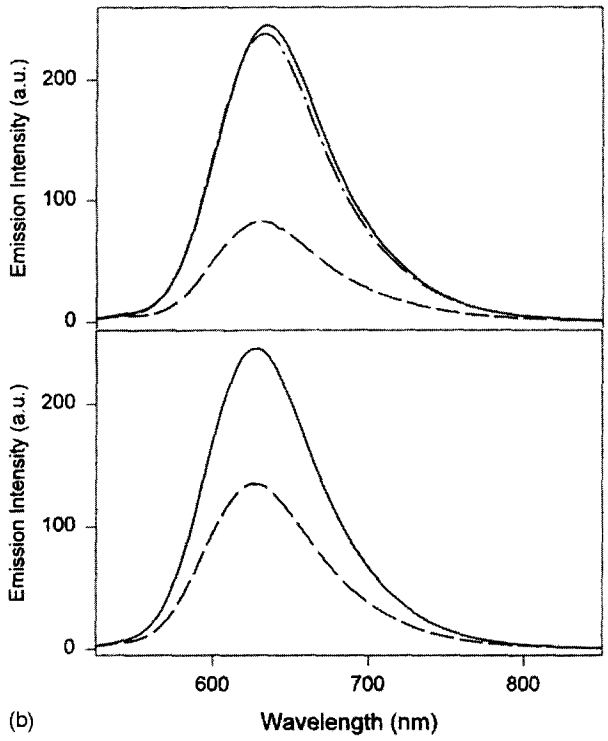
Emission Intensity (a.u.)
200
100
0
Emission Intensity (a.u.)
200
100
0
600
700
800
(b)
Wavelength (nm)

FIG. 45b

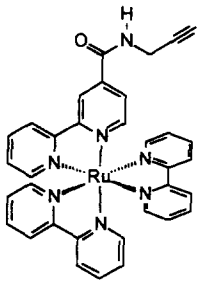
H
O
N
N
N
N
Ru
N
N
N

42

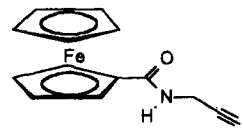
Fe
O
N
H

43

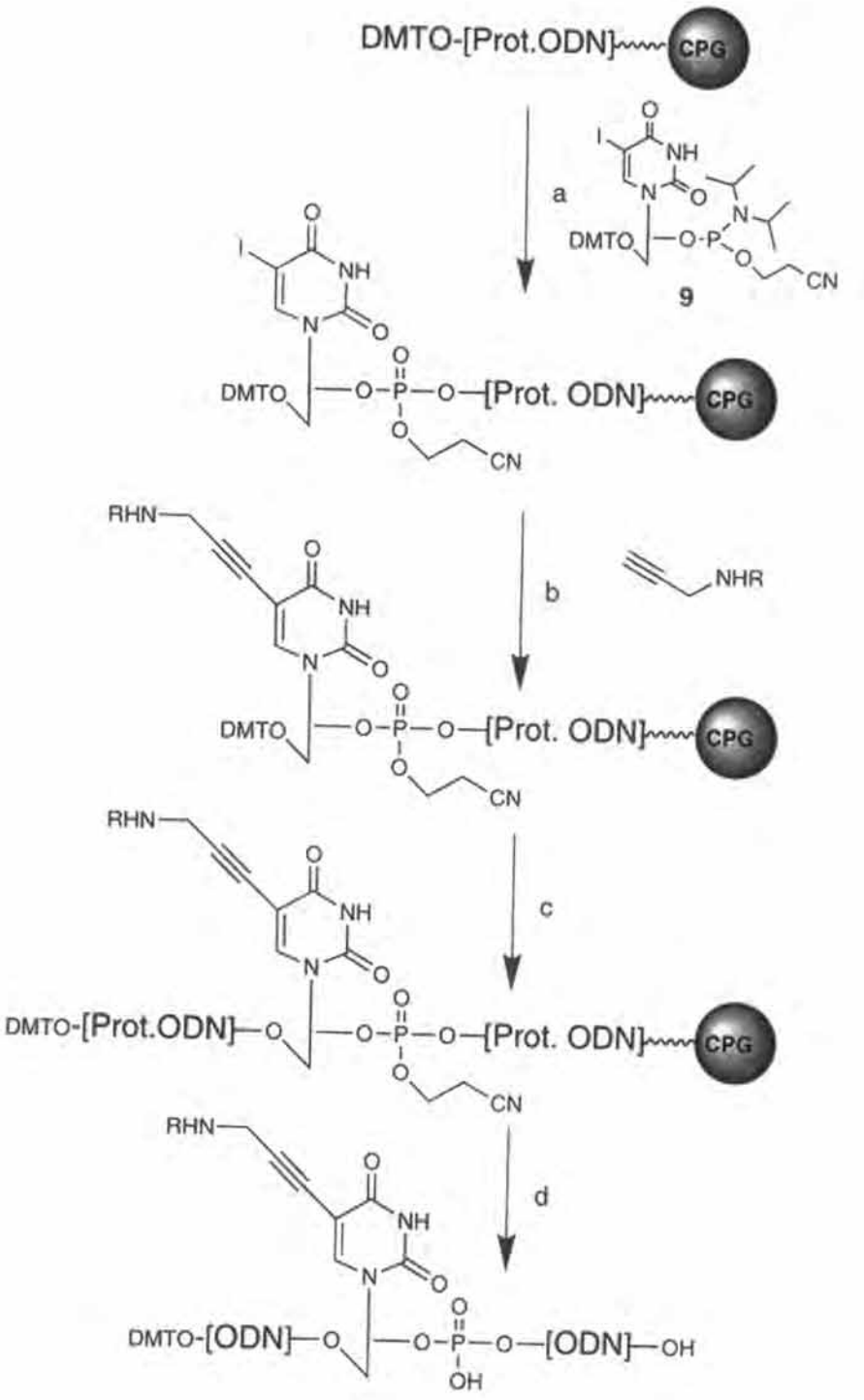

FIG. 46. On-column attachment of redox- and photo-active groups to DNA oligomers. Reproduced with permission from Ref. (*159*). Copyright 1999, American Chemical Society.

The ferrocenyl group appears to be well suited for the development of redox-active oligonucleotides given its stability, diverse substitution chemistry, and its amenable stereochemistry. There have been reports of the terminal attachment of ferrocenyl groups to oligonucleotides using simple derivatives, including ferrocenylhexanol as a phosphoramidite (*165,166*). Ferrocenyl–nucleosides were first synthesized by Gautheron and co-workers (*167*) as possible antitumour agents, and more recently attempts have been made to incorporate this type of compound directly into DNA strands using automated methods (*163,164*). Oligonucleotides containing C5–ethynylferrocene–dT **44** were found to undergo cyclization during deprotection and cleavage from the solid support in aqueous NH_3 to form the ferrocenyl–furano–pyrimidone, **45**, Fig. 47 (*163*). Such cyclization reactions are known for alkynyl–thymidine derivatives and have previously been reported for C5–ethynylferrocene–dT (*167*). The reaction is base catalyzed, and generally strong base has been used. However, this is not necessary as the ferrocenyl group activates the C≡C bond towards nucleophilic attack.

The crystal and molecular structure of the **44**, **45**, and C5–vinylferrocenyl–thymidine show that the substituted cyclopentadienyl ring is essentially co-planar with the nucleobase (*164*). DFT calculations indicate that, irrespective of the extent of saturation in the bridging C_2-unit in ethynyl–, vinyl– or ethyl–ferrocenyl–C5–thymidine, a similar amount of spin density is transferred to the nucleobase (Fig. 48). The reduction potentials for these compounds are shifted little compared to the parent ferrocenyl derivatives.

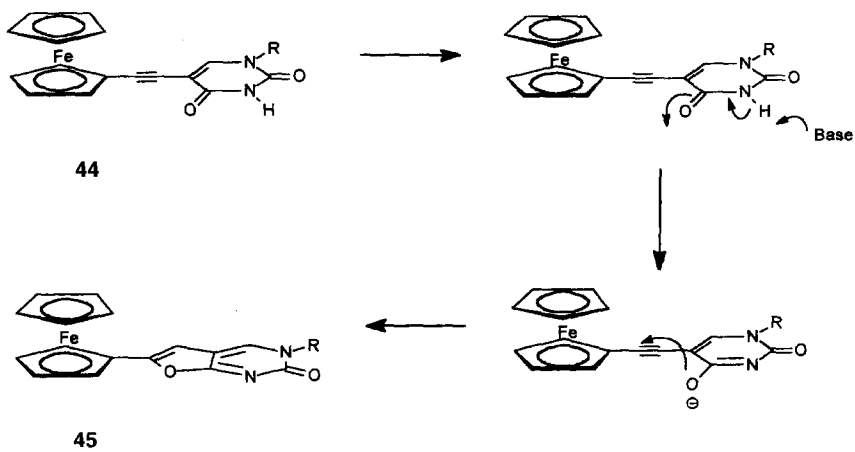

FIG. 47. Mechanism for the base-catalyzed cyclization of **44** → **45**. Adapted from Ref. (*163*).

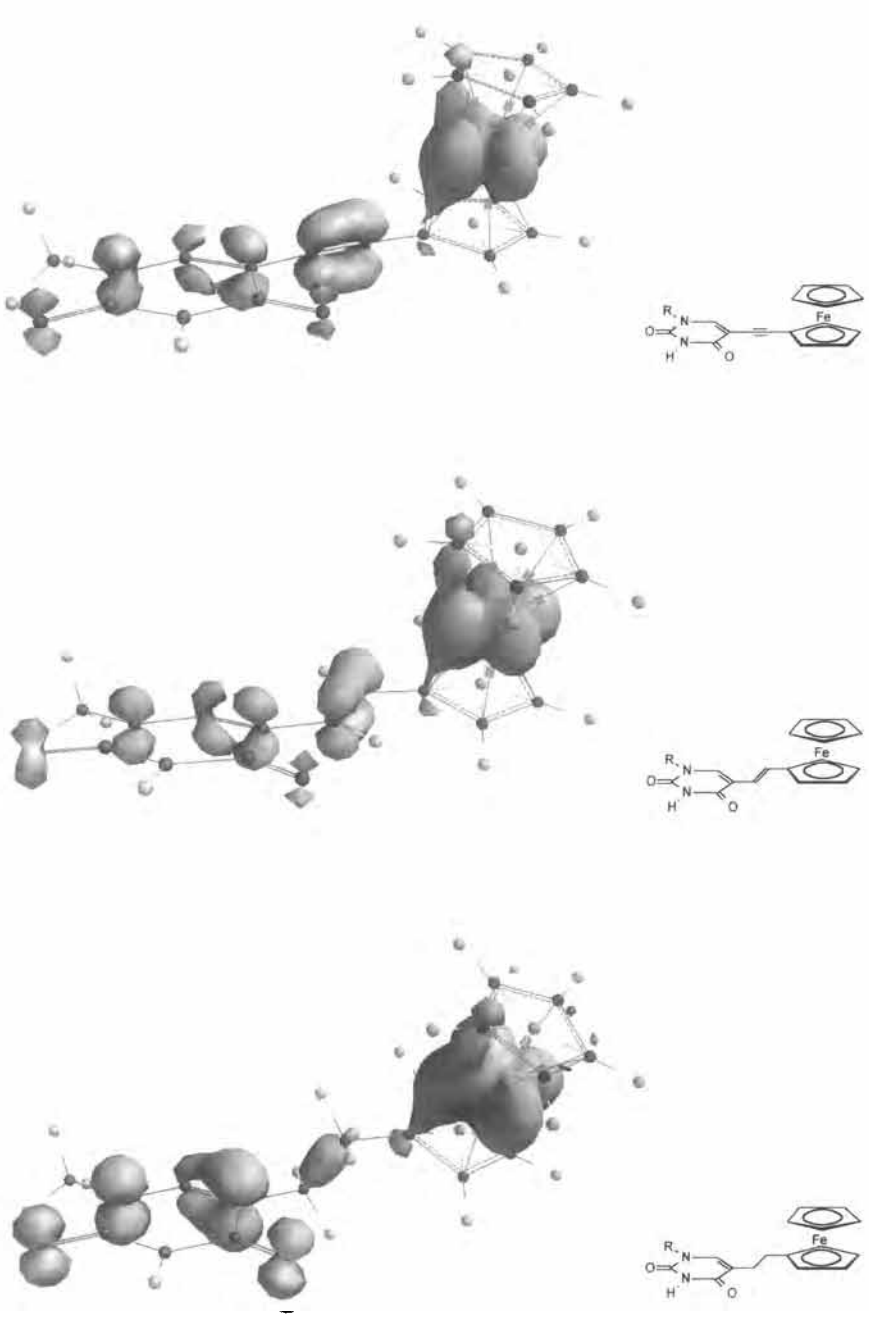

FIG. 48. Calculated structures for one-electron oxidized C5–ferrocenyl-modified dT derivatives, illustrating distribution of spin-density as a function of linkage. Ref. (*164*).

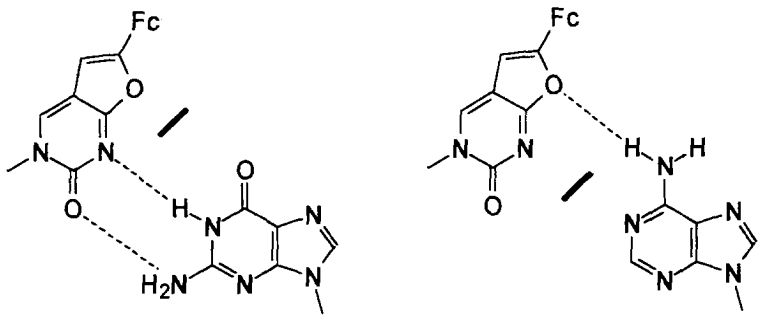

FIG. 49. Base-pairing of **45** with G and A. The former is preferred, as reported in Ref. (*163*).

Thermal denaturation studies on 15-mer oligomers indicated that **45** has a preference for base-pairing with dG compared to dA (Fig. 49) (*163*). Subsequently, it has been found that **44** can be incorporated into DNA oligomers intact using alternative reagents and work-up procedures. However, the oligomers produced contain a 1:1 mixture of **44**:**45** (*164*).

V. DNA and Nanotechnology

The use of DNA as a material for nanotechnology applications (*27,168*) is an increasingly considered option, owing to several factors. Foremost are the well-established rules for building molecular architectures using the complementary base-pairing principles (*26*). In addition, the polymeric nature, ease of synthesis (chemical or biological), and possible biological manipulation of DNA further enhance its suitability for new technological applications. Also, the increasing evidence for DNA-mediated charge transfer has increased interest in the possibility of a DNA-based molecular electronics.

Several reports have sought to explore the suitability of DNA as the conduit of charge transfer by direct measurement of its electrical conductivity across an electrode junction. Porath *et al.* (*169*) have reported large-bandgap semiconducting behavior for poly(dG)–poly(dC) (30 bp $\sim$ 10.4 nm long) spanning an 8 nm gap between two Pt electrodes. In contrast, conductivity measurements performed on 16 μm long ds-λ–DNA connecting two superconducting Re/C electrodes found conduction over a wide temperature range (RT and 1K) with a low resistance

per molecule (< 100 kΩ (*170*). Furthermore, the observed proximity-induced superconductivity below the transition temperature of the contacts (1 K) indicated the molecules to be conducting. It was, however, emphasized that the role of the contact between the electrode and DNA may be crucial to the measured properties, but that these are poorly defined in this and other systems (*170*).

A rather better defined electrode–DNA interface is seen in the elegant approach to making DNA-based metallic interconnects of Braun *et al.* (*171*). Here the structural and molecular recognition properties of DNA are used to template a silver wire between two gold electrodes. Figure 50 outlines the procedure. To each electrode surface is chemisorbed a thiol-modified 12-mer oligonucleotide (Electrode A–oligoA: Electrode B–oligo B). To this λ-DNA, containing "sticky-ends" complementary to the sequences A and B, is added which spans the 12–16 μm gap. A 0.1 M $AgNO_3$ basic aqueous solution (0.05 M, ammonium hydroxide, pH = 10.5) is then added to ion-exchange the Na^+ ions. Then the Ag^+/DNA complex is reduced, using basic hydroquinone, to form small metallic silver aggregates bound to the DNA. Further treatment with acidic solution of hydroquinone and Ag^+ ions yields a silver wire ~12 μm long and 100 nm wide.

The choice of metal ion in this work is interesting since it has been known for a considerable time that Ag^+ is a rare example of a d-block metal ion that does not disrupt the duplex DNA structure (*172,173*). Rationalization of this effect has tended to focus on the possible base-pair crosslinking due to the preferred linear coordination geometry of Ag^I ions (*174*). The importance of $Ag^+ \cdots$ DNA coordination chemistry to the procedure described is not clear. However, reports that other metal ions, e.g., Pd^{II} (*175*), can be plated to DNA to fabricate metallic wires (Fig. 51) suggests that this may not be essential.

The possibility for a truly molecular DNA-based device is illustrated by the intriguing, so-called, metal- or *M*-DNA. This form of DNA was reported by Lee *et al.* in 1993 and is formed at pH > 8 (typically pH = 8.5) in the presence of various species of divalent metal ion, e.g., Zn^{II}, Ni^{II}, and Co^{II}, but not Mg^{II} or Ca^{II} (*176*). The *B*-DNA → *M*-DNA transition occurs with the release of protons, and titration with $NiCl_2$ indicates one proton is released per metal ion per base pair. On the basis of ^1H NMR studies the imino T–H3 and G–H1 protons are lost, accounting for the need for basic conditions. Electronic absorption and CD spectra are relatively unperturbed in the transformation, suggesting a *B*-type structure is retained. The authors report that all bacterial and synthetic DNA, with the exception of perhaps poly[d(AT)], undergo this interconversion, which is reversible on addition of ethyl-

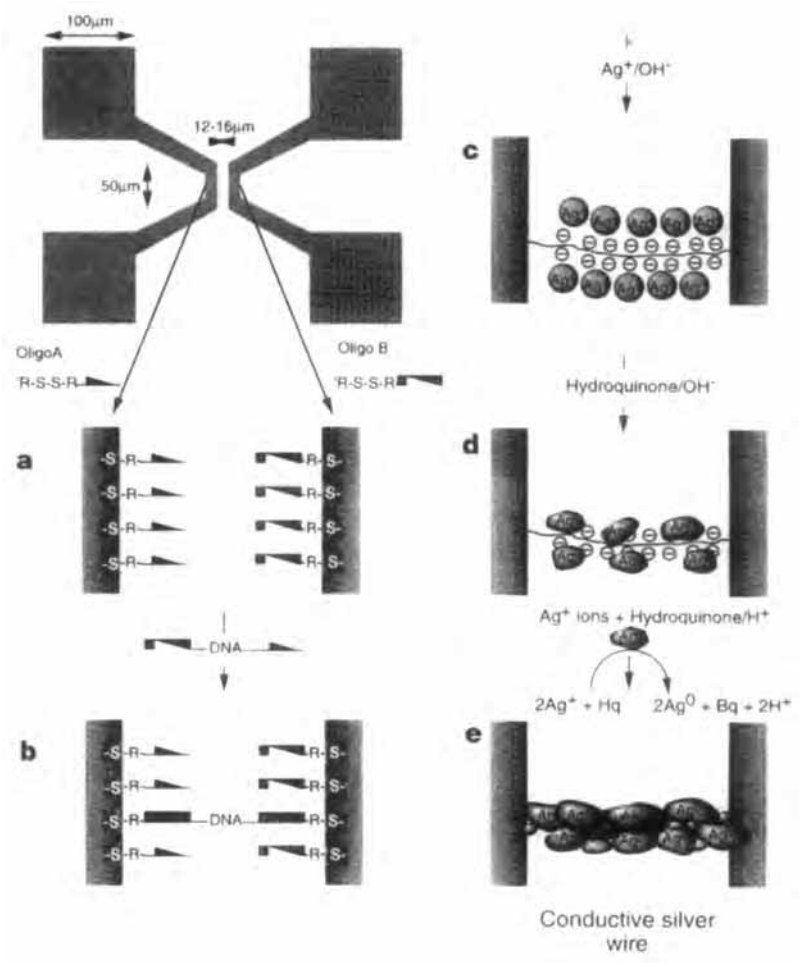

FIG 50. Construction of a silver wire connecting two gold electrodes. The top left image shows the electrode pattern (0.5×0.5 mm) used in the experiments. The two 50 μm long, parallel electrodes are connected to four (100×100 μm) bonding pads. (a) Oligonucleotides with two different sequences attached to the electrodes. (b) λ-DNA bridge connecting the two electrodes. (c) Silver-ion-loaded DNA bridge. (d) Metallic silver aggregates bound to the DNA skeleton. (e) Fully developed silver wire. Reproduced with permission from Ref. (*171*). Copyright 1998, *Nature* (London).

enediaminetetraacetic acid (EDTA). On the basis of these data, the $N1_{purine}$–metal–$N3_{pyrimidine}$ metal-modified base-pairing scheme has been proposed for the structure of *M*-DNA (Fig. 52).

Recent investigations into the charge-transport properties of *M*-DNA have indicated highly conducting behavior (*177*). Fluorescence lifetime

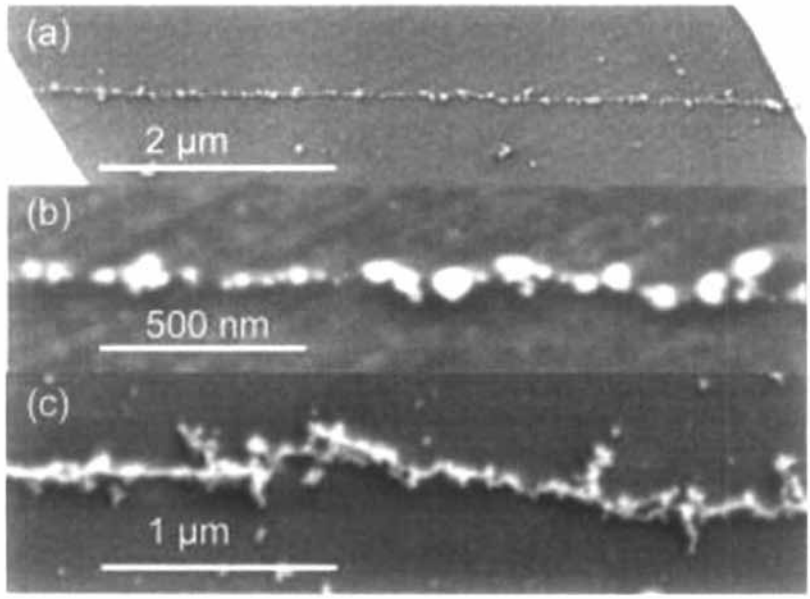

FIG. 51. Scanning electron microscope image of different stages of metalization of DNA. (a) Linear chain of separated palladium clusters connecting two gold contacts; (b) magnification of (a) showing clusters with diameter > 40 nm; (c) continuous coated DNA strand after one development step with a diameter larger than 40 nm. Reproduced with permission from Ref. (*175*). Copyright 2001, American Institute of Physics.

measurements indicated a very rapid component ($\tau \leq 10$ ps) to the decay kinetics for 20-mer duplexes containing terminal fluorescein donor and rhodamine acceptor groups; a feature characteristic of rapid charge transfer. Longer, 54-base-pair, duplexes showed similar behavior. Interestingly, the addition of the sequence-specific DNA-binding protein re-established much of the fluorescence in these longer oligomers, suggesting attenuation of the charge transfer.

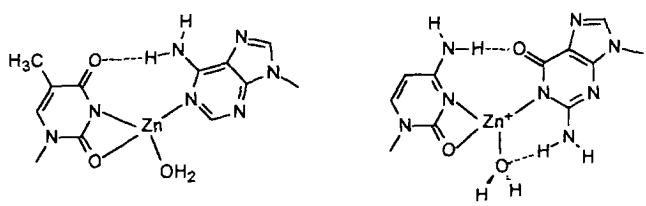

FIG. 52. Suggested base-pairing scheme for metal derivatized *M*-DNA where the imino protons of N3–T and N1–G are replaced by a divalent metal ion. Adapted from Ref. (*177*).

Subsequent conductivity measurements have been made on bundles of phage λ-DNA spanning a 10 μm spacing between gold electrodes (*178*). For regular *B*-DNA, semiconductor-like behavior was observed in the current–voltage curves with a band gap of approx. 200 meV. For *M*-DNA metallic-like conduction was apparent with no observable plateau region in the *I–V* curve (Fig. 53).

No satisfactory explanation for the mechanism of charge transfer through *M*-DNA has yet been put forward. The lack of accessible redox chemistry for Zn^{II} argues against a metal-based pathway. Furthermore, while the suggested coordination modes are plausible there is little precedent. The work of Kimura and Kikuto (*179*) has demonstrated that Zn^{II} in cyclen complexes has a highly specific interaction with N3T sites even in duplex DNA. However, the similar ability to form *M*-DNA with Ni^{II} and Co^{II} raises some interesting questions regarding the metal–ion binding. Crystallographically characterized complexes (*180*) of Ni^{II} and Co^{II} indicate typical binding patterns, e.g., G–N7, A–N7, and hence binding at the center of the duplex would be surprising.

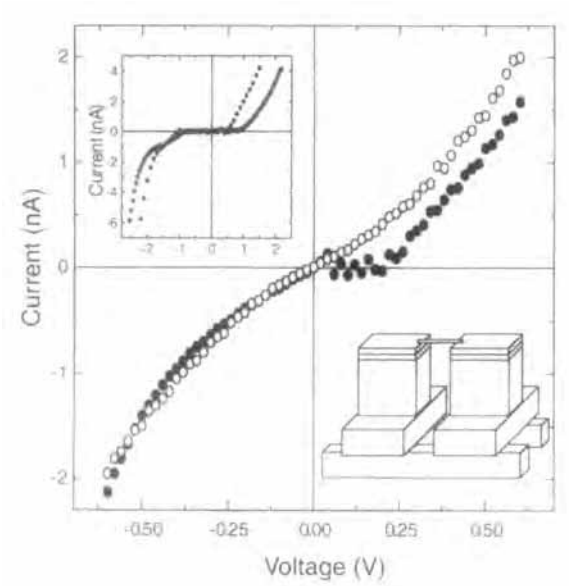

FIG. 53. Current–voltage curves measured in vacuum at RT on *M*-DNA (open circles) and B-DNA (closed circles). The former indicates semiconductor-like behavior and the latter metal-like. Reproduced with permission from Ref. (*178*). Copyright 2001, American Physics Society.

Further work will be required to clarify the structural details of this interesting new form of DNA.

The attachment of DNA to inorganic substrates is a key aspect of many anticipated (nano)technological applications. Both in fundamental measurements, as mentioned above, and in future device applications the benefits of a well-defined interface between DNA and an electrode material are important. Methods for immobilizing DNA oligonucleotides to metallic substrates such as Au and Pt are now straightforward and use thiol-terminated oligomers (*181*). The thiol groups anchor the DNA spontaneously to the metal surface and either single- or double-stranded DNA can be assembled in this way (Fig. 54).

This has been exploited in the elegant work of Alivisatos *et al.* (*182*) and Mirkin and co-workers (*168,183–185*) who have used DNA-recognition processes to organize Au nanoparticles into structured assemblies. The

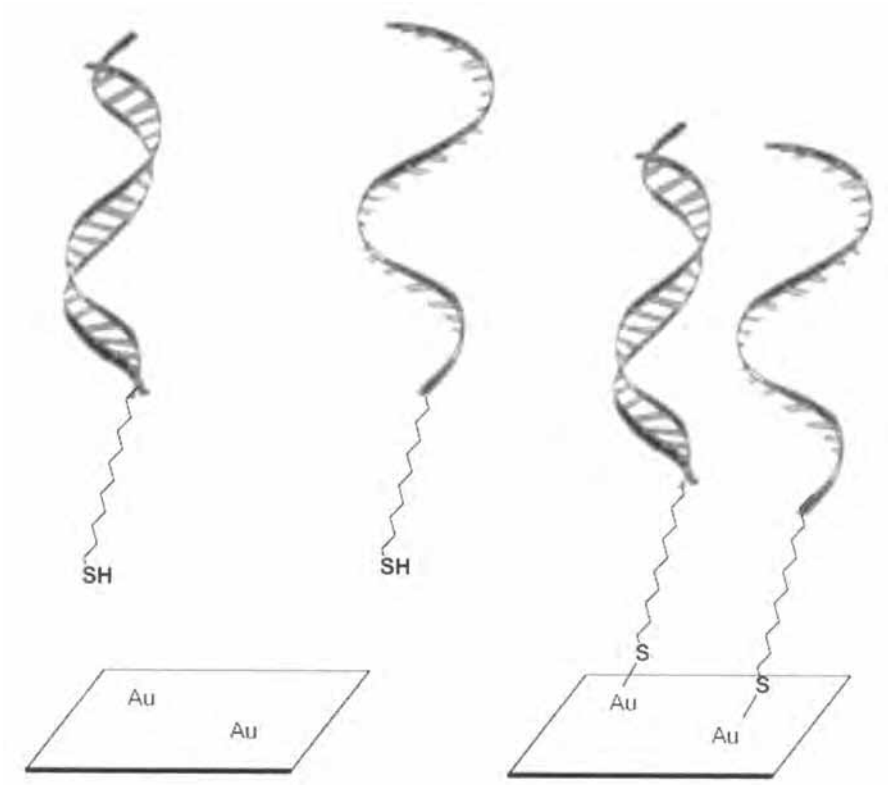

FIG. 54. Schematic illustrating the formation of DNA-monolayers by Au–thiol interactions.

latter group has used sticky-end duplex DNA as a crosslinkage via hybridization with complementary sequences (Fig. 55). The resulting assembly of the gold particles induces a red → blue color change due to perturbations of the plasmon band, and this has been used to develop a highly sensitive colorimetric test for DNA sequences (*183*). The assembly process generates an ABAB periodicity that can be seen in assemblies of nanoparticles of different sizes (Fig. 56). This building process has also been performed at surfaces to build up multilayered structures (*184*).

A similar approach to building DNA–nanoparticle networks has been reported by Niemeyer (*186,187*). Here biotinylated duplex DNA is used as a spacer and the binding event for self-assembly involves the highly specific biotin–streptavidin interaction. A range of discrete aggregates and extended networks has been prepared (Fig. 57). While these DNA–protein conjugates lie outside the scope of this review, one aspect is especially relevant. Divalent ions, in the form of Mg^{2+}, have been used to induce structural changes of these assemblies (*186*). Explanations are based upon supercoiling between DNA molecules bound to adjacent streptavidin binding sites (Fig. 58). This raises the possibility of using metal ion · · · DNA interactions to control, or switch, DNA-based assemblies.

In comparision with metal or insulating oxides, the attachment of oligonucleotides to semiconductor surfaces has been little considered. One such example of DNA-modified semiconductor materials is metal sulfide/selenide nanoparticles (*188*) which were functionalized with DNA in a similar manner to the gold particles. For silicon substrates the lack of suitable chemistries for covalent modification of the semiconductor surface has limited development. However, the molecular chemistry at semiconductor solids has been significantly advanced by the pioneering work of Chidsey on the reactivity of hydrogen-terminated silicon (*189, 190*). Hydrogen-terminated silicon surfaces are formed on etching with aqueous ammonium fluoride or hydrofluoric acid and are an integral step in the fabrication of semiconductor devices. The surface generated by this treatment can react with a range of molecular functional groups, such as alkene (*191,192*), alkyne (*191*), and alcohols (*193*), to form covalently-modified surfaces (Fig. 59). *This chemistry differs fundamentally from typical methods used for derivatizing silicon that rely on reaction with the insulating native oxide.*

Smith and co-workers (*194*) have used this chemistry to prepare carboxyl-modified Si(111) surfaces at which polylysine-tethered DNA is electrostatically adsorbed (Fig. 60). An alternative approach involved covalent attachment of a pre-synthesized oligonucleotide bearing a terminal carboxyl group to an amine-modified Si(001) surface (*195*).

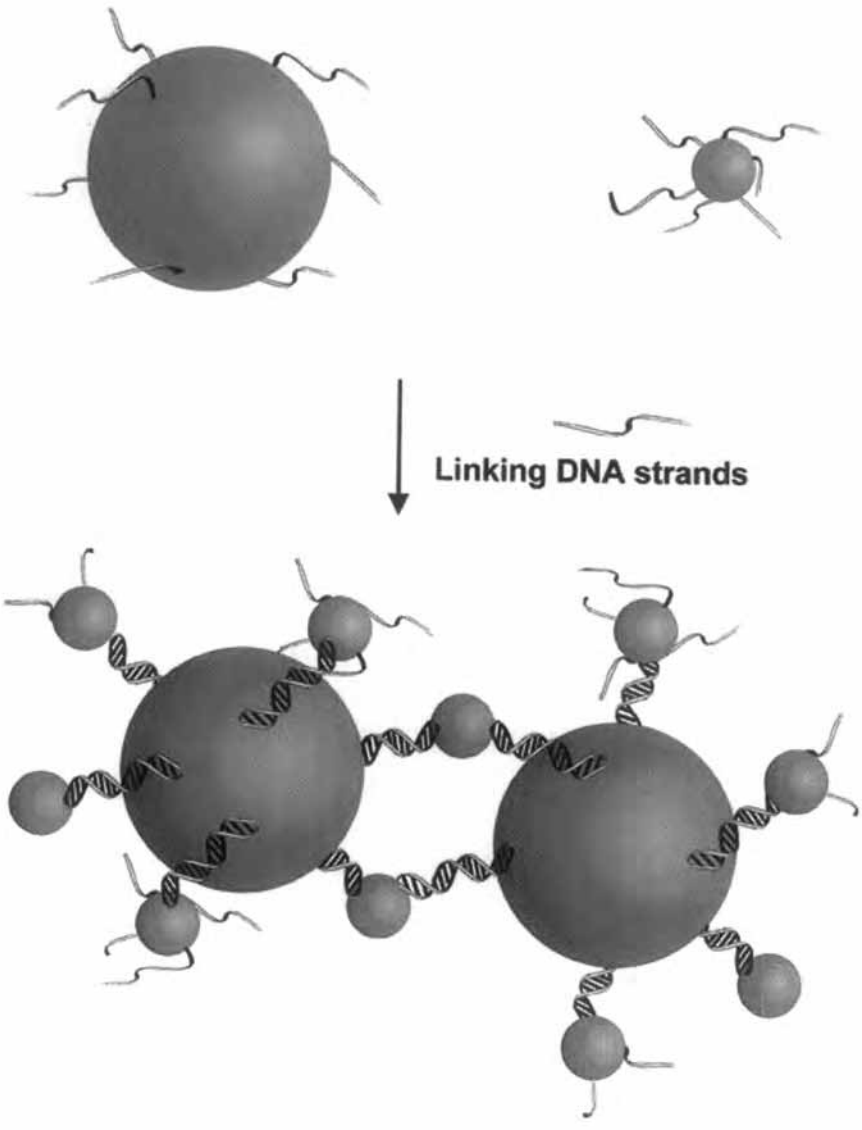

FIG. 55. DNA assembly of gold nanoparticles. Different sized particles (typically, 8 and 30 nm) are assembled alternately through DNA sequence specificity. Reproduced with permission from Ref. (*185*). Copyright 2000, American Chemical Society.

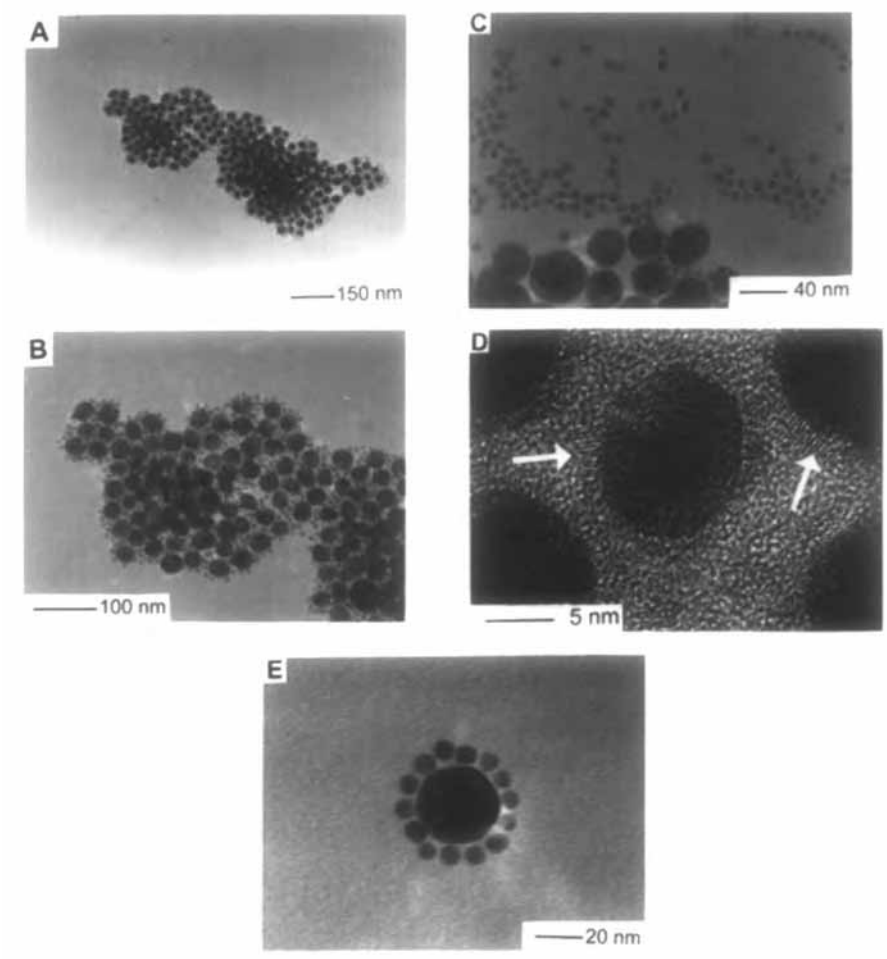

FIG. 56. TEM images of DNA-linked gold network: (a) an assembly of 8 and 30 nm gold particles; (b) higher resolution image of (a); (c) control experiment without DNA; (d) HR–TEM image of a portion of a hybrid Au/quantum dot (QD) assembly. The lattice fringes of the QDs, which resemble fingerprints, appear near each Au nanoparticle. (e) A satellite structure formed using a 60-fold excess of the 8 nm particles. Reproduced with permission from Ref. (*185*). Copyright 2000, American Chemical Society.

More recently, it has been shown that DNA oligomers can be synthesized directly on modified semiconductor surfaces using automated methods (*196*). The silicon surfaces are first modified to give a terminal, protected, hydroxyl group at which automated phosphoramidite chemistry can be performed (Fig. 61). Semiconductor processing methods

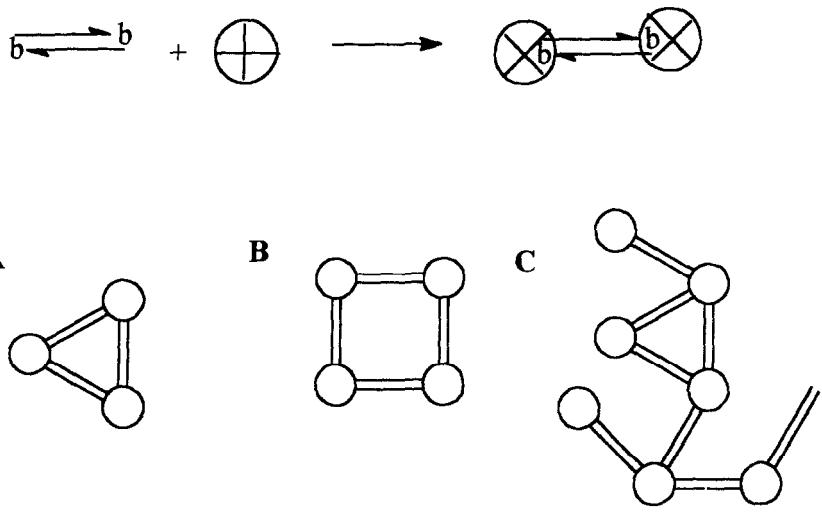

FIG. 57. DNA–nanoparticle assembly based on biotin–streptavidin binding. Discrete, **A** and **B**, and extended, **C**, networks have been constructed. Adapted from Ref. (*186*).

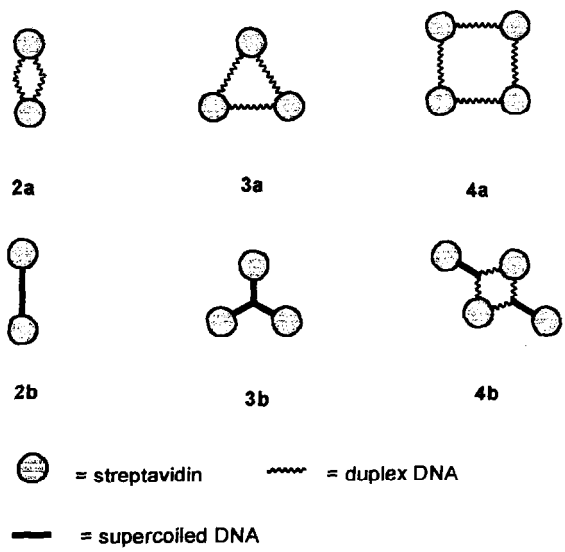

FIG. 58. Metal ion modulation of DNA–nanoparticle constructs based upon supercoiling. Adapted from Ref (*186*). Structures labelled (a) and (b) are before and after metal ion addition, respectively.

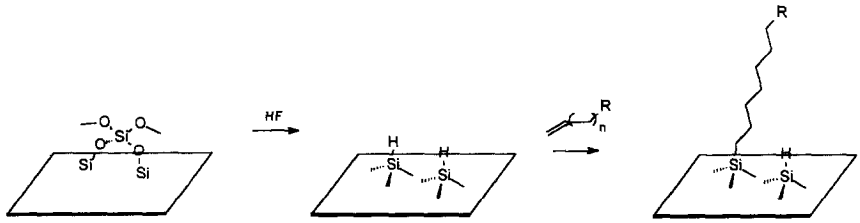

FIG. 59. Molecular modification of semiconductor silicon surfaces. Removal of the oxide generates a hydrogen-terminated layer that reacts with a range of molecular functional groups including alkenes.

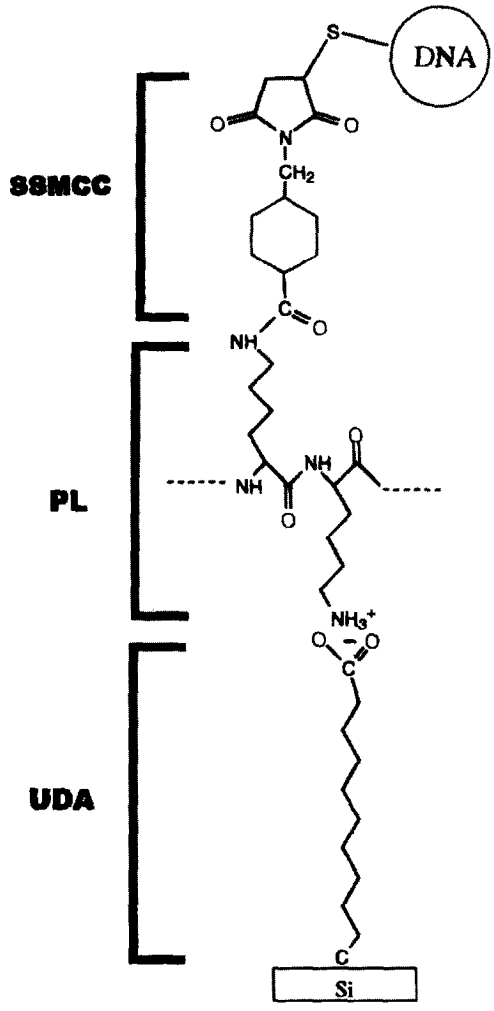

FIG. 60. Schematic illustrating electrostatic immobilization of DNA to a carboxyl-modified Si(111) surface. Reproduced with permission from Ref. (*194*). Copyright 2000, American Chemical Society.

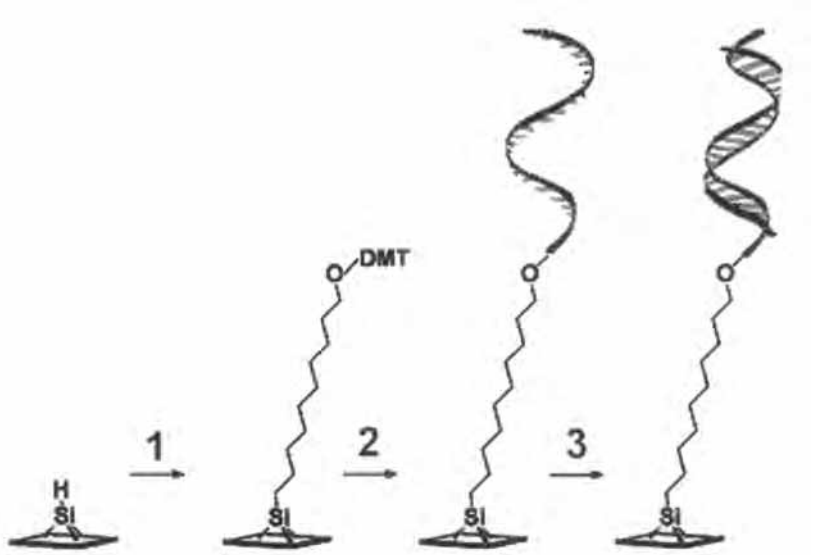

FIG. 61. Schematic illustrating the on-chip synthesis of DNA oligomers at silicon surfaces. Reproduced with permission from Ref. (*196*). Copyright 2001, Wiley–VCH.

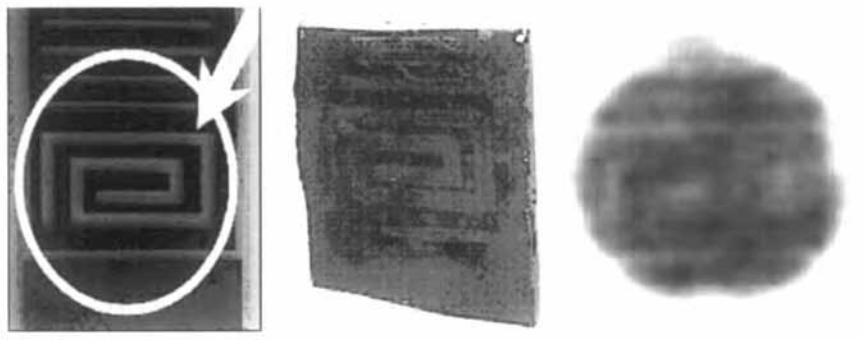

FIG. 62. A DNA-patterned Si surface formed by photolithography and anodic etching to form porous silicon regions. The surface was functionalized with a 17-mer oligonucleotide according to Fig. 61. Left, the mask; center, Si wafer after on-chip DNA synthesis; right, a phosphorimage after hybridization with a complementary ^{32}P-labelled oligonucleotide. The light regions (in the center image) are porous silicon and these correspond with the dark regions of ds-DNA (right). Reproduced with permission from Ref. (*196*). Copyright 2001, Wiley–VCH.

can be exploited, such as photolithography to generate patterned DNA surfaces (Fig. 62). The silicon-bound oligonucleotides have a surface coverage similar to thiol-derivatized oligomers on gold surfaces and can act as substrates for T4 polynucleotide kinase. DNA-mediated charge transfer was observed, binding the redox-active intercalator methylene blue to the silicon-bound duplex DNA.

VI. Conclusion

This review has aimed to bring into focus a variety of DNA-related chemistries that have an inorganic perspective. The coordination chemistry of DNA is well established but continues to expand and be better understood in both real and model systems. The use of DNA in nanotechnology applications, including its use as a template for forming metallic connections, will benefit from the detailed understanding that such studies provide. The controversial topic of DNA-mediated charge transport will also benefit from the availability of better defined systems. These are now appearing through a combination of metallonucleosides and solid-phase automated synthesis. In fact, redox-labeled oligonucleotides on Au electrodes are now available commercially as gene-sensing technology (eSensor^{TM}) (*197*). The recent inclusion of semiconductor silicon as a material at which DNA oligomers can be automatically synthesized (*196*) creates numerous new possibilities for the design of molecular devices. From the breadth of topics considered herein, spanning supramolecular chemistry, biological chemistry, drug design, and nanotechnology, it is obvious that metal ion $\cdots$ DNA interactions will continue to warrant investigation for many years to come.

References

1. Watson, J. D.; Crick, F. H. C. *Nature* **1953**, *171*, 737.
2. http://www.ornl.gov/hgmis/
3. Sherman, S. E.; Lippard, S. J. *Chem. Rev.* **1987**, *87*, 1153.
4. Lempers, E.; Reedijk, J. *Adv. Inorg. Chem.* **1991**, *37*, 175.
5. Lippert, B. In "Cisplatin: Chemistry and Biochemistry of a Leading Anticancer Drug"; Lippert, B., Ed.; HVCA, Zurich and Wiley-VCH: Weinheim, **1999**; p. 379.
6. Spingler, B.; Whittington, D. A.; Lippard, S. J. *J. Inorg. Biochem.* **2001**, *86*, 440.
7. Takahara, P. M.; Rosenzweig, A. C.; Frederick, C. A.; Lippard, S. J. *Nature* **1995**, *377*, 649.

8. Guo, Z. J.; Sadler, P. J. *Adv. Inorg. Chem.* **2000**, *49*, 183.
9. Chen, Y.; Parkinson, J. A.; Guo, Z. J.; Brown, T.; Sadler, P. J. *Angew. Chem. Int. Ed.* **1999**, *38*, 2060.
10. Sava, G.; Alessio, E.; Bergamo, A.; Mestroni, G. In "Metallo-pharmaceuticals"; Clarke, M. J., Sadler, P. J., Eds.; Springer: Berlin, **1999**; Vol. 1, p. 143.
11. Keppler, B. K. "Metal Complexes in Cancer Chemotherapy"; VCH: Weinheim, Germany, **1993**.
12. Ohndorf, U. M.; Rould, M. A.; He, Q.; Pabo, C. O.; Lippard, S. J. *Nature* **1999**, *399*, 708.
13. Marzilli, L. G.; Saad, J. S.; Kuklenyik, Z.; Keating, K. A.; Xu, Y. H. *J. Am. Chem. Soc.* **2001**, *123*, 2764.
14. Parkinson, J. A.; Chen, Y.; Murdoch, P. D.; Guo, Z. J.; Berners-Price, S. J.; Brown, T.; Sadler, P. J. *Chem. Eur. J.* **2000**, *6*, 3636.
15. Jamieson, E. R.; Lippard, S. J. *Chem. Rev.* **1999**, *99*, 2467.
16. Reedijk, J. *Chem. Rev.* **1999**, *99*, 2499.
17. Ziegler, C. J.; Silverman, A. P.; Lippard, S. J. *J. Biol. Inorg. Chem.* **2000**, *5*, 774.
18. Sandman, K. E.; Marla, S. S.; Zlokarnik, G.; Lippard, S. J. *Chem. Biol.* **1999**, *6*, 541.
19. Cox, J. W.; Berners-Price, S. J.; Davies, M. S.; Qu, Y.; Farrell, N. *J. Am. Chem. Soc.* **2001**, *123*, 1316.
20. Farrell, N. In "Polynuclear Charged Platinum Complexes as a New Class of Anticancer Agents"; Kelland, L. R., Farrell, N., Eds.; Humana Press: Totowa, NJ, **2000**, p. 321.
21. Komeda, S.; Lutz, M.; Spek, A. L.; Chikuma, M.; Reedijk, J. *Inorg. Chem.* **2000**, *39*, 4230.
22. Velders, A. H.; Kooijman, H.; Spek, A. L.; Haasnoot, J. G.; de Vos, D.; Reedijk, J. *Inorg. Chem.* **2000**, *39*, 2966.
23. Guo, M. L.; Guo, Z. J.; Sadler, P. J. *J. Biol. Inorg. Chem.* **2001**, *6*, 698.
24. Alessio, E.; Iengo, E.; Serli, B.; Mestroni, G.; Sava, G. *J. Inorg. Biochem.* **2001**, *86*, 21.
25. Holmlin, R. E.; Dandliker, P. J.; Barton, J. K. *Angew. Chem. Int. Ed.* **1997**, *36*, 2714.
26. Seeman, N. C. *Angew. Chem. Int. Ed.* **1998**, *37*, 3220.
27. Bashir, R. *Superlattices and Microstructures* **2001**, *29*, 1.
28. Muller, J.; Drumm, M.; Boudvillain, M.; Leng, M.; Sletten, E.; Lippert, B. *J. Biol. Inorg. Chem.* **2000**, *5*, 601.
29. Lippert, B.; Leng, M. In "Topics in Biological Inorganic Chemistry"; Clarke, M. J., Sadler, P. J., Eds.; Springer: Berlin, **1999**; Vol. 1, p. 118.
30. Janik, M. B. L.; Lippert, B. *J. Biol. Inorg. Chem.* **1999**, *4*, 645.
31. Janik, M. B. L.; Hegmans, A.; Freisinger, E.; Lippert, B. *J. Biol. Inorg. Chem.* **1999**, *4*, 130.
32. van der Veer, J. L.; Ligtvoet, H.; van den Elst, H.; Reedijk, J. *J. Am. Chem. Soc.* **1986**, *108*, 3860.
33. Gibson, D.; Lippard, S. J. *Inorg. Chem.* **1987**, *26*, 2275.
34. Lepre, A. C.; Chassot, L.; Costello, C. E.; Lippard, S. J. *Biochemistry* **1990**, *29*, 811.
35. Bouvillain, M.; Dalbies, R.; Aussourd, C.; Leng, M. *Nucl. Acid Res.* **1995**, *23*, 2381.
36. Lui, Y.; Pacifico, C.; Natile, G.; Sletten, E. *Angew. Chem. Int. Ed. Engl.* **2001**, *40*, 1226.
37. Kikuta, E.; Murata, M.; Katsube, N.; Koike, T.; Kimura, E. *J. Am. Chem. Soc.* **1999**, *121*, 5426.
38. Aoki, S.; Sugimura, C.; Kimura, E. *J. Am. Chem. Soc.* **1998**, *120*, 10094.
39. Aoki, S.; Honda, Y.; Kimura, E. *J. Am. Chem. Soc.* **1998**, *120*, 10018.
40. Kuklenyik, Z.; Marzilli, L. G. *Inorg. Chem.* **1996**, *35*, 5654.
41. Young, M. A.; Jayaram, B.; Beveridge, D. L. *J. Am. Chem. Soc.* **1997**, *119*, 59.

42. Hamelberg, D.; McFail-Isom, L.; Dean Williams, L.; Wilson, W. D. *J. Am. Chem. Soc.* **2000**, *122*, 10513.
43. Tereshko, V.; Minasov, G.; Egli, M. *J. Am. Chem. Soc.* **1999**, *121*, 3590.
44. Tereshko, V.; Wilds, C. J.; Minasov, G.; Prakash, T. P.; Maier, M. A.; Howard, A.; Wawrzak, Z.; Manoharan, M.; Egli, M. *Nucl. Acid Res.* **2001**, *29*, 1208.
45. Hud, N. V.; Fiegon, J. *J. Am. Chem. Soc.* **1997**, *119*, 5756.
46. Han, W.; Lindsay, S. M.; Dlakic, M.; Harrington, R. E. *Nature* **1997**, *386*, 563.
47. Freisinger, E.; Schimanski, A.; Lippert, B. *J. Biol. Inorg. Chem.* **2001**, *6*, 378.
48. Freisinger, E.; Schneider, A.; Drumm, M.; Hegmans, A.; Meier, S.; Lippert, B. *J. Chem. Soc., Dalton Trans.* **2000**, 3281.
49. Zamora, F.; Witkowski, H.; Freisinger, E.; Muller, J.; Thormann, B.; Albinati, A.; Lippert, B. *J. Chem. Soc., Dalton Trans.* **1999**, 175.
50. Schall, O. F.; Gokel, G. W. *J. Org. Chem.* **1996**, *61*, 1449.
51. De Wall, S. L.; Barbour, L. J.; Schall, O. F.; Gokel, G. W. *J. Chem. Cryst.* **2000**, *30*, 227.
52. Gibson, A. E.; Price, C.; Clegg, W.; Houlton, A. *J. Chem. Soc., Dalton Trans.* **2002**, *131*.
53. Adamiak, D. A.; Saenger, W. *Acta Cryst.* **1980**, *B36*, 2585.
54. Swaminathan, P.; Sundaralingam, M. *Acta Cryst.* **1980**, *B36*, 2590.
55. Price, C.; Elsegood, M. R. J.; Clegg, W.; Houlton, A. *J. Chem. Soc., Chem. Commun.* **1995**, 2285.
56. Price, C.; Shipman, M. A.; Rees, N. H.; Elsegood, M. R. J.; Edwards, A. J.; Clegg, W.; Houlton, A. *Chem. Eur. J.* **2001**, *7*, 1194.
57. Shipman, M. A.; Price, C.; Elsegood, M. R. J.; Clegg, W.; Houlton, A. *Angew. Chem. Int. Ed.* **2000**, *39*, 2360.
58. Shipman, M. A.; Price, C.; Gibson, A. E.; Elsegood, M. R. J.; Clegg, W.; Houlton, A. *Chem. Eur. J.* **2000**, *6*, 4371.
59. Rother, I. B.; Freisinger, E.; Erxleben, A.; Lippert, B. *Inorg. Chim. Acta* **2000**, *300–302*, 339.
60. Meiser, C.; Song, B.; Freisinger, E.; Peilert, M.; Sigel, H.; Lippert, B. *Chem. Eur. J.* **1997**, *3*, 388.
61. Kickham, J. E.; Loeb, S. J.; Murphy, S. L. *Chem. Eur. J.* **1997**, *3*, 1203.
62. Sponer, J. E.; Leszczynski, J.; Glahe, F.; Lippert, B.; Sponer, J. *Inorg. Chem.* **2001**, *40*, 3269.
63. Pearson, C.; Beauchamp, A. L. *Inorg. Chem.* **1998**, *37*, 1242.
64. Sheldrick, W. S.; Gunther, B. J. *J. Organomet. Chem.* **1989**, *375*, 233.
65. Houlton, A.; Price, C.; Clegg, W.; Shipman, M. A., unpublished.
66. Raudaschl-Seiber, G.; Schollhorn, H.; Thewalt, U.; Lippert, B. *J. Am. Chem. Soc.* **1985**, *107*, 3591.
67. Kang, C.; Zhang, X.; Moyzis, R.; Rich, A. *Nature* **1992**, *356*, 126.
68. Laughlan, G.; Murchie, A. I. H.; Norman, D. G.; Moore, M. P.; Moody, P. C. E.; Lilley, D. M. J.; Luisi, B. *Science* **1994**, *265*, 520.
69. Fedoroff, O. Y.; Rangan, A.; Chemeris, V. V.; Hurley, L. H. *Biochemistry* **2000**, *39*, 15083.
70. Han, H. Y.; Langley, D. R.; Rangan, A.; Hurley, L. H. *J. Am. Chem. Soc.* **2001**, *123*, 8902.
71. Sun, D. Y.; Hurley, L. H. In "Drug–Nucleic Acid Interactions"; **2001**; Vol. 340, p. 573.
72. Sigel, R. K. O.; Freisinger, E.; Lippert, B. *Chem. Commun.* **1998**, 219.
73. Sigel, R. K. O.; Freisinger, E.; Lippert, B. *J. Biol. Inorg. Chem.* **2000**, *5*, 287.
74. Chaput, J. C.; Switzer, C. *Proc. Natl. Acad. Sci. U.S.A* **1999**, *96*, 10614.
75. Lippert, B. *Coord. Chem. Rev.* **2000**, *200–202*, 487.
76. de Meester, P.; Skapski, A. C. *J. Chem. Soc. A* **1971**, 2167.

77. Terzis, A.; Beauchamp, A. L.; Rivest, R. *Inorg. Chem.* **1973**, *12*, 1166.
78. Suggs, W.; Dube, M. J.; Nichols, M. *Chem. Commun.* **1993**, 307.
79. Zangrando, E.; Pichierri, F.; Randaccio, L.; Lippert, B. *Coord. Chem. Rev.* **1996**, *156*, 275.
80. Lippert, B. *Coord. Chem. Rev.* **1999**, *182*, 263.
81. Hegmans, A.; Zangrando, E.; Freisinger, E.; Pichierri, F.; Randaccio, L.; Mealli, C.; Gerdan, M.; Trautwein, A. X.; Lippert, B. *Chem. Eur. J.* **1999**, *5*, 3010.
82. Dale, R. M. K.; Livingston, D. C.; Ward, D. C. *Proc. Natl. Acad. Sci. USA* **1973**, *70*, 2238.
83. Dale, R. M. K.; Martin, E.; Livingston, D. C. *Biochemistry* **1975**, *14*, 2447.
84. Buncel, E.; Norris, A. R.; Racz, W.; Taylor, S. E. *J. Chem. Soc., Chem. Commun.* **1979**, 562.
85. Schollhorn, H.; Thewalt, U.; Lippert, B. *J. Chem. Soc. Chem. Commun.* **1986**, 258.
86. Hopp, M.; Erxleben, A.; Rombeck, I.; Lippert, B. *Inorg. Chem.* **1996**, *35*, 397.
87. Rauter, H.; Mutikainen, I.; Blomberg, M.; Lock, C. J. L.; Amo-Ochoa, P.; Freisinger, E.; Randaccio, L.; Zangrando, E.; Chiarparin, E.; Lippert, B. *Angew. Chem. Int. Ed. Engl.* **1997**, *36*, 1296.
88. Zamora, F.; Kunsman, M.; Sabat, M.; Lippert, B. *Inorg. Chem.* **1997**, *36*, 1583.
89. Zamora, F.; Zangrando, E.; Furlan, M.; Randaccio, L.; Lippert, B. *J. Organomet. Chem.* **1998**, *552*, 127.
90. Zamora, F.; Amo-Ochoa, P.; Fischer, B.; Schimanski, A.; Lippert, B. *Angew. Chem. Int. Ed.* **1999**, *38*, 2274.
91. Schimanski, A.; Freisinger, E.; Erxleben, A.; Lippert, B. *Inorg. Chim. Acta* **1998**, *283*, 223.
92. Clarke, M. J.; Taube, H. *J. Am. Chem. Soc.* **1975**, *97*, 1397.
93. Krentzein, H. J.; Clarke, M. J.; Taube, H. *Bioinorg. Chem.* **1975**, *4*, 143.
94. Romerosa, A.; Suarez-Varela, J.; Hidalgo, M. A.; Avila-Roson, J. C.; Colacio, E. *Inorg. Chem.* **1997**, *36*, 3784.
95. Price, C.; Elsegood, M. R. J.; Clegg, M.; Rees, N. H.; Houlton, A. *Angew. Chem. Int. Ed. Engl.* **1997**, *36*, 1762.
96. Price, C.; Shipman, M. A.; Gummerson, S. L.; Houlton, A.; Clegg, W.; Elsegood, M. R. J. *J. Chem. Soc. Dalton Trans.* **2001**, 353.
97. Ryabov, A. D. *Chem. Rev.* **1990**, *90*, 403.
98. Velders, A. H.; van der Geest, B.; Kooijman, H.; Spek, A. L.; Haasnoot, J. G.; Reedijk, J. *Eur. J. Inorg. Chem.* **2001**, 369.
99. Sponer, J.; Sponer, J. E.; Gorb, L.; Leszczynski, J.; Lippert, B. *J. Phys. Chem. A* **1999**, *103*, 11406.
100. Muller, J.; Zangrando, E.; Pahlke, N.; Freisinger, E.; Randaccio, L.; Lippert, B. *Chem. Eur. J.* **1998**, *4*, 397.
101. Pichierri, F.; Holthenrich, D.; Zangrando, E.; Lippert, B.; Randaccio, L. *J. Biol. Inorg. Chem.* **1996**, *1*, 439.
102. Price, C.; Rees, N. H.; Elsegood, M. R. J.; Clegg, W.; Houlton, A. *J. Chem. Soc., Dalton Trans.* **1998**, 2001.
103. Muller, J.; Sigel, R. K. O.; Lippert, B. *J. Inorg. Biochem.* **2000**, *79*, 261.
104. Lehn, J.-M. "Supramolecular Chemistry: Concepts and Perspectives"; VCH: Weinheim, **1995**.
105. Harriman, A.; Magda, D. J.; Sessler, J. L. *Chem. Commun.* **1991**, 345.
106. Harriman, A.; Kubo, Y.; Sessler, J. L. *J. Am. Chem. Soc.* **1992**, *114*.
107. Sessler, J. L.; Wang, B.; Harriman, A. *J. Am. Chem. Soc.* **1993**, *115*, 10418.
108. Sessler, J. L.; Wang, B.; Harriman, A. *J. Am. Chem. Soc.* **1995**, *117*, 704.

109. Price, C.; Aslanoglu, M.; Isaac, C. J.; Elsegood, M. R. J.; Clegg, W.; Horrocks, B. R.; Houlton, A. *J. Chem. Soc., Dalton Trans.* **1996**, 4115.
110. Houlton, A.; Isaac, C. J.; Gibson, A. E.; Horrocks, B. R.; Clegg, W.; Elsegood, M. R. J. *J. Chem. Soc., Dalton Trans.* **1999**, 3229.
111. Encinas, S.; Simpson, N. R. M.; Andrews, P.; Ward, M. D.; White, C. M.; Armaroli, N.; Barigelletti, F.; Houlton, A. *New J. Chem.* **2000**, *24*, 987.
112. Constable, E. C.; Fallahpour, R.-A. *J. Chem. Soc., Dalton Trans.* **1996**, 2389.
113. Ward, M. D.; Barigelletti, F. *Coord. Chem. Rev.* **2001**, *216*, 127.
114. Navarro, J. A. R.; Lippert, B. *Coord. Chem. Rev.* **1999**, *185–186*, 653.
115. Sigel, R. K. O.; Lippert, B. *Chem. Commun.* **1999**, 2167.
116. Sponer, J.; Sabat, M.; Burda, J. V.; Doody, A. M.; Leszczynski, J.; Hobza, P. *Biomol. Struc. Dyn.* **1998**, *16*, 139.
117. Bruning, W.; Sigel, R. K. O.; Freisinger, E.; Lippert, B. *Angew. Chem. Int. Ed.* **2001**, *40*, 3397.
118. Cheong, C.; Moore, P. B. *Biochemistry* **1992**, *31*, 8406.
119. Lippert, B.; Lock, C. J. L.; Speranzini, R. A. *Inorg. Chem.* **1981**, *20*, 808.
120. Dieter-Wurm, I.; Sabat, M.; Lippert, B. *J. Am. Chem. Soc.* **1992**, *114*, 357.
121. Menzer, S.; Sabat, M.; Lippert, B. *J. Am. Chem. Soc.* **1992**, *114*, 4644.
122. Schreiber, A.; Luth, M. S.; Erxleben, A.; Fusch, E. C.; Lippert, B. *J. Am. Chem. Soc.* **1996**, *118*, 4124.
123. Metzger, S.; Lippert, B. *J. Am. Chem. Soc.* **1996**, *118*, 12467.
124. Sigel, R. K. O.; Freisinger, E.; Metzger, S.; Lippert, B. *J. Am. Chem. Soc.* **1998**, *120*, 12000.
125. Meiser, C.; Freisinger, E.; Lippert, B. *J. Chem. Soc., Dalton Trans.* **1998**, 2059.
126. Freisinger, E.; Meier, S.; Lippert, B. *J. Chem. Soc., Dalton Trans.* **2000**, 3274.
127. Sigel, R. K. O.; Thompson, S. M.; Freisinger, E.; Lippert, B. *Chem. Commun.* **1999**, 19.
128. Luth, M. S.; Freisinger, E.; Lippert, B. *Chem. Eur. J.* **2001**, *7*, 2104.
129. Sigel, R. K. O.; Thompson, S. M.; Freisinger, E.; Glahe, F.; Lippert, B. *Chem. Eur. J.* **2001**, *7*, 1968.
130. Luth, M. S.; Freisinger, E.; Glahe, F.; Lippert, B. *Inorg. Chem.* **1998**, *37*, 5044.
131. Rauter, H.; Hillgeris, E. C.; Lippert, B. *Chem. Commun.* **1992**, 1385.
132. Rauter, H.; Hillgeris, E. C.; Erxleben, A.; Lippert, B. *J. Am. Chem. Soc.* **1994**, *116*, 616.
133. Navarro, J. A.; Janik, M. B. L.; Freisinger, E.; Lippert, B. *Inorg. Chem.* **1999**, *38*, 426.
134. Navarro, J. A. R.; Freisinger, E.; Lippert, B. *Eur. J. Inorg. Chem.* **2000**, 147.
135. Uchida, K.; Toyama, A.; Tamura, M.; Sugimura, M.; Mitsumori, F.; Furukawa, Y.; Takeuchi, H.; Harada, I. *Inorg. Chem.* **1989**, *28*, 2067.
136. Price, C.; Mayeux, A.; Horrocks, B. R.; Clegg, W.; Houlton, A. *Angew. Chem. Int. Ed.*, **2002**, *41*, 1047.
137. Kickham, J. E.; Loeb, S. J.; Murphy, S. L. *J. Am. Chem. Soc.* **1993**, *115*, 7031.
138. Chen, H.; Ogo, S.; Fish, R. H. *J. Am. Chem. Soc.* **1996**, *118*, 4993.
139. Chen, S.-C. *J. Organomet. Chem.* **1980**, *202*, 183.
140. Pratviel, G.; Bernadou, J.; Meunier, B. *Adv. Inorg. Chem.* **1998**, *45*, 251.
141. Dreyer, G. B.; Dervan, P. B. *Biochemistry* **1985**, *24*, 968.
142. Sigman, D. S. *Acc. Chem. Res.* **1986**, *19*, 180.
143. Thorp, H. H. *Adv. Inorg. Chem.* **1995**, *43*, 127.
144. Sigel, A.; Sigel, H. *Metal Ions in Biol. Sys.* **1996**, *33*, 678.
145. Napier, M. E.; Loomis, C. R.; Sistare, M. F.; Kim, J.; Eckhardt, A. E.; Thorp, H. H. *Bioconjugate Chem.* **1997**, *8*, 906.
146. Bannwarth, W.; Schmidt, D.; Stallard, R. L.; Hornung, C.; Knorr, R.; Muller, F. *Helv. Chim. Acta* **1988**, *71*, 2085.

147. Bannwarth, W.; Schmidt, D. *Tetra. Lett.* **1989**, *30*, 1513.
148. Tesler, J.; Cruickshank, K. A.; Schanze, K. S.; Netzel, T. L. *J. Am. Chem. Soc.* **1989**, *111*, 7221.
149. Meggers, E.; Kusch, D.; Giese, B. *Helv. Chim. Acta* **1997**, *80*, 640.
150. Hu, X.; Smith, G. D.; Sykora, M.; Lee, S. J.; Grinstaff, M. W. *Inorg. Chem.* **2000**, *39*, 2500.
151. Bashkin, J. K.; Frolova, E. I.; Sampath, U. *J. Am. Chem. Soc.* **1994**, *116*, 5981.
152. Bergstrom, D. E.; Gerry, N. *J. Am. Chem. Soc.* **1994**, *116*, 12067.
153. Magda, D.; Crofts, S.; Lin, A.; Miles, D.; Wright, M.; Sessler, J. L. *J. Am. Chem. Soc.* **1997**, *119*, 2293.
154. Manchanda, R.; Dunham, S. U.; Lippard, S. J. *J. Am. Chem. Soc.* **1996**, *118*, 5144.
155. Schliepe, J.; Berghoff, U.; Lippert, B.; Cech, D. *Angew. Chem. Int. Ed.* **1996**, *35*, 646.
156. Schmidt, K. S.; Filippov, D. V.; Meeuwenoord, N. J.; van der Marel, G. A.; van Boom, J. H.; Lippert, B.; Reedijk, J. *Angew. Chem. Int. Ed.* **2000**, *39*, 375.
157. Hurley, D. J.; Tor, Y. *J. Am. Chem. Soc.* **1998**, *120*, 2194.
158. Kahn, S. I.; Beilstein, A. E.; Tierney, M. T.; Sykora, M.; Grinstaff, M. W. *Inorg. Chem.* **1999**, *38*, 5999.
159. Kahn, S. I.; Grinstaff, M. W. *J. Am. Chem. Soc.* **1999**, *121*, 4704.
160. Kahn, S. I.; Beilstein, A. E.; Grinstaff, M. W. *Inorg. Chem.* **1999**, *38*, 418.
161. Beilstein, A. E.; Grinstaff, M. W. *Chem. Commun.* **2000**, 509.
162. Tierney, M. T.; Sykora, M.; Kahn, S. I.; Grinstaff, M. W. *J. Phys. Chem. B* **2000**, *104*, 7574.
163. Yu, C. J.; Yowanto, H.; Wan, Y.; Meade, T. J.; Chong, Y.; Strong, M.; Donilon, L. H.; Kayyem, J. F.; Gozin, M.; Blackburn, G. F. *J. Am. Chem. Soc.* **2000**, *122*, 6767.
164. Pike, A.; Ryder, L. C.; Clegg, W.; Horrocks, B. R.; Houlton, A.; Connolly, B. A. *Chem. Eur. J.*, in press.
165. Ihara, T.; Maruo, Y.; Takenada, S.; Takagi, M. *Nucl. Acid Res.* **1996**, *24*, 4273.
166. Ihara, T.; Nakayama, M.; Murata, M.; Nakano, K.; Maeda, M. *Chem. Commun.* **1997**, 1609.
167. Meunier, P.; Ouattara, I.; Gautheron, B.; Tirouflet, J.; Camboli, D.; Besancon, J. *Eur. J. Med. Chem.* **1991**, *26*, 351.
168. Storhoff, J. J.; Mirkin, C. A. *Chem. Rev.* **1999**, *99*, 1849.
169. Porath, D.; Bezryadin, A.; de Vries, S.; Dekker, C. *Nature* **2000**, *403*, 635.
170. Kasumov, A. Y.; Kociak, M.; Gueron, S.; Reulet, B.; Volkov, V. T.; Klinov, D. V.; Bouchiat, H. *Science* **2001**, *291*, 280.
171. Braun, E.; Eichen, Y.; Sivan, U.; Ben-Yoseph, G. *Nature* **1998**, *391*, 775.
172. Yamane, T.; Davidson, N. *Biochim. Biophys. Acta* **1962**, *55*, 609.
173. Yamane, T.; Davidson, N. *Biochim. Biophys. Acta* **1962**, *55*, 780.
174. Menzer, S.; Sabat, M.; Lippert, B. *J. Am. Chem. Soc.* **1992**, *114*, 4644.
175. Richter, J.; Mertig, M.; Pompe, W.; Monch, I.; Schackert, H. K. *Appl. Phys. Lett.* **2001**, *78*, 536.
176. Lee, J. S.; Latimer, L. J. P.; Reid, R. S. *Biochem. Cell Biol.* **1993**, *71*, 162.
177. Aich, P.; Labiuk, S. L.; Tari, L. W.; Delbaere, L. J. T.; Roesler, W. J.; Falk, K. J.; Steer, R. P.; Lee, J. S. *J. Mol. Biol.* **1999**, *294*, 477.
178. Rakitin, A.; Aich, A.; Papadopoulos, C.; Kobzar, Y.; Vedeneev, A. S.; Lee, J. S.; Xu, J. M. *Phys. Rev. Lett.* **2001**, *86*, 3670.
179. Kimura, E.; Kikuta, E. *J. Biol. Inorg. Chem.* **2000**, *5*, 139.
180. Allen, F. H.; Kennard, O. *Chem. Des. Autom. News* **1993**, *8*, 31.
181. Kelley, S. O.; Jackson, N. M.; Hill, M. G.; Barton, J. K. *Angew. Chem. Int. Ed.* **1999**, *38*, 941.

182. Alivisatos, A. P.; Johnsson, K. P.; Peng, X. G.; Wison, T. E.; Loweth, C. J.; Bruchez, M. P.; Schultz, P. G. *Nature* **1996**, *382*, 609.
183. Storhoff, J. J.; Elghanian, R.; Mucic, R. C.; Mirkin, C. A.; Letsinger, R. L. *J. Am. Chem. Soc.* **1998**, *120*, 1959.
184. Taton, T. A.; Mucic, R. C.; Mirkin, C. A.; Letsinger, R. L. *J. Am. Chem. Soc.* **2000**, *122*, 6305.
185. Mirkin, C. A. *Inorg. Chem.* **2000**, *39*, 2258.
186. Niemeyer, C. M.; Adler, M.; Lenhert, S.; Gao, S.; Fuchs, H.; Chi, L. *ChemBioChem* **2001**, *2*, 260.
187. Niemeyer, C. M. *Chem. Eur. J.* **2001**, *7*, 3189.
188. Mitchell, G. P.; Mirkin, C. A.; Letsinger, R. L. *J. Am. Chem. Soc.* **1999**, *121*, 8122.
189. Linford, M. R.; Chidsey, C. E. D. *J. Am. Chem. Soc.* **1993**, *115*, 12631.
190. Linford, M. R.; Fenter, P. M.; Chidsey, C. E. D. *J. Am. Chem. Soc.* **1995**, *117*, 3145.
191. Buriak, J. M. *Chem. Commun.* **1999**, 1051.
192. Bateman, J. E.; Eagling, R. D.; Worrall, D. R.; Horrocks, B. R.; Houlton, A. *Angew. Chem. Int. Ed.* **1998**, *37*, 2683.
193. Cleland, G.; Horrocks, B. R.; Houlton, A. *J. Chem. Soc., Faraday Trans.* **1995**, *91*, 4001.
194. Strother, T.; Cai, W.; Zhao, X.; Hamers, R. J.; Smith, L. M. *J. Am. Chem. Soc.* **2000**, *122*, 1205.
195. Strother, T.; Hamers, R. J.; Smith, L. M. *Nucl. Acid Res.* **2000**, *28*, 3535.
196. Pike, A. R.; Lie, L. H.; Eagling, R. D.; Ryder, L. C.; Patole, S. N.; Connolly, B. A.; Horrocks, B.; Houlton, A. *Angew. Chem. Int. Ed.* **2002**, *41*, 615.
197. Yu, C. J.; Wan, Y.; Yowanto, H.; Li, J.; Tao, C.; James, M. D.; Tan, C. L.; Blackburn, G. F.; Meade, T. J. *J. Am. Chem. Soc.* **2001**, *123*, 11155.

ADVANCES IN THE CHEMISTRY OF CHLOROCYCLOPHOSPHAZENES

VADAPALLI CHANDRASEKHAR* and
VENKATASUBBAIAH KRISHNAN

Department of Chemistry, Indian Institute of Technology, Kanpur 208 016, India

I. Introduction

Cyclophosphazenes are a fascinating group of inorganic heterocyclic compounds whose chemistry is multi-faceted, well developed and reasonably well understood. They are closely related to the linear polyphosphazenes; this relationship is unlike any other existing between ring-polymer systems. Although cyclic siloxanes and polysiloxanes have a close interrelationship, the number and types of cyclophosphazene derivatives that are known, together with their exact counterparts in polyphosphazenes, underscore the utility of cyclophosphazenes as *models* for the more complex polyphosphazenes. The literature on cyclophosphazenes has appeared earlier in the form of books (*1,2*), chapters of books (*3–5*), authoritative compilations of data (*6,7*), and several reviews (*8–21*). The current literature on this subject is reported annually in the Specialist Periodic Reports published by the Royal Society of chemistry (*22*). This review deals mostly with chlorocyclo-

0898-8838/02 $35.00

phosphazenes and their reactions. Aspects relating to the structure and bonding of these compounds are not dealt with here.

Cyclophosphazenes are inorganic heterocyclic ring compounds containing an $[N{=}PX_2]$ repeat unit in a valence-unsaturated skeleton that are isoelectronic with the corresponding siloxanes which contain the $[OSiX_2]$ repeat unit. Within these compounds phosphorus is pentavalent and tetracoordinate while nitrogen is trivalent and dicoordinate. While phosphorus has two exocyclic substituents, nitrogen has none. The most common members of this family of compounds are the chlorocyclophosphazenes, $N_3P_3Cl_6$ **1** and $N_4P_4Cl_8$ **2**. These compounds are also commercially available and serve as the starting materials for the rich and diverse chemistry of cyclophosphazenes. Fluorocyclophosphazenes have received less attention than the chloro analogs, although in recent years there has been an interest in this class of compound and in the differences in reactivity between the P–Cl and P–F bonds, due to the unique character of the latter bond type. The chemistry of fluorocyclophosphazenes has been a subject of a recent critical review (*23*). The bromocyclophosphazenes, although known, have been even less studied than the fluoro derivatives (*24,25*). This is probably because of the cumbersome preparative procedures involved in the synthesis of these compounds.

The cyclophosphazene ring systems constitute a regular and homologous series and the ring size varies considerably. For the series $[NPF_2]_n$, compounds from $n = 3$ to 40 are known (*23*). The cyclophosphazene with the smallest ring size is the four-membered cyclodiphosphazene $[NP(NR_2)_2]_2$, $R = i\text{-Pr}$, **3** (*26*). The largest structurally characterized ring system is the 24-membered permethyl ring $[NP(Me)_2]_{12}$ **4** (*27*). This variation in ring size is quite remarkable for a homologous series of inorganic rings. Figure 1 shows some typical examples of cyclophosphazene derivatives.

Although cyclophosphazenes are among the oldest inorganic rings to be known (along with S_4N_4), having been prepared by Liebig and Wöhler as early as 1834 and studied in detail by Stokes in 1895–97 (*28–32*), it is only since the 1960s that the chemistry of these ring systems has been explored in great detail. Interest in the chemistry of cyclophosphazenes comes from different directions. Firstly, the replacement of halogens on halogenocyclophosphazenes by a variety of nucleophiles has been a fertile area of research fraught with many interesting problems connected with the question of regio- and stereo-selectivity of the substitution reaction, the kinetics of the reactions involved, and the structural elucidation of the products formed (*14,18*). Secondly, substituted cyclophosphazenes can serve as excellent ligands for a number of

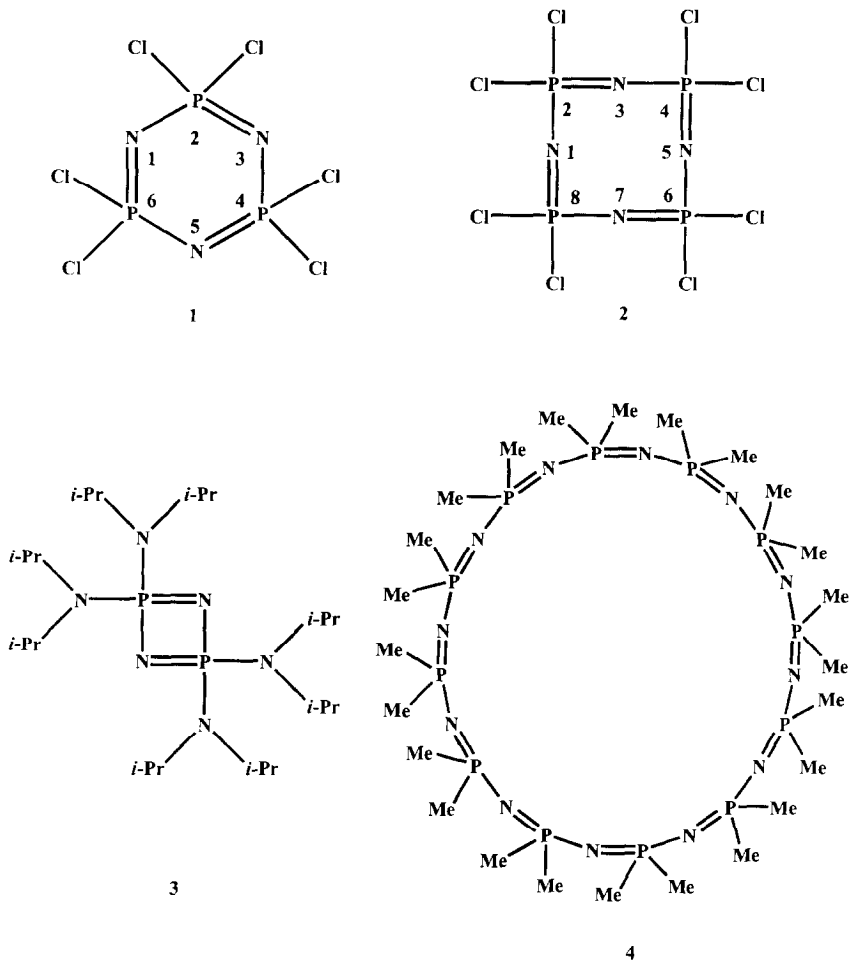

FIG. 1. Representative examples of cyclophosphazenes.

transition metal ions. Unlike the other ubiquitous inorganic heterocyclic ring (cage), S_4N_4, that loses the integrity of its cage structure in many of its reactions with metal ions, cyclophosphazene ligands are quite robust and display interesting coordination behavior. The use of cyclophosphazenes as scaffolds for the construction of new ligand systems has been an active area of research in recent times (*19,33*). A third, and perhaps the most important, reason for the sustained interest in these inorganic rings stems from the discovery that $N_3P_3Cl_6$ **1** can be polymerized to the linear polymer $[NPCl_2]_n$ **5**. Although the polymer **5**

is itself not very useful, owing to the hydrolytic sensitivity of the P–Cl bonds, several hundred stable polymers have been prepared by the replacement of chlorine atoms on **5** by a variety of substituents (*34*) (Fig. 2).

The nomenclature and numbering system adopted in this article is the one currently widely used in the literature and corresponds closely to the one suggested by Shaw (*13,17*). Only the chemistry of chlorocyclophosphazenes is dealt with in this review. The structural and bonding aspects are not considered here.

II. Preparative Methods

The traditional and most extensively used method of synthesis of chlorocyclophosphazenes $[NPCl_2]_n$ involves the reaction of finely ground ammonium chloride with phosphorus pentachloride in a high boiling solvent such as *sym*-tetrachloroethane. This reaction affords a mixture of cyclic and linear products from which the individual products have to be separated, usually by fractional distillation in high vacuum (*1, 5, 17,18,35–39*), (Eq. 1):

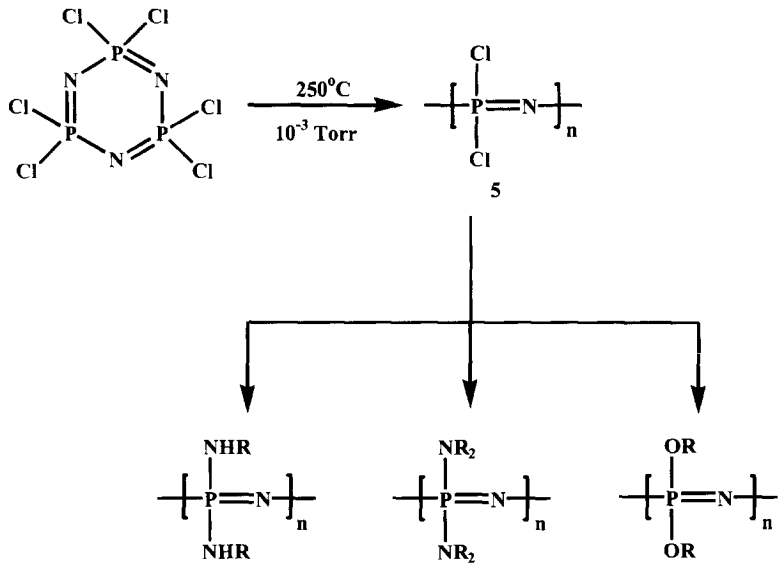

FIG. 2. Synthesis of polyorganophosphazenes.

$$n\mathrm{PCl_5} + n\mathrm{NH_4Cl} \xrightarrow[\triangle]{\text{s-TCE}} [\mathrm{PNCl_2}]_n + 4n\mathrm{HCl} \quad (1)$$

An alternative method of synthesis of $N_3P_3Cl_6$ has been developed recently, based on the reaction of tris (trimethylsilyl) amine and phosphorus pentachloride (*40*). This reaction either preferentially leads to the formation of $N_3P_3Cl_6$ or to an N-silylated phosphoranimine intermediate $Cl_3P{=}NSiMe_3$, depending on the reaction conditions used. Thus the reaction between tris (trimethylsilylamine) and PCl_5 in methylene chloride at 40°C affords a mixture of cyclo and linear phosphazenes, which has been shown by an NMR analysis to contain up to 76% of $N_3P_3Cl_6$ (Eq. 2).

$$n\mathrm{N(SiMe_3)_3} + n\mathrm{PCl_5} \xrightarrow[40°\mathrm{C}]{\mathrm{CH_2Cl_2}} [\mathrm{PNCl_2}]_n + 3n\mathrm{Me_3SiCl} \quad (2)$$

Yields : $n = 3$ (76%); $n = 4$ (4%); $n = 5$ (5%); $n = 6$ (3%); others 12%

If this procedure could be adapted for large-scale preparations it would be an attractive alternative to the NH_4Cl/PCl_5 reaction. The proposed mechanism of this reaction is given in Fig. 3. The first step in the reaction is the formation of the phosphoranimine **6** which further reacts with PCl_5 to generate the linear molecule $[Cl_3PNPCl_3]^+[PCl_6]^-$. Chain growth takes place by the reaction of the latter with **6**. Although this mechanism is very similar to that proposed for the PCl_5/NH_4Cl reaction by Emsley (*38*), Allcock (*40*) suggests that the chain closure reaction proceeds by an intermolecular process rather than an intramolecular one. The chain termination is believed to be assisted by $N(SiMe_3)_3$. The evidence for this proposal is from the observations that (a) the linear fragment $[Cl_3PNPCl_2NPCl_3]^+[PCl_6]^-$ affords, upon reaction with $N(SiMe_3)_3$, mainly $N_3P_3Cl_6$ and (b) oligomeric linear chain compounds such as $[Cl_3P[NPCl_2]_nNPCl_3]^+[PCl_6]^-$, $n = 0$, 1, or 2, do not undergo cyclization on their own in boiling methylene chloride in the absence of the added amine. The phosphoranimine **6** and its fluoroalkoxy analog $(CF_3CH_2O)_3P{=}NSiMe_3$ **7** are valuable intermediates for the preparation of polyphosphazenes. Thus Allcock and co-workers have shown that **6** can be polymerized by PCl_5 to afford polydichlorophosphazene $[NPCl_2]_n$ with a low poly dispersity index (*41*). Also, new telechelic polyphosphazenes have been prepared by the use of this monomer (*42*). Matyajaszewski has shown that **7** can be polymerized using a fluoride initiator such as *n*-Bu_4NF(*43*) (Fig. 4).

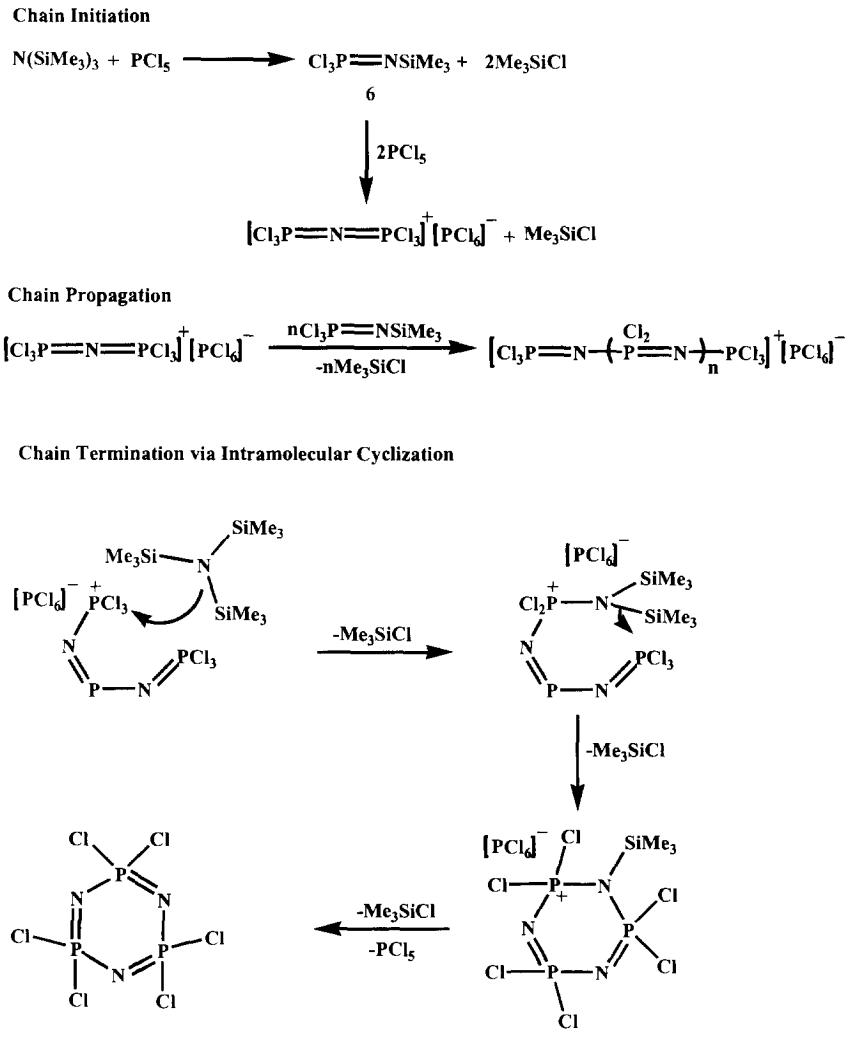

FIG. 3. Mechanism of the $N(SiMe_3)_3/PCl_5$ reaction.

The most convenient method of synthesis of fluorocyclophosphazenes consists of metathetical halogen exchange reactions of the chloro analogs, effected by an appropriate fluorinating agent. Thus the synthesis of $N_3P_3F_6$ is carried out by the reaction of $N_3P_3Cl_6$ with sodium fluoride in acetonitrile (*44*). Many other fluorinating agents are known (*23*). Bromocyclophosphazenes have been commonly prepared by the

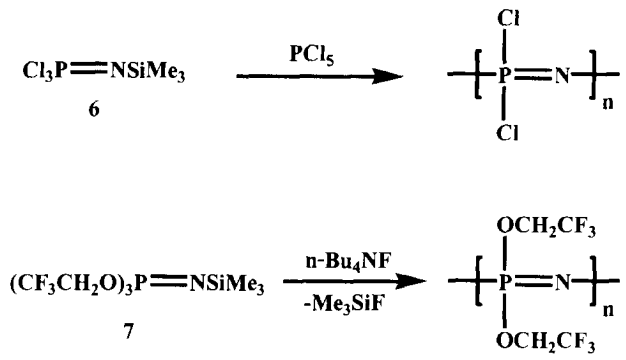

FIG. 4. Preparation of polyphosphazenes from acyclic phosphoranimines.

reaction of NH_4Br with a mixture of PBr_3 and Br_2 (*24,25*). Cyclophosphazenes containing a P–I bond have been synthesized by the reaction of hydrido phosphazenes with iodine in carbon tetrachloride (*45*). On the other hand, cyclophosphazenes containing isothiocyanato groups (*46–48*) and cyano groups (*49*) have been synthesized from the corresponding chlorocyclophosphazenes by a metathesis reaction involving the reagent KNCS or KCN. The use of 18-crown-6-ether or a phase-transfer catalyst greatly facilitates the reaction. The isothiocyanato derivative could be converted to the corresponding thiourethane or thiourea derivative by reaction with alcohols or amines respectively. Figure 5 summarizes these reactions.

Azido cyclophosphazenes are also known (*50–56*). The hexaazido derivative $N_3P_3(N_3)_6$ is extremely shock sensitive and has been known to explode (*50*). However, with other appropriate substituents present on the cyclophosphazene skeleton, if azido substituents are also introduced on the cyclophosphazene such compounds seem to be more stable. These types of mixed substituent cyclophosphazene, containing the azido group as one type of substituent, can be prepared by the reaction of the corresponding chlorocyclophosphazene with sodium azide in presence of the phase-transfer catalyst *n*-Bu_4NBr (*55,56*) (Fig. 6). Such azidocyclophosphazenes are of interest because they can be further elaborated by utilizing the nitrene generation type of reactivity of the azido functionality. Nitrene insertion products were observed with some of these aryloxy derivatives such as $N_3P_3(OC_6H_5)_5N_3$. Also, some of the aryloxy and alkoxy azides undergo a Staudinger reaction with several phosphorus (III) compounds to afford phosphinimines (*56*).

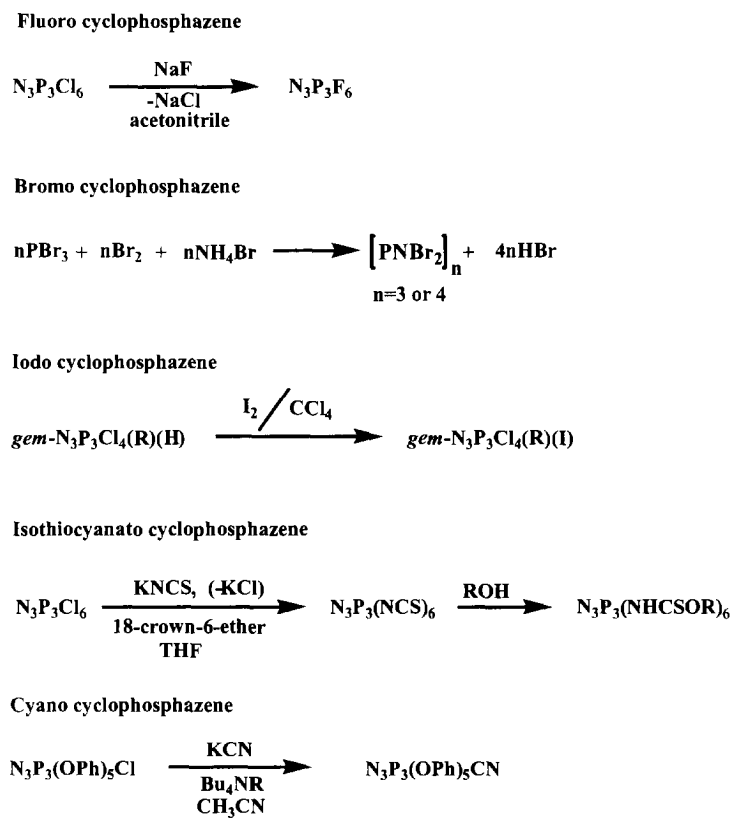

FIG. 5. Preparation of halogeno and pseudohalogeno cyclophosphazenes.

Although the most widely studied examples of cyclophosphazenes are the six- and eight-membered rings, four membered rings containing a P_2N_2 framework can be synthesized. This may be contrasted with the instability of cyclobutadiene in organic systems. The strategy for the synthesis of the four-membered P–N rings is the *in situ* generation of the phosphonitrile $R_2P{\equiv}N$ by the decomposition of the phosphorus azide R_2PN_3 [R = $(i\text{-Pr})_2N$]. The di-isopropylamino substituents on phosphorus serve as ideal sterically suited substituents for the isolation of the four-membered rings. In the absence of other trapping agents the *phosphonitrile* dimerizes to afford the cyclodiphosphazene **3** (Eq. 3) (*26*):

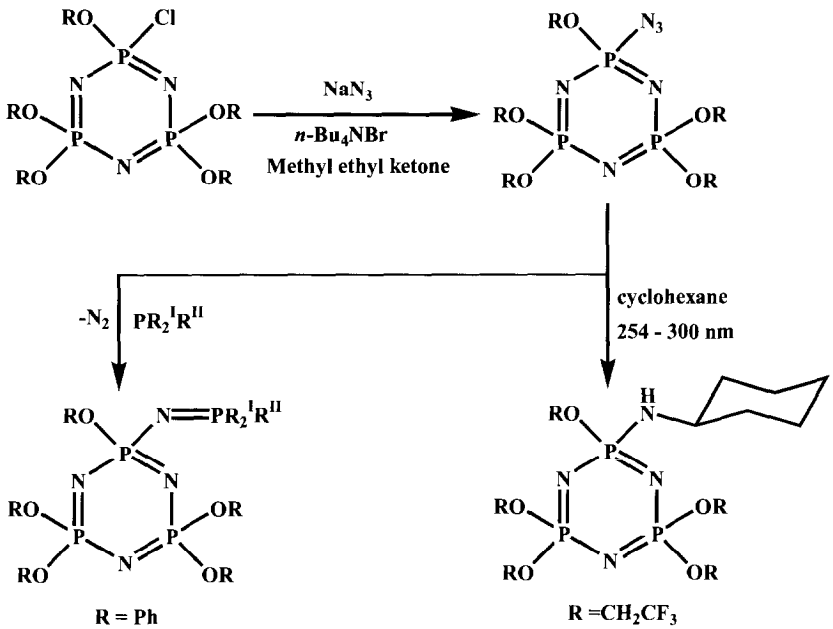

FIG. 6. Formation of stable azido phosphazenes and some of their reactions.

$$R_2PN_3 \longrightarrow [R_2P{\equiv}N] \longrightarrow \text{(3)}$$

R = N(*i*-Pr)$_2$

A related synthesis involves the decomposition of $[(NR_2)_2P(S)CHN_2\text{-}P(NR_2)_2]$ (*57,58*).

III. Chlorine Replacement Reactions

Nucleophilic substitution reactions involving the replacement of chlorine (or bromine or fluorine) atoms on the phosphorus have been among the most well studied reactions of cyclophosphazenes

(*8,14,17,18*). These reactions constitute the core of cyclophosphazene chemistry and serve as the principal method for increasing the number and types of cyclophosphazenes. By means of these reactions a large number of other cyclophosphazenes containing P–N, P–O, P–S, P–C and even P–M bonds can be prepared from halogenocyclophosphazenes. Such reactions are also important from the point of view of preparing polyorganophosphazenes. Since the dichloropolyphosphazene $[NPCl_2]_n$ is unstable with respect to the hydrolysis of P–Cl bonds, the chlorine atoms must be replaced by other substituents in order to confer stability to the polymer. This is accomplished by the nucleophilic substitution reactions involving the replacement of chlorine atoms on the polymer (Fig. 2). Therefore an understanding of the potential and limitations of the reactions of various nucleophilic reagents with halogenocyclophosphazenes is beneficial for their application in polymeric systems. Often it is easier to carry out the reactions on the rings $N_3P_3Cl_6$ and $N_4P_4Cl_8$ as model systems before reactions are attempted, adapted and applied to the polymeric system (*9,18*).

An additional academic curiosity has also driven the study of these reactions in great detail by various research groups all over the world. It can be readily seen that the sequential replacement of halogens from $N_3P_3Cl_6$ and $N_4P_4Cl_8$ introduces a number of different possibilities in terms of regio- and stereoisomer formation and selection. This can be easily understood by looking at the halogen replacement reactions of $N_3P_3Cl_6$. Since all the phosphorus centers are equivalent in this compound, replacement of the first chlorine atom by a nucleophile affords a single isomer $N_3P_3Cl_5R$. However, when a second molecule of the nucleophile reacts with this compound it has the option of reacting at a PCl_2 center or a P(Cl)(NHR) center. This can lead to the formation of geminal or non-geminal isomers (Fig. 7). It can also be seen that for the non-geminal compound a further elaboration in terms of *cis* and *trans* stereoisomers is possible. This situation is also found for the tris and tetrakis substituted derivatives, $N_3P_3Cl_3R_3$ and $N_3P_3Cl_2R_4$. The pentakis and hexakis products do not have the possibility of isomer formation. Allen has made a comprehensive survey on the regio- and stereochemical control that is observed in the substitution reactions of halogenocyclophosphazenes (14). In addition to the regio- and stereoisomers that are possible, it may also be noted that the stereoisomers *trans*-$N_3P_3X_4R_2$, *trans*-$N_3P_3X_3R_3$, and *trans*-$N_3P_3X_2R_4$ would also have the possibility of optical isomerism as the enantiomers of these compounds would be non-superimposable.

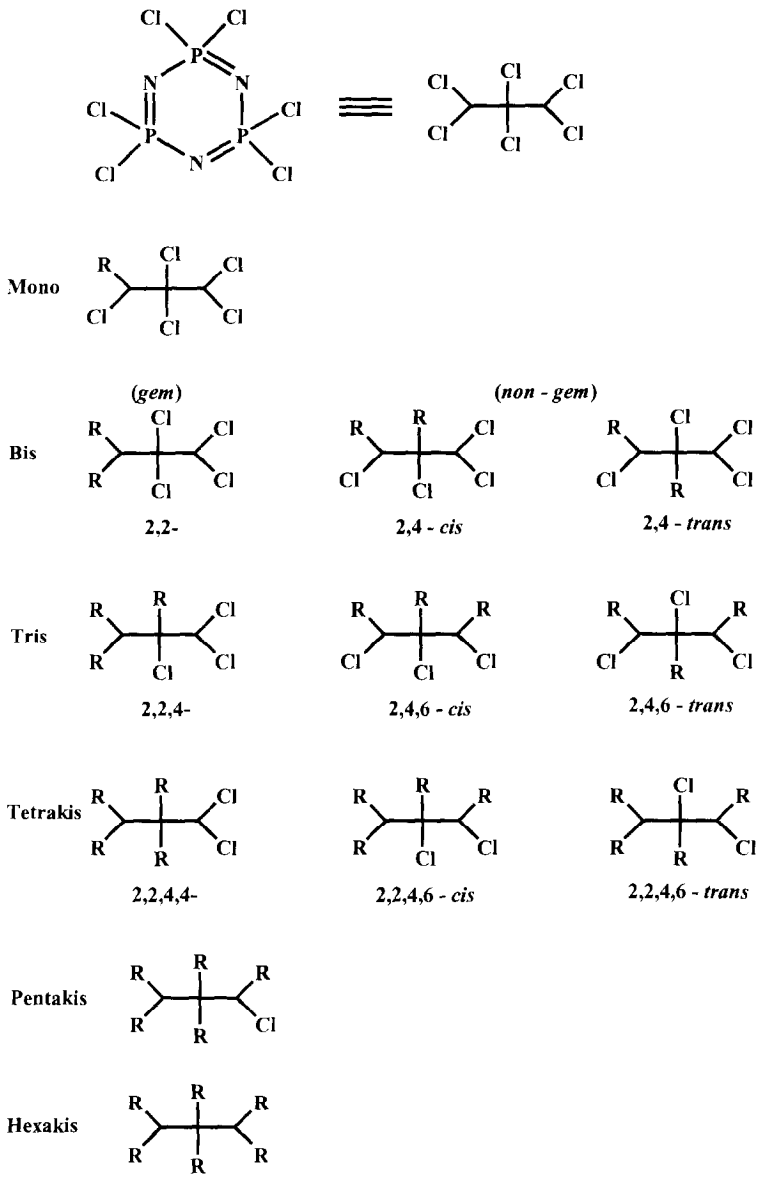

FIG. 7. Total number of regio- and stereoisomers possible in the chlorine replacement reactions of $N_3P_3Cl_6$.

The complexity of the substitution reaction pathway intensifies in the replacement reactions of the tetrameric halides $N_4P_4X_8$. A total of 33 isomers is possible (*17,18*).

Although replacement reactions of the pentameric system are also known, these have not been as well studied (*14*). The following account gives a description of some of the different types of nucleophilic substitution reactions that have been well studied. The sequential replacement of chloride substituents by fluoride has been studied, and is discussed elsewhere (*14, 23*).

A. Reactions of Amines with $N_3P_3Cl_6$ and $N_4P_4Cl_8$

1. $N_3P_3Cl_6$

The reactions of $N_3P_3Cl_6$, $N_3P_3Br_6$, and $N_3P_3F_6$ with a number of primary and secondary amines have been well studied (*14,18*). The reactivity follows the order P–Br > P–Cl > P–F which also reflects the ease of the P–X bond cleavage. Representative examples of the reactions of $N_3P_3Cl_6$ and the products isolated are given in Table I (*59–83*). Among the three halides, the reactions of the trimeric chloride have been most well studied. This is because, while $N_3P_3F_6$ is relatively sluggish in its reactions with amines (because of the strong P–F bond, the poor leaving ability of F^-, and the highly planar nature of the $N_3P_3F_6$ ring) (*84*), the tedious and complicated synthesis of $N_3P_3Br_6$ has prevented its widespread use and stunted its chemistry (*85*). However, the paucity of data on the fluorides and the bromides is more than made up by the wealth of information known about the replacement reactions of the amines with $N_3P_3Cl_6$.

The details of the kinetics of the reactions and the reaction mechanisms are dealt with elsewhere (*14*). Some of the general trends of the above reactions are:

(1) There is a reasonably good stoichiometric control observed in these aminolysis reactions. Therefore, in principle, the extent of chlorine replacement can be regulated by the ratio of the reactants. If mixtures of products are formed, these are generally amenable to separation by column chromatography. Separation of individual stereoisomers is often accomplished by procedures such as fractional crystallization.

(2) In most cases, pentasubstituted products have not been obtained. Also, with primary amines, the actual isolation of the tris- substituted derivatives has remained rare.

TABLE I

REACTIONS OF SELECTED AMINES WITH $N_3P_3Cl_6$ [a,b] (REPRODUCED WITH PERMISSION FROM REF. (*14*). COPYRIGHT: AMERICAN CHEMICAL SOCIETY)

No.	Amine HNRR′		Products $N_3P_3(NRR')_nCl_{6-n}$			Ref.
	R	R′	$n = 2$	$n = 3$	$n = 4$	
1	H	H	g	ni	ni	*59,60*
2[c]	H	Me	ng(t > c) > g	ni	ni	*61,62*
3	H	Et	ng(t)	ng(tr)	g(tr)	*63*
4	H	CH_2CH_2Cl	g	tr(u)	g	*64*
5	H	CH_2CH_2OMe	ng	tr(u)	g	*64*
6	H	CH_2CH_2COOEt	g	ni	g	*65*
7	H	CH_2Ph	g > ng	ni	g	*66*
8	H	*i*-Pr	ng(t > c) > g	ni	g	*63,67*
9	H	Ph	g, ng	s	g	*68,69*
10[d,e]	H	C_6H_4-*p*-X (X = OCH_3, CH_3)	ng(c = t), g	g = ng(c = t)	g	*68,69*
11	H	*t*-Bu	g	ni	g	*70*
12	H	C_6H_{11}, C_5H_9, C_3H_7	g	ni	g	*71*
13	H	Adamantyl	g	ni	g	*72*
14	Me	Me	ng(t > c)	(ng, t > c), g	ng(c)	*73–76*
15	Et	Et	ng(t > c)	ng(t > c), g	ng(t > c)	*77*
16	NC_2H_4(aziridine)		g = ng(c < *t*)	g = ng(c < t)	g = ng(c = t)	*78–79*
17	NC_5H_{10}(piperidine)		ng(t > c)	ng(t) > g	ng(c)	*80*
18	NC_4H_8(pyrrolidine)		t > c	ng, g	c > t	*81*
19	Morpholine		t > c	tr	tr	*81*
20	Me	Ph	ng(c = t)	ng(c) = g	ni	*82*
21	C_6H_{11}	C_6H_{11}	ng			*83*
22	$C_6H_5CH_2$	$C_6H_5CH_2$	ng			*66*

[a] g = geminal, ng = non-geminal, t = *trans*, c = *cis*, tr = trace amounts, ni = not isolated (or identified), s = identified spectroscopically, u = isomers isolated, configuration not assigned.

[b] In most cases mono- and per-substituted derivatives are isolated; pentakis derivatives are rare.

[c] Hexakis derivative not isolated.

[d] Use of triethyl amine affords exclusively geminal product.

[e] Pentakis product isolated.

(3) Although complete replacement of chlorine atoms can be accomplished with most kinds of amines, this becomes difficult in the reactions with sterically hindered amines. Thus in the reactions of $N_3P_3Cl_6$ with cyclohexylamine (*71*) and adamantyl amine (*72*), the yields of fully substituted products are low. In the reactions of $N_3P_3Cl_6$ with further sterically encumbered amines such as

dicyclohexylamine (*83*) and dibenzylamine (*66*), the substitution of chlorine atoms does not proceed beyond the bis stage.

The regio and stereo selectivity observed in the reactions of $N_3P_3Cl_6$ with various amines presents a complicated picture, and the complications are exacerbated by the finding that amine hydrochlorides formed as side products in the reactions may actually be involved in *cis–trans* isomerization of the aminocyclophosphazene products (*14*). Secondly, nucleophilic solvents such as acetonitrile have also been implicated in such isomerizations. Additionally, there are clear solvent effects in certain reactions in determining the nature of the regioisomer formed (*14*). Notwithstanding these complications, it is still possible to infer some general patterns in the aminolysis reactions. These are summarized below:

(a) Substitution reactions of $N_3P_3Cl_6$ with secondary amines produce mainly *non-geminal* products with usually *trans* products predominating. The only exception to this trend is aziridine, which reacts to give both the geminal and the non-geminal products in approximately equal amounts (*78–79*). Solvent effects are seen; e.g., the use of acetonitrile in many reactions (except with N-methyl aniline) seems to promote the formation of non-geminal products at the tris stage of substitution while the use of aromatic solvents seems to increase the amount of geminal isomer formed (*14*).

(b) The reactions of $N_3P_3Cl_6$ with primary amines is much more complex. As one proceeds from ammonia to progressively more sterically hindered amines the situation becomes interesting. Ammonia reacts with $N_3P_3Cl_6$ to give exclusively a geminal product, $N_3P_3Cl_4(NH_2)_2$ (*59,60*). In contrast the reactions with methyl (*61,62*) and ethyl amines (*63*) proceed to give the non-geminal products $N_3P_3Cl_4(NHR)_2$. However, as the steric bulk of the amine is further increased, as happens with *t*-butyl amine, a geminal product is formed, which is contrary to the expectations based on steric grounds (*70*). In addition to the above steric effect there also appears to be an electronic effect operating as well. Thus β-haloethyl amines react with $N_3P_3Cl_6$ in diethylether to give geminal products (in this reaction, again, a solvent effect is seen; thus, changing the solvent to acetonitrile leads to the formation of the non-geminal product, also, albeit in lower yield than the geminal product) (*64*). Reactions of anilines afford non-geminal products at the bis stage. However, use of a trialkylamine as the base leads to the formation of geminal products (*68,89*). As

mentioned earlier, tris products have rarely been isolated. As the reactions proceed to the tetrakis stage, most of the primary amines afford only geminal products.

(c) In addition to the above, an interesting observation has been made by Shaw in one of the early experiments to determine the role of the incoming nucleophile on the regioselection of the product formed. Thus, while *t*-butylamine as an incoming nucleophile favors the formation of a geminal product in its reaction with $N_3P_3Cl_5(NHEt)$, ethylamine directs the formation of a non-geminal product in its reaction with $N_3P_3Cl_5$(*t*-BuNH) (*86*). The reasons for these reactivity differences are now understood and are discussed below.

Detailed kinetic investigations on several systems have been carried out and have helped to unravel many of the factors involved in the divergent reaction pathways discussed above (*14,87–93*). The mechanistic pathways involved in the aminolysis reactions of chlorocyclophosphazenes are summarized in Fig. 8.

In the S_N2 pathway two types of transition states have been proposed:

(a) Formation of a neutral five-coordinate phosphorus intermediate followed by the expulsion of the leaving group. This transition state is non-polar [Fig. 8(A)].

(b) A concerted S_N2 mechanism similar to that found in the carbon system, involving a polar transition state [Fig. 8(B)].

Analysis of the kinetic parameters has shown that S_N2 reactions are characterized by a $\Delta H^{\neq}$ term associated with the ease of formation of the neutral five-coordinate intermediate (*87–93*). Thus, in the first stage of chlorine substitution in $N_3P_3Cl_6$ with an amine, this factor should be related to the steric bulk of the amine. The more hindered the amine, the higher this value should be. Thus the $\Delta H^{\neq}$ obtained in the reaction of $N_3P_3Cl_6$ with methylamine is lower than that obtained in a similar reaction involving *t*-butylamine (Table II). Also, the ease of five-coordinate intermediate formation can be related to the rigidity of the cyclotriphosphazene involved. Thus a perfectly planar $N_3P_3F_6$ would be expected to form this five-coordinate intermediate with greater difficulty than $N_3P_3Cl_6$ and hence $\Delta H^{\neq}$ would be expected to be higher for the former than for the latter in a reaction where the nucleophile and other conditions are constant (Table II). Similarly, since $N_4P_4Cl_8$ is puckered and not planar, it would be expected to form the five-coordinate intermediate with greater ease, as relatively less geo-

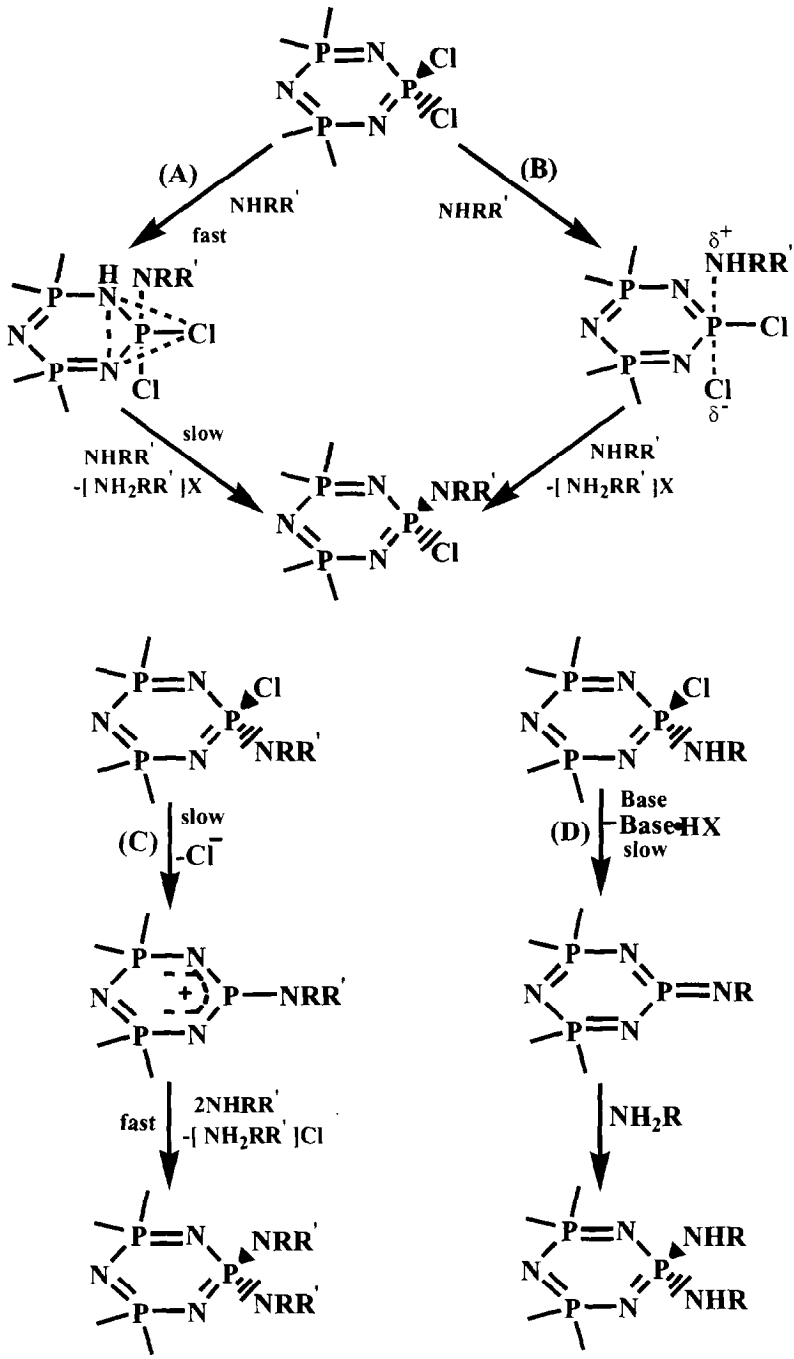

FIG. 8. Mechanistic pathways involved in the chlorine replacement reaction of chlorocyclophosphazenes: (A) = S_N2 (non-polar); (B) = S_N2 (concerted); (C) = S_N1; (D) = S_N1(CB).

TABLE II

SELECTED ACTIVATION PARAMETERS FOR CYCLOPHOSPHAZENE AMINOLYSIS REACTIONS (REPRODUCED WITH PERMISSION FROM REF. (*14*). COPYRIGHT: AMERICAN CHEMICAL SOCIETY)

Phosphazene[a]	Solvent	Product		
		$\Delta H^{\neq}$, kJ mol^{-1}	$\Delta S^{\neq}$, J K^{-1} mol^{-1}	Ref.
$N_3P_3Cl_5NHMe$	thf	2.9	−205	*87*
$N_3P_3Cl_5NMe_2$	thf	7.1	−197	*73*
$N_3P_3Cl_5NMe_2$	CH_3CN	20.7	−128.0	*73*
$N_3P_3F_5NMe_2$	CH_3CN	53.1	−128.7	*73*
$N_3P_3Cl_5NC_5H_{10}$	thf	12.1	−188	*88*
$N_3P_3Cl_5NHCMe_3$	thf	47.6	−125.9	*89*
$N_3P_3Cl_5NHCMe_3$	CH_3CN	20.3	−205.7	*89*
$N_4P_4Cl_7NHCMe_3$	CH_3CN	8.2	−201.6	*89*
$N_3P_3Cl_5NHPh$	CH_3CN	29.1[b]	−203.9[b]	*90*
$N_3P_3Cl_5NHC_6H_4$-*p*-OMe	thf	21.9[b]	−261.7[b]	*90*
$N_3P_3Cl_5NHC_6H_4$-*p*-OMe	CH_3CN	25.2[b]	−189.5[b]	*90*
cis-$N_3P_3Cl_4(NMe_2)_2$	thf	8.8	−238.0	*91*
trans-$N_3P_3Cl_4(NMe_2)_2$	thf	28.5	−159.0	*91*
trans-$N_3P_3Cl_4(NMe_2)_2$	CH_3CN	10.6	−189.7	*92*
2,4-$N_3P_3Cl_4(NHC_6H_4$-*p*-$OMe)_2$	thf	29.1[b]	−278.2[b]	*90*
trans-2,4,6-$N_3P_3Cl_3(NMe_2)_3$	CH_3CN	14.0	−196.4	*92*
cis-2,2,4,6-$N_3P_3Cl_2(NMe_2)_4$	CH_3CN	21.0	−217.2	*92*

[a] Obtained in the reaction of the amine and the parent phosphazene.
[b] Error estimated as < 5%.

metric adjustments would have to be made. This is reflected not only in the fact that $N_4P_4Cl_8$ reacts much faster with amines in comparison with $N_3P_3Cl_6$ (see above) but also that the $\Delta H^{\neq}$ term is lower when one compares analogous reactions in the same reaction conditions (*89*) (Table II).

A detailed examination of the kinetics of dimethylaminolysis of $N_3P_3Cl_6$ by Krishnamurthy and co-workers has revealed that there is a gradual and subtle mechanistic change that occurs as the degree of replacement of chlorines increases (*92*). While the first chlorine replacement follows an S_N2 pathway involving the formation of a neutral five-coordinate intermediate [Fig. 8(A)], at the second stage the mechanism can be induced to follow a concerted path [Fig. 8(B)] by using acetonitrile as the solvent. The polar transition state of the concerted path reaction pathway is stabilized in acetonitrile. This postulate has sup-

port from the following observation. In comparison with the formation of $N_3P_3Cl_5(NMe_2)$ ($\Delta H^{\neq}$, 20.7 kJ mol^{-1}), the formation of *trans*-$N_3P_3Cl_4(NMe_2)_2$ in acetonitrile is accompanied by a *decrease* in $\Delta H^{\neq}$ (10.6 kJ mol^{-1}). This indicates that the neutral five-coordinate intermediate formation is not in operation. If it were the case, the $\Delta H^{\neq}$ would be expected to increase in view of the increased steric constraint in forming the transition state leading to the bis product. Additionally, the $\Delta S^{\neq}$ term has been found to become more negative in the latter case; this suggests that a polar transition state is involved, which is favored in polar solvents like acetonitrile and is reflected in large negative values of $\Delta S^{\neq}$. This trend continues up to the tris stage. However, the replacement of a chlorine atom from *trans*-$N_3P_3Cl_3(NMe_2)_3$ involves a sudden mechanistic change to a dissociative S_N1 pathway involving the heterolytic cleavage of the P–Cl bond [Fig. 8(C)]. It has been proposed that the combined mesomeric electron release by all of the NMe_2 groups leads to the dissociation of the P–Cl bond. Interestingly, the X-ray structure of *trans*-$N_3P_3Cl_3(NMe_2)_3$ shows that one of the P–Cl bonds is longer than the others. It is the preferential dissociation of this bond that results in the predominant *cis*-stereoselectivity in the tetrakis product *cis*-$N_3P_3Cl_2(NMe_2)_4$. Further evidence of the existence of this pathway is obtained in the dimethylaminolysis of $N_3P_3Cl(OPh)_5$ (*92*). In this instance also an S_N1 pathway is preferred over the S_N2 pathway because of a similar combined mesomeric release of the five phenoxy groups which eases the heterolytic dissociation of the P–Cl bond in solution. It is likely that the trace formation of geminal products in the reactions of $N_3P_3Cl_6$ with secondary amines may be occurring as a result of the competing S_N1 reaction pathway.

The formation of geminal products with primary amines should necessarily involve a mechanism that differs from the one discussed above. It has been proposed that a hydrogen abstraction from a P(Cl)(NHR) center (as a result of HCl elimination) can lead to the formation of a three-coordinate phosphorus (V) intermediate, which is sterically strained and is also electrophilic. Consequently the incoming nucleophile attacks this center (in preference to a PCl_2 center) and the result is the formation of a geminal product [Fig. 8(D)]. A tertiary alkylamine or any other base can accelerate the proton abstraction mechanism. Conclusive evidence for this mechanism, labeled as $S_N1(CB)$ (CB = conjugate base), has been provided by Krishnamurthy and colleagues, who have shown that $N_3P_3Cl_5(NH\text{-}p\text{-}C_6H_4\text{–}OMe)$ reacts with a second mole of the amine in the presence of a tertiary base to afford a geminal product, $N_3P_3Cl_4(NH\text{-}p\text{-}C_6H_4\text{–}OMe)_2$ (*90*). The kinetics of the reaction show that it is a first-order process, which is consistent with

the proposal. Also, the three-coordinate intermediate has been trapped and products resulting from its reaction with other nucleophiles such as methanol have been isolated (*90*).

The role of the incoming nucleophile in determining the structure of the compound may be traced to competitive rates between proton abstraction (S_N1 CB) and bimolecular (S_N2) pathways. If the latter is slower (as is likely when the incoming nucleophile is the sterically hindered *t*-butylamine) the proton abstraction becomes more competitive and geminal products are formed. With less hindered amines such as ethylamine as the incoming nucleophiles the competition favors the *normal* S_N2 pathway leading to non-geminal products. Similarly, domination of the proton abstraction pathway at the higher stages of substitution leads to the preponderance of geminal tetrakis products in the reaction of $N_3P_3Cl_6$ with primary amines. The geminal product preference of (2-haloethyl) amines has been explained on the basis of their lower basicity. As a result, these amines are likely to be less nucleophilic and higher activation energies are expected in S_N2 pathways. Because of this, the dissociative pathway becomes more competitive and geminal products are formed. If one increases the basicity of the amine by using (2-methoxyethyl) amine, once again the normal pathway is followed and non-geminal products are formed (*64*). In the case of aziridine, where the exocyclic substituent is both small and weakly electron releasing, both the dissociative (S_N1) and associative (S_N2) pathways might be equally competitive and therefore geminal as well as non-geminal products are formed in this case (*78,79*).

The preference for the formation of a given stereoisomer seems to be governed by more subtle reasons. These are discussed elsewhere (*14*).

2. $N_4P_4Cl_8$

The reactions of $N_4P_4Cl_8$ with amines proceed much faster than for $N_3P_3Cl_6$. Thus, for example, *t*-butylamine reacts about 200 times faster with $N_4P_4Cl_8$ than with $N_3P_3Cl_6$ (*89*). A primary reason for this enhanced reactivity appears to be the greater skeletal flexibility of the eight-membered ring. From the limited kinetic studies that are known for the aminolysis of $N_4P_4Cl_8$ it appears that the dominant reaction pathway, at least for the initial stages of halogen replacement, is of the S_N2 type, involving the formation of the neutral five-coordinate intermediate. It appears that because of the greater flexibility of the eight-membered ring the enthalpy of activation for the formation of such an intermediate is relatively less. Probably because of this, other reaction pathways become far less important and a predominantly non-geminal

mode of substitution is observed. The greater reactivity of $N_4P_4Cl_8$ is also manifested in its reactions with bulky amines. Thus, while $N_3P_3Cl_6$ in its reaction with dibenzylamine even under harsh reaction conditions affords only the bis-substituted product $N_3P_3Cl_4(NR_2)_2$, a similar reaction of $N_4P_4Cl_8$ proceeds more readily and a product with substitution of up to four chlorine atoms is realized, $N_4P_4Cl_4(NR_2)_4$ (*93*). With amines such as cyclohexyl amine (*71*) and adamantyl amine (*72*), fully substituted products are obtained.

At the second stage of chlorine substitution in the tetramers there is a greater statistical probability for the incoming nucleophile to attack the phosphorus adjacent to $\equiv$P(Cl)(NHR), viz. P4 or P8, rather than the remote phosphorus, viz. P6 (Fig. 9). However, this statistical effect is countered by the electron releasing effect of the substituent already present on P2, which tends to deactivate P2 as well as P4 and P8 towards further nucleophilic substitution. It is observed that reactive amines such as dimethylamine (*94*) or ethylamine (*95*) react with $N_4P_4Cl_8$ and

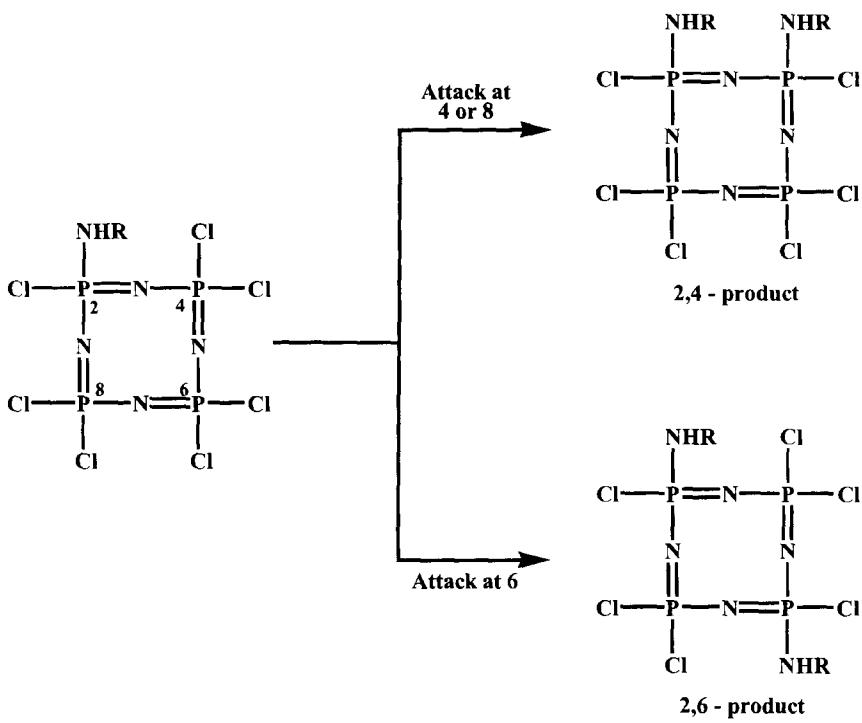

FIG. 9. Regio isomers of *non-gem* $N_4P_4Cl_6(NHR)_2$.

form 2-*trans*-6 products, whereas sluggishly reacting amines such as *t*-butylamine (*96*), dibenzylamine (*93*), or N-methylaniline (*97*) afford both 2,4 and 2,6 substituted products. A remarkable feature of the study of the reactions of $N_4P_4Cl_8$ with N-methylaniline is the isolation of five stereo isomers out of a possible ten at the tetrakis stage of substitution (*97*).

In addition to the normal pathways encountered so far, an unusual reaction pathway leading to the formation of bicyclic phosphazenes is observed in the reactions of $N_4P_4Cl_8$ with amines. This reaction was initially discovered in the aminolysis reactions of 2-*trans*-6-$N_4P_4Cl_6(NHEt_2)_2$ **8**. Thus, the reaction of **8** with an excess of dimethylamine in diethyl ether as the solvent affords the normal compound 2-*trans*-6- $N_4P_4(NMe_2)_6(NHEt)_2$ **9**. In contrast if the reaction is carried out in boiling chloroform an unusual transannular bridged bicyclic compound, $N_4P_4(NMe_2)_5(NHEt)(NEt)$ **10**, is isolated (*98–100*) (Fig. 10). While the normal amino derivative $N_4P_4(NHR)_8$ **11** is formed in the reaction of primary amines with the tetrameric chloride **2**, the formation of the bicyclic product **12** occurs if the reactions are carried out in a solvent like chloroform (*98,101*) (Fig. 10). It has been observed that the relative yields of the normal and bicyclic product are dependent on a number of factors (*102,103*).

From the synthetic studies that have been carried out it is clear that the formation of bicyclic product does not take place *before* at least four chlorine atoms are replaced by amino groups in $N_4P_4Cl_8$ (*103–106*). Also, the tetrakis amino substituted cyclotetraphosphazenes such as $N_4P_4Cl_4(NMe_2)_2(NHEt)_2$ do not yield bicyclic products if they are reacted with a tertiary amine alone. It appears that the bicyclic product formation takes place by a proton-abstraction–chloride-departure mechanism involving a bis phosphinium intermediate (Fig. 11). Another route to the bicyclic product formation is through dealkylation-cum-transannular attack. In the reactions of $N_4P_4Cl_8$ with the bulky dibenzylamine a bicyclic phosphazene $N_4P_4(NR_2)_6(NR)$ ($R = CH_2C_6H_5$) is formed where the bridgehead is an amino substituent that undergoes a dealkylation reaction (*93*).

B. Reactions with Oxygen and Sulfur Nucleophiles

1. Hydrolysis

The simplest of the reactions of $N_3P_3Cl_6$ with nucleophiles containing oxygen involves hydrolysis. Complete replacement of all the chlorine atoms by hydroxyl groups should give rise to $N_3P_3(OH)_6$. However, the

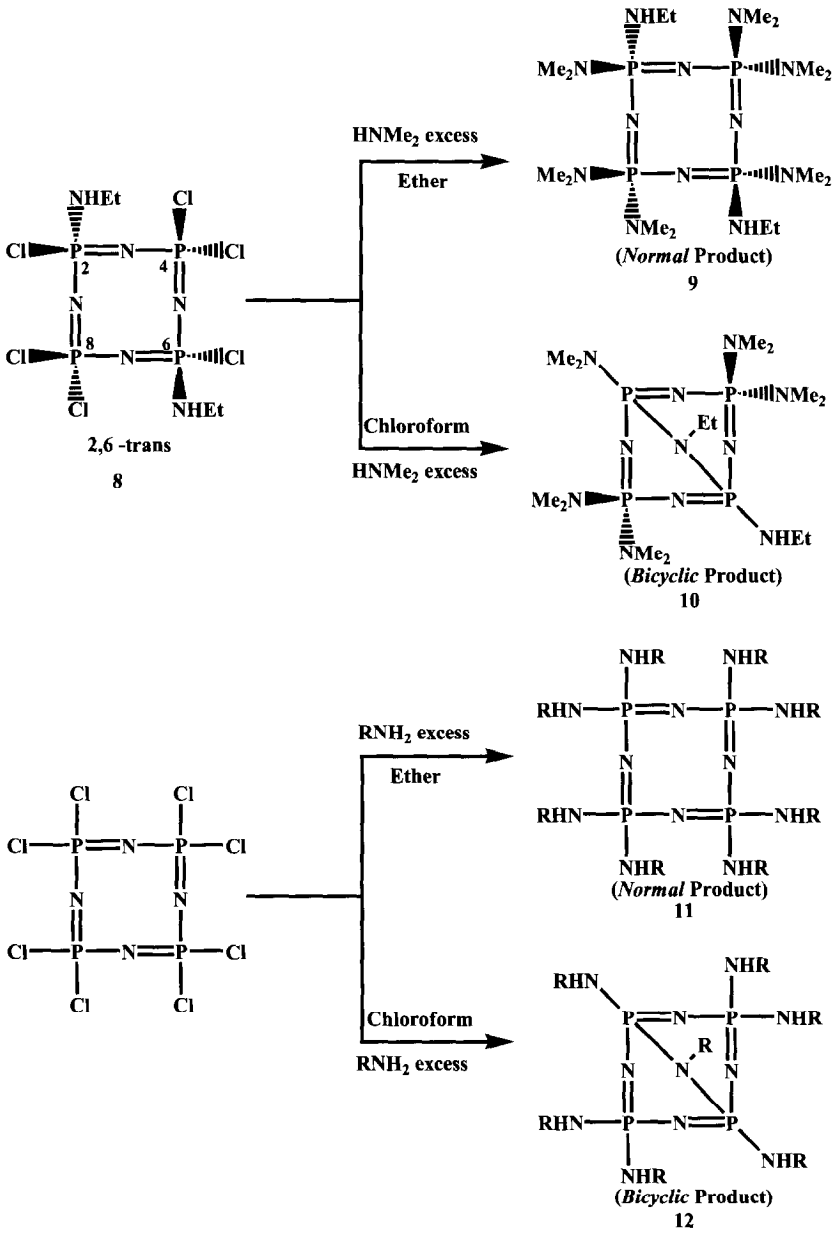

FIG. 10. Formation of bicyclic products in the aminolysis reaction of the tetrameric compounds.

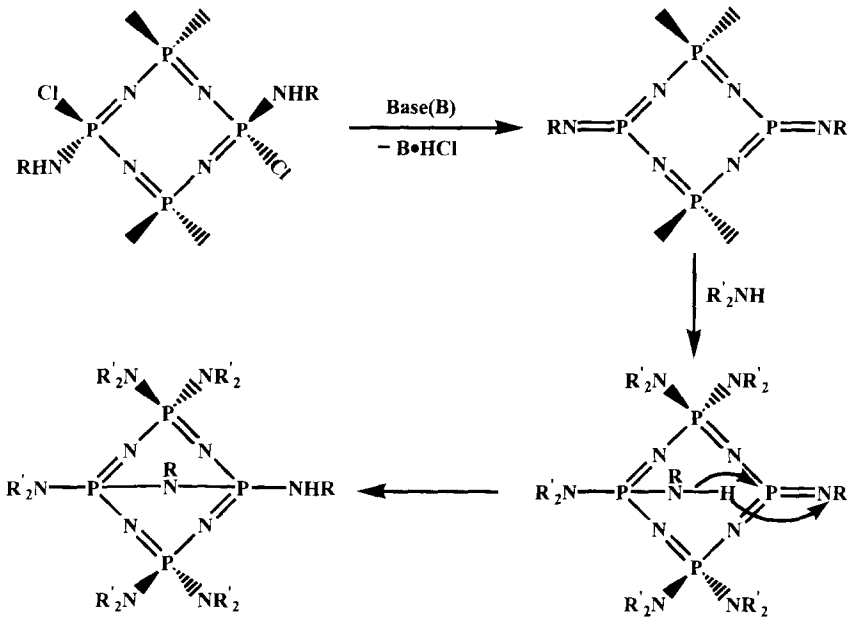

FIG. 11. Mechanism of bicyclic product formation.

latter is unstable in its hydroxy form and tautomerizes to the metaphosphimic acid $[NHP(O)OH]_3$, which hydrolyzes further to the eventual products, phosphoric acid and ammonia (*1,4, 14,18*).

However, in comparison with complete hydrolysis, the sequential and partial hydrolysis reactions are of greater interest from two points of view. Apart from academic curiosity, there is an important reason for studying the interaction of water with $N_3P_3Cl_6$. It has been very well established that water has a beneficial as well as a detrimental role in the polymerization of $N_3P_3Cl_6$ (*107*). Thus, while at low concentrations water seems to facilitate the polymerization, at larger concentrations it leads to crosslinking reactions. Haw has studied the hydrolysis reaction of $N_3P_3Cl_6$ in a THF solution by monitoring the ^{31}P NMR spectra (*108*). Products obtained by the replacement of from one to three chlorine atoms could be detected and identified by ^{31}P NMR. The first step in the reaction is the generation of the monohydroxy derivative $N_3P_3Cl_5OH$ **13** that exists in its tautomeric form **14** (Fig. 12). This species has been implicated as a possible polymerization catalyst in the ring-opening polymerization of $N_3P_3Cl_6$ (*108*). From the monohydroxy derivative, replacement of chlorine atoms proceeds both geminally and

13 14

FIG. 12. Monohydroxy cyclotriphosphazene and its tautomer.

non-geminally. In contrast to the above study, a controlled hydrolysis of $N_3P_3Cl_6$ with the hydrated salt $[Ph_4As]^+Cl^-$. H_2O leads to the isolation of the anionic species $[NPCl_2NPCl(O)NHPCl(O)]^-$ (*109*).

Studies on partially hydroxylated products of organocyclophosphazenes have clearly shown that such compounds exhibit tautomerism involving O → N hydrogen transfer. The crystal structures of $N_3P_3Ph_2(OMe)_3(O)H$ (*110*), $N_3P_3Cl_2(NEt_2)_3(O)H$ (*111*), and $N_3P_3(OPh)_5(O)H$ (*112*) have shown clearly the presence of cyclophosphazadiene structures in the solid state. The fluxional behavior of these tautomers was studied by variable temperature NMR (*113*).

2. *Reactions of Trimeric and Tetrameric Halides with Hydroxy and Mercapto Reagents*

Alcohols and phenols (mostly as the sodium salts) react with chlorocyclophosphazenes to yield fully substituted cyclophosphazenes. A variety of alkoxides and aryloxides have been employed. These include simple alkoxides (*14,114*), fluorine substituted alkoxides (*115*), vinyloxides (*116,117*), simple aryloxides (*118–122*), sterically hindered aryloxides (*123*), aryloxides containing various substituents (*124–127*), higher fused-ring benzenoid oxides (*128*), steroid salts (*129*), etc. With anthryl oxide, the mono-substituted derivative $N_3P_3Cl_5OR$ and the gem-tetrakis derivative $N_3P_3Cl_2(OR)_4$ were isolated (*123*). The reactions of substituted cyclophosphazenes $N_3P_3X_5(NPPh_3)$ (X = F, Cl) with methoxide were studied. These reactions also proceed to complete substitution (*130*). Unlike the aminolysis reactions, kinetic investigations on the reactions with alkoxides or aryloxides have been very limited. Although product distribution studies suggest that in the reactions of $N_3P_3Cl_6$ with most alkoxides and aryloxides a non-geminal pathway is observed (*14*), certain aryloxides such as 2,6-dichlorophenoxide (*123*) react in a geminal manner. Cyclophosphazenes $N_3P_3(OR)_6$ and

$N_4P_4(OR)_8$ (R = $C_6H_4C_6H_4OC_8H_{17}$ and $C_6H_4CH{=}NC_6H_4OC_7H_{15}$) have been prepared and shown to exhibit liquid-crystalline behavior (*131*).

Pentakis derivatives $N_3P_3(OR)_5Cl$ **15** have been isolated in the reactions of $N_3P_3Cl_6$ with NaOPh (*118*) or $NaOC_6H_4$-*p*-CH_3 (*119*) (Fig. 13). These products are of considerable value as model compounds containing a single replaceable chlorine atom. Recently the compound $N_3P_3(OCH_2CF_3)_5Cl$ **16** has been synthesized from $N_3P_3(OCH_2CF_3)_6$ by a controlled hydrolysis followed by a suitable exchange reaction with PCl_5 (*56*).

Reactions of thiolates with chlorocyclophosphazenes are found to proceed in an exclusive geminal pathway (*14*).

Alkoxy cyclophosphazenes undergo thermal rearrangement reactions. Of these the most well studied examples are various kinds of methoxy substituted cyclophosphazenes. Thus methoxy cyclophosphazenes $[NP(OMe)_2]_n$, n = 3–6, rearrange upon heating in vacuum to *cyclophosphazanes*, the rearrangement consisting of the transfer of an alkyl group (from P–O–R) to a ring nitrogen atom (Fig. 14) (*18, 132,133*). The driving force for this reaction is the formation of the thermodynamically stable P=O bond. The geminal derivatives $N_3P_3R_2(OMe)_4$(R = Ph or *t*-BuNH) yield fully as well as partially rearranged products. The partially rearranged products differ in the location of the N-methyl substituent (*132*).

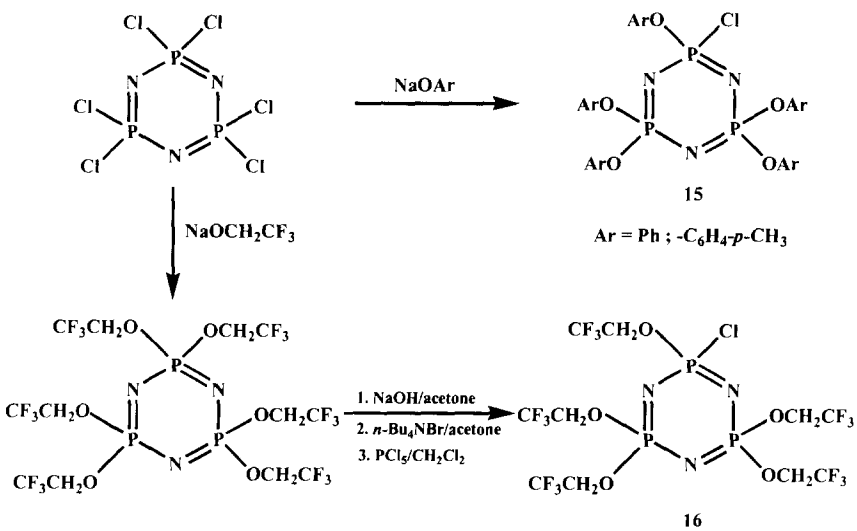

FIG. 13. Synthesis of $N_3P_3(OR)_5Cl$.

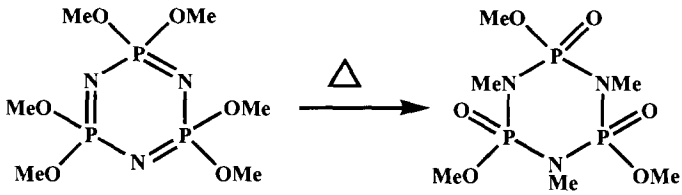

Cyclophosphazene **Cyclophosphazane**

17 **18**

FIG. 14. Rearrangement of $N_3P_3(OMe)_6$.

The rearrangement reactions can be initiated by the addition of alkyl iodide, suggesting that an intermolecular process triggers the initiation of the rearrangement. Thus, scrambled cross-alkylated products are formed when $N_3P_3(OMe)_6$ and $N_3P_3(OCD_3)_6$ are heated together (*114*). A similar scrambling has also been detected when *trans*-$N_3P_3(OCH_2Ph)_3(O\text{–}C_6H_4\text{-}p\text{-}CH_3)_3$ is thermolyzed with *trans*-$N_3P_3(OCH_3)_3(O\text{–}C_6H_4\text{-}p\text{-}CH_3)_3$ (*134,135*). It is important to note that fluoroalkoxy cyclophosphazenes and aryloxy cyclophosphazenes do not undergo rearrangement reactions.

C. Cyclophosphazenes Containing P–C Bonds

There are five synthetic methods that are currently known for the synthesis of cyclophosphazenes containing P–C bonds. These are: (a) direct synthesis involving a condensation reaction between (usually) two reagents; a more special class of these reactions is the cyclization (ring closure) reaction of an appropriately constructed synthon by the reaction with a suitable reagent; (b) Friedel–Crafts reactions on halogenocyclophosphazenes; (c) reactions of organolithium reagents with halogenocyclophosphazenes; (d) reactions of Grignard reagents with halogenocyclophosphazenes; and (e) reactions of a combination of a Grignard and organocopper (I) reagents. The last of these methods is also a potent route for the preparation of hydridocyclophosphazenes that contain a P–H bond.

1. Direct Synthesis

Cyclization of linear fragments is one of the successful synthetic methods of preparing alkyl- or aryl-substituted cyclophosphazenes. An excellent synthon of this type is the Bezman's salt

$[Ph_2P(NH_2)NP(NH_2)Ph_2]^+Cl^-$, **19**, which is prepared by the reaction of Ph_2PCl_3 and ammonia (*136*). This synthon has a preformed N–P–N–P–N unit and can be readily cyclized to a six or higher membered ring upon reaction with an appropriate reagent (*137*). An important application of the use of the Bezman's salt approach has been the synthesis of metallocyclophosphazenes of the type **20**, which contain an early transition metal in the framework of the cyclophosphazene skeleton [Fig. 15(A)] (*138*). A modification of the Bezman's salt to design a chiral synthon allowed the synthesis of an optically pure cyclophosphazene (*139*).

Condensation reactions involving the elimination of Me_3SiX (X = Br, F) from N–(silyl)P–(halogeno) phosphoranimines is also a good method for the synthesis of fully substituted alkyl or aryl cyclophosphazenes. Thus, the phosphoranimine **21** has been found to thermolyze to afford fully substituted cyclic trimers or tetramers [Fig. 15(B)] (*140*). Interestingly, if the leaving group on phosphorus is changed from the halogen to trifluoroethoxy, thermolysis of the latter affords a linear polyphosphazene (*140*).

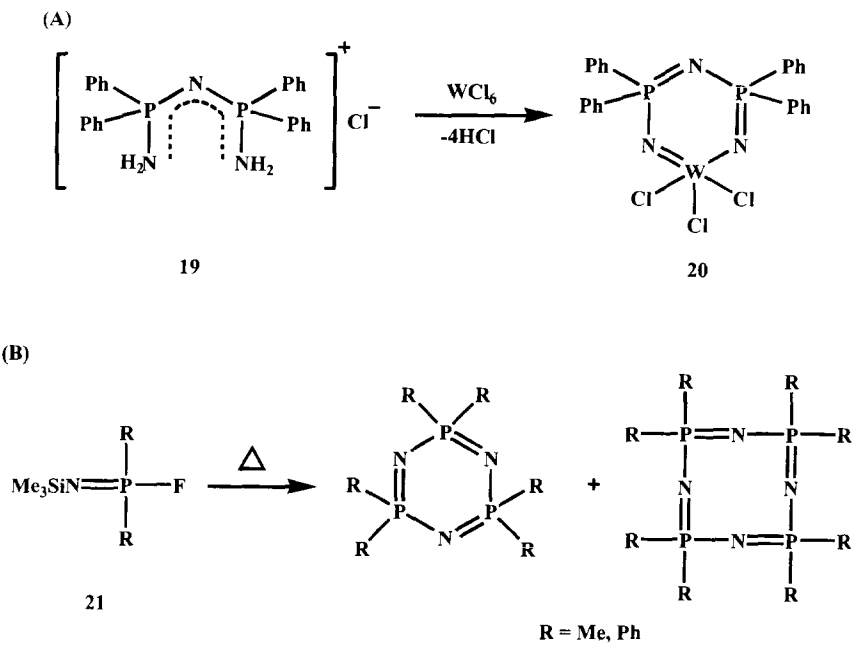

FIG. 15. (A) Cyclization reaction to afford a metallocyclophosphazene (*20*); (B) thermolysis of N-silyl-P-(fluoro)phosphoranimine (*21*) to afford alkyl cyclophosphazenes.

2. Friedel–Crafts Reaction

The Friedel–Crafts reaction of $N_3P_3Cl_6$ with benzene and aluminum chloride takes place to afford geminally substituted products *gem*-$N_3P_3Cl_4Ph_2$ and *gem*-$N_3P_3Cl_2Ph_4$. The yields of the hexakis product $N_3P_3Ph_6$ are quite low, however. This reaction is carried out in the presence of triethylamine, which reduces the reaction time and increases the yield of the bis product as well (*141*). In contrast to the Friedel–Crafts reactions involving $N_3P_3Cl_6$, those with the tetrameric chloride $N_4P_4Cl_8$ are quite complex. Only very low yields of a ring-degraded product, *gem*-$N_3P_3Cl_4(Ph)(NPPh_3)$, could be isolated in these reactions (*14,17*). The ionization of the P–Cl bond from the $\equiv$P(R)(Cl) moiety in the presence of aluminum chloride is the key step in this reaction. The three-coordinate phosphorus-containing species that would be generated as a result of this ionization is involved in a further electrophilic substitution with the arenes to afford the arylated cyclophosphazene products. $N_3P_3F_6$, containing the strong P–F bond, is not susceptible to ionization and hence Friedel–Crafts reactions do not occur with this substrate (*14*).

3. Reactions with Organometallic Reagents

The reactions of organometallic reagents with chlorocyclophosphazenes are quite complex and depend on several variables, such as (a) the ring size of the cyclophosphazene, (b) the nature of the organometallic reagent, and (c) the reaction conditions including the type of solvent used, the temperature of the reaction, etc. (*10*).

In the *normal* nucleophilic substitution reactions encountered so far, the most important and often the only event was the replacement of the halogen on the phosphorus by the nucleophile (irrespective of the mechanistic pathway involved). In the reactions of chlorocyclophosphazenes with organometallic reagents, RM, another principal competing reaction is the elimination of RCl (instead of M–Cl). This reaction, also known as the metal–halogen exchange reaction, is more prominent with chlorocyclophosphazenes than with fluorocyclophosphazenes and leads to the generation of a three-coordinate phosphorus species **22** (Fig. 16). Such a species can lead to a variety of products, including ring degradation products. The reactions with various types of organometallic reagents are discussed in the following.

a. Organolithium Reagents The reactions of fluorocyclophosphazenes with organolithium reagents have received more attention than those of chlorocyclophosphazenes. This is because, in the reactions of the latter

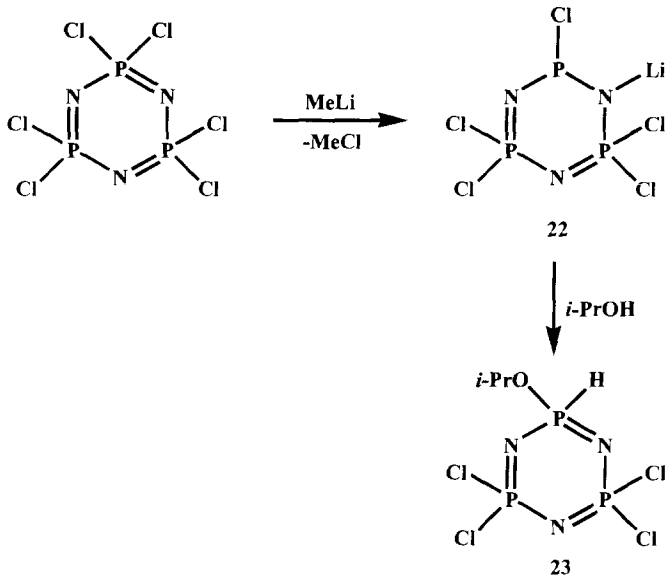

FIG. 16. Metal–halogen exchange reaction.

with the RLi types of reagent, ring-cleaved products are more common than normal substituted derivatives. Thus, for example, the reaction of methyl lithium or phenyl lithium with $N_3P_3Cl_6$ affords only minor quantities of organocyclophosphazenes (*142*). One of the probable reasons for the ring cleavage is the ready elimination of RCl rather than LiCl in these reactions to afford the metal–halogen exchanged intermediate **22**. A controlled reaction of $N_3P_3Cl_6$ with methyl lithium at −20° °C in THF followed by work-up with *i*-propanol gives a hydridocyclophosphazene *gem*-$N_3P_3Cl_4$(*i-PrO*)(*H*) **23** (*143*) whose formation is clear evidence for the involvement of the metal–halogen exchanged intermediate (Fig. 16). The subject of hydridophosphazenes is discussed in a later section. In contrast, the reaction of the fluorinated derivative with alkyl lithium reagents is a rich source for the generation of P–C bonds (*23*).

b. Reactions with Grignard Reagents The reaction of Grignard reagents with chlorocyclophosphazenes is dependent on the type of solvent used, the size of the cyclophosphazene ring, substituents present on the cyclophosphazene, and the nature of the magnesium reagent.

Initial investigations on the reaction of $N_3P_3Cl_6$ with phenyl magnesium bromide in diethyl ether revealed the formation of acyclic phenylated products $Ph_3P{=}NPPh_2{=}NH.HX$ (X = Cl or Br) as well as a small amount of $N_3P_3Ph_6$ (*144,145*). On the other hand, the reaction of $N_3P_3Cl_6$ with diphenylmagnesium in ether afforded a complex mixture of $N_3P_3Cl_5NPPh_3$, $N_3P_3Cl_5NP(Ph)(NPPh_3)_2$, and a bi(cyclophosphazene) $(N_3P_3Cl_4Ph)_2$ (*146,147*).

A reinvestigation of the Grignard reaction using THF as the solvent proved more fruitful. A number of alkyl and aryl Grignard reagents were used. Only two products were detected: a mono-substituted product $N_3P_3Cl_5R$ **24** and a P–P-linked bicyclophosphazene $(N_3P_3Cl_4R)_2$ **25** (Fig. 17). The yields of the two products depend on the nature of the R group. With sterically less hindered alkyl groups and with the phenyl group, the bicyclophosphazene is the principal product. With sterically hindered alkyl groups, a larger yield of the mono-substituted product is obtained (*148,149*). The mechanism of this reaction has been investigated and also involves, as the first step, a metal–halogen exchange reaction by elimination of RCl.

The mono-alkylated species $N_3P_3Cl_5R$ is a good synthon for the generation of geminally substituted products by further reaction with Grignard reagents (Eq. 4) (*150*)

$$N_3P_3Cl_5R + R'MgX \longrightarrow 2,2\text{-}N_3P_3Cl_4(R)(R') \qquad (4)$$

An interesting application of the above methodologies has been in the synthesis of methylsilane- and methylsiloxane-linked cyclotriphosphazenes (*151*). Since the above methodology does not achieve the

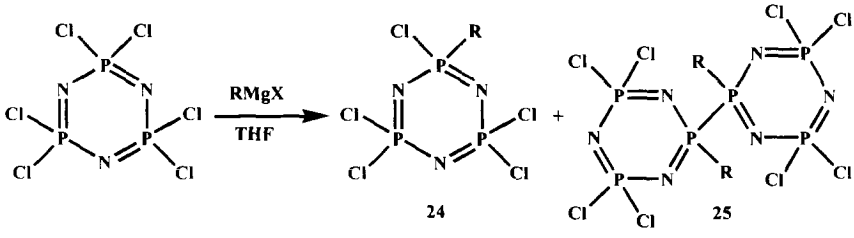

PhMgCl	**0%**	**100%**
MeMgCl	**15%**	**85%**
***n*-BuMgCl**	**69%**	**31%**
Me_3SiCH_2MgCl	**100%**	**0%**

FIG. 17. Mono and bi(cyclophosphazenes) from the Grignard reaction of $N_3P_3Cl_6$.

synthesis of the non-geminally substituted derivatives, an indirect method of synthesis has been developed. Alkylation of *non-gem* $N_3P_3(NMe_2)_nCl_{6-n}$ ($n = 3, 4$) with Grignard reagents followed by elimination of the NMe_2 group by HCl treatment affords the desired products (*152*). Use of an excess of the Grignard reagent together with a minimum amount of solvent (diethyl ether) has been found to be necessary to minimize an ether-cleaved alkoxy-substituted product $N_3P_3(NMe_2)_3(R)_2(OEt)$.

The reaction of $N_4P_4Cl_8$ with Grignard reagents is more complex. Thus the reaction with phenyl magnesium bromide leads to both substitution and ring cleavage. Mixtures of products are obtained: 2,2,4,4-$N_4P_4Cl_4Ph_4$, 2,2-$N_3P_3Cl_4(Ph)(NPPh_3)$, along with a small amount of $N_4P_4Ph_8$ (*153,154*).

c. Reactions of Alkyl Grignard Reagents in Conjunction with Organocopper Reagents A variation of the Grignard reaction of $N_3P_3Cl_6$ involves the use of an additional organocopper reagent [*n*-$Bu_3PCuI]_4$. These reactions lead mainly to the formation of *gem*-dialkyl compounds $N_3P_3Cl_4R_2$ (*155–162*). The reaction with alkyl Grignards are more successful. With aryl reagents, although geminal products have been isolated, ring-cleaved products are also formed (*10*). The reaction mechanism has been investigated and it is found that the interaction of $N_3P_3Cl_6$ with the Grignard reagent in the presence of the copper reagent leads to the formation of a bimetallic complex **26** (*162*) in which the magnesium is coordinated to nitrogen atoms and the Cu(I) is coordinated to the phosphorus(III) center. The intermediate on work-up with *i*-propanol leads to the formation of a hydrido cyclophosphazene *gem*-$N_3P_3Cl_4(R)(H)$ **27**. On the other hand, interaction of the bimetallic intermediate **26** with another equivalent of the Grignard reagent leads to *gem*-$N_3P_3Cl_4(R)(R')$ **28**. These reactions are summarized in Fig. 18. An additional variation in the utilization of this reaction involves the reaction of the intermediate **26** with aldehydes and ketones to afford *gem*-alkyl (hydroxyalkyl) compounds *gem*-$N_3P_3Cl_4(R)(C)(OH)R'R''$ **29** (*162*).

The hydrido phosphazenes **27** themselves are quite valuable reagents and can be converted into halogenocyclophosphazenes upon treatment with chlorine, bromine, or iodine. The elusive cyclophosphazenes containing a P–I bond have been synthesized in this manner (*43*). Another application of the hydrido phosphazenes is their deprotonation, leading to phosphazene anions, which provide a valuable route for other P–C compounds (*161*). The phosphazene anions can also be generated by the cleavage of the bicyclophosphazenes **25** with $LiBEt_3H$ (*163*).

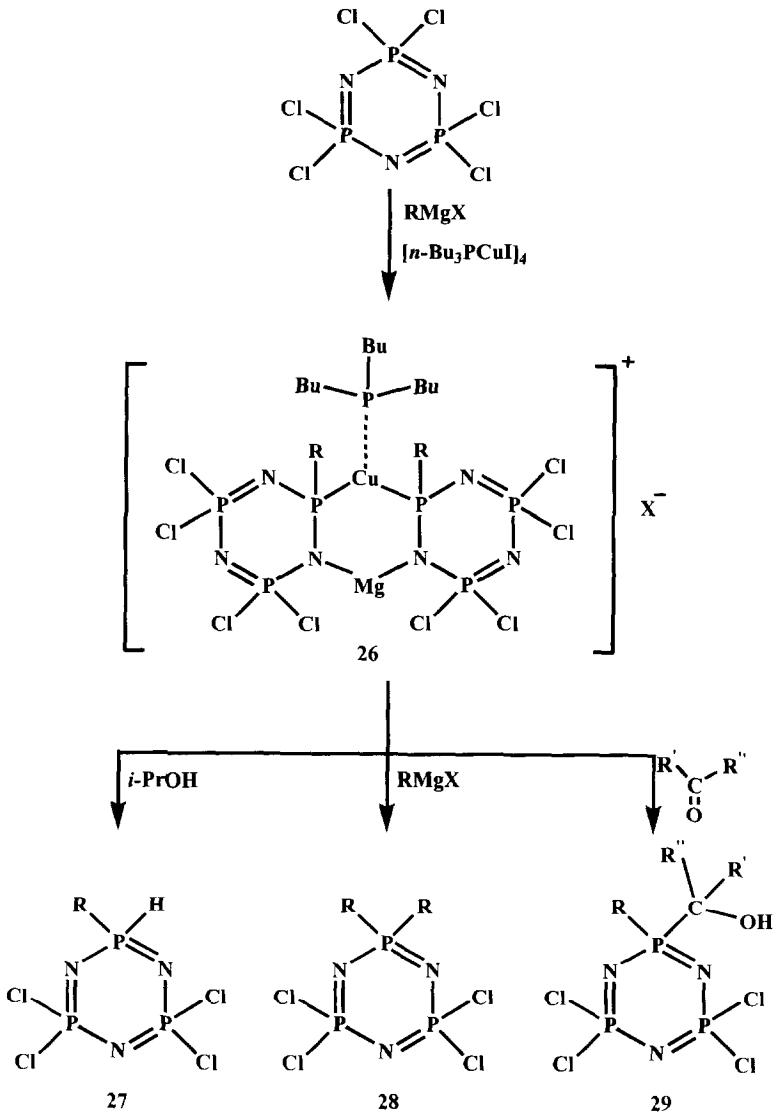

FIG. 18. The reaction of $N_3P_3Cl_6$ with RMgX/[n-$Bu_3PCuI]_4$.

Another method of the synthesis of hydridophosphazenes involves the ring closure reaction of the Bezman's reagent (*164–166*). Recently the first example of a trihydrocyclophosphazene **30** has been synthesized (*167*).

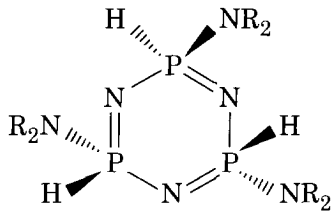

R = cyclohexyl

30

d. Alkylation with Organoaluminum Reagents Among the other prominent methods of generating a P–C bond is the use of organoaluminum reagents. The reaction of $N_3P_3Cl_6$ with trimethyl aluminum has been investigated. In this reaction the per substituted derivative $N_3P_3Me_6$(46%) and the ring-opened product $[Me_3PNP(Me)_2P(Me)_2NH]^+Cl^-$ are the principal products. Alkylation of *gem*-$N_3P_3Cl_4Me_2$ with trimethyl aluminum gave mainly the tetrakis derivative $N_3P_3Cl_2Me_4$ along with *tris*- $N_3P_3Cl_3Me_3$ (*168*).

D. Reactions of Chlorocyclophosphazenes with Difunctional Reagents

The reactions of chlorocyclophosphazenes with difunctional reagents such as diamines, diols, or amino alcohols can in principle lead to the formation of several products. These are shown in Fig. 19. The reactions of these reagents with the chlorocyclophosphazenes are discussed below.

1. $N_3P_3Cl_6$

The reactions of the six-membered chlorocyclophosphazene were studied with a number of aliphatic diamines (*169–175*), aromatic diamines (*176*), aliphatic diols (*177–179*), aromatic diols (*180,181*) and compounds containing amino and hydroxyl functional groups (*169,170,182*). This subject has been reviewed (*11,16,20*). There are at least five different reaction products that are possible (Fig. 19). Replacement of two chlorine atoms from the *same* phosphorus atom produces a spirocyclic product. Replacement of two chlorine atoms from two different phosphorus atoms in the same molecule produces an ansa product. Reaction of only one end of the difunctional reagent, resulting in the substitution of only one chlorine atom, leads to an open-chain compound. Intermolecular bridged compounds are formed when the difunc-

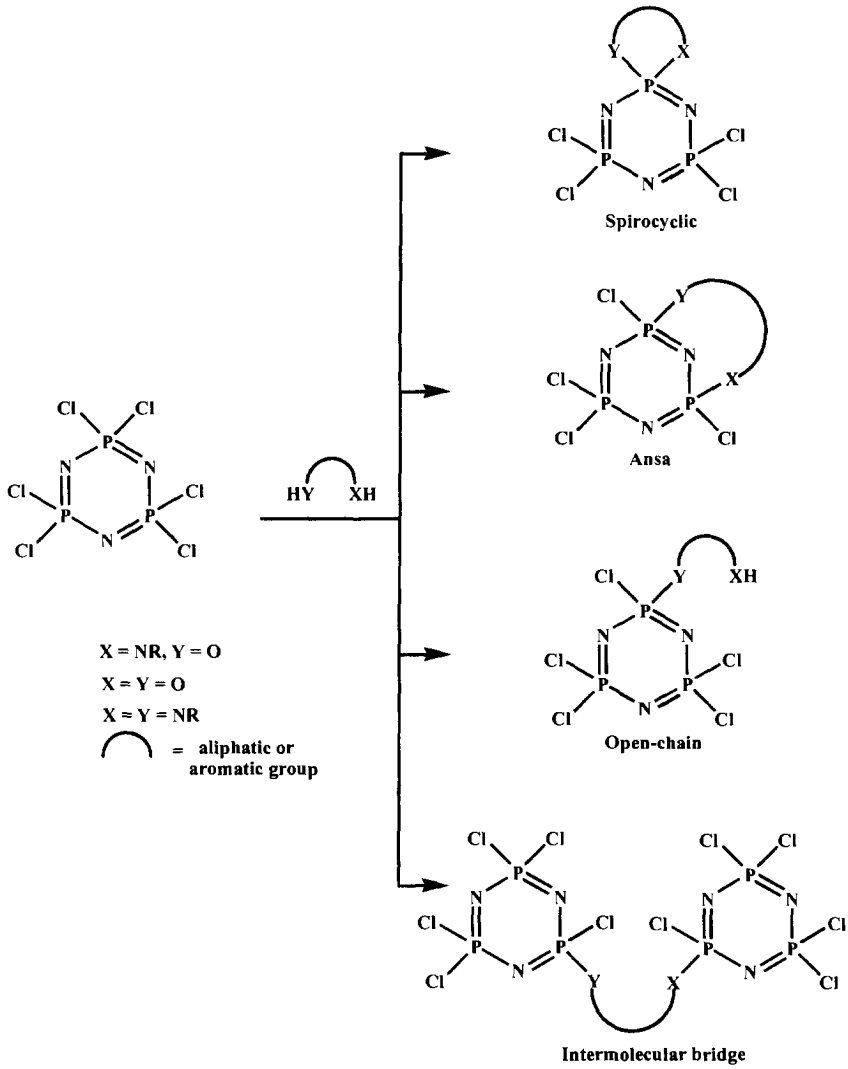

FIG. 19. The possible products in the reaction of difunctional reagent with $N_3P_3Cl_6$.

tional reagent reacts with two molecules of the cyclophosphazene. Finally, ring-degraded products are formed in the reactions of certain aromatic ortho dinucleophiles.

With aliphatic diols, although mixtures of products are formed, the predominant products are spirocycles (*11,177*). The reactions with the sodium salts of etheroxy diols such as tetra- and pentaethylene glycols

affords a mixture of spirocyclic and ansa products which can be separated by column chromatography (*183*). In the reaction with 1,3-propanediol an unusual spiro–ansa product containing both a spirocyclic and an ansa arrangement were isolated (*177,178*). Primary diamines react with chlorocyclophosphazenes to afford monospiro products primarily, although with amines such as 1,3-diaminopropane, mono-, di- and trispiro products have been isolated (*174*). Secondary aliphatic diamines as well as amino alcohols (*169–170,173*) and other types of difunctional reagents such as dihydrazidophosphoric acid (*184–186*) result in spirocyclic products. With unsymmetric difunctional reagents such as N-methyl ethanolamine, the di- and trispiro products also show *cis–trans* isomerization (*170,171*). Intermolecular bridged compounds are formed in the reactions with long-chain aliphatic diamines (*16,187*). Ansa products have been rare and require indirect synthetic approaches. The reaction of $N_3P_3(CH_3)Cl_5$ with 1-amino propanol gives an open chain compound, *gem*-$N_3P_3(CH_3)(NH(CH_2)_3OH)Cl_4$, that undergoes intramolecular cyclization upon treatment with a base to afford the ansa product **31** (*188*). In an alternative approach, *non-gem*-$N_3P_3(OCH_2CF_3)_4Cl_2$ has been shown to react with both aliphatic and aromatic difunctional reagents to form ansa compounds **32** (*189*).

Most aromatic difunctional reagents react with $N_3P_3Cl_6$ to afford spirocyclic products (*20,176,180,181,189,190*). With catechol, the trispiro product is observed (*190*). This product was shown to function as a host in the formation of several inclusion adducts, including polymers (*191*). Ring degradation of the cyclophosphazene ring occurs in the reaction with *o*-amino phenol as well as in the reaction with catechol in the presence of a triethylamine (*192*).

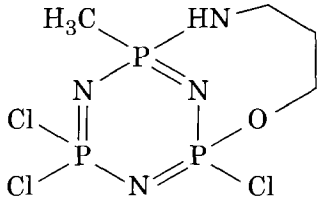

31

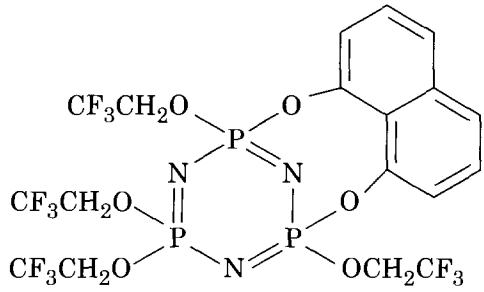

32

Recently Brandt and co-workers have delineated the relative importance of thermodynamic *vs.* supramolecular factors in the direction of product formation. Thus, in the normal course of reaction $N_3P_3Cl_6$ would react with a bis-naphthol to afford a spirocyclic product **33**. However, upon using a pre-formed cyclophosphazene containing a crown-architecture **34**, the encapsulation of Na^+ ions by the crown preferentially orients the difunctional reagent towards the non-geminal chlorines and the spirocycle formation is inhibited (Fig. 20) (*193,194*). Two types of ansa product **35** and **36** are formed. An interesting host–guest complexation-driven regioselectivity has also been reported by Brandt and co-workers. They have observed that the P–N–P crown reacts with aliphatic diamines at *low temperatures* to produce interesting ansa–ansa, doubly bridged or singly bridged compounds. It is

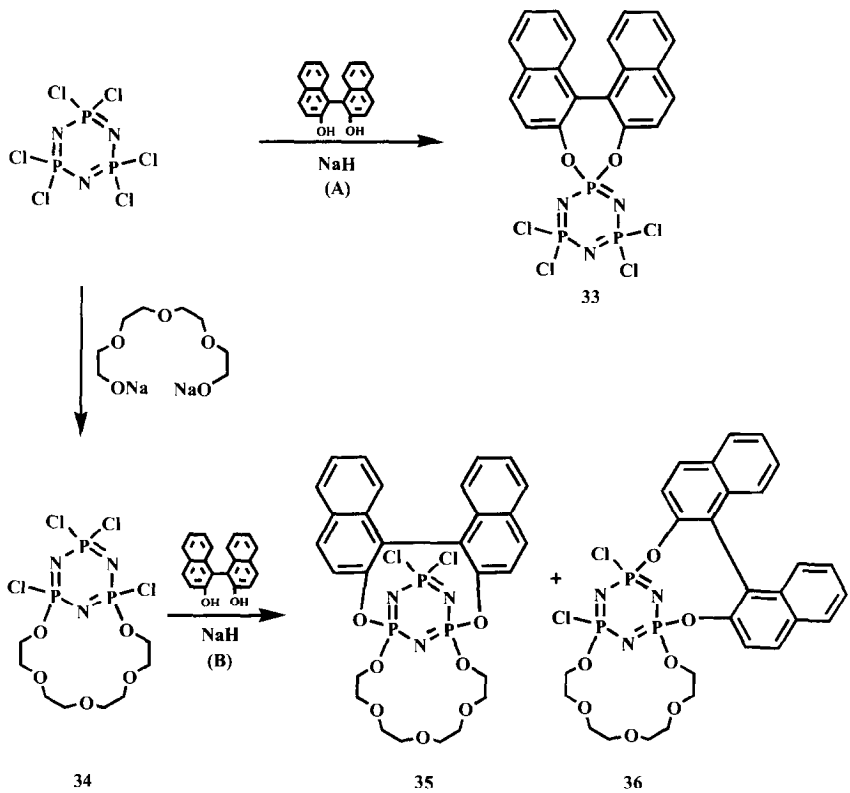

FIG. 20. Thermodynamic (A) *vs.* supramolecular effect (B) in the formation of spirocyclic and ansa products.

believed that the initial complexation of the diamine to the crown activates the P–Cl bonds selectively and initially forms an open-chain derivative, which leads to other products (*195*).

2. $N_4P_4Cl_8$

The reactions of the eight-membered ring with difunctional reagents are much less studied (*196–198*). This is primarily because of greater product instability. However, monospiro products have been isolated and characterized in the reactions of $N_4P_4Cl_8$ with 1,3-diaminopropane, 1,3-propanediol, and N-methylethanolamine (*196*). Monospirocyclic products have also been isolated in the reactions with 2,2′-methylene-bis(4,6-di-*t*-butylphenol). Mono and dispiro (2,2-6,6) products were obtained in reactions with N,N′-diisopropylpropane–1,3-diaminopropane (*199*). The reactions of 1,1′-ferrocene diol with $N_4P_4Cl_8$ have been investigated. These lead to the formation of monoansa product 2,4-$N_4P_4Cl_6(FcO_2)$. In contrast, the reactions with the corresponding dithia or diselena derivatives afford monospirocycles (*200*).

IV. Phosphazene-Based Dendrimers

The multi-functional nature of chlorocyclophosphazenes allows these compounds to be utilized as dendrimer cores. $N_3P_3Cl_6$ and $N_4P_4Cl_8$ offer six and eight branching points, which is significantly more than the ones available with conventional organic cores, permitting the ready accommodation of a larger number of peripheral units around the cyclophosphazene framework. This in turn implies that spherical dendrimeric architecture is attained more quickly using a lesser number of synthetic steps. Both convergent and divergent synthetic methodologies have been used towards the assembly of cyclophosphazene-based dendrimers.

Togni and co-workers have used the convergent methodology to link phosphine-containing chiral ferrocene ligands on the cyclophosphazene core to obtain dendrimeric structures of the type **37** (Fig. 21) (*201*). The reaction with the cyclophosphazene end occurs by the replacement of the P–Cl bond and by the formation of the P–O bond. The dendrimers contain twelve and sixteen ferrocene moieties respectively. The phosphine units present can coordinate to Rh(I) to afford metallic dendrimers, which have been shown to be excellent catalysts for the enantioselective hydrogenation of dimethyl itaconate. The product

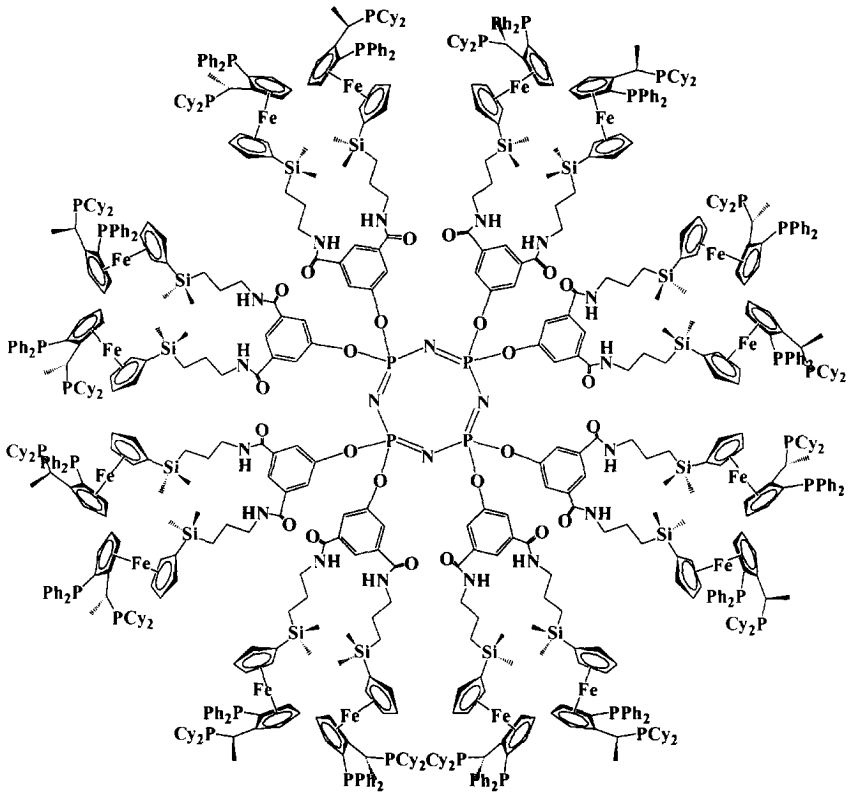

37

FIG. 21. A dendrimer based on the eight-membered P–N ring.

obtained has 98% ee. Clearly this kind of approach allows the possibility of developing a new generation of catalytic systems.

Majoral and co-workers have utilized a divergent synthetic strategy to prepare phosphazene dendrimers. Their strategy consists of using the functional cyclophosphazene $N_3P_3(O\text{–}C_6H_4\text{-}p\text{-}CHO)_6$ as the dendrimeric core (*202,203*). This molecule consists of six peripheral CHO groups which have been used in condensation reactions with N-methyl hydrazine to afford hydrazones containing six reactive NH groups that can be involved in reaction with chlorophosphines to generate phosphine-terminated cyclophosphazenes. A Staudinger reaction with the phosphorus azide $N_3P(S)(O\text{–}C_6H_4\text{-}p\text{-}CHO)_2$ gives the first-generation dendrimer **38** which contains twelve peripheral CHO groups (Fig. 22).

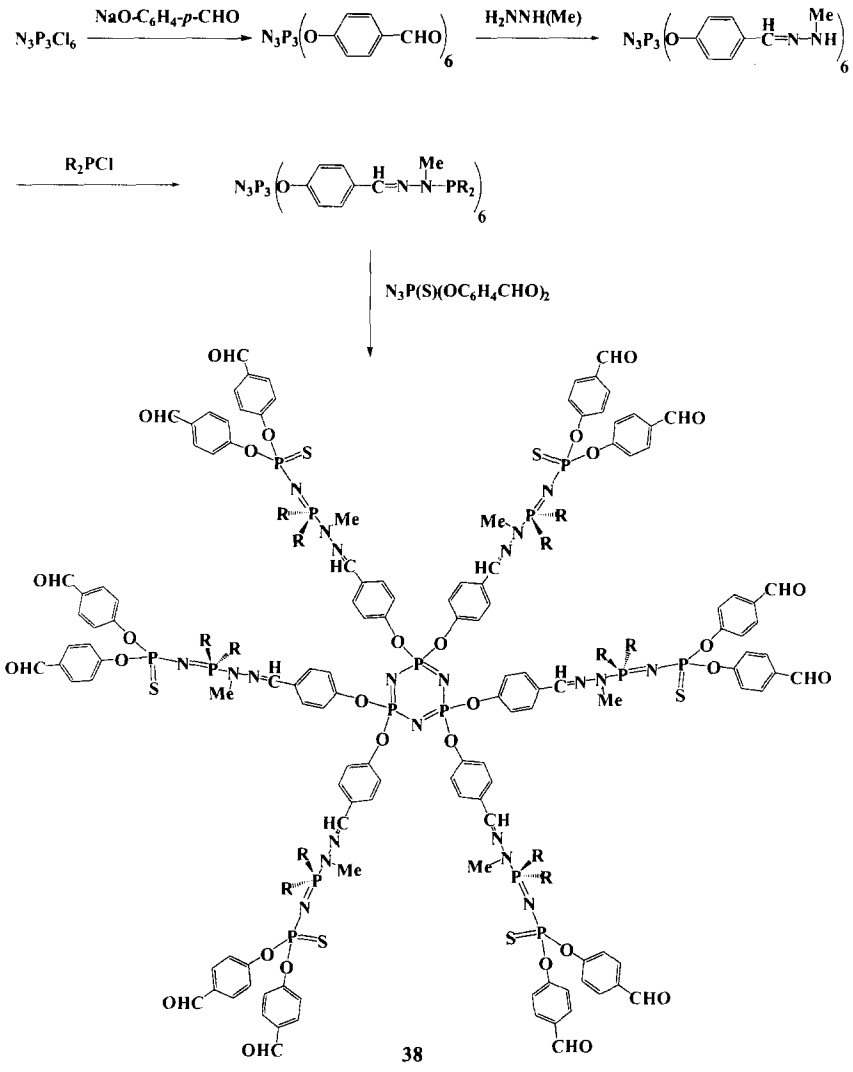

First generation dendrimer

FIG. 22. Synthesis of a divergent dendrimer.

This methodology has been repeated to give dendrimers up to the third generation. A variation of this strategy consists of utilizing the phosphine Ph_2PCH_2OH in a Mannich-type reaction with the terminal NH group on the cyclophosphazene in the second step of the dendrimer

synthesis. Remarkably, Majoral and co-workers have also shown that even after the dendrimer synthesis is accomplished the inner voids of the main dendrimer can be further activated to generate reactive sites. These can be elaborated to produce secondary dendrimeric structures within the space of the primary *mother dendrimer* (*204*). Labarre and co-workers have also claimed the synthesis of cyclophosphazene dendrimers up to the fifth generation by using the combination of $N_3P_3Cl_6$ and long-chain aliphatic diamines (*205*). A hexa-armed star-like poly(β-benzyl-L-aspartates) has been assembled using hexakis (4-aminophenoxy)cyclotriphosphazene as the core (*206*).

V. Cyclophosphazene-Based Ligands and their Coordination Chemistry

The coordination and organometallic chemistry of cyclophosphazenes has been a subject of two previous and one recent reviews (*10,19,21*). The ring nitrogen atoms of the cyclophosphazene skeleton possess a lone pair of electrons and in principle these can participate in interaction with appropriate transition metal ions. Although the basicity of the ring nitrogen atoms in the parent chlorocyclophosphazenes is quite low, it can be enhanced by placing appropriate electron-releasing substituents on phosphorus. Thus peralkylated cyclophosphazenes $[NP(Me_2)]_n$ or aminocyclophosphazenes such as $[NP(NRR')_2]_n$ have been viewed as possible ligand systems. Six-membered cyclophosphazene ligands based on the above design did not coordinate to transition metal ions but were quite readily protonated to give compounds of the type $[N_3P_3(NMe_2)_6H]_2^+ X^{2-}$; $X = CoCl_4$ or $Mo_6O_{19}^{2-}$ (*207,208*). Increasing the ring size does impart favorable coordination properties. Thus in the complex $N_4P_4(NMe_2)_8W(CO)_4$ the coordination to tungsten occurs through a cyclophosphazene as well as the exocyclic dimethylamino nitrogen (*209*). While $N_4P_4Me_8$ forms a diprotonated complex upon interaction with platinum or cobalt halides in a protic solvent (*210,211*), it coordinates to Cu(II) through one of the ring nitrogen atoms while the opposite nitrogen is protonated (*212*). In contrast, the complex $N_4P_4(NHMe)_8.PtCl_2$ contains coordination of two antipodal ring nitrogen atoms in a *cis* manner with the platinum (*210,213,214*). Higher membered rings such as $N_5P_5Me_{10}$ (*215,216*), $N_6P_6Me_{12}$ (*217*), $N_6P_6(NMe_2)_{12}$ (*218–220*), and $N_8P_8Me_{16}$ (*221*) have been investigated as ligands and are found to be effective in coordination to first-row transition metal ions.

The phosphorus atom of the cyclophosphazene ring can also be involved in interaction with transition metal atoms either by a coordinate or by a covalent linkage. The former occurs with hydridocyclophosphazenes by a tautomerization of the P–H to result in a P(III) center (*222*). The covalent mode of linkage occurs by the reaction of the appropriate organometallic or metal fragment with the halogenocyclophosphazenes (*223*).

A more attractive utility of cyclophosphazenes consists of utilizing their multi-functional periphery (reactive P–Cl bonds), which allows the construction of appropriate coordination ligands. In the past few years this aspect has been receiving considerable attention and a number of coordinating ligands have been prepared. In this approach a suitable coordinating group is incorporated on the phosphazene skeleton (*21*). Apart from the generation of ligands containing a large number of coordination sites, the well developed nucleophilic substitution chemistry of chlorocyclophosphazenes allows the design of ligands with varying coordinating capabilities such as the number, nature, and stereochemical disposition of the coordination sites. Table III summarizes some selected ligand systems prepared utilizing this concept. The earlier studied examples of this approach include acetylenic phosphazenes (*224*), phosphine-containing derivatives (*225,226*), carboranyl-substituted phosphazenes (*227*), etc.

Among the various ligands listed in Table III, the pyrazolyl family of ligands has received considerable attention (*228–242*). Polymeric ligands based on this family are also known (*234*). Several modes of coordination have been observed. The metal complexes showing these various coordination modes are shown in Fig. 23. One of the common ways of interaction of the pyrazolyl cyclophosphazenes with a transition metal ion is through the two pyrazolyl nitrogen atoms (the pyrazolyl substituents being in a geminal or a non-geminal disposition) along with a ring nitrogen atom [Fig. 23(A)] (*21*, *229*). Two geminal pyrazolyl nitrogen atoms and a ring nitrogen atom are also involved in some examples [Fig. 23(B)] (*233*). Lanthanide ions have also been found to be coordinated by the hexakis derivative $N_3P_3(3,5\text{-}Me_2Pz)_6$ (*236*). In this case the substituted cyclotriphosphazene ring supplies five coordination sites: four pyrazolyl nitrogen atoms and one cyclophosphazene ring nitrogen atom [Fig. 23(C)]. In the complex $N_3P_3(3,5\text{-}Me_2Pz)_6.CuCl_2.PdBr_2$ the palladium ion is coordinated by *only* geminal pyrazolyl nitrogens [Fig. 23(D)] (*239*). Exclusive non-geminal pyrazolyl nitrogen atom coordination is also accomplished by a specific ligand design [Fig. 23(E)] (*232*). In the above instances where the cyclophosphazene ring nitrogen is involved in coordination to the metal ion, the phos-

TABLE III

SOME MULTI-SITE LIGANDS CONTAINING NITROGEN DONOR SITES AND METAL COMPLEXES DERIVED FROM THEM

Ligand	Complex (Ref.)
$N_3P_3(3,5\text{-}Me_2Pz)_6$, L1	L1 · $CuCl_2$ (*229*); L1 · $SmCl_3$ (*236*); L1 · $2CuCl_2$ (*237*); [{$N_3P_3(Me_2Pz)_5O$} · ($2CuCl_2$)(3,5-Me_2PzH)] (*237*); L1 · $2CuI_2$ (*238*); L1 · $2ZnCl_2$ (*238*); L1 · $CuCl_2$ · $PdBr_2$ (*239*)
gem-$N_3P_3Ph_2(3,5\text{-}Me_2Pz)_4$, L2	L2 · $NiCl_2$ (*240*); L2 · $Cu(ClO_4)_2 \cdot 2H_2O$ (*230*); L2 · $Cu(ClO)_4 \cdot 2$ImH (*230*); L2 · $CuCl_2$ (*241*)
gem-$N_3P_3Ph_2(Pz)_4$, L3	L3 · $CoCl_2$ (*242*)
gem-$N_3P_3(NH_2)_2(3,5\text{-}Me_2Pz)_4$, L4	L4 · $CoCl_2$ (*231*)
gem-$N_3P_3Ph_4(Me_2Pz)_2$, L5	L5 · $W(CO)_3$ (*233*); L5 · $Mo(CO)_3$ (*233*) L6·$PdCl_2$ (*232*)
non-gem-cis-$N_3P_3(OPh)_4(3,5\text{-}Me_2Pz)_2$, L6	
$N_3P_3(OC_5H_4N)_6$, L7	[2 · $N_3P_3(2\text{-}OC_5H_4N)_6$ · 2CuCl · $CuCl_2$]$^{2+}$ · $2Cl^-$ (*248*); [N_3P_3{(4-$OC_5H_4N)_6Mn(CO)_3$(bipy)}$_6$]($ClO_4)_6$ (*243*)
gem-$N_3P_3[NH(CH_2)_2NH](NMe_2)_4$, L8	L8 · $PdCl_2$ (*247*); [{$N_3P_3(NMe_2)_4[NH(CH_2)_2NH_2]OH$} · $PdCl_2$] (*247*); [{$N_3P_3(NMe_2)_4[N(CH_2)_2NH_2]$ · $PdCl_2$} · O] (*247*)
$N_3P_3(OPh)_5$(-*o*-$NHCH_2C_5H_4N$), L9	L9 · $PdCl_2$ (*245*); 2L9 · $Cu(NO_3)_2$ (*245*); L9 · $Cu(NO_3)_2$ (*245*)
$N_3P_3(OC_6H_4\text{-}p\text{-}tBu)_5(O\text{–}C_6H_4\text{-}p\text{-}CH_2CN)$[a], *L10*	L10 · Fe(Cp)($Ph_2P(CH_2)_2PPh_2$)]PF_6 (*246*)
$N_3P_3(O_2C_{10}H_6N_2)_3$[a], L11	L11 · $(CoL)_3$ (*244*); L = 3,5-di-*tert*-butyl-*o*-benzoquinone

[a] Although metal complexes have been reported with these ligands, they have not been structurally characterized.

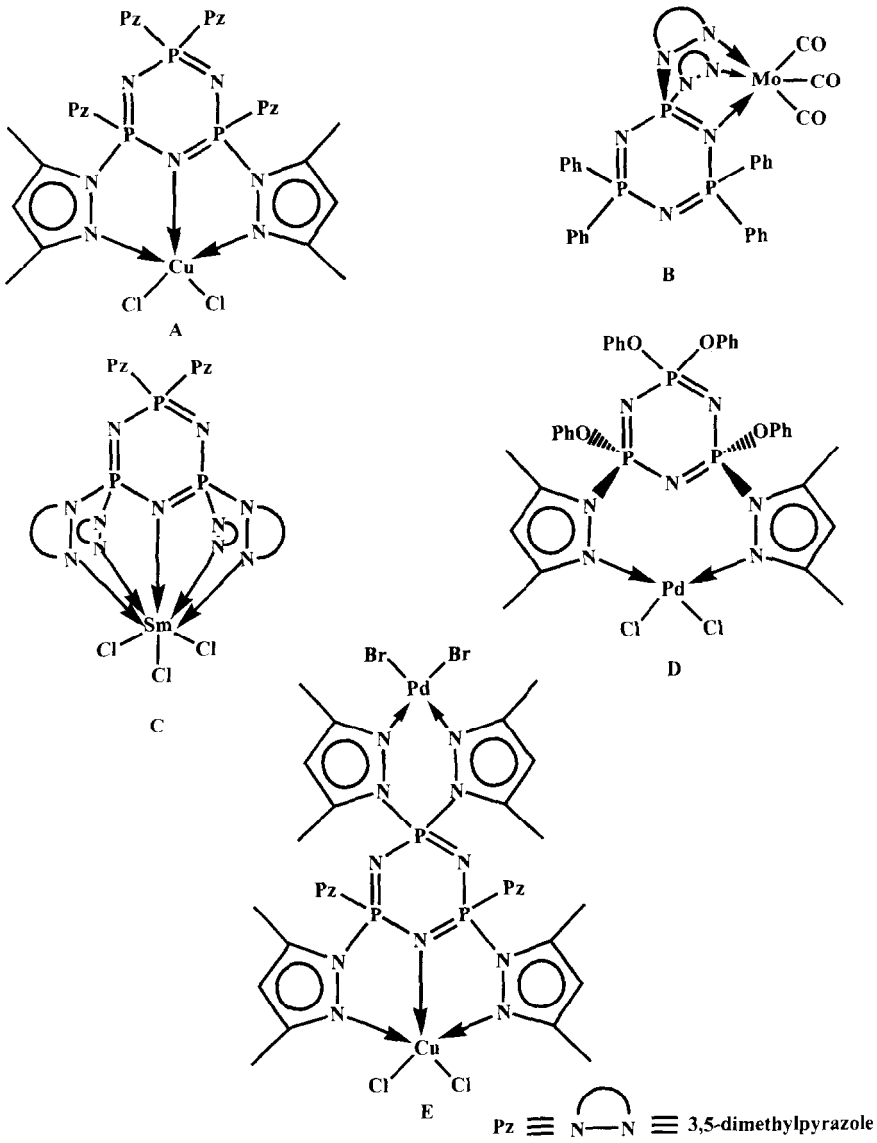

FIG. 23. Modes of coordination of pyrazolyl cyclophosphazenes.

phazene ring undergoes a distortion from planarity with the nitrogen involved in coordination suffering the maximum displacement from the average plane of the cyclophosphazene ring. An additional structural feature that is manifested upon coordination is the lengthening

of the P–N bonds flanking the site of coordination (*21*). Many of the diamagnetic complexes prepared from pyrazolylcyclophosphazenes show stereochemical non-rigidity in solution (*238*). Homo- and heterobimetallic compounds can be prepared in a stepwise manner by using these ligands (*237–239*) (Eqs. 5–7). A summary of the coordination behavior of pyrazolylcyclophosphazenes and other ligands built using the cyclophosphazene ring as the scaffold is given in Table III.

$$N_3P_3(3,5\text{-}Me_2Pz)_6 \xrightarrow{CuCl_2} N_3P_3(3,5\text{-}Me_2Pz)_6 \cdot CuCl_2 \quad (5)$$

$$N_3P_3(3,5\text{-}Me_2Pz)_6 \cdot CuCl_2 \xrightarrow{CuCl_2} N_3P_3(3,5\text{-}Me_2Pz)_6 \cdot 2CuCl_2 \quad (6)$$

$$N_3P_3(3,5\text{-}Me_2Pz)_6 \cdot CuCl_2 \xrightarrow{PdBr_2} N_3P_3(3,5\text{-}Me_2Pz)_6 \cdot CuCl_2 \cdot PdBr_2 \quad (7)$$

Another attractive approach of utilizing $[NP(NHR)_2]_n$ as ligands consists in deprotonating the NH groups (*249–252*). Steiner and co-workers have shown that $N_3P_3R_6$(R = NHC_6H_{11}; NHPh) can be readily and completely deprotonated to generate the dimeric complex $[\{N_3P_3(NC_6H_{11})_6\}_2(thf)_4Li_{12}]$ (*249*) (Eq. 8).

$$N_3P_3(NHC_6H_{11})_6 \xrightarrow{6n\text{-}BuLi} [N_3P_3(NC_6H_{11})_6]^{6-} \cdot 6Li^+ \quad (8)$$

Interestingly, this highly charged compound is soluble in a wide range of organic solvents. In this compound the lithium anions are bound to the central P_3N_9 core (Fig. 24). The phosphazene rings are highly non-planar within this structure. Trianionic derivatives $[N_3P_3(NHR)_3(NR)_3]^{3-}$ have also been prepared. These contain the protonated amino substituents in a stereo-specific non-geminal *cis* orientation (Eq. 9) (*250*).

$$N_3P_3(NHPh)_6 \xrightarrow{6n\text{-}BuLi} cis\text{-}[N_3P_3(NPh)_3(NHPh)_3]^{3-} \cdot 3Li^+ \quad (9)$$

The eight membered 2,4,6,8 *trans*-$N_4P_4(NHC_6H_{11})_4$ could also be deprotonated to afford the tetraanionic derivatives (*251*).

The NH protons can also be deprotonated in reactions with metal alkyls to generate compounds with a very high metal content (*252*) (Eqs. 10,11).

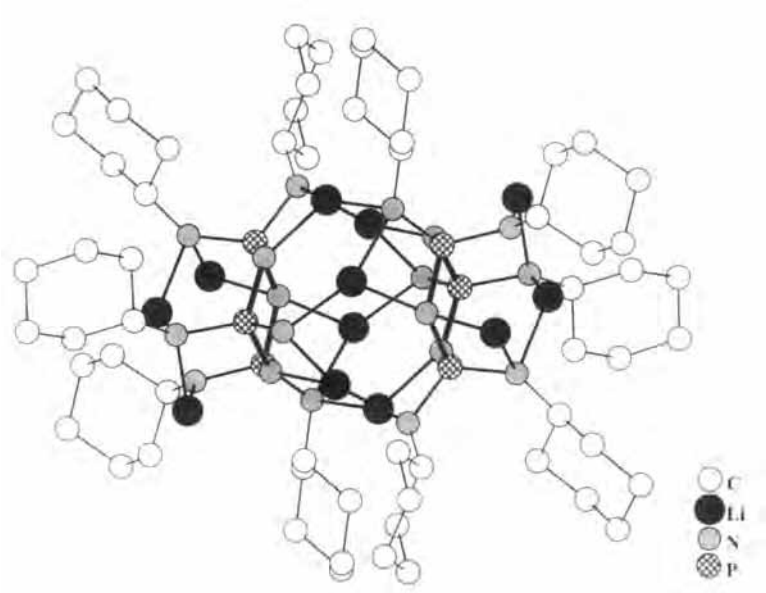

FIG. 24. Molecular structure of $[\{N_3P_3(NC_6H_{11})_6\}_2(thf)_4Li_{12}]$ (hydrogens, solvent molecule, and two cyclohexyl groups are omitted for clarity).

$$N_3P_3(NHC_6H_{11})_6 \xrightarrow[THF]{5Me_3Al} [\{N_3P_3(NC_6H_{11})_6\}(thf{\bullet}MeAl)(Me_2Al)] + 6CH_4 \quad (10)$$

$$N_3P_3(NHC_6H_{11})_6 \xrightarrow{6Et_2Zn} [N_3P_3(NC_6H_{11})_6(EtZn)_6] + 6C_2H_6 \quad (11)$$

The cyclophosphazene ring assumes a highly puckered conformation in both the zinc and aluminum complexes, indicating its remarkable flexibility to adapt to the coordination requirement of the metals.

VI. Conclusions

The chemistry of chlorocyclophosphazenes continues to be of great interest. Many of the mechanistic features involving the aminolysis reactions are now understood. However, rigorous kinetic studies on reactions of chlorocyclophosphazenes with other types of nucleophiles are quite rare. The most promising utility of the chlorocyclophosphazenes is their reactive periphery combined with a robust framework. It

is expected that the future course of cyclophosphazene chemistry will center around these properties. The reactive periphery allows the construction of a number of multi-site ligands. This makes it possible for the cyclophosphazene unit to be used as a convenient core to build dendrimeric structures.

ACKNOWLEDGEMENTS

VC is thankful to the Department of Science and Technology and the Council of Scientific and Industrial Research, India, for financial support.

REFERENCES

1. Allcock, H.R. "Phosphorus–Nitrogen Compounds"; Academic Press: New York, 1972.
2. Allcock, H. R. "Heteroatom Ring Systems and Polymers"; Academic Press: New York, 1967.
3. Roesky, H. W. In "The Chemistry of Inorganic Ring Systems"; Steudel, R., Ed.; Elsevier: Amsterdam, 1992.
4. Allen, C. W. In "The Chemistry of Inorganic Homo and Heterocycles"; Haiduc, I.; Sowerby, D. B., Eds.; Academic Press: New York, 1987, Vol. 2.
5. Heal, H. G. "The Inorganic Heterocyclic Chemistry of Sulfur, Nitrogen and Phosphorus"; Academic Press: New York, 1980.
6. Keat, R.; Shaw, R. A. In "Organic Phosphorus Chemistry"; Kosalopoff, G. M.; Maier, L., Eds.; Wiley: New York, 1973, Vol. 6.
7. Krishnamurthy, S. S.; Woods, M. *Annu. Rep. NMR Spectrosc.* **1987**, *19*, 175.
8. Allcock, H. R. *Chem. Rev.* **1972**, *72*, 315.
9. Allcock, H. R. *Acc. Chem. Res.* **1979**, *12*, 351.
10. Allcock, H. R.; Desorcie, J. L.; Riding, G. H. *Polyhedron* **1987**, *6*, 119.
11. Shaw, R. A. *Phosphorus, Sulfur Silicon* **1989**, *45*, 103.
12. Shaw, R. A. *Pure Appl. Chem.* **1980**, *52*, 1063.
13. Shaw, R. A. *Chem. Rev.* **1962**, *62*, 247.
14. Allen, C. W. *Chem. Rev.* **1991**, *91*, 119.
15. Allen, C. W. *Coord. Chem. Rev.* **1994**, *130*, 137.
16. Labarre, J. F. *Topics Curr. Chem.* **1985**, *129*, 173.
17. Krishnamurthy, S. S.; Sau, A. C.; Woods, M. *Adv. Inorg. Rad. Chem.* **1978**, *21*, 41.
18. Chandrasekhar, V.; Thomas, K. R. J. *Struct. Bond.* **1993**, *81*, 41.
19. Chandrasekhar, V.; Thomas, K. R. J. *Appl. Organomet. Chem.* **1993**, *7*, 1.
20. Chandrasekhar, V.; Muralidhara, M. G.; Selvaraj, I. I. *Heterocycles* **1990**, *31*, 2231.
21. Chandrasekhar, V.; Nagendran, S. *Chem. Soc. Rev.* **2001**, *30*, 193.
22. Allen, C. W. In "Organophosphorus Compounds" (Specialist Periodic Reports); Royal Society of Chemistry, London, 1986–1999.
23. Elias, A. J.; Shreeve, J. M. *Adv. Inorg. Chem.* **2001**, *52*, 335.
24. John, K.; Moeller, T. *Inorg. Synth.* **1963**, *7*, 76.
25. Krishnamurthy, S. S.; Rao, M. N. S.; Woods, M. *J. Inorg. Nucl. Chem.* **1979**, *41*, 1093.

26. Baceiredo, A.; Bertrand, G.; Majoral, J. P.; Sicard, G.; Jaud, J.; Galy, J. *J. Am. Chem. Soc.* **1984**, *106*, 6088.
27. Oakley, R. T.; Rettig, S. J.; Paddock, N. L.; Trotter, J. *J. Am. Chem. Soc.* **1985**, *107*, 6923.
28. Liebig, J. *Justus. Liebigs. Ann. Chem.* **1834**, *11*, 139.
29. Stokes, H. N. *Am. Chem. J.* **1895**, *17*, 275.
30. Stokes, H. N. *Ber.* **1895**, *28*, 437.
31. Stokes, H. N. *Am. Chem. J.* **1896**, *18*, 780.
32. Stokes, H. N. *Am. Chem. J.* **1897**, *19*, 782.
33. Thomas, K. R. J.; Chandrasekhar, V.; Pal, P.; Scott, S. R.; Hallford, R.; Cordes, A. W. *Inorg. Chem.* **1993**, *32*, 606.
34. Mark, J. E.; Allcock, H. R.; West, R. "Inorganic Polymers"; Prentice Hall, Englewood Cliffs, NJ, 1992.
35. Allcock, H. R.; Stinnett, S. J.; Tedder, J. B.; Adams, R. A. *U. S. Patent 4,656,017*, 1987.
36. Tanino, H.; Okamoto, T.; Ueyama, S.; Fujikawa, K.; Tsumiyama, T. *U.S. Patent 4,522, 689*, 1985.
37. Fekete, T. M.; Start, J. F. *U.S. Patent 4,046, 857*, 1977.
38. Emsley, J.; Udy, P. *J. Chem. Soc. A* **1970**, 3025.
39. Becke-Goehring, M.; Fluck, E. *Angew. Chem. Int. Ed. Engl.* **1962**, *1*, 281.
40. Allcock, H. R.; Crane, C. A.; Morrissey, C. T.; Olshavsky, M. A. *Inorg. Chem.* **1999**, *38*, 280.
41. Honeyman, C. H.; Manners, I.; Morissey, C. T.; Allcock, H. R. *J. Am. Chem. Soc.* **1995**, *117*, 7035.
42. Allcock, H. R.; Nelson, J. M.; Prange, R.; Crane, C. A.; de Denus, C. R. *Macromolecules* **1999**, *32*, 5736.
43. Montague, R. A.; Matyjaszewski, K. *J. Am. Chem. Soc.* **1990**, *112*, 6721.
44. Schmutzler, R. *Inorg. Synth.* **1967**, *9*, 75.
45. Allcock, H. R.; Harris, P. J. *Inorg. Chem.* **1981**, *20*, 2844.
46. Allcock, H. R.; Rutt, S. J.; Parvez, M. *Inorg. Chem.* **1991**, *30*, 1776.
47. Tesi, G.; Otto, R. J. A.; Sherif, F. G.; Audrieth, L. F. *J. Am. Chem. Soc.* **1960**, *82*, 528.
48. Walsh, E. J.; Derby, E.; Smegal, J. *Inorg. Chim. Acta* **1976**, *16*, L9.
49. Allcock, H. R.; Rutt, S. J.; Parvez, M. *J. Am. Chem. Soc.* **1986**, *108*, 6089.
50. Grundmann, C.; Ratz, R. *Z. Naturforsch.* **1955**, *10b*, 116.
51. Muller, U.; Schmock, F. *Z. Naturforsch.* **1980**, *35b*, 1529.
52. Roesky, H. W.; Banek, M. *Z. Naturforsch.* **1979**, *34b*, 752.
53. Sharts, C. M.; Bilbo, A. J.; Gentry, D. R. *Inorg. Chem.* **1966**, *5*, 2140.
54. Wilson, M.; Sanchez, M.; Labarre, J. *Inorg. Chim. Acta* **1987**, *136*, 53.
55. McIntosh, M. B.; Hartle, T. J.; Allcock, H. R. *J. Am. Chem. Soc.* **1999**, *121*, 884.
56. Allcock, H. R.; McIntosh, M. B.; Hartle, T. J. *Inorg. Chem.* **1999**, *38*, 5535.
57. Granier, M.; Bacieredo, A.; Dartiguenave, Y; Dartiguenave, M.; Menu, M.-J.; Bertrand, G. *J. Am. Chem. Soc.* **1990**, *112*, 6277.
58. Rolland, H.; Ocando-Mavarez, E.; Potin, P.; Majoral, J.-P.; Bertrand, G. *Inorg. Chem.* **1991**, *30*, 4095.
59. Fiestel, G. R.; Moeller, T. *J. Inorg. Nucl. Chem.* **1967**, *29*, 2731.
60. Fincham, J. K.; Hursthouse, M. B.; Parkes, H. G.; Shaw, L. S.; Shaw, R. A. *Acta Crystallogr. Sect. B* **1986**, *42*, 462.
61. Brian, Z.; Goldschmidt, J. M. E. *Synth. React. Inorg. Met. Org.* **1978**, *8*, 185.
62. Lehr, W.; *Z. Anorg. Chem.* **1967**, *352*, 27.
63. Das, R. N.; Shaw, R. A.; Smith, B. C.; Woods, M. *J. Chem. Soc., Dalton Trans.* **1973**, 709.

64. Allen, C. W.; Mackay, J. A. *Inorg. Chem.* **1986**, *25*, 4628.
65. Smarddijk, A. A.; De Ruiter B.; van der Huizen, A. A.; van de Grampel, J. C. *Recl. Trav. Chim. Pays-Bas* **1982**, *101*, 270.
66. Hasan, M.; Shaw, R. A.; Woods, M. *J. Chem. Soc., Dalton Trans.* **1975**, 2202.
67. Lingley, D. J.; Shaw, R. A.; Woods, M.; Krishnamurthy, S. S. *Phosphorus Sulfur* **1978**, *4*, 379.
68. Desai, V. B.; Shaw, R. A.; Smith, B. C. *J. Chem. Soc. A* **1970**, 2023.
69. Ganapathiappan, S.; Krishnamurthy, S. S. *J. Chem. Soc., Dalton Trans.* **1987**, 579.
70. Das, S. K.; Keat, R.; Shaw, R. A.; Smith, B. C. *J. Chem. Soc. A* **1965**, 5032.
71. Chandrasekhar, V.; Vivekanandan, K.; Nagendran, S.; Senthil Andavan, G. T.; Weathers, N. R.; Yarbrough, J. C.; Cordes, A. W. *Inorg. Chem.* **1998**, *37*, 6192.
72. Krause, W. E.; Parvez, M.; Visscher, K. B.; Allcock, H. R. *Inorg. Chem.* **1996**, *35*, 6337.
73. Goldschmidt, J. M. E.; Licht, E. *J. Chem. Soc. A* **1971**, 2429.
74. Keat, R.; Shaw, R. A. *J. Chem. Soc* . **1965**, 2215.
75. Green, B; Sowerby, D. B. *J. Inorg. Nucl. Chem. Lett.* **1971**, *33*, 3687.
76. Goldschmidt, J. M. E.; Sadeh, U. *J. Inorg. Nucl. Chem.* **1980**, *42*, 618.
77. Lingley, D. J.; Shaw, R. A.; Yu, H. S. *Inorg. Nucl. Chem. Lett.* **1980**, *16*, 219.
78. van der Huizen, A. A.; Jekel, A. P.; Rusch, J.; van de Grampel, J. C. *Recl. Trav. Chim. Pays-Bas* **1981**, *100*, 343.
79. van der Huizen, A. A.; van de Grampel, J. C.; Rusch, J. W.; Wilting, T.; Bolhius, F.; Meetsma, A. *J. Chem. Soc., Dalton Trans.* **1986**, 1317.
80. Keat, R.; Shaw, R. A. *J. Chem. Soc. A* **1966**, 908.
81. Brian, Z.; Goldschmidt, J. M. E. *J. Chem. Soc. Dalton Trans.* **1979**, 1017.
82. Krishnamurthy, S. S.; Sudheendra Rao, M. N. S.; Vasudeva Murthy, A. R.; Shaw, R. A. Woods; M. *Ind. J. Chem. Sect. A* **1976**, *14*, 823.
83. Ray, S. K.; Shaw, R. A. *J. Chem. Soc.* **1961**, 872.
84. Evans, T.; Allcock, H. R. *Inorg. Chem.* **1979**, *18*, 2342.
85. Krishnamurthy, S. S.; Rao, M. N. S.; Woods, M. *J. Inorg. Nucl. Chem.* **1979**, *41*, 1093.
86. Keat, R.; Shaw, R. A. *Angew. Chem. Int. Ed. Engl.* **1968**, *7*, 212.
87. Goldschmidt, J. M. E.; Licht, E. *J. Chem. Soc., Dalton Trans.* **1972**, 728.
88. Goldschmidt, J. M. E.; Licht, E. *J. Chem. Soc., Dalton Trans.* **1979**, 1012.
89. Krishnamurthy, S. S.; Sundaram, P. M. *J. Chem. Soc., Dalton Trans.* **1982**, 67.
90. Ganapathiappan, S.; Krishnamurthy, S. S. *J. Chem. Soc., Dalton Trans.* **1987**, 585.
91. Goldschmidt, J. M. E.; Goldstein, R. *J. Chem. Soc., Dalton Trans.* **1981**, 1283.
92. Katti, K. V.; Krishnamurthy, S. S. *J. Chem. Soc., Dalton Trans.* **1985**, 285.
93. Krishnamurthy, S. S.; Sundaram, P. M.; Woods, M. *Inorg. Chem.* **1982**, *21*, 406.
94. Millington, D.; Sowerby, D. B. *J. Chem. Soc., Dalton Trans.* **1972**, 2035.
95. Krishnamurthy, S. S.; Sau, A. C.; Vasudeva Murthy, A. R.; Keat, R.; Shaw, R. A.; Woods, M. *J. Chem. Soc., Dalton Trans.* **1976**, 1405.
96. Krishnamurthy, S. S.; Sau, A. C.; Vasudeva Murthy, A. R.; Keat, R.; Shaw, R. A.; Woods, M. *J. Chem. Soc., Dalton Trans.* **1977**, 1980.
97. Krishnamurthy, S. S.; Rao, M. N. S.; Vasudeva Murthy, A. R.; Shaw, R. A.; Woods, M. *Inorg. Chem.* **1978**, *17*, 1527.
98. Sau, A. C.; Dhathathreyan, K. S.; Narayanaswamy, P. Y.; Krishnamurthy, S. S. *Inorg. Synth.* **1989**, *25*, 15.
99. Krishnamurthy, S. S.; Sau, A. C.; Vasudeva Murthy, A. R.; Shaw, R. A.; Woods, M; Keat, R. *J. Chem. Res. (S)* **1977**, 70.
100. Cameron, T. S.; Mannan, K. H.; Krishnamurthy, S. S.; Sau, A. C.; Vasudeva Murthy, A. R.; Keat, R.; Shaw, R. A.; Woods, M. *Chem. Commun.* **1975**, 975.
101. Krishnamurthy, S. S.; Ramachandran, K.; Woods, M. *J. Chem. Res. (S)* **1979**, 92.

102. Krishnamurthy, S. S.; Ramachandran, K.; Sau, A. C.; Shaw, R. A.; Vasudeva Murthy, A. R.; Woods, M. *Inorg. Chem.* **1979**, *18*, 2010.
103. Krishnamurthy, S. S. *Main Group Chem. News* **1997**, 12.
104. Contractor, S. R.; Kilic, Z.; Shaw, R. A. *J. Chem. Soc., Dalton Trans.* **1987**, 2023.
105. Narayanaswamy, P. Y.; Dhathathreyan, K. S.; Krishnamurthy, S. S. *Inorg. Chem.* **1985**, *24*, 640.
106. Narasimhamurthy, S.; Thirupathi, N.; Murugavel, R.; Krishnamurthy, S. S. *Phosphorus, Sulfur, Silicon* **1994**, *93–94*, 221.
107. Allcock, H. R.; Gardener, J. E.; Smeltz, K. M. *Macromolecules* **1975**, *8*, 36.
108. Gabler, D. G.; Haw, J. F. *Inorg. Chem.* **1990**, *29*, 4018.
109. De Ruiter, B.; Winter, H.; Wilting, T.; van de Grampel, J. C. *J. Chem. Soc., Dalton Trans.* **1984**, 1027.
110. Dhathathreyan, K. S.; Krishnamurthy, S. S.; Vasudeva Murthy, A. R.; Cameron, T. S.; Chan, C.; Shaw, R. A.; Woods, M. *Chem. Commun.* **1980**, 231.
111. Bullen, G. J.; Dann, P. E.; Evans, M. L.; Hursthouse, M. B.; Shaw, R. A.; Wait, K.; Woods, M.; Yu, H. S. *Z. Naturforsch.* **1976**, *31b*, 995.
112. Parvez, M.; Kwon, S.; Allcock, H. R. *Acta Cryst.* **1991**, *47c*, 466.
113. Dhathathreyan, K. S.; Krishnamurthy, S. S.; Vasudevamurthy, A. R.; Shaw, R. A.; Woods, M. *J. Chem. Soc., Dalton Trans.* **1982**, 1549.
114. Ferrar, W. T.; DiStefano, F. V.; Allcock, H. R. *Macromolecules* **1980**, *13*, 1345.
115. Schmulz, J. L.; Allcock, H. R. *Inorg. Chem.* **1975**, *14*, 2433.
116. Ramachandran, K.; Allen, C. W. *Inorg. Chem.* **1983**, *22*, 1445.
117. Brown, D. E.; Allen, C. W. *Inorg. Chem.* **1987**, *26*, 934.
118. Dell, D.; Fitzsimmons, B. W.; Keat, R.; Shaw, R. *J. Chem. Soc. A* **1966**, 1680; McBee, E. T.; Okuhara, K.; Morton, C. *Inorg. Chem.* **1966**, *5*, 455.
119. Karthikeyan, S.; Krishnamurthy, S. S. *Z. Anorg. Allg. Chem.* **1984**, *513*, 231.
120. Dell, D.; Fitzsimmons, B. W.; Shaw, R. A. *J. Chem. Soc. A* **1965**, 4070.
121. Kumar, D.; Fohlen, G. M.; Parker, J. H. *J. Polym. Sci. Polym. Chem. Ed.* **1983**, *21*, 3155.
122. Dhathathreyan, K. S.; Krishnamurthy, S. S.; Woods, M. *J. Chem. Soc., Dalton Trans.* **1982**, 2151.
123. Allcock, H. R.; Ngo, D. C.; Parvez, M.; Visscher, K. *J. Chem. Soc., Dalton Trans.* **1992**, 1687.
124. Allcock, H. R.; Ngo, D. C.; Parvez, M.; Visscher, K. *Inorg. Chem.* **1994**, *33*, 2090.
125. Allcock, H. R.; Al-Shali, S.; Ngo, D. C.; Visscher, K.; Parvez, M. *J. Chem. Soc., Dalton Trans.* **1996**, 3549.
126. Bandoli, G.; Gleria, M.; Lombardo, G. M.; Pappalardo, G. C. *J. Chem. Soc., Dalton Trans.* **1995**, 1749.
127. Bandoli, G.; Casellato, U.; Gleria, M.; Graasi, A.; Montoneri, E.; Pappalardo, G. C. *J. Chem. Soc., Dalton Trans.* **1989**, 757.
128. Allcock, H. R.; Al-Shali, S.; Ngo, D. C.; Visscher, K.; Parvez, M. *J. Chem. Soc., Dalton Trans.* **1995**, 3521.
129. Allcock, H. R.; Fuller, T. J.; Matsumura, K. *J. Org. Chem.* **1981**, *46*, 13.
130. Kumaraswamy, K. C.; Krishnamurthy, S. S. *Inorg. Chem.* **1986**, *25*, 920.
131. Moriya, K.; Kawanishi, Y.; Yano, S.; Kajiwara, M. *Chem. Commun.* **2000**, 1111.
132. Dhathathreyan, K. S.; Krishnamurthy, S. S.; Vasudeva Murthy, A. R.; Shaw, R. A.; Woods, M. *J. Chem. Soc., Dalton Trans.* **1981**, 1928.
133. Fitzsimmons, B. W.; Hewlett, C.; Shaw, R. A. *J. Chem. Soc.* **1965**, 7432.
134. Karthikeyan, S.; Vyas, K.; Krishnamurthy, S. S.; Cameron, T. S.; Vincent, B. R. *J. Chem. Soc., Dalton Trans.* **1988**, 1371.
135. Karthikeyan, S.; Krishnamurthy, S. S. *J. Chem. Soc., Dalton Trans.* **1991**, 299.

136. Bezman, I. I.; Smalley, J. H. *Chem. Ind. (London)* **1963**, 163.
137. Herring, D. L.; Douglas, C. M. *Inorg. Chem.* **1964**, *3*, 428.
138. Witt, M.; Roesky, H. W. *Chem. Rev.* **1994**, *94*, 1163.
139. Schmulbach, C. D.; Derderian, C.; Zeck, O.; Sahuri, S. *Inorg. Chem.* **1971**, *10*, 195.
140. Neilson, R. H.; Wisian-Neilson, P. *Chem. Rev.* **1988**, *88*, 541.
141. McBee, E. T.; Okuhara, K.; Morton, C. J. *Inorg. Chem.* **1965**, *4*, 1672.
142. Harris, P. J.; Fadeley, C. L. *Inorg. Chem.* **1983**, *22*, 561.
143. Winter, H.; van de Grampel, J. C. *J. Chem. Soc., Dalton Trans.* **1986**, 1269.
144. Biddlestone, M.; Shaw, R. A. *J. Chem. Soc. A* **1969**, 178.
145. Biddlestone, M.; Shaw, R. A. *J. Chem. Soc., Dalton Trans.* **1975**, 2527.
146. Biddlestone, M.; Shaw, R. A.; Taylor, D. *Chem. Commun.* **1969**, 320.
147. Biddlestone, M.; Shaw, R. A. *Chem. Commun.* **1968**, 407.
148. Harris, P. J.; Desorcie, J. L.; Allcock, H. R. *Chem. Commun.* **1981**, 852.
149. Allcock, H. R.; Desorcie, J. L.; Harris, P. J. *J. Am. Chem. Soc.* **1983**, *105*, 2814.
150. Harris, P. J.; Williams, K. B.; Fisher, B. L. *J. Org. Chem.* **1984**, *49*, 406.
151. Allcock, H. R.; Brennan, D. J.; Graaskamp, J. M.; Parvez, M. *Organometallics* **1986**, *5*, 2434.
152. Allcock, H. R.; Desorcie, J. L.; Wagner, L. J. *Inorg. Chem.* **1985**, *24*, 333.
153. Biddlestone, M.; Shaw, R. A. *Chem. Commun.* **1965**, 205.
154. Biddlestone, M.; Shaw, R. A. *J. Chem. Soc. A* **1970**, 1750.
155. Harris, P. J.; Allcock, H. R. *J. Am. Chem. Soc.* **1978**, *100*, 6512.
156. Allcock, H. R.; Harris, P. J. *J. Am. Chem. Soc.* **1979**, *101*, 6221.
157. Allcock, H. R.; Harris, P. J. *Inorg. Chem.* **1981**, *20*, 2844.
158. Allcock, H. R.; Harris, P. J. *Chem. Commun.* **1979**, 714.
159. Allcock, H. R.; Harris, P. J.; Connolly, M. S. *Inorg. Chem.* **1981**, *20*, 11.
160. Harris, P. J.; Schwalke, M. A.; Liu, V.; Fisher, B. L. *Inorg. Chem.* **1983**, *22*, 1812.
161. Allcock, H. R.; Harris, P. J.; Nissan, R. A. *J. Am. Chem. Soc.* **1981**, *103*, 2256.
162. Buwalda, P. L.; Steenberger, A.; Oosting, G. E.; van de Grampel, J. C. *Inorg. Chem.* **1990**, *29*, 2658.
163. Allcock, H. R.; Connolly, M. S.; Whittle, R. R. *Organometallics* **1983**, *2*, 1514.
164. Schmidpeter, A.; Ebeling, J. *Angew. Chem. Int. Ed. Engl.* **1968**, *7*, 209.
165. Schmidpeter, A.; Ebeling, J.; Stray, H.; Weingand, C. *Z. Anorg. Allg. Chem.* **1972**, *394*, 171.
166. Bermann, M.; van Wazer, J. R. *Inorg. Chem.* **1972**, *11*, 209.
167. Schick, G.; Raab, M.; Gudat, D.; Nieger, M.; Niecke, E. *Angew. Chem. Int. Ed. Engl.* **1998**, *37*, 2390.
168. Jackson, L. A.; Harris, P. J. *Inorg. Chem.* **1988**, *27*, 4338.
169. Krishnamurthy, S. S.; Ramachandran, K.; Vasudeva Murthy, A. R.; Shaw, R. A.; Woods, M. *J. Chem. Soc., Dalton Trans.* **1980**, 840.
170. Chandrasekhar, V.; Krishnamurthy, S. S.; Manohar, H.; Vasudeva Murthy, A. R.; Shaw, R. A.; Woods, M. *J. Chem. Soc., Dalton Trans.* **1984**, 621.
171. Chandrasekhar, V.; Krishnamurthy, S. S.; Vasudeva Murthy, A. R.; Shaw, R. A.; Woods, M. *Inorg. Nucl. Chem. Lett.* **1981**, *17*, 181.
172. Chandrasekhar, V.; Reddy, N. S. *Heterocycles* **1989**, *28*, 611.
173. Ruiter, B. D.; Kuipers, G.; Bijlaart, J. H.; van de Grampel, J. C. *Z. Naturforsch.* **1982**, *37b*, 1425.
174. Sampath Kumar, E.; Muralidhara, M. G.; Chandrasekhar, V. *Polyhedron* **1995**, *14*, 1571.
175. Deutsch, W. F.; Shaw, R. A. *J. Chem. Soc., Dalton Trans.* **1988**, 1757.
176. Allcock, H. R.; Diefenbach, U.; Pucher, S. R. *Inorg. Chem.* **1994**, *33*, 3091.

177. Alkubaisi, A. H.; Parkes, H. G.; Shaw, R. A. *Heterocycles* **1989**, *28*, 347.
178. Contractor, S. R.; Hursthouse, M. B.; Parkes, H. G.; Shaw, L. S.; Shaw, R. A.; Yilmaz, H. *Chem. Commun.* **1984**, 675.
179. Muralidhara, M. G.; Grover, N.; Chandrasekhar, V. *Polyhedron* **1993**, *12*, 1509.
180. Allcock, H. R.; Kugel, R. L. *Inorg. Chem.* **1966**, *5*, 1016.
181. Brandt, K.; Jedlinski, Z. *J. Org. Chem.* **1980**, *45*, 1672.
182. Kumara Swamy, K. C.; Krishnamurthy, S. S. *Ind. J. Chem.* **1984**, *23A*, 717.
183. Brandt, K.; Kupka, T.; Drodz, J.; van de Grampel, J. C.; Meetsma, A.; Jekel, A. P. *Inorg. Chim. Acta* **1995**, *228*, 187; Brandt, K.; Porwolik, I.; Kupka, T.; Olejnik, A.; Shaw, R. A.; Davies, D. B. *J. Org. Chem.* **1995**, *60*, 7433.
184. Engelhardt, U.; Diefenbach, U. *Z. Naturforsch.* **1990**, *44B*, 612.
185. Engelhardt, U.; Diefenbach, U.; Damerius, R. *Z. Naturforsch.* **1990**, *45B*, 457.
186. Diefenbach, U.; Engelhardt, U. *Z. Anorg. Allg. Chem.* **1992**, *609*, 67.
187. Castera, P.; Faucher, J.-F.; Labarre, J.-F.; Perly, B. *J. Mol. Struct.* **1987**, *160*, 365.
188. Harris, P. J.; Williams, K. B. *Inorg. Chem.* **1984**, *23*, 1496.
189. Allcock, H. R.; Turner, M. L.; Visscher, K. B. *Inorg. Chem.* **1992**, *31*, 4354.
190. Allcock, H. R.; Walsh, E. J. *Inorg. Chem.* **1971**, *10*, 1643.
191. Primrose, A. P.; Parvez, M.; Allcock, H. R. *Macromolecules* **1997**, *30*, 670.
192. Allcock, H. R.; Kugel, R. L.; Moore, G. Y. *Inorg. Chem.* **1975**, *14*, 2831.
193. Brandt, K.; Porwolik, I.; Olejnik, A.; Shaw, R. A.; Davies, D. B.; Hursthouse, M. B.; Sykara, G. D. *J. Am. Chem. Soc.* **1996**, *118*, 4496.
194. Brandt, K.; Porwolik-Czomperlik, I.; Siwy, M.; Kupka, T.; Shaw, R. A.; Davies, D. B.; Hursthouse, M. B.; Sykara, G. D. *J. Am. Chem. Soc.* **1997**, *119*, 12432.
195. Brandt, K.; Porwolik, I.; Siwy, M.; Kupka, T.; Shaw, R. A.; Davies, D. B.; Hursthouse, M. B.; Sykara, G. D. *J. Am. Chem. Soc.* **1997**, *119*, 1143.
196. Chandrasekhar, V.; Karthikeyan, S.; Krishnamurthy, S. S.; Woods, M. *Ind. J. Chem.* **1985**, *24A*, 379.
197. Alkubaisi, A. H.; Shaw, R. A. *Phosphorus, Sulfur, Silicon* **1989**. *45*, 7.
198. Chivers, T.; Hedgeland, R. *Can. J. Chem.* **1972**, *50*, 1017.
199. Kumaraswamy, S.; Vijjulatha, M.; Muthaiah, C.; Kumara Swamy, K. C.; Engelhardt, U. *J. Chem. Soc., Dalton Trans.* **1999**, 891.
200. Herberhold, M.; Hofmann, A.; Milius, W. *Z. Anorg. Allg. Chem.* **1997**, *623*, 545.
201. Schneider, R.; Köllner, C.; Weber, I.; Togni, A. *Chem. Commun.* **1999**, 2415.
202. Galliot, C.; Prévoté, Caminade, A.-M.; Majoral, J.-P. *J. Am. Chem. Soc.* **1995**, *117*, 5470.
203. Slany, M.; Bardajì, M.; Casanove, M.-J.; Caminade, A.-M.; Majoral, J.-P.; Chandret, B. *J. Am. Chem. Soc.* **1995**, *117*, 9764.
204. Galliot, C.; Larré, C.; Caminade, A.-M.; Majoral, J.-P. *Science* **1997**, *277*, 1981.
205. Sournies, F.; Crasnier, F.; Graffeuil, M.; Faucher, J.-P.; Lahana, R.; Labarre, M.-C.; Labarre, J.-F. *Angew. Chem. Int. Ed. Engl.* **1995**, *34*, 578.
206. Inoue, K.; Sakai, H.; Ochi, S.; Itaya, T.; Tanigaki, T. *J. Am. Chem. Soc.* **1994**, *116*, 10783.
207. Allcock, H. R.; Bissel, E. C.; Shawl, L. J. *Inorg. Chem.* **1973**, *12*, 2963.
208. MacDonald, A. L.; Trotter, J. *Can. J. Chem.* **1974**, *52*, 734.
209. Calhoun, H. P.; Paddock, N. L.; Trotter, J. *J. Chem. Soc., Dalton Trans.* **1973**, 2708.
210. O'Brien, J. P.; Allen, R. W.; Allcock, H. R. *Inorg. Chem.* **1979**, *18*, 2230.
211. Trotter, J.; Whitlow, S. H. *J. Chem. Soc. A* **1970**, 460.
212. Trotter, J.; Whitlow, S. H. *J. Chem. Soc. A* **1970**, 455.
213. Allcock, H. R.; Allen, R. W.; O'Brien, J. P. *J. Am. Chem. Soc.* **1977**, *99*, 3984.
214. Allen, R. W.; O'Brien, J. P.; Allcock, H. R. *J. Am. Chem. Soc.* **1977**, *99*, 3987.

215. Calhoun, H. P.; Trotter, J. *J. Chem. Soc., Dalton Trans.* **1974**, 382.
216. Paddock, N. L.; Ranganathan, T. N.; Wingfield, J. N. *J. Chem. Soc., Dalton Trans.* **1972**, 1578.
217. Paddock, N. L.; Ranganathan, T. N.; Rettig, S. J.; Sharma, R.; Trotter, J. *Can. J. Chem.* **1981**, *59*, 2429.
218. Calhoun, H. P.; Paddock, N. L.; Wingfield, J. N. *Can. J. Chem.* **1975**, *53*, 1765.
219. Marsh, W. C.; Trotter, J. *J. Chem. Soc. A* **1971**, 1482.
220. Harrison, W.; Trotter, J. *J. Chem. Soc., Dalton Trans.* **1973**, 61.
221. Gallicano, K. D.; Paddock, N. L.; Rettig, S. J.; Trotter, J. *Can. J. Chem.* **1981**, *59*, 2435.
222. Schmidpeter, A.; Blanck, K.; Hess, H.; Riffel, H. *Angew. Chem. Int. Ed. Engl.* **1980**, *19*, 650.
223. Allcock, H. R.; Suszko, P. R.; Wagner, L. J.; Whittle, R. R.; Boso, B. *J. Am. Chem. Soc.* **1984**, *106*, 4966.
224. Allcock, H. R.; Nissan, R. A.; Harris, P. J.; Whittle, R. R. *Organometallics* **1984**, *3*, 432.
225. Allcock, H. R.; Manners, I.; Mang, M. N.; Parvez, M. *Inorg. Chem.* **1990**, *29*, 522.
226. Allcock, H. R.; Lavin, K. D.; Tollefson, N. M.; Evans, T. L. *Organometallics* **1983**, *2*, 267.
227. Allcock, H. R.; Scopelianos, A. G.; Whittle, R. R.; Tollefson, N. M. *J. Am. Chem. Soc.* **1983**, *105*, 1316.
228. Gallicano, K. D.; Paddock, N. L. *Can. J. Chem.* **1982**, *60*, 521.
229. Thomas, K. R. J.; Chandrasekhar, V.; Pal, P. S.; Scott, R.; Hallford, R.; Cordes, A. W. *Inorg. Chem.* **1993**, *32*, 606.
230. Thomas, K. R. J.; Tharmaraj, P.; Chandrasekhar, V.; Bryan, C. D.; Cordes, A. W. *Inorg. Chem.* **1994**, *33*, 5382.
231. Thomas, K. R. J.; Chandrasekhar, V.; Vivekanandan, K.; Senthil Andavan, G. T.; Nagendran, S.; Kingsley, S.; Tiekink, E. R. T. *Inorg. Chim. Acta* **1999**, *286*, 127.
232. Chandrasekaran, A.; Krishnamurthy, S. S.; Nethaji, M. *Inorg. Chem.* **1993**, *32*, 6102.
233. Chandrasekaran, A.; Krishnamurthy, S. S.; Nethaji, M. *J. Chem. Soc., Dalton Trans.* **1994**, 63.
234. Chandrasekhar, V.; Athimoolam, A. P.; Vivekanandan, K.; Nagendran, S. *Tetrahedron Lett.* **1999**, *40*, 1185.
235. Thomas, K. R. J.; Chandrasekhar, V.; Zanello, P.; Laschi, P. *Polyhedron* **1997**, *16*, 1003.
236. Koo, B. H.; Byun, Y.; Hong, E.; Kim, Y.; Do, Y. *Chem. Commun.* **1998**, 1227.
237. Thomas, K. R. J.; Chandrasekhar, V.; Pal, P. S.; Scott, R.; Hallford, R.; Cordes, A. W. *J. Chem. Soc., Dalton Trans.* **1993**, 2589.
238. Byun, Y.; Min, D.; Do, J.; Yun, H.; Do, Y. *Inorg. Chem.* **1996**, *35*, 3981.
239. Thomas, K. R. J.; Chandrasekhar, V.; Bryan, C. D.; Cordes, A. W. *J. Coord. Chem.* **1995**, *35*, 337.
240. Thomas, K. R. J.; Tharmaraj, P.; Chandrasekhar, V.; Tiekink, E. R. T. *J. Chem. Soc., Dalton Trans.* **1994**, 1301.
241. Thomas, K. R. J.; Tharmaraj, P.; Chandrasekhar, V.; Scott. S. R.; Cordes, A. W. *Polyhedron* **1995**, *14*, 977.
242. Thomas, K. R. J.; Chandrasekhar, V.; Scott. S. R.; Cordes, A. W. *Polyhedron* **1995**, *14*, 1607.
243. Carriedo, G. A.; Elipe, P. G.; Alonso, F. J. G.; Fernández-Catuxo, L.; Díaz, M. R.; Granda, G. *J. Organomet. Chem.* **1995**, *498*, 207.
244. Jung, O. S.; Kim, Y. T.; Lee, Y.-A.; Kim, Y. J.; Chae, H. K. *Inorg. Chem.* **1999**, *38*, 5457.
245. Diefenbach, U.; Kretschmann, M.; Stromburg, B. *Chem. Ber.* **1996**, *129*, 1573.
246. Díaz, C.; Izquierdo, G. *Polyhedron* **1999**, *18*, 1479.

247. Chandrasekaran, A.; Krishnamurthy, S. S.; Nethaji, M. *Inorg. Chem.* **1994**, *33*, 3085.
248. Ainscough, E. W.; Brodie, A. M.; Depree, C. V. *J. Chem. Soc., Dalton Trans.* **1999**, 4123.
249. Steiner, A.; Wright, D. S. *Angew. Chem. Int. Ed. Engl.* **1996**, *35*, 636.
250. Lawson, G. T.; Rivals, F.; Tascher, M.; Jacob, C.; Bickley, J. F.; Steiner, A. *Chem. Commun.* **2000**, 341.
251. Steiner, A.; Wright, D. S. *Chem. Commun.* **1997**, 283.
252. Lawson, G. T.; Jacob, C.; Steiner, A. *Eur. J. Inorg. Chem.* **1999**, 1881.

SELF-ASSEMBLY OF PORPHYRIN ARRAYS

LAURA BALDINI* and CHRISTOPHER A. HUNTER†

*Dipartimento di Chimica Organica e Industriale, Università degli Studi di Parma, Parco Area delle Scienze, 17/A, 43100 Parma, Italy

†Centre for Chemical Biology, Krebs Institute for Biomolecular Science, Department of Chemistry, University of Sheffield, Sheffield S3 7HF, United Kingdom

I. Introduction

The rich photochemical and redox properties of porphyrins make them attractive targets for the assembly of oligomeric and polymeric arrays that may exhibit novel photonic or electronic properties. Energy and electron transfer reactions within chromophore arrays have been exploited by Nature to sustain life through the complex process of photosynthesis. Attempts to artificially reproduce this process have been directed to the synthesis of simple models able to mimic components of the natural systems, with the aim of better understanding the light harvesting systems and reaction centers and of using this understanding to construct artificial devices to capture, store and transfer solar energy. The interest in constructing multi-porphyrin systems is therefore shared by a number of scientists working in different fields ranging from biology to material science. The ultimate goal is to achieve complete control over the spatial disposition and orientation

0898-8838/02 $35.00

of the chromophores within the array and thereby regulate any photo-induced energy or electron transfer properties.

Self-assembly of complementary subunits via non-covalent interactions such as hydrogen-bonding or metal–ligand interactions is an attractive synthetic approach to the controlled oligomerization of monomers to form large supramolecular architectures (*1,2*). By a judicious choice of components, complex well-defined chromophore arrays can be constructed in a single step (*3,4*). Chemists have taken inspiration from Nature in designing subunits able to self-associate to form higher order assemblies via weak interactions, trying to emulate the high specificity of protein folding, formation of the DNA double helix, and cellular recognition processes. The key to self-assembly is the ability to manipulate the process of molecular recognition: subunits which display complementarity in their geometry and functionality spontaneously aggregate, forming supramolecular structures, when mixed under appropriate conditions. The instructions for the assembly process are contained in the stereochemical features of the building blocks. The use of weak reversible interactions means that the process is under thermodynamic control, and the final structure is obtained by equilibration to a global energy minimum: dynamic assembly and disassembly of the system allows proof-reading and error checking. In order to generate stable assemblies using this approach, many weak binding interactions are generally required to overcome the entropy losses associated with the organization of multiple components into a single supramolecular structure. To maximize the stability of the assembly, losses in conformational entropy must be minimized, and therefore rigid preorganized subunits are generally desirable (*5*).

Many different interactions have been exploited in self-assembly (*4*), such as hydrogen-bonding, metal–ligand, hydrophobic, and van der Waals interactions. Hydrogen-bonding and metal–ligand, interactions afford the best control over the directionality of the resulting bond and therefore the geometry of the final assembly. Metal–ligand interactions are particularly attractive, since varying the metal and donor atoms offers a wide range of thermodynamic bond strength, kinetic lability, geometry, and stoichiometry of interaction.

Self-assembled structures can be *closed* if all the potential binding sites are utilized, or *open* if they are not. Closed assemblies have a definite geometry and stoichiometry, while open assemblies exist as mixtures of oligomers or polymers of varying stoichiometry. In addition, the self-assembled structure can be classified as *cooperative* if the multiple binding interactions reinforce each other to yield enhanced stability, or *trivial* if the binding interactions do not cooperate in the

assembly process. Examples of the four classes of assembly are illustrated in Scheme 1.

The stability of a trivial assembly is simply determined by the thermodynamic properties of the discrete intermolecular binding interactions involved. Cooperative assembly processes involve an intramolecular cyclization, and this leads to an enhanced thermodynamic stability compared with the trivial analogs. The increase in stability is quantified by the parameter EM, the effective molarity of the intramolecular process, as first introduced in the study of intramolecular covalent cyclization reactions (*6,7*). EM is defined as the ratio of the binding constant of the intramolecular interaction to the binding constant of the corresponding intermolecular interaction (Scheme 2). The former can be determined by measuring the stability of the self-assembled structure, and the latter value is determined using simple monofunctional reference compounds.

The value of EM for a cooperative self-assembled structure provides a measure of the monomer concentration at which trivial polymeric structures start to compete, and therefore EM represents the upper limit of the concentration range within which the cooperative structure is stable (Scheme 2). The lower limit of this range is called the critical self-assembly concentration (csac) and is determined by the stoichiometry of the assembly and the strength of the non-covalent binding interactions: weaker interactions and larger numbers of components raise the csac and narrow the stability window of the assembly (*8*). Theoretical treatments of the thermodynamics of the self-assembly process have been reported by Hunter (*8*), Sanders (*9*), and Mandolini (*10*). The value of EM is lowered by enthalpic contributions associated with

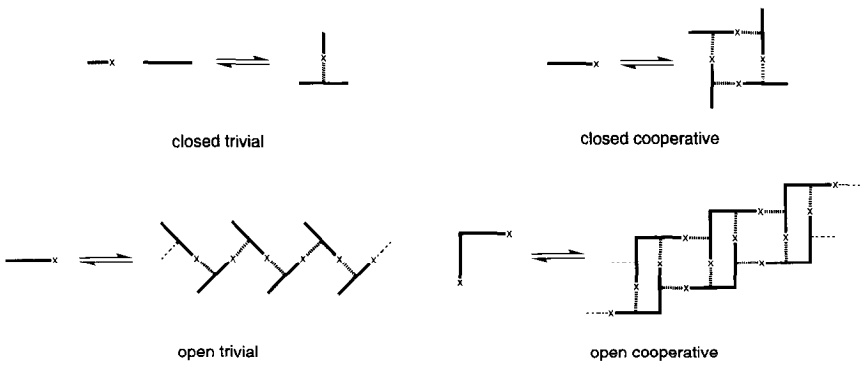

SCHEME 1

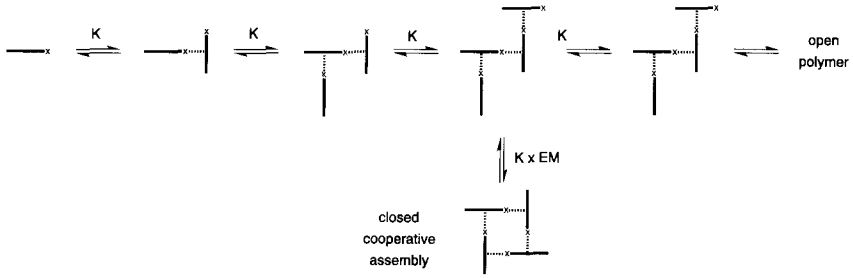

SCHEME 2

unfavorable strain energy upon ring closure and entropic contributions associated with losses of conformational degrees of freedom in flexible systems. Thus, in order to achieve the highest EM, the monomers must be carefully designed to achieve high complementarity (thus forming strainless rings) and rigidity (to minimize the loss of conformational entropy); i.e., the degree of preorganization determines EM.

The characterization of self-assembled structures is a much more challenging task than the identification of covalent reaction products. Self-assembly processes are reversible, and the products by their very nature are kinetically labile and sensitive to changes in environment. Thus changes in concentration may alter the balance in the equilibrium between different possible self-assembled structures. For example, a system which has a low EM will form only a closed cooperative structure in dilute solution and is likely to form open trivial polymers in the solid state. Thus, although X-ray diffraction can be used whenever a single crystal is available, the result may not be representative of the equilibria present in solution. Invasive techniques such as mass spectrometry perturb the equilibria by changing the environment and so may not provide an accurate picture of the species that are present in solution. In general, a range of different techniques must be applied to build up evidence for the structures of self-assembled complexes in solution, and the most useful methods vary from one system to another. Titrations give information on the stability of the complex and can distinguish between cooperative and trivial structures. Structural information is available from NMR and optical spectroscopy, although the high symmetry of self-assembled multi-component structures often precludes detailed structure determination by these methods. An assessment of molecular weight and hence the stoichiometry of the assembly is therefore crucial. FAB (*11,12*), ESI (*13*) and MALDI–TOF (*14,15*) mass spectrometry have been successfully used to detect the presence

of assemblies in the gas phase. Vapor pressure osmometry is a useful non-invasive technique for determining the approximate molecular weight in solution (*16*). Gel permeation chromatography and pulse gradient spin echo ^{1}H NMR experiments have also been used to determine molecular weights in solution (*17*).

Porphyrins represent ideal building blocks for the synthesis of oligomeric and polymeric arrays via the self-assembly technique. They are rigid, can easily be functionalized, and a number of different metals can be inserted in the center of the macrocycle. The central metal of the porphyrin is coordinated to four nitrogens and can accept either one or two additional apical donor atoms to give a square pyramidal or octahedral coordination sphere respectively. In recent years, a number of self-assembled porphyrin arrays have been reported, held together by either hydrogen–bonding or metal–ligand coordination interactions. It is only the latter type of assembly that we will deal with here, focusing on coordination oligomers where the key oligomerization interactions involve ligand binding to the central metal of a metalloporphyrin. Porphyrin coordination assemblies where the oligomerization interaction involves a peripheral ligand on the porphyrin coordinated to an external metal ion have also been prepared, but systems of this type will not be discussed here (*2*).

II. Trivial Closed Assemblies

A. Porphyrins as Ligands

The simplest way in which two porphyrins can interact to generate a self-assembled dimeric structure requires the presence of a donor group on the periphery of one component which coordinates to the metal center of the other. In order to generate exclusively a 1:1 complex, there should be no other ligand binding sites, and the central metal must accept only one ligand in the axial position. This is possible when the metal is 5-coordinate (e.g., zinc), or if the 6th position of a 6-coordinate metal is occupied by a kinetically inert ligand (e.g., Ru(II) coordinated to CO). The geometry of the assembly is determined by the ligand, namely the orientation of the donating electron pair with respect to the porphyrin ring.

A number of dimers featuring an orthogonal disposition of the porphyrin planes have been prepared. The perpendicular geometry is achieved using a 4-pyridyl unit linked through the porphyrin *meso* posi-

tion. Fleischer and Shachter (*18*) and Li and Xu (*19*) reported the formation of perpendicular dimers (**1**) upon coordination of a 4-pyridyl porphyrin to a zinc porphyrin (Fig. 1). Both assemblies were characterized by ^{1}H NMR spectroscopy: the pyridyl protons are upfield shifted as a result of the shielding effect due to the large ring current created by the zinc porphyrin π-system. The association constants, though not determined, are expected to be of the order of $10^3\ M^{-1}$ and are too small for complexation to be investigated using UV–Vis absorption spectroscopy. Using time-resolved fluorescence experiments, Li and Xu determined an inter-porphyrin singlet state energy transfer in the dimer with a rate constant of $1.1 \times 10^{10}\ s^{-1}$. They also obtained a crystal structure for zinc(II) tetraphenylporphyrin coordinated to copper(II) meso-5-(4-pyridyl)-octamethylporphyrin (**2**) which showed a distorted perpendicular geometry for the dimer.

Imamura (*11,20,21*) synthesized several similar perpendicular dimers exploiting axial coordination of the 4-pyridyl free-base porphyrin to Ru(II)CO (**3**) and Os(II)CO (**4**) porphyrins (Fig. 1). The pyridine–ruthenium and pyridine–osmium interactions are much stronger than the pyridine–zinc interaction, and the complexes are perfectly stable in solution and can be isolated by precipitation. One of the ruthenium dimers was characterized by FAB–MS (*11*). Complexation is accompanied by characteristic changes in ^{1}H NMR chemical shift, indicating

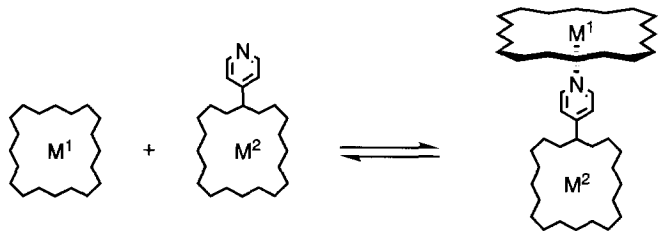

(1) M^1 = Zn
M^2 = 2H

(2) M^1 = Zn
M^2 = Cu

(3) M^1 = Ru(CO)
M^2 = 2H, Zn

(4) M^1 = Os(CO)
M^2 = 2H

FIG. 1. Trivial closed dimers assembled from 4-pyridyl porphyrins.

binding of the pyridine ligands to the ruthenium centers: typically, upfield shifts of 7 ppm and 2 ppm are observed for the α and β pyridyl protons respectively. The shielding effects on the free-base porphyrin NH protons were large enough for tautomerism to be observed directly at low temperature and an activation energy E_a to be measured as 40.5 kJ mol^{-1} for the exchange process (*21*). For all of the complexes, the UV–Vis absorption spectra are essentially the sum of the respective monomer absorptions, and cyclic voltammetry has confirmed that there is no electrochemical communication between the porphyrin subunits: they are reduced and oxidized independently (*20,21*). This behavior was attributed to the perpendicular arrangement of the chromophores which prevents interaction of the π-systems. An X-ray crystal structure of one of the ruthenium dimers shows that, in the solid state, the geometry of the assembly deviates from the perpendicular arrangement in a manner similar to that observed for the zinc complex, and this is attributed to crystal-packing effects (*20*).

If more than one 4-pyridine moiety is introduced in the *meso* positions of the free-base porphyrin, it is possible to obtain self-assembled trimers, tetramers, and pentamers with the same perpendicular arrangement of the porphyrins. Fleischer and Schachter (*18*) used pyridine–zinc interactions to assemble two different trimers in solution (**5**, Fig. 2a and **6**, Fig. 2b), while Imamura (*11,20,21*) and Alessio (*22*) synthesized a number of perpendicular ruthenium and osmium oligomers (**7** (*11,20,21*), Fig 2a; **8** (*21*), Fig. 2b; **9** (*21*), Fig. 2c; **10** (*21*), and **11** (*22*), Fig. 2d). The chemical shift of the ^{1}H NMR signal due to the free-base porphyrin NH protons provides a diagnostic tool for determining the stoichiometry of these complexes, because the ring current effects of the metalloporphyrins are additive, and the NH signal is shifted upfield by about 0.5 ppm by each coordinated metalloporphyrin (*21*). All these complexes exhibit the same stability, UV–Vis absorption, and redox properties as the corresponding dimers. The separation of the π-systems is too large for any strong inter-chromophore interactions.

To substitute the strongly bound axial CO ligand of the ruthenium or osmium center, it is necessary to employ more drastic conditions than simple stirring at room temperature. Imamura (*11,20*) used photolysis to synthesize porphyrin trimers on the basis of simultaneous coordination of two 4-pyridyl porphyrins to the same ruthenium porphyrin (**12**, Fig. 3). Some interesting photophysical behavior was observed for these systems. The trimers have an extra UV–Vis absorption band at about 450 nm which is ascribed to metal–ligand charge transfer (MLCT), a $d\pi(Ru(II))$–$\pi^*(OEP)$ transition. This band shows a bathochromic shift in more polar solvents, and decreased in intensity when

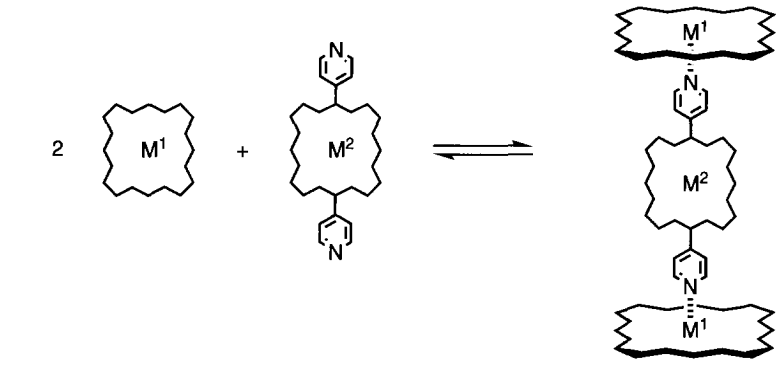

(5) M^1 = Zn
M^2 = 2H

(a)

(7) M^1 = Ru(CO), Os(CO)
M^2 = 2H

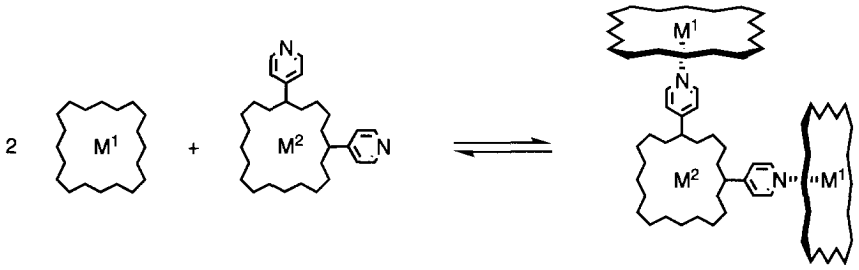

(6) M^1 = Zn
M^2 = 2H

(b)

(8) M^1 = Os(CO)
M^2 = 2H

FIG. 2. Trivial closed trimers (a,b), tetramers (c), and pentamers (d) assembled on multidentate 4-pyridyl porphyrin ligands.

an oxidizing agent was added to convert Ru(II) to Ru(III). Cyclic voltammetry showed that the redox potentials of the axial free-base porphyrins are not changed by coordination to ruthenium.

The geometry of the assembly can be altered by using a 3-pyridyl substituent on the porphyrin periphery. The donor nitrogen atom is oriented at an angle with respect to the porphyrin plane, and this has been exploited in the assembly of oblique dimeric, trimeric, and pentameric structures from free base mono- (**13** (*12*) and **14** (*23*), Fig 4a), bis-

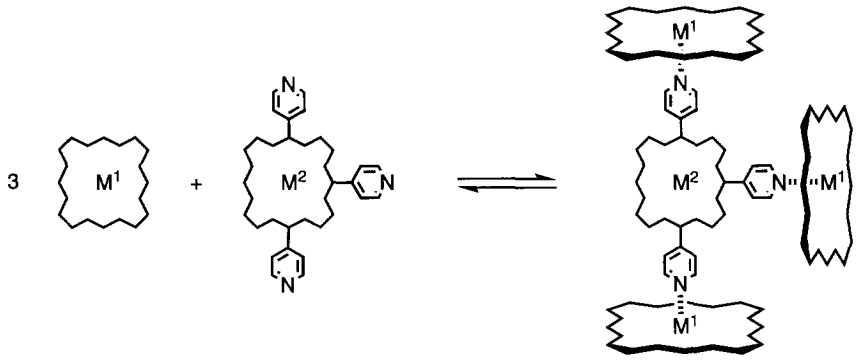

(c)

(9) M^1 = Os(CO)
M^2 = 2H

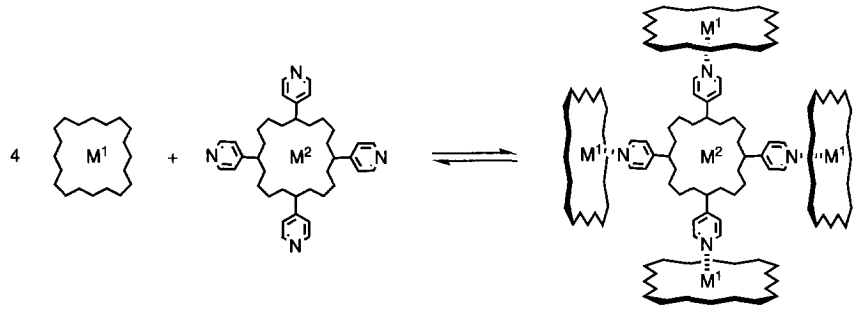

(d)

(10) M^1 = Os(CO)
M^2 = 2H
(11) M^1 = Ru(CO)
M^2 = 2H, Zn

(**15** (*12*), Fig. 4b), or tetrapyridyl porphyrins (**16** (*24*), Fig. 4c) coordinated to the metal centers of Ru(II)CO and Os(II)CO porphyrins (*24*). In the ^{1}H NMR spectrum there is a complexation-induced upfield shift of 0.3 ppm for the metalloporphyrin alkyl substituents, confirming the oblique geometry (in the perpendicular analog these protons were unaffected by assembly, because they do not sit over the face of the free-base porphyrin ligand) (*12*). Alessio (*23*) reported the X-ray crystal structure of the dimer **14**, and the angle between the mean planes of the two porphyrins is 43°. Substitution at the 3-position of the pyridine gives rise to atropisomers, and these can be observed in slow exchange in the ^{1}H NMR spectrum of the trimer **15** (Fig. 4b): the ratio of the $\alpha\alpha$ and

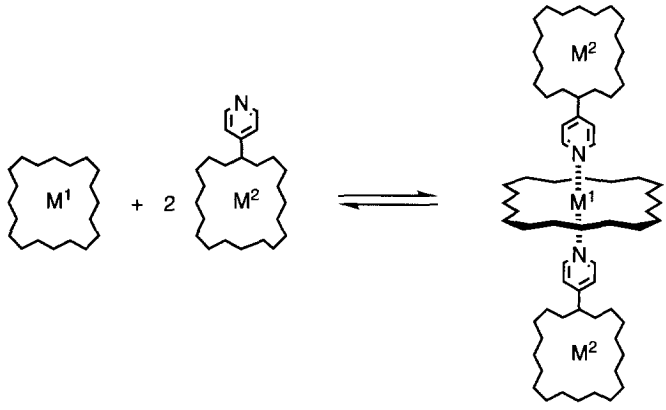

(12) M^1 = Ru
M^2 = 2H, Zn

FIG. 3. A trivial closed trimer assembled on a six-coordinate metalloporphyrin.

$\alpha\beta$ forms is approximately 2:3 (*12*). In the X-ray crystal structure of the pentameric array **16** (Fig. 4c), only the $\alpha\beta\alpha\beta$ atropisomer is observed (*24*). The properties of these systems are very similar to those of the perpendicular structures, and there is no evidence of any interaction between the chromophores. The UV–Vis absorption spectra do not differ from the sum of the individual components, and the redox behavior of the dimer **13** shows that the two components have independent elec-

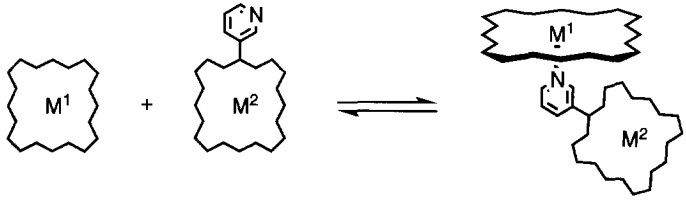

(13) M^1 = Os(CO)
M^2 = 2H

(a)

(14) M^1 = Ru(CO)
M^2 = 2H, Zn

FIG. 4. Trivial closed dimers (a), trimers (b), and pentamer (c) assembled from 3-pyridyl porphyrins.

(b)

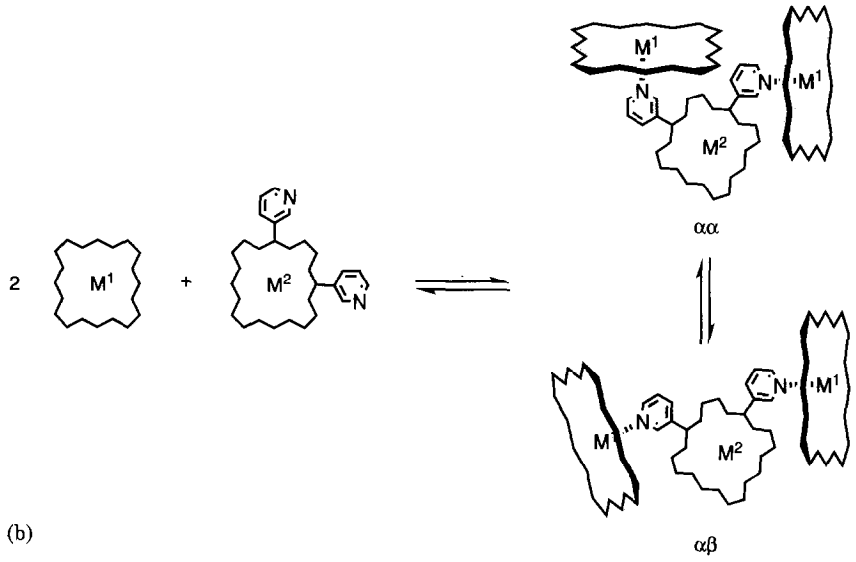

(15) M^1 = Os(CO)
M^2 = 2H

(c)

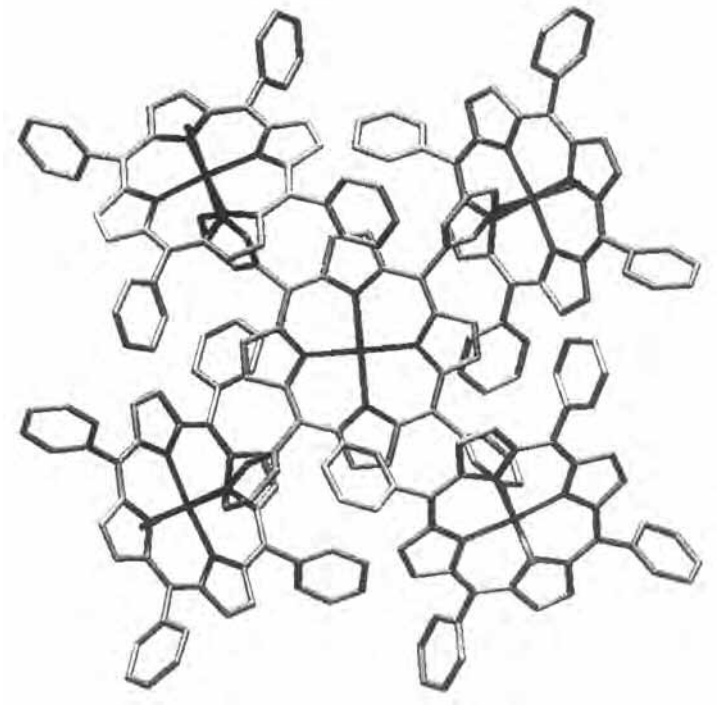

trochemical properties. An extensive study of the photophysical behavior of the dimeric and pentameric porphyrin assemblies was carried out by Prodi (*25*).

Sanders (*14*) has exploited the strong and selective coordination of phosphine donor groups to Ru(II) to construct hetero-dimetallic porphyrin dimers (**17**, Fig. 5). An alkyne–phosphine moiety introduced on the periphery of a free base or metalloporphyrin (M = Zn or Ni) spontaneously coordinates to a Ru(II)(CO) porphyrin when the two porphyrins are mixed in a 1:1 ratio. Coordination is characterized by a downfield shift of the ^{31}P resonance ($\Delta\delta^{31}P = 19$ ppm). There is no evidence of self-coordination of the zinc porphyrin: at 10^{-6} M in toluene, there is no shift in the Soret band in the UV–Vis absorption spectrum. The Ni–Ru dimer was observed by MALDI–TOF mass spectrometry. Heating the Ru(II)CO porphyrin with 2 equivalents of the phosphine porphyrins led to quantitative formation of trimeric assemblies.

Groves (*26,27*) has constructed an artificial membrane bound electron transfer system taking advantage of this class of porphyrin assembly. A manganese porphyrin functionalized with long steroidal chains is inserted into a synthetic lipid bilayer. The plane of the porphyrin is oriented parallel to the phospholipid bilayer interface, so that the central metal is exposed for coordination to zinc porphyrins equipped with imidazole ligands. Three anionic groups on the zinc porphyrin periphery lie at the membrane surface and are able to interact with *ferri*-cytochrome *c* in solution. Thus a self-assembled ternary system is formed where the zinc porphyrin bridges the manganese porphyrin in

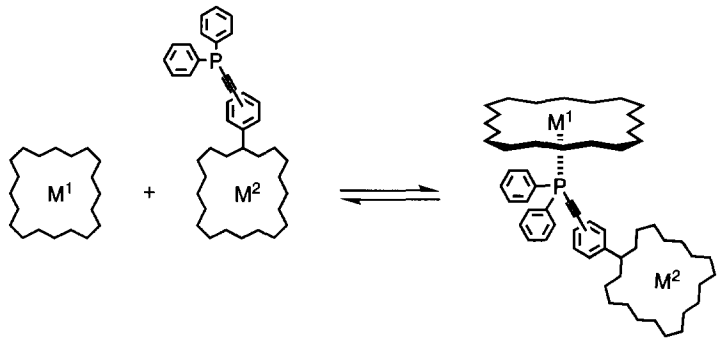

(17) M^1 = Ru(CO)
M^2 = 2H, Zn, Ni

FIG. 5. Trivial closed dimer assembled via phosphorus–ruthenium coordination.

the membrane and the cytochrome *c* in the aqueous phase. An extensive study of electron transfer from the manganese redox center to the *ferri*-cytochrome *c* was carried out.

Sanders (*28,29*) has assembled very large porphyrin arrays by combining this coordination approach with covalently linked oligomers. He explored the possibility of coordinating a monomeric dipyridyl porphyrin to a covalent Ru(II)CO porphyrin oligomer (*28*) and of coordinating covalent pyridyl porphyrin oligomers to monomeric Ru(II)CO porphyrins (*29*). With the first approach, the team assembled arrays of 11 and 21 porphyrins by reaction of a central di- and tetra- 4-pyridyl porphyrin with two and four porphyrin pentamers respectively. The second approach enabled them to make an array of six porphyrins, three ruthenium monomeric porphyrins coordinated to a tripyridyl porphyrin trimer, as well as a dendritic 7-porphyrin assembly where two pyridyl porphyrin trimers were coordinated to a single ruthenium porphyrin.

B. Non-Porphyrin Ligands

Simple bidentate ligands are able to bridge two metalloporphyrins to yield a three-component assembly. Fuhrhop (*30*) reported the pyrazine bridged Fe(II)protoporphrin complex (**18**, Fig. 6a) that exhibits photoinduced electron transfer between the two metalloporphyrins. High-spin Fe(III)tetraphenylporphyrin dinuclear complexes where the bridging ligands are hydroquinone dianions were synthesized by Hendrickson (*31*). 1,4-diazabicyclo[2.2.2]octane (DABCO), pyrazine, 4,4′-bipyridine, 1,2-bis(4-pyridyl)ethane, and *trans*-1,2-bis(4-pyridyl)ethylene were shown by Endo (*32*) to bridge two Ru(II)(CO)octaethylporphyrins, giving stable assemblies (**19–23**, Fig. 6a). Cyclic voltammetry revealed that the complexes undergo two electron oxidation steps. The first oxidation occurs at the porphyrin π-system, whereas the second is on the metal centers. Triple-decker Ru(II)octaethylporphyrin complexes were also prepared with pyrazine and 4,4′-bipyridine bridges (*33*) (**24** and **25**, Fig. 6b). Electrochemical studies proved that the two ends of the complex can interact with each other.

An extended bipyridinic ligand was synthesized by Tykwinski (*34*) and was shown by ^{1}H NMR spectroscopy and single crystal X-ray crystallography to axially coordinate to two Ru(II)(CO) porphyrins (**26**, Fig. 7).

Zinc porphyrins also interact with diaza ligands to form dimeric assemblies, but these systems have significantly lower kinetic and thermodynamic stability. The zinc porphyrin–DABCO system has been widely studied by Sanders (*35*) and Anderson (*36,37*), while Ballester

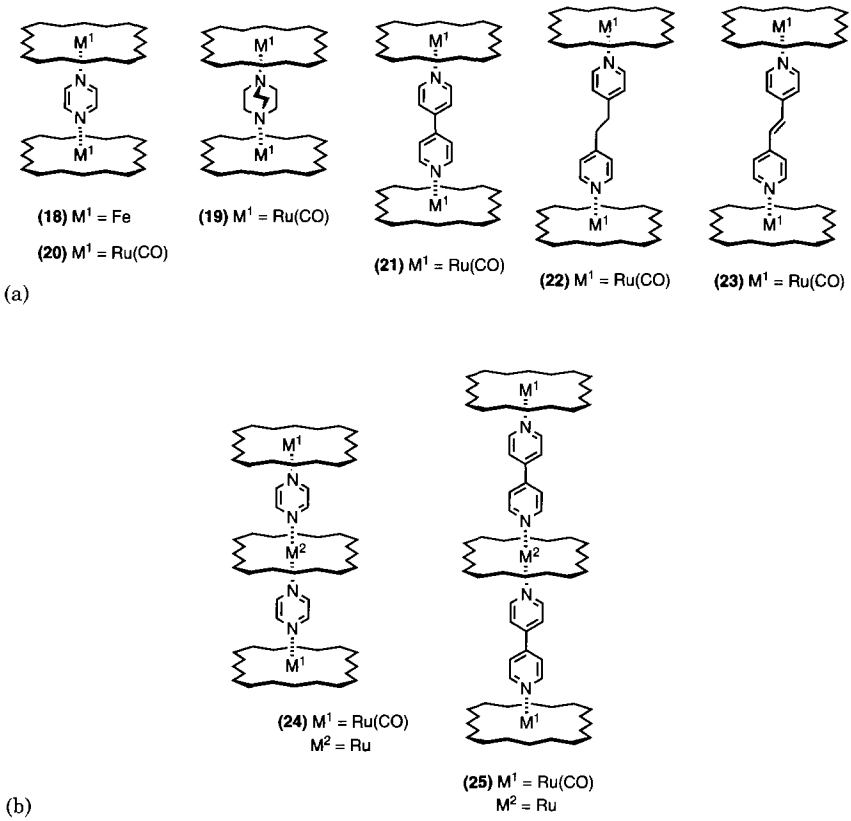

FIG. 6. Trivial closed dimeric (a) and trimeric (b) sandwich complexes assembled on bidentate ligands.

(*38*) reported a computational study that applies the *ab initio* SCF–GIAO method to the calculation of the ^{1}H NMR chemical shifts of zinc porphyrin–DABCO complexes. The experimental measurement of zinc porphyrin–DABCO microscopic binding constants requires the combined use of both ^{1}H NMR and UV–Vis absorption methods. At UV–Vis concentrations (10^{-6} M), only the 1:1 complex (**27**) is formed with an association constant of 10^4–10^5 M^{-1} in chlorinated organic solvents (Fig. 8a). At NMR concentrations (10^{-3} M), when 0.5 equivalents of DABCO are added, the 2:1 DABCO-bridged complex (**28**) is formed, but this opens up to give the 1:1 complex in excess DABCO (Fig. 8b).

Chichak and Branda reported the synthesis of two supramolecular systems where two (**29**) (*39*) or six (**30**) (*40*) Ru(II)CO porphyrins are

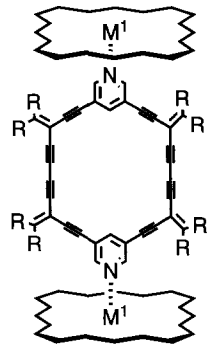

(26) M^1 = Ru(CO)
R = Me, Ph

FIG. 7. An extended dimeric sandwich complex assembled on a bidentate ligand.

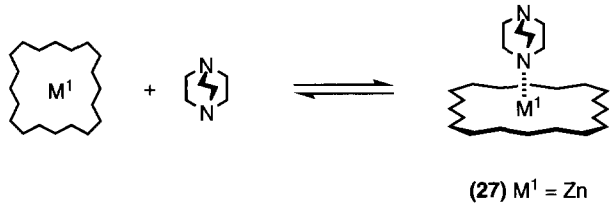

(27) M^1 = Zn

(a)

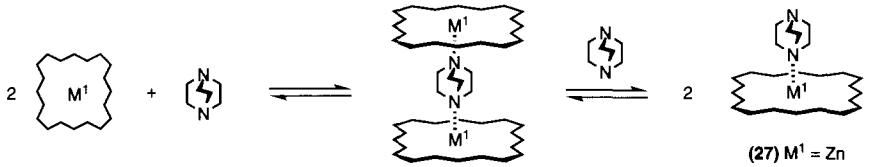

(28) M^1 = Zn

(27) M^1 = Zn

(b)

FIG. 8. Trivial closed DABCO zinc porphyrin complexes.

coordinated to the peripheral pyridyl groups of transition metal complexes (Ru, Os, or Fe) (Fig. 9). The multicomponent assemblies are therefore held together by two types of metal–ligand interaction that confer a very well-defined geometry. The assemblies are formed quantitatively upon mixing the ruthenium porphyrin with the transition metal complex. The UV–Vis absorption spectra of both systems are essentially the sum of the absorptions of the components, but fluorescence experiments revealed electronic communication between the chromophores.

Sanders (*41,42*) studied the ability of several multi-pyridine ligands to coordinate zinc and Ru(II)CO porphyrins and then act as templates for the synthesis of macrocyclic porphyrin oligomers. Once coordinated to the template, the reactive ends of the porphyrins are brought together, and cyclization is favored (*43,44*). Alternatively, the templates can be exploited in the synthesis of linear porphyrin oligomers, since they can act as scavengers that remove the cyclizable components of a reaction mixture (*45*). An X-ray crystal structure of a central tripyridyl triazine ligand axially coordinated to three Ru(II)CO porphyrins highlights the complementarity of this ligand for trimer formation (*29*) (**31**, Fig. 10).

A four-component self-assembling system was described by Kuroda (*46*). Two rhodium porphyrins are coordinated by the terminal pyridine groups of an extended ligand constructed from a tartrate derivative.

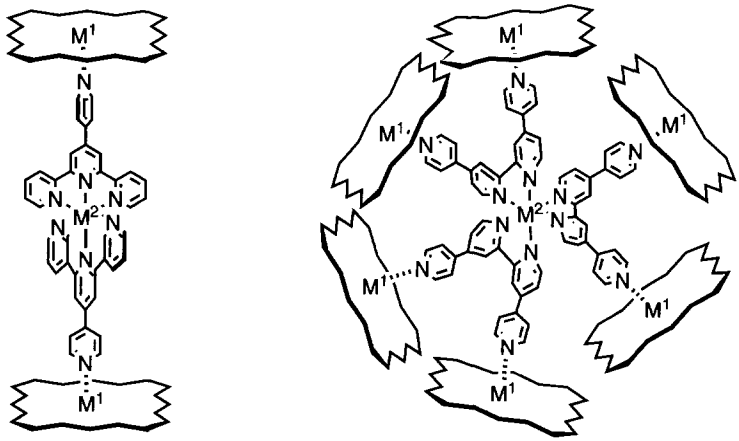

(29) M^1 = Ru(CO)
M^2 = Ru, Os

(30) M^1 = Ru(CO)
M^2 = Ru, Fe

FIG. 9. Trivial closed assemblies based on multidentate transition metal complexes.

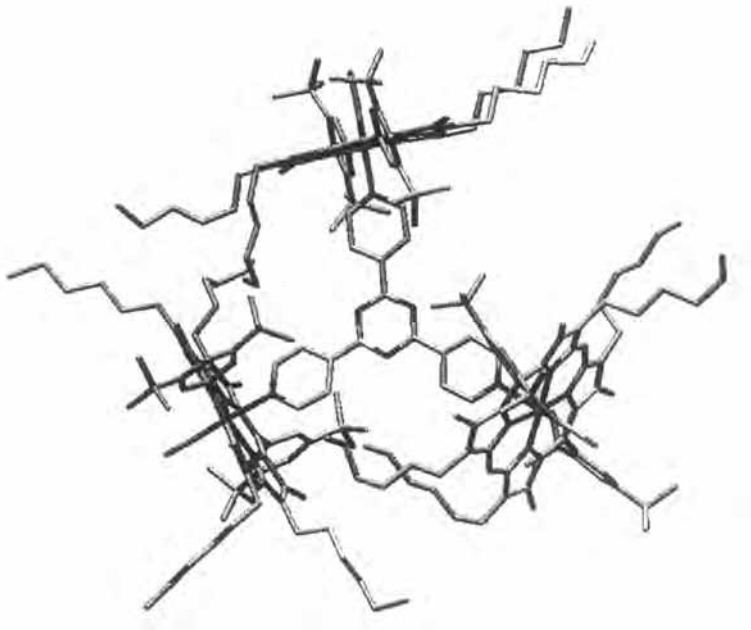

FIG. 10. Trivial closed trimer assembled on a trispyridine ligand.

The hydroxyl and carbonyl groups of the tartrate skeleton simultaneously interact via hydrogen-bonding with the amido groups of a modified free-base porphyrin. Another complex assembly that exploits multiple types of interaction was reported by Whitesides (*47*). He prepared two systems where a hydrogen-bonded isocyanuric acid–melamine rosette was functionalized on the periphery with imidazole groups. Addition of a zinc porphyrin yielded a supramolecular aggregate in which the imidazole moieties coordinated to the metalloporphyrins. The stoichiometry, structure, and stability of the assembly were investigated by ^{1}H NMR and UV–Vis absorption spectroscopy, ESI–MS and size exclusion chromatography. The imidazole groups do not affect the stability of the rosette assembly, but strongly coordinate the zinc porphyrin units (for a model system, $K \approx 10^5\ M^{-1}$).

The axial coordination of metalloporphyrins to a pyridyl ligand was successfully exploited by two groups to produce porphyrin-stoppered rotaxanes. Sanders (*48*) assembled a rotaxane by simply mixing the constituent parts. Zn(II), Ru(II)CO, and Rh(II)Cl porphyrins were used as stoppers. Branda (*49*) reported the stoppering of a pseudorotaxane by adding two equivalents of a Ru(II)CO porphyrin that coordinated to

two pyridine groups on the ends of the thread component. The stoppers could be displaced with an excess of a competitive pyridine ligand.

III. Cooperative Closed Assemblies

The assembly of two or more subunits to form a superstructure where at least one cooperative intramolecular ring closure takes place permits the assembly of stable complexes using relatively weak interactions.

A. Homo-Assemblies

When the metalloporphyrin bears a donor group on its periphery, it can behave as a self-complementary ditopic unit capable of metal–ligand induced dimerization. Many systems have been synthesized using different metals, ligands, and spacers. The length and geometry of the spacer groups determine the stoichiometry of the assembly process.

1. Dimers

The ligand group can be introduced either on the *meso* or on the β-pyrrole position of the porphyrin ring, but the synthesis of the *meso*-functionalized derivatives is easier and has been more widely exploited. Balch (*50–53*) reported that the insertion of trivalent ions such as Fe(III) (**32**) and Mn(III) (**33**) into octaethyl porphyrins functionalized at one *meso* position with a hydroxy group (oxophlorins) leads to the formation of a dimeric head-to-tail complex in solution (Fig. 11a) (*50,51*). An X-ray crystal structure was obtained for the analogous In(III) complex (**34**), and this confirmed the head-to-tail geometry that the authors inferred for the other dimers in solution (*53*) (Fig. 11b). The dimers are stable in chloroform but open on addition of protic acids or pyridine (*52*). The Fe(III) octaethyloxophlorin dimer (*52*) is easily oxidized by silver(I) salts. The one-electron oxidation is more favorable than for the corresponding monomer or μ-oxo dimer, presumably because of the close interaction of the π-systems in the self-assembled dimer.

Goff (*54*) synthesized an Fe(III) porphyrin with a 2-hydroxyphenyl group at one *meso* position (**35**, Fig. 12a). Under basic conditions, the system spontaneously dimerizes due to phenolate–Fe(III) coordination. The complex is very stable and was isolated and fully characterized. In the solid state, the X-ray crystal structure confirmed the structure of the assembly as a macrocyclic head-to-tail dimer with two intermolecu-

(a)

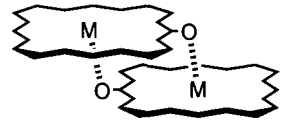

(32) M = Fe(III)

(33) M = Mn(III)

(34) M = In(III)

(b)

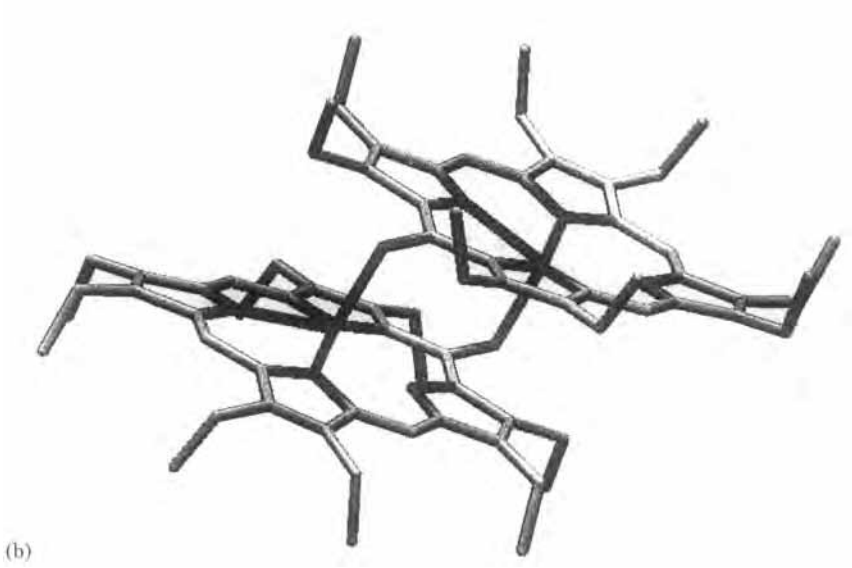

FIG. 11. Cooperative closed dimers assembled from oxophlorins.

lar phenoxide–Fe(III) interactions (Fig. 12b). ^{1}H NMR and UV–Vis absorption studies indicate the presence of a five-coordinate high-spin Fe(III) complex, showing that the head-to-tail geometry is retained in solution. The complex can be opened by addition of two equivalents of a protic acid to generate the monomeric porphyrin, and the dimer can be reformed by treatment with base. Chemical reduction of Fe(III) to Fe(II) with sodium dithionite also dissociates the dimer. Goff (*55*) also reported a Mn(III) head-to-tail dimer (**36**) which has the same geometry (Fig. 12a). On mixing the Mn(III)Cl and Fe(III)Cl porphyrins under basic conditions the heterometallic dimer was detected, but the thermodynamically more stable complex is the homometallic Fe(III) dimer, and the heterodimer could not be isolated.

(a)

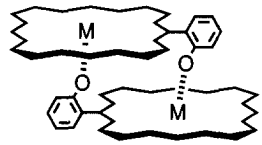

(35) M = Fe(III)

(36) M = Mn(III)

(b)

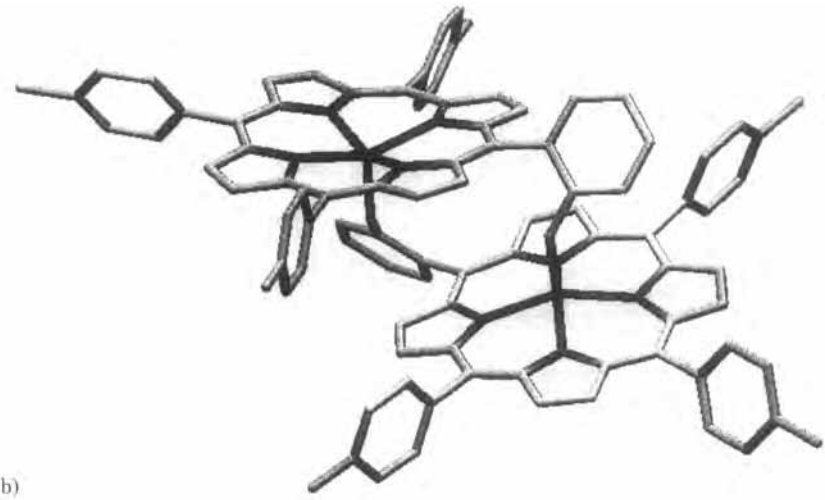

FIG. 12. Cooperative closed dimers assembled from phenol-functionalized porphyrins.

A number of porphyrin dimers and oligomers have been synthesized to examine the factors affecting energy and electron transfer reactions of the special pair of bacteriochlorophylls that are found in photosynthetic reaction centers. This special pair is the key component in the energy transfer between the light-harvesting antenna complexes and the reaction center itself. The special pair are separated by a distance of about 3.2 Å, are nearly parallel in orientation, and have partial overlap of the π-orbitals. This slipped cofacial orientation is considered important for efficient energy and electron transfer. Kobuke and Miyaji (*16*) reported a zinc porphyrin bearing two N-methylimidazolyl *meso* substituents oriented *trans* across the porphyrin ring (**37**), and this forms a slipped cofacial dimer by coordination of the imidazolyl moieties to the zinc centers (Fig. 13). The dimer self-assembles at concentrations as low as 10^{-6} M, and fluorescence studies show that it is

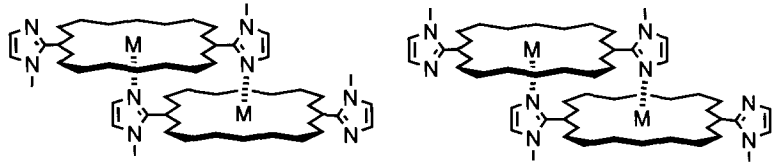

(37) M = Zn **(38)** M = Mg

FIG. 13. Cooperative closed dimers assembled from imidazole-functionalized porphyrins.

stable down to 10^{-9} M. The structure of the dimeric assembly was confirmed by ^{1}H NMR spectroscopy and VPO measurements. Attempts to form a mixed dimer with the corresponding free-base porphyrin failed, and this indicates that a simple imidazole–zinc interaction cannot compete with the cooperativity of two such interactions in the macrocyclic dimer. In the UV–Vis absorption spectrum of the dimer, the Soret band shows a splitting of 18 nm, and the Q bands are red shifted. The fluorescence maxima are also shifted to longer wavelengths, and these features show that there is strong exciton coupling of the chromophores similar to that found in the special pair. Substitution of the central zinc with magnesium in the *cis* analog produced a system which starts to dimerize at a concentration of 10^{-8} M (*56*) (**38**, Fig. 13).

Porphyrins functionalized with 2-pyridyl groups at the *meso* position have proved to be very effective for the self-assembly of metalloporphyrin dimers (Fig. 14a,b). In the X-ray crystal structure of the zinc porphyrin dimer (**39**), synthesized by Knapp and co-workers, (*57*), the porphyrins are closely stacked with a mean plane separation of 3.3 Å. This leads to exciton coupling of the chromophores, and in the UV–Vis absorption spectrum characteristic splitting of the Soret band and a red shift of the Q bands are observed. A similar structure has been reported by Gerasimchuk (*58*) for the analogous magnesium porphyrin (**40**), and again the UV–Vis absorption spectrum shows excitonic interactions between the chromophores. Dilution experiments enabled the authors to measure an association constant of 5×10^5 M^{-1} for formation of the magnesium dimer. Addition of competitive donor ligands such as acetone, DMF, DMSO, or pyridine leads to dissociation of the dimer. The corresponding Ru(II)CO porphyrin forms a similar head-to-tail dimer (**41**) (*13*). The increased stability of the pyridine–ruthenium interaction means that these dimers are fully assembled in solution and can be readily isolated. Pyridine, 4-cyanopyridine, 3- or 4-pyridyl free-base porphyrins were introduced in the 6th coordination site of

(a)

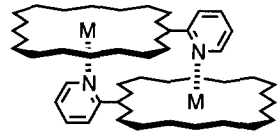

(39) M = Zn

(40) M = Mg

(41) M = Ru(CO)

(42) M = Ru(Py)

(43) M = Ru(PyCN)

(46) M = Rh(III)Cl

(b)

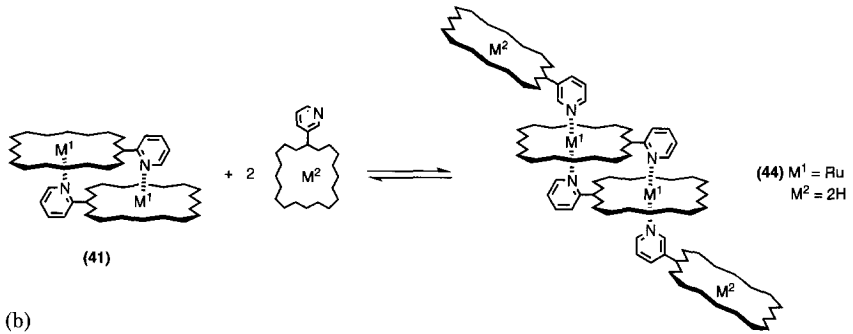

(c)

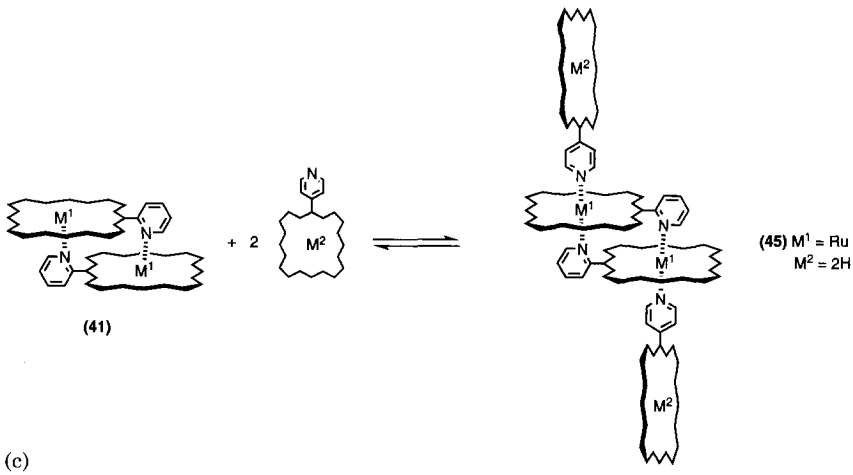

FIG. 14. Cooperative closed dimers (a) and tetramers (b,c) assembled from pyridine-functionalized porphyrins.

the ruthenium centers upon photoirradiation of the reaction mixture (**42**, **43**, Fig. 14a; **44**, Fig. 14b; **45**, Fig. 14c). All the assemblies show characteristic excitonic interactions between the porphyrin subunits in the UV–Vis absorption spectrum. The strong interaction between the cofacial ruthenium porphyrin rings is reflected in the stepwise oxidation of the porphyrin units and metal centers and in the intervalence charge-transfer bands observed in the near-IR absorption spectrum, which are due to a mixed-valence Ru(III), Ru(II) state. Upfield shifts in the ^{1}H NMR spectrum of the pyridyl protons enabled Aoyama (*59*) to detect the presence in solution of the head-to-tail dimer of the related Rh(III)Cl porphyrin (**46**, Fig. 14a).

The aniline–zinc porphyrin interaction has also been exploited to form dimers. Hunter (*60*) reported the dimerization of porphyrins functionalized at one *meso* position with *ortho* or *meta* aniline groups (**47**, **48**, Fig. 15). Both compounds showed concentration-dependent ^{1}H NMR spectra with large upfield shifts for the aniline protons. The dimerization constants are 160 and 1080 M^{-1} respectively for **47** and **48**, and these values are an order of magnitude higher than the association constants of simple reference complexes ($K = 10$ and 130 M^{-1} respectively), which is indicative of cooperative self-assembly. The complexation-induced changes in chemical shift were used to obtain three-dimensional structures of the dimers.

When the donor group is attached at a β-pyrrole position rather than the *meso* position, the properties of the assemblies change. Knapp (*57*) synthesized a series of β-pyrrole 2-pyridyl substituted zinc porphyrins (**49**, Fig. 16) and showed that dimerization takes place provided the *meso*-substituents are not too bulky: ^{1}H NMR and VPO measurements showed that the porphyrin, which bears heptyl substituents, dimerizes in solution, whereas the phenyl analog does not. The complexation-induced changes in chemical shift suggest a stacked structure for the dimer.

A dimer made up of two zinc porphyrins bearing a 7-azabicyclo[2.2.1]heptadiene fused at the C2–C3 β-positions was reported by Knapp (*61*). The compound was designed to dimerize with a pyrrole-over-pyrrole geometry similar to that found in the photosynthetic special pair. Dimerization at 10^{-3} M was confirmed by VPO and ^{1}H NMR spectroscopy. Dilution to 10^{-5} M or addition of DMAP caused disaggregation of the complex. In the solid state, this compound assembles as a cyclic hexamer with the vicinal porphyrin planes almost perpendicular.

If the ligand is not directly linked to the porphyrin periphery but is held at a distance from the chromophore by a rigid spacer, more open

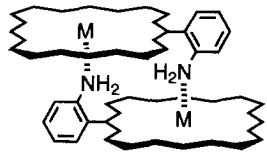

(47) M = Zn

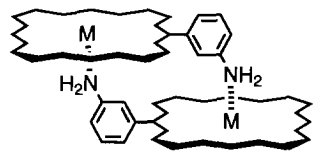

(48) M = Zn

FIG. 15. Cooperative closed dimers assembled from aniline-functionalized porphyrins.

macrocyclic structures can be assembled, and these can exhibit host–guest properties. Hunter (*62*) showed that the porphyrin derivative (**50**) dimerizes in solution, and that the assembly (**51**) is stable down to concentrations of 10^{-8} M (Fig. 17). The cooperative assembly process leads to a high stability constant ($2 \times 10^8\ M^{-1}$, cf. simple reference complexes for which $K \approx 10^3\ M^{-1}$). Upfield shifts of the pyridyl protons in the ^1H NMR spectrum, redshifts of the UV–Vis absorption bands, and emission maxima as well as VPO measurements confirmed the geometry and stoichiometry of the assembly. The self-assembled macrocycle proved to be an efficient receptor for terephthalic acid derivatives ($K \approx 10^3\ M^{-1}$ in chloroform).

Bied-Charreton (*63*) showed by ^1H NMR spectroscopy that a zinc porphyrin bearing a primary amino group attached via a flexible spacer to the *meta* position of a *meso*-phenyl ring spontaneously dimerizes in solution via NH_2–Zn coordination. The corresponding *ortho* derivative shows an equilibrium between the dimeric form and the intramolecularly coordinated monomer. ESR spectroscopy was used to demonstrate the same behavior in the corresponding cobalt porphyrin (*64*).

A novel zinc porphyrin dimer (**52**) with a boronic ester linkage was prepared by Shinkai (Fig. 18) (*65*). The authors introduced an additional

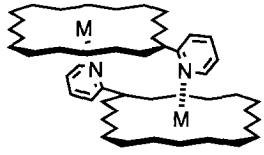

(49) M = Zn

FIG. 16. Cooperative closed dimers assembled from porphyrins functionalized with pyridine at the β-pyrrole position.

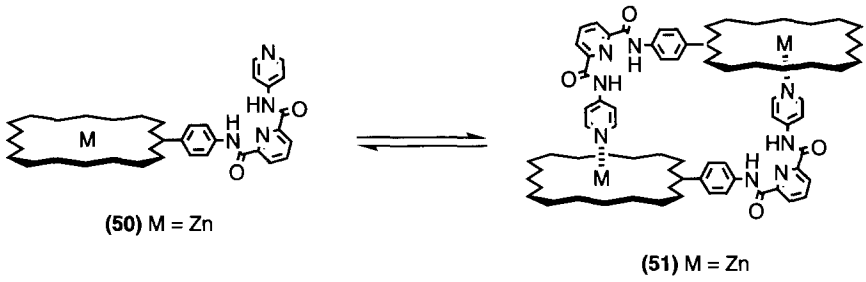

FIG. 17. Cooperative closed dimer assembled from extended pyridine-functionalized porphyrins to form a cavity for guest complexation.

recognition process that occurs upon mixing the *meso*-dicatechol zinc porphyrin and pyridine-3-boronic acid dimethyl ester. The boronic acid derivative reacts with the cathecol moiety to yield a self-complementary complex that dimerizes through two intermolecular zinc–pyridine interactions. The dimerization constant determined by UV–Vis absorption spectroscopy is $1 \times 10^4\,M^{-1}$ (cf. simple reference complex for which $K = 340\,M^{-1}$). The 2 + 2 stoichiometry was confirmed by VPO measurements.

A porphyrin array in which the assembly properties can be regulated by light was synthesized by Burrell (*66*). This zinc porphyrin has a pyridine group attached to the β-pyrrole position via an alkene linkage that can be either *cis* or *trans*. In the *trans* form, the porphyrin self-assembles into a trivial open polymer (**53**) (see Section IV.A) with an angle of 64° between the coordinating ligand and the porphyrin plane in the solid state. However, in the *cis* form, the porphyrin assembles into a cooperative closed dimer (**54**) with an angle of 32° between the two porphyrin planes. The *trans* polymeric form may be converted into the *cis* dimer by irradiation at 400 nm (Fig. 19).

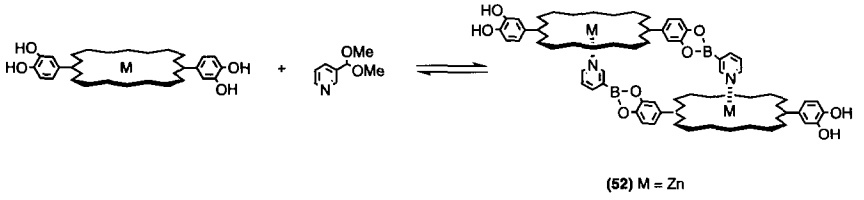

FIG. 18. Cooperative closed dimer assembled using boronic esters as well as zinc–pyridine coordination.

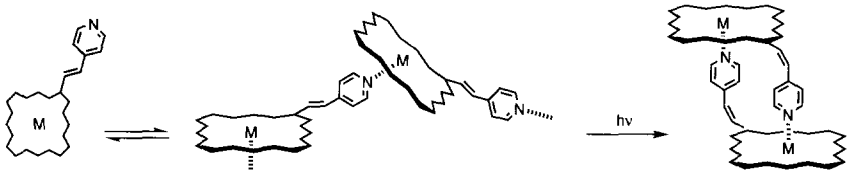

(53) M = Zn (54) M = Zn

FIG. 19. A pyridine-functionalized porphyrin that can be photoswitched between a trivial open polymer and a cooperative closed dimer.

2. *Higher Oligomers*

The self-assembly of cyclic dimers is entropically favored over the assembly of higher cyclic oligomers, but the assembly of larger oligomers is possible if the geometry of the monomer is incompatible with dimerization.

Wojaczynski and LatosGrazynski (*67–70*) reported the self-assembly of metalloporphyrins with a hydroxy substituent on the β-pyrrole position. The trivalent metal complexes (Fe(III), Ga(III), Mn(III)) form cyclic head-to-tail trimers quantitatively (**55**, **56**, **57**, Fig. 20a). The structures were confirmed by mass spectroscopy and ^{1}H NMR spectrometry, the upfield shift of the 3-pyrrole proton being particularly diagnostic. An X-ray crystal structure was also obtained for the iron trimer **55** (*70*) (Fig. 20b). The UV–Vis absorption spectra of all of these trimers are characterized by band broadening and, in the iron and gallium trimers, by a blue shift of the Soret band. The assemblies are opened on addition of protic acids or bases. Mixed metal trimers were also identified in solution by ^{1}H NMR and mass spectrometry, but they could not be isolated. Comparison of these systems with the corresponding oxophlorins discussed in the previous section illustrates how a very simple modification in the position of the donor group on the porphyrin ring causes a dramatic change in the self-assembly properties, in this case from dimer to trimer.

A related study, aimed at demonstrating how a change in the structure of the ligand covalently bound to the porphyrin modified the self-assembling properties of the system, was reported by Hunter (*71*)[1]. The

[1]In this paper, we reported the self-assembly of a macrocyclic trimer based on an isomer of the dimer system. The assignment of this structure was based on VPO measurements, but subsequent experiments suggest that this system is predominantly a dimer in solution. It appears that the monomer is not sufficiently rigid to prevent collapse to the entropically favored dimer.

(a)

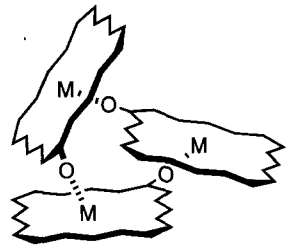

(55) M = Fe(III)
(56) M = Ga(III)
(57) M = Mn(III)

(b)

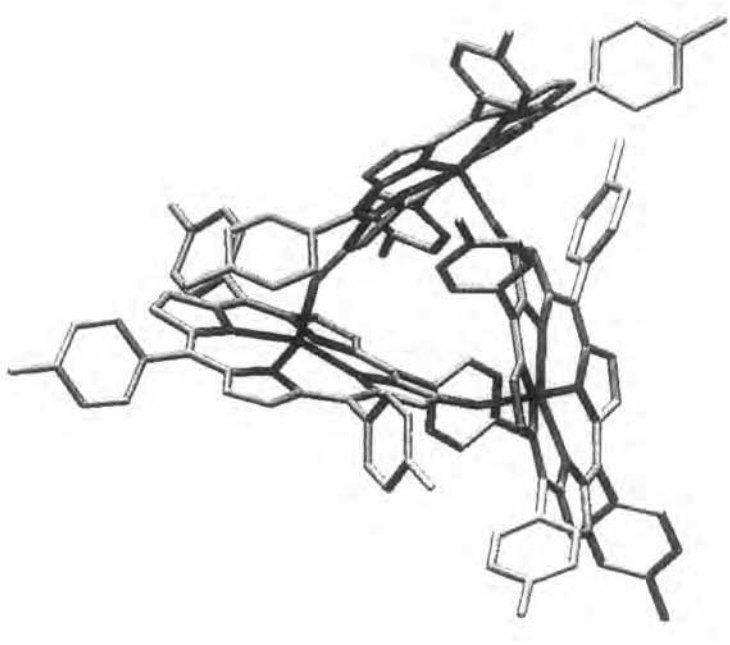

FIG. 20. Cooperative closed trimers.

team showed that changing the angle between the pyridine ligand and the porphyrin plane from 90° to 180° would lead to self-assembly of a cyclic tetramer (**58**) instead of a dimer (Fig. 21). Tetramer formation was confirmed by ^{1}H NMR and UV–Vis spectroscopy and VPO measurements. However, the tetramer is significantly less stable than the dimer, with an association constant of 10^{12}–10^{13} M^{-3}. The effective molarity for intramolecular cyclization of the tetramer (0.6–0.9 M) is

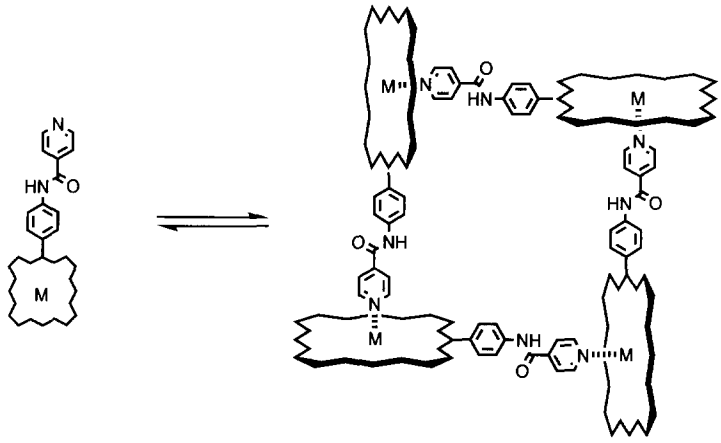

(58) M = Zn

FIG. 21. A cooperative closed tetramer.

not so different from the value measured for the dimer (6 M), but, because the cooperativity is shared out between four molecules instead of two, the concentration at which self-assembly takes place differs by orders of magnitude: 10^{-5} M for the tetramer and 10^{-9} M for the dimer.

Ru(II)(CO) and Ru(II)Py porphyrins functionalized at one *meso* position with a 4-pyridyl group were prepared by Imamura (*72,73*). Intermolecular pyridine–ruthenium interactions lead to the formation of cyclic tetramers (**59**, **60**, Fig. 22). These tetramers are much more stable than the corresponding zinc systems and can be observed by FAB mass spectrometry. In the UV–Vis absorption spectrum the Soret bands are broadened with respect to the corresponding ruthenium porphyrin monomer, but there are no significant inter-chromophore interactions. The tetramer can be dissociated by adding pyridine. The rate of this reaction is faster for the Ru(II)CO system than for the Ru(II)Py system. The first ligand substitution is the rate-determining step, and once this has occurred the other substitutions follow rapidly, so that the structure quickly falls apart and no acyclic intermediates are observed. This is a hallmark of the dissociation of a cooperative self-assembled structure. The redox behavior of the assemblies, studied by means of cyclic voltammetry, is characterized by two four-electrons oxidation processes, the first of them proceeding stepwise. The pyridine ligands in the Ru(II)Py tetramer were replaced by another pyridyl porphyrin, generating an eight-porphyrin array (**61**) (*74*).

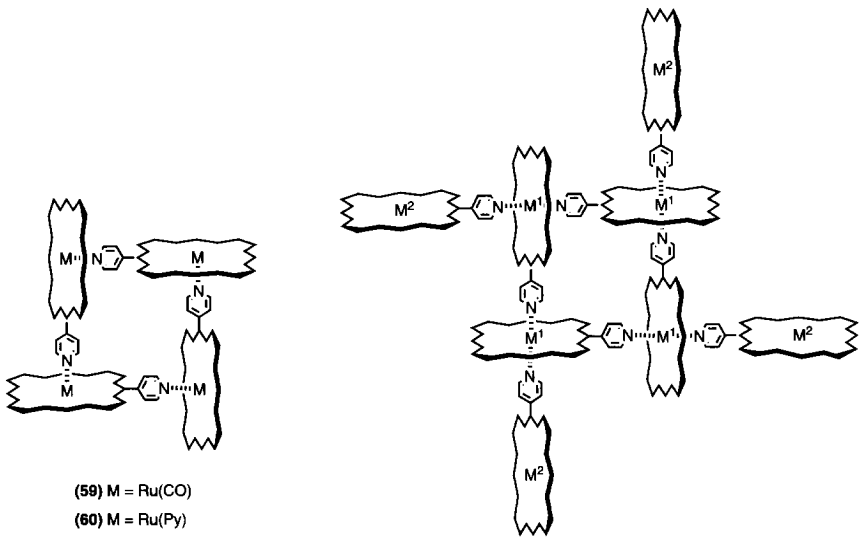

FIG. 22. Cooperative closed tetramers and octamer.

B. HETERO-ASSEMBLIES

1. Porphyrins as Ligands

A free-base porphyrin functionalized at two *meso* positions with 3- or 4-pyridyl groups can act as a bidentate ligand for covalent zinc porphyrin dimers to give trimeric assemblies (*75–78*). The pyridyl groups can be introduced either *trans* (5,15) or *cis* (5,10) across the porphyrin (**62**, Fig. 23a; **63** and **64**, Fig. 23b). UV–Vis titration experiments with the *trans* ligand yielded an association constant of $7 \times 10^6\,M^{-1}$ for the formation of **62**, while with the *cis* ligands the authors measured an association constant of $5 \times 10^6\,M^{-1}$ for the 3-pyridyl (**63**) and $2 \times 10^7\,M^{-1}$ for the 4-pyridyl derivative (**64**). The difference reflects the complementarity of the ligand geometries with respect to the zinc binding sites in the porphyrin dimer.

If the free-base porphyrin is tetrasubstituted at the *meso* positions with 3- or 4-pyridyl ligands, pentamers are obtained on coordination to zinc porphyrin dimers (*79*) (**65**, **66**, Fig. 24). With the 3-pyridyl derivative all the porphyrin planes are coplanar, whereas in the case of the 4-pyridyl derivative the ligand porphyrins are approximately perpendicular to the plane of the zinc porphyrins. Quenching of the zinc porphyrin

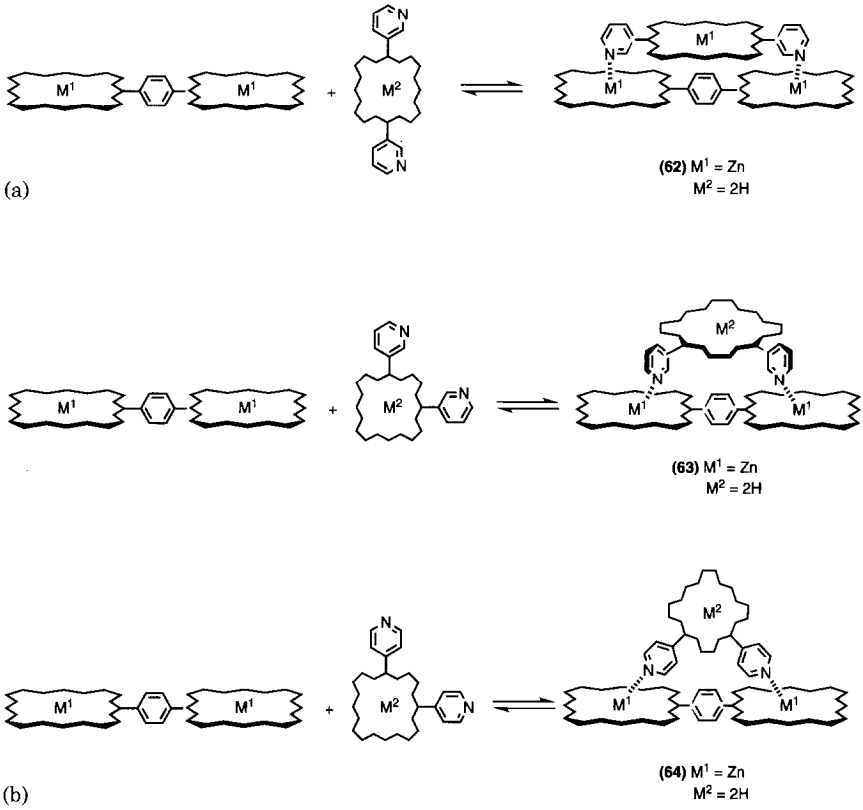

FIG. 23. Two-component cooperative closed trimers.

fluorescence in these assemblies is attributed to singlet energy transfer from the zinc porphyrins to the free-base porphyrin. A similar pentameric assembly was reported by Gunter (*80*), who showed that a tetrapyridyl porphyrin formed a 1:2 complex with a zinc porphyrin dimer. If the porphyrin guest bears only two pyridyl groups, a 1:1 complex is formed with an association constant of about $10^8\ M^{-1}$. Hunter also reported the assembly of a pentameric array from a tetrapyridyl porphyrin and a zinc porphyrin dimer with complementary geometries (*81*). The microscopic association constant for each binding event is $2 \times 10^6\ M^{-1}$, measured by UV–Vis absorption spectroscopy. Fluorescence titrations together with time-resolved experiments proved that the assembly functions as a simple light-harvesting system in which the antenna zinc porphyrins transfer incident excitation energy to the inner free-base component.

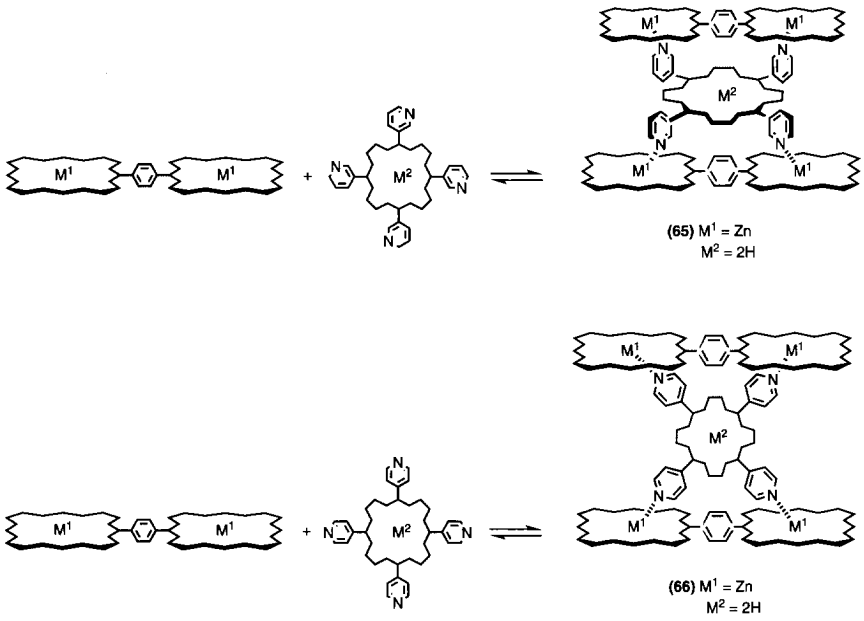

FIG. 24. Three-component cooperative closed pentamers.

In order to mimic the electron transfer processes in photosynthetic systems, Hunter (*82*) designed a stable self-assembling complex (**67**) with a well-defined structure (Fig. 25). Two complementary porphyrin subunits were synthesized: a zinc porphyrin dimer containing a naphthalenediimide spacer and a free-base porphyrin functionalized with two pyridine ligands. Two cooperative pyridine–zinc interactions lead to a stable 1:1 complex, and the association constant was determined to be $3 \times 10^8\ M^{-1}$ by fluorescence spectroscopy. In the complex, the fluorescence of the free-base porphyrin is quenched by photoinduced electron transfer to the naphthalenediimide acceptor. The authors suggest that electron transfer occurs through space or through the solvent between the chromophores that are held 10 Å apart rather than through the covalent framework of the molecules. A related complex lacking the electron acceptor group was synthesized as a control, and it displays energy transfer from the zinc porphyrins to the free-base porphyrin but no electron transfer.

Sanders (*83*) constructed a supramolecular assembly of heterometallic porphyrins held together by different types of metal–ligand interaction. The team exploited the different kinetic and thermodynamic properties of the pyridine–zinc, carboxylate–tin, and pyridine–

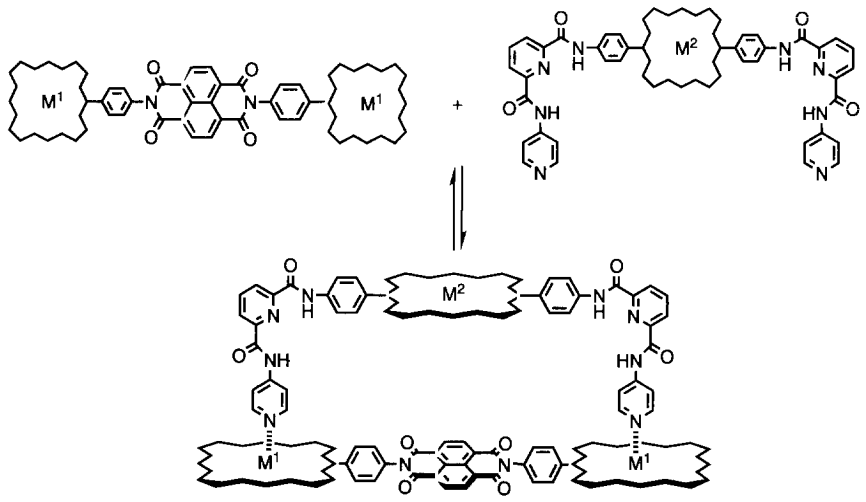

(67) $M^1 = Zn$
$M^2 = 2H$

FIG. 25. A cooperative closed trimer that exhibits intramolecular electron and energy transfer.

ruthenium interactions to generate a heterodimer and a heterotrimer (**68**, **69**, Fig. 26).

Macrocyclic receptors made up of two, four or six zinc porphyrins covalently connected have been used as hosts for di- and tetrapyridyl porphyrins, and the association constants are in the range 10^5–10^6 M^{-1}, reflecting the cooperative multipoint interactions (*84–86*). These host–guest complexes have well-defined structures, like Lindsey's "wheel and spoke" architecture (**70**, Fig. 27a), and have been used to study energy and electron transfer between the chromophores. A similar host–guest complex (**71**, Fig. 27b) was reported by Slone and Hupp (*87*), but in this case the host was itself a supramolecular structure. Four 5,15-dipyridyl zinc porphyrins coordinated to four rhenium complexes form the walls of a macrocyclic molecular square. This host binds *meso*-tetrapyridyl and 5,15-dipyridyl porphyrins with association constants of 4×10^7 M^{-1} and 3×10^6 M^{-1} respectively.

2. *Non-Porphyrin Ligands*

Coordination complexes with a ladder structure have been developed by Anderson (*36,37*). These ladders are prepared from covalently linked

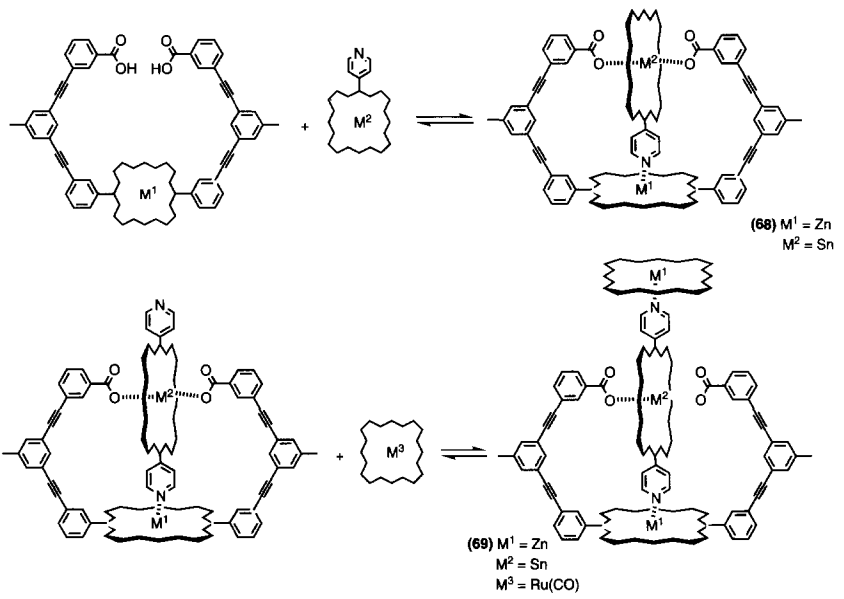

FIG. 26. Cooperative closed dimer and trimer featuring multi-point binding interactions.

metalloporphyrin oligomers by coordination to bidentate ligands. Anderson's first ladder complexes (*36*) were prepared from a butadieyne-linked zinc porphyrin dimer by coordination to DABCO, 4,4′-bipiperidine and 4,4′-bipyridine. In the absence of a coordinating ligand the zinc porphyrin dimer aggregates, but when one equivalent of DABCO is added the 2:2 ladder complex (**72**) is formed quantitatively (Fig. 28). Initially, the free porphyrin dimer and the ladder complex are in slow exchange on the NMR timescale, but in the presence of excess DABCO the ladder starts to break up to give a 1:2 complex (**73**) and the system enters the fast-exchange regime. The association constant for ladder formation determined by UV–Vis absorption spectroscopy is 4×10^{21} M^{-3}(EM = 0.3 M). The UV–Vis absorption spectra for this system show some interesting features. In both the aggregated and ladder forms, the porphyrin Q bands are significantly redshifted (up to 80 nm) with respect to the monomer spectrum, and the Soret band is split. This is due to increased planarity and conjugation in the complex compared to the single-strand dimer.

Anderson has produced a range of improved zinc porphyrin–DABCO ladder complexes where an aromatic substituent in the *meso* position reduces aggregation (*37*). The ^{1}H NMR spectra show a characteristic

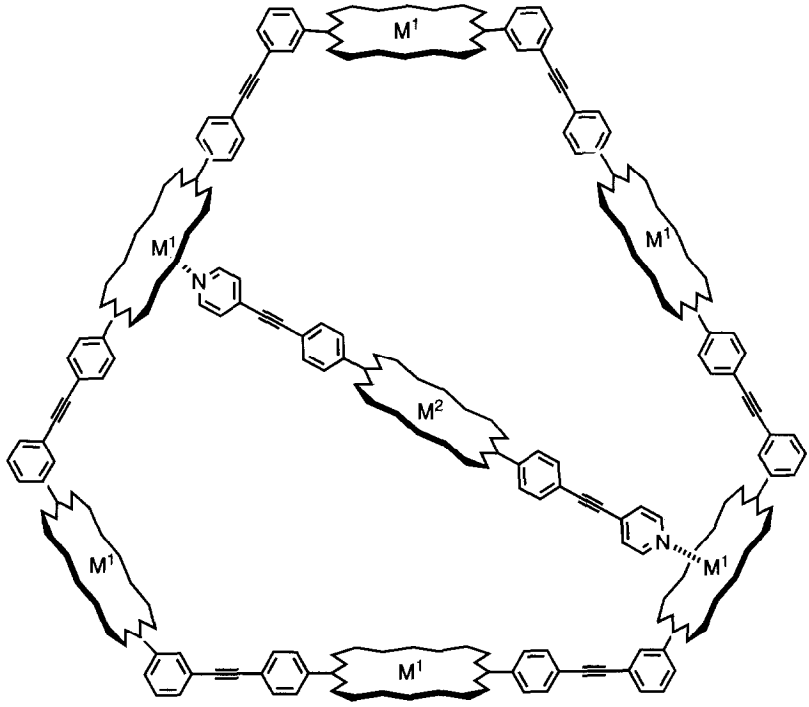

(a)

(70) M^1 = Zn
M^2 = 2H

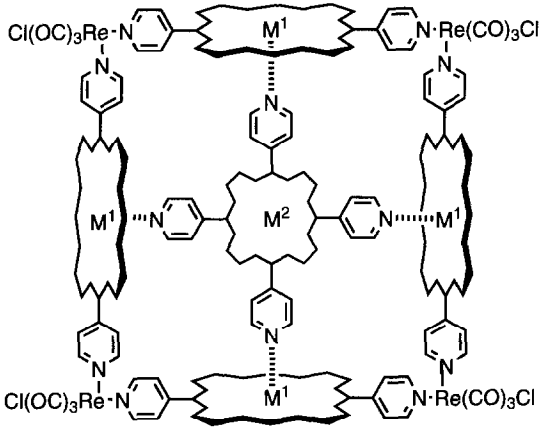

(71) M^1 = Zn
M^2 = 2H

(b)

FIG. 27. Two-component cooperative closed heptamer (a) and pentamer (b).

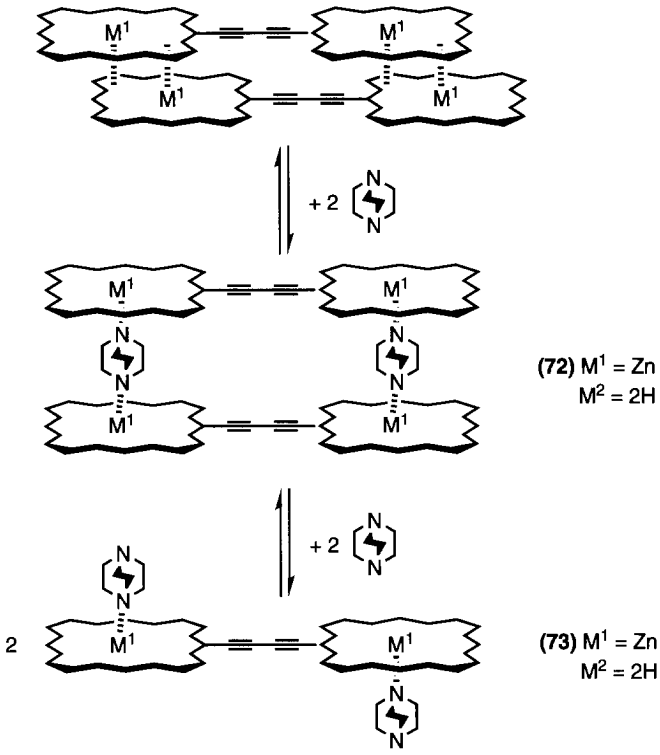

FIG. 28. Anderson's prototype DABCO ladder assembly.

upfield shift of 0.35 ppm for the porphyrin β-pyrrole protons due to shielding from the second porphyrin strand. The DABCO signals are shifted upfield to about −4 ppm on coordination to the zinc porphyrins, and for the pentameric system three different bound DABCO signals are observed, corresponding to the three different DABCO environments. Ladder formation is a two-state cooperative all-or-nothing process, and intermediates are not observed in the ^{1}H NMR spectra. In mixtures of oligomers, self-sorting takes place. For example, in a mixture of dimer, trimer, and DABCO, only the two homo-ladders, $(\text{dimer})_2 \cdot (\text{DABCO})_2$ and $(\text{trimer})_2 \cdot (\text{DABCO})_3$, are observed. At 10^{-6} M concentrations, the dimer does not completely form the ladder complex, whereas the higher oligomers do, before opening takes place in the presence of excess DABCO. The longer ladders are more stable due to cooperativity between the multiple binding interactions. This is best illustrated by the concentration at which the ladder is half-assembled:

the values range from 10^{-5} M for the monomer to 10^{-9} M for the hexamer. A linear relationship between the free energy of self-assembly and the number of porphyrins in the oligomer indicates that each rung of the ladder contributes equally to the stability of the system. The Hill coefficients are all greater than one and increase from dimer to hexamer, reflecting greater cooperativity despite the higher molecularity of the hexamer. Any of a number of bidentate nitrogen donor ligands can be used to assemble these ladders, including porphyrins themselves. An example is Anderson's triple strand array (**74**, Fig. 29) (*88*). The trimeric assembly is too stable for the stability constant to be determined by UV–Vis absorption spectroscopy, but it is in the range 10^{16}–10^{19} M^{-2}.

Crossley (*89*) described the self-assembly of a spherical cage-like structure made up of two zinc porphyrin dimers bound to a tetramine ligand. The 2:1 complex is stable at 10^{-6} M concentrations, but addition of excess of ligand causes dissociation of the capsule with formation of a 1:1 complex.

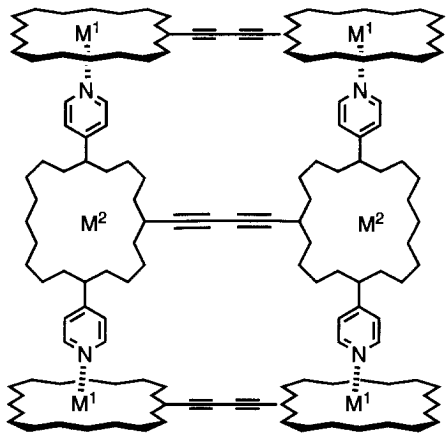

(74) M^1 = Zn
M^2 = 2H

FIG. 29. A cooperative closed hexamer.

IV. Trivial Open Assemblies

The optical and electrochemical properties of porphyrins make these chromophores useful building blocks for the synthesis of electro- and photoactive polymers. Two types of linear polymers have been constructed using the self-assembly approach: homo-polymeric assemblies and hetero- or "shish kebab" polymers.

A. Homo-Polymeric Assemblies

A polymeric structure can be generated by intermolecular coordination of a metalloporphyrin equipped with a suitable ligand. Fleischer (*18,90*) solved the crystal structure of a zinc porphyrin with one 4-pyridyl group attached at the *meso* position. In the solid state, a coordination polymer is formed (**75**, Fig. 30). The authors reported that the open polymer persists in solution, but the association constant of $3 \times 10^4\ M^{-1}$ is rather high, and it seems more likely, in the light of later work on closed macrocycles (see above), that this system forms a cyclic tetramer at 10^{-3} M concentrations in solution (*71,73*).

Hunter (*60*) reported a self-assembled open polymer formed by a zinc porphyrin bearing one *para*-aniline substituent at the *meso* position. The *ortho*- and *meta*-analogs discussed above form closed dimers, but the geometry of the *para*-derivative precludes this, and polymerization is the only alternative (**76**, Fig. 31). Although the dilution experiments could be fitted to a non-cooperative polymerization model with a pairwise association constant ($K = 190\ M^{-1}$) practically identical to that found for simple aniline–zinc porphyrin complexes ($K = 130\ M^{-1}$), broadening of the ^1H NMR spectrum at high concentrations is characteristic of oligomerization.

Smith (*91*) reported an X-ray crystal structure of a zinc porphyrin polymer (**77**, Fig. 32) where, unusually, the coordination bond is between a nitro group and the zinc center. The tetranitroporphyrin is highly substituted, and the resulting steric hindrance causes the macrocycle to be noticeably distorted. Adjacent porphyrin planes in the polymer are almost orthogonal. However, there is no evidence of polymerization in solution, and the nitro–zinc interaction is probably too weak to maintain this structure outside the solid state.

B. Hetero-Polymeric Assemblies

When a bidentate ligand bridges two metalloporphyrins, a linear polymeric chain is formed. This arrangement has been dubbed "shish

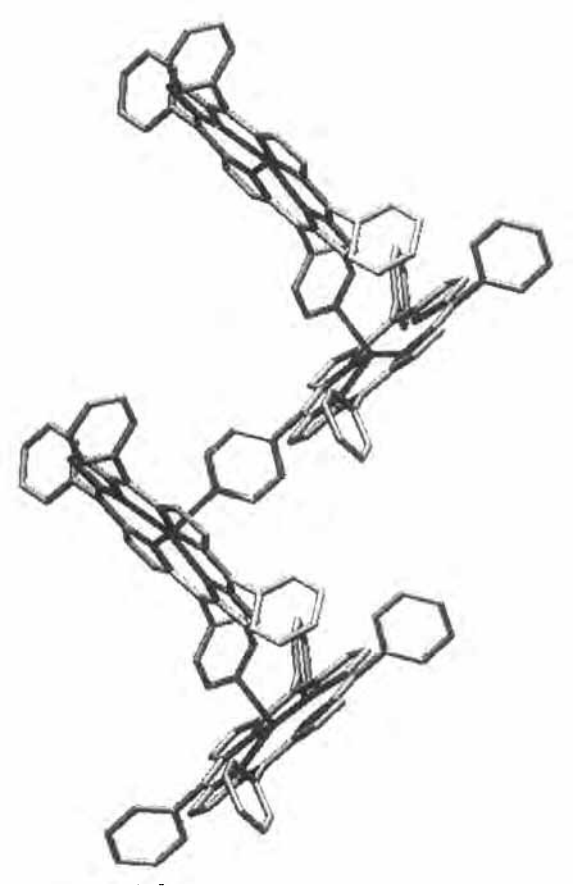

FIG. 30. A trivial open polymer assembled from pyridine-functionalized porphyrins.

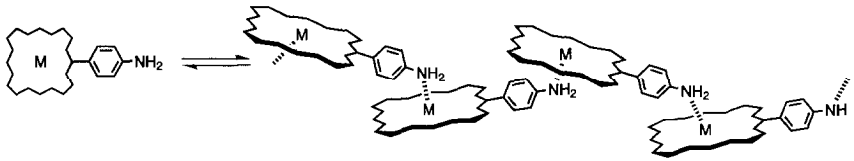

(76) M = Zn

FIG. 31. A trivial open polymer assembled from aniline-functionalized porphyrins.

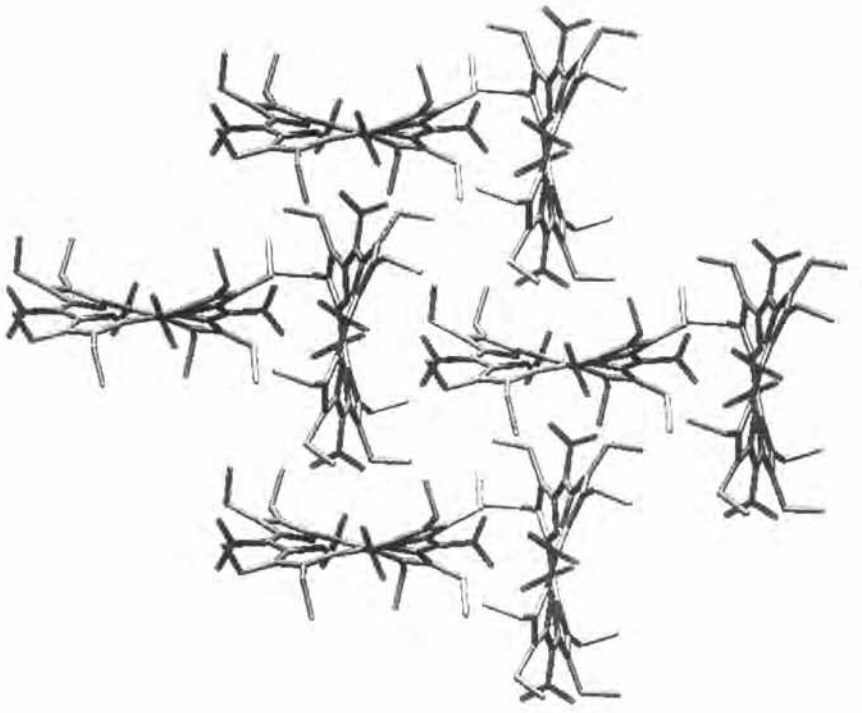

FIG. 32. Crystal packing diagram for **77**, suggestive of polymerization through nitro–zinc coordination interactions.

kebab". Polymers of this type have been studied particularly with regard to their conductivity properties.

Launay (*92*) reported the synthesis of shish-kebab ruthenium porphyrin polymers with pyrazine and 4,4′-azopyridine as the bridging ligand (**78**, **79**, Fig. 33). The synthesis was accomplished by photoirradiation to decarbonylate the Ru(II)CO center after coordination of the first axial ligand. The structures were characterized by the upfield shifts of the ligand protons in the ^{1}H NMR spectra. Since the bridging and terminating ligands give rise to different signals, it was possible to determine the number of porphyrins present in the oligomers: 13 ± 1 for the azopyridine oligomer, and 5 ± 1 for the pyrazine system. In the UV–Vis absorption spectra, the authors were able to identify a metal-to-axial ligand charge transfer band. The Soret band is blue-shifted in the case of the pyrazine-bridged oligomer as a result of exciton coupling between neighboring chromophores (*93*). In the pyrazine oligomer, the bulky porphyrins protect the inner metal–ligand moiety

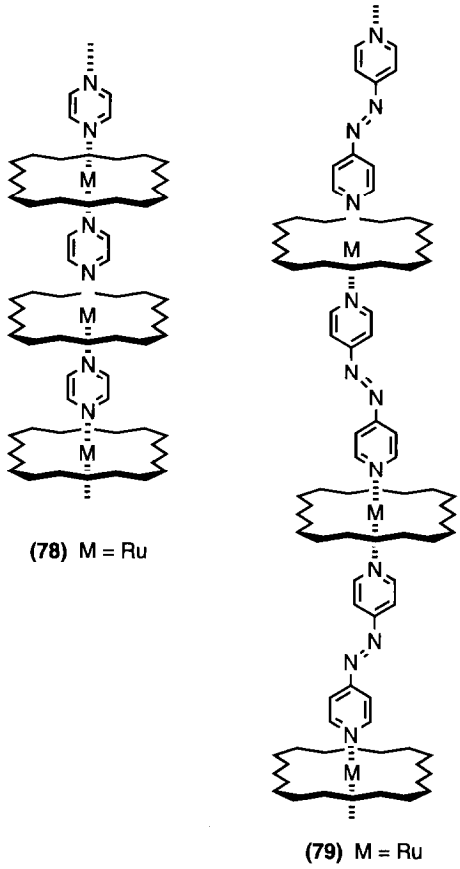

FIG. 33. Trivial open shish-kebab polymers.

from externally added oxidants. Cyclic voltammetry was used to investigate the influence of the pH on intramolecular electron transfer. In the azopyridine complex, addition of 0.5 equivalents of H^+ per monomeric unit led to oxidation of half of the Ru(II) centers to Ru(III) and reduction of one ligand in every four to 1,2-bis(4-pyridyl)hydrazine. The resulting mixed valence state gave rise to a near IR intervalence transition, Ru(II)–Ru(III).

Reed (*94,95*) treated Fe(III) and Mn(III) tetraphenylporphyrins with imidazolate anions to obtain polymers that precipitate in high yields. When the ligand is added in excess, the simple 1:2 complex is formed. In the X-ray crystal structure of the Mn(III) polymer, a zig-zag chain is

observed with alternating short–short and long–long coordination bonds, because the manganese ions are alternately in high and low spin states.

Maldotti (*96*) studied the kinetics of the formation of the pyrazine-bridged Fe(II) porphyrin shish-kebab polymer by means of flash kinetic experiments. Upon irradiation of a deaerated alkaline water/ethanol solution of Fe(III) protoporphyrin IX and pyrazine with a short intense flash of light, the 2:1 Fe(II) porphyrin $(\text{pyrazine})_2$ complex is formed, but it immediately polymerizes with second-order kinetics. This can be monitored in the UV–Vis absorption spectrum, with the disappearance of a band at 550 nm together with the emergence of a new band due to the polymer at 800 nm. The process is accelerated by the addition of LiCl, which augments hydrophobic interactions, and is diminished by the presence of a surfactant. A shish-kebab polymer is also formed upon photoreduction of Fe(III) porphyrins in presence of piperazine or 4,4′-bipyridine ligands (*97*).

The synthesis of iron, ruthenium, and osmium octaethylporphyrin polymers bridged by pyrazine, 4,4′-bipyridine, and DABCO was developed by Collman (*98–100*). The Ru(II) and Os(II) shish-kebab structures precipitate as insoluble polymers after stoichiometric amounts of the bidentate ligand are stirred with the neutral metalloporphyrin dimers (*100*), whereas the Fe(II) polymer is obtained from the monomeric metalloporphyrin (*99*). If the ligand is added in excess, the 2:1 complex is formed. The length of the polymers was determined by analysis of the IR spectra, in which the authors identified the centrosymmetric pyrazine ring-stretching mode which is active only when it binds to the metal in a monodentate way, i.e., at the polymer terminus. Typical chain lengths are 40 (Fe), 25 (Ru), and 20 (Os). Conductivity measurements on compacted powders of the polymer revealed that the conductivity dramatically increases on oxidative doping, the relative order being Os > Ru > Fe and pyrazine > bipyridine > DABCO. The oxidation is metal-centered, and so the order of conductivity is explained in terms of the better ability of the aromatic pyrazine ligand to transfer electrons between the M(II) and M(III) centers, i.e., mixing its π^* orbital with the d_π orbital of the metal. Shish-kebab polymers of Ru(III) tetraphenylporphyrins bridged by 4,4′-bipyridine and other diaza ligands have been obtained as films deposited on a substrate by electrolytic oxidation of the 2:1 Ru(II) porphyrin $(\text{ligand})_2$ complex in solution (*101*).

Hanack has reviewed a number of phthalocyanine and tetrabenzoporphyrin shish-kebab porphyrin polymers (*102*).

V. Cooperative Open Assemblies

Metalloporphyrins can also self-assemble in a cooperative open arrangement, generating polymeric structures with additional stability due to the intramolecular ring closure processes. The simplest strategy is to equip a six-coordinate metalloporphyrin with two ligands. Surprisingly, three of the systems reported have used magnesium porphyrins, which are generally 5-coordinate in solution and do not readily bind a 6th ligand. All of these examples should therefore be viewed with caution (*56,65,103*).

Kobuke and Miyaji (*56*) reported the formation of a self-assembled polymer of a 5,15-bisimidazolyl magnesium porphyrin (**80**, Fig. 34). The imidazolyl moieties coordinate the Mg centers of the adjacent porphyrins, giving a slipped cofacial arrangement to the structure. The evidence for oligomerization comes from ^{1}H NMR spectroscopy at 10^{-3} M concentrations: by integrating signals assigned to the terminal and internal subunits, the authors determined an average of 2.3 porphyrin units in the oligomer. UV–Vis absorption spectroscopy showed that intermolecular complexation persists down to concentrations of 10^{-6} M. Thus it seems most likely that this system forms a stable dimeric assembly and that there is some weaker aggregation at higher concentrations, but polymers are not formed.

Magnesium–hydroxyl interactions have been used in the same way with a *p*-hydroquinone unit attached at the *meso* position of a magnesium porphyrin (*103*). Again, the evidence for oligomerization comes from ^{1}H NMR spectroscopy, and the results can equally be interpreted as dimerization rather than polymerization.

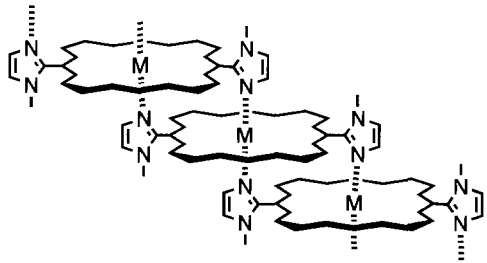

(80) M = Mg

FIG. 34. A cooperative open polymer assembled from imidazole-functionalized porphyrins.

Shinkai (*65*) exploited the boronic acid–diol motif mentioned above to self-assemble a polymer based on pyridine–magnesium porphyrin interactions. In this case, the evidence for polymerization comes from light-scattering experiments in dilute solution which yielded an average molecular weight of 10^9 g mol^{-1} for this system.

Hunter designed a Co(II) porphyrin equipped with two pyridyl groups connected via a spacer to the *meso* positions *trans* across the porphyrin to form open polymeric assemblies in solution via pyridine–cobalt coordination (**81**, Fig. 35) (*17*). Cooperative assembly of stable complexes was observed by UV–Vis absorption spectroscopy at 10^{-6} M concentrations ($K \approx 10^3$ M^{-1} for simple reference complexes). Pulse-gradient spin echo (PGSE) ^{1}H NMR experiments yielded a diffusion coefficient for the oligomer that was significantly smaller than the diffusion coefficients of monomeric or dimeric reference compounds, indicating the formation of a high molecular weight species. Size-exclusion chromatography (SEC) experiments yielded more precise information about the size of the polymer: at low concentrations short oligomers formed, but at 10^{-2} M concentrations soluble polymeric assemblies, approximately 100 units long, were formed. Cobalt porphyrins equipped with just one pyridine ligand were used as chain capping agents and could be added to the polymer to reduce the average chain length.

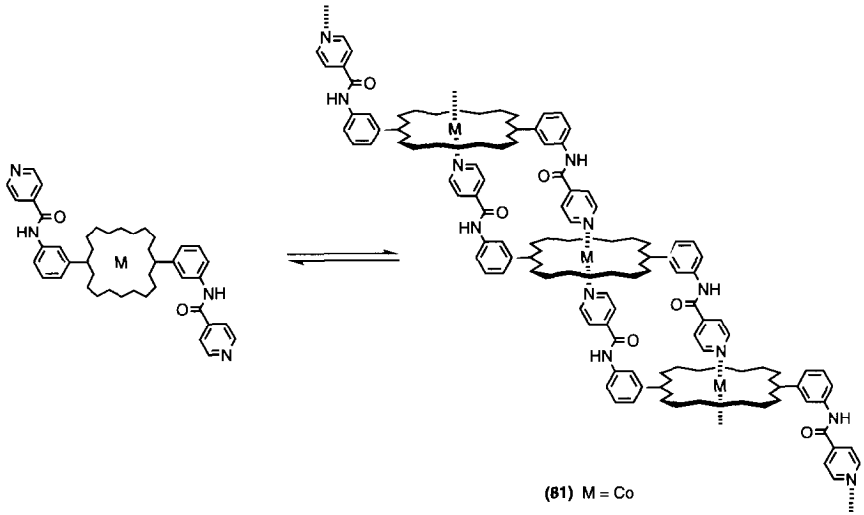

FIG. 35. A cooperative open polymer assembled from pyridine-functionalized porphyrins.

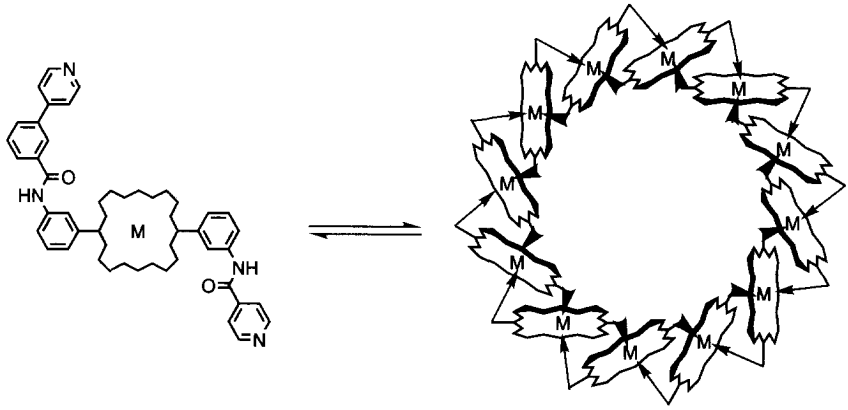

FIG. 36. Closed cooperative dodecamer.

This work was extended to the construction of large cyclic assemblies. By altering the lengths and geometries of the two porphyrin ligands, the system can be biased to form a helical polymer or a closed macrocyclic structure (*104*). The ligand geometries are such that metal–ligand coordination gives a 30° angle between adjacent porphyrin planes, and SEC at concentrations less than 5×10^{-4} M suggests that the porphyrin self-assembles into a macrocyclic dodecamer (**82**, Fig. 36). The intramolecular interactions of the macrocyclization process provide extra stability relative to the intermolecular interactions of a linear polymerization process, and so the dodecamer is fully assembled at concentrations at which the linear system forms only short oligomers. At higher concentrations (> EM $\approx$ 0.5 mM), the dodecamer opens up, and longer polymers are formed. This macrocycle architecture is similar to the bacterial light-harvesting complexes, where close coupling of the chromophores around the ring facilitates fast and efficient energy transfer to the reaction center, but no photochemical properties have been reported.

REFERENCES

1. Philp, D.; Stoddart, J. F. *Angew. Chem., Int. Ed. Engl.* **1996**, *35*, 1155.
2. Wojaczynski, J.; Latos-Grazynski, L. *Coord. Chem. Rev.* **2000**, *204*, 113.
3. Lawrence, D. S.; Jiang, T.; Levett, M. *Chem. Rev.* **1995**, *95*, 2229.
4. Conn, M. M.; Rebek, J. *Chem. Rev.* **1997**, *97*, 1647.
5. Whitesides, G. M.; Mathias, J. P.; Seto, C. T. *Science* **1991**, *254*, 1312.
6. Kirby A. J. *Adv. Phys. Org. Chem.* **1980**, *17*, 183.

7. Mandolini, L. *Adv. Phys. Org. Chem.* **1986**, *22*, 1.
8. Chi, X. L.; Guerin, A. J.; Haycock, R. A.; Hunter, C. A.; Sarson, L. D. *J. Chem. Soc., Chem. Commun.* **1995**, 2563.
9. Anderson, H. L.; Anderson, S.; Sanders, J. K. M. *J. Chem. Soc., Perkin Trans. 1* **1995**, 2231.
10. Galli, C.; Mandolini, L. *Eur. J. Org. Chem.* **2000**, 3117.
11. Kimura, A.; Funatsu, K.; Imamura, T.; Kido, H.; Sasaki, Y. *Chem. Lett.* **1995**, 207.
12. Kariya, N.; Imamura, T.; Sasaki, Y. *Inorg. Chem.* **1998**, *37*, 1658.
13. Funatsu, K.; Imamura, T.; Ichimura, A.; Sasaki, Y. *Inorg. Chem.* **1998**, *37*, 4986.
14. Darling, S. L.; Stulz, E.; Feeder, N.; Bampos, N.; Sanders, J. K. M. *New J. Chem.* **2000**, *24*, 261.
15. Stulz, E.; Mak, C. C.; Sanders, J. K. M. *J. Chem. Soc., Dalton Trans.* **2001**, 604.
16. Kobuke, Y.; Miyaji, H. *J. Am. Chem. Soc.* **1994**, *116*, 4111.
17. Michelsen, U.; Hunter, C. A. *Angew. Chem., Int. Ed.* **2000**, *39*, 764.
18. Fleischer, E. B.; Shachter, A. M. *Inorg. Chem.* **1991**, *30*, 3763.
19. Li, M.; Xu, Z.; You, X. Z.; Huang, X. Y.; Zheng, X. G.; Wang, H. Z. *Inorg. Chim. Acta* **1997**, *261*, 211.
20. Funatsu, K.; Kimura, A.; Imamura, T.; Ichimura, A.; Sasaki, Y. *Inorg. Chem.* **1997**, *36*, 1625.
21. Kariya, N.; Imamura, T.; Sasaki, Y. *Inorg. Chem.* **1997**, *36*, 833.
22. Alessio, E.; Macchi, M.; Heath, S.; Marzilli, L. G. *Chem. Commun.* **1996**, 1411.
23. Alessio, E.; Geremia, S.; Mestroni, S.; Iengo, E.; Srnova, I.; Slouf, M. *Inorg. Chem.* **1999**, *38*, 869.
24. Alessio, E.; Geremia, S.; Mestroni, S.; Srnova, I.; Slouf, M.; Gianferrara, T.; Prodi, A. *Inorg. Chem.* **1999**, *38*, 2527.
25. Prodi, A.; Indelli, M. T.; Kleverlaan, C. J.; Scandola, F.; Alessio, E.; Gianferrara, T.; Marzilli, L. G. *Chem. Eur. J.* **1999**, *5*, 2668.
26. Groves, J. T.; Fate, G. D.; Lahiri, J. *J. Am. Chem. Soc.* **1994**, *116*, 5477.
27. Lahiri, J.; Fate, G. D.; Ungashe, S. B.; Groves, J. T. *J. Am. Chem. Soc.* **1996**, *118*, 2347.
28. Mak, C. C.; Bampos, N.; Sanders, J. K. M. *Chem. Commun.* **1999**, 1085.
29. Darling, S. L.; Mak, C. C.; Bampos, N.; Feeder, N.; Teat, S. J.; Sanders, J. K. M. *New J. Chem.* **1999**, *23*, 359.
30. Fuhrhop, J. H.; Baccouche, M.; Bunzel, M. *Angew. Chem., Int. Ed. Engl.* **1980**, *19*, 322.
31. Kessel, S. L.; Hendrickson, D. N. *Inorg. Chem.* **1980**, *19*, 1883.
32. Endo, A.; Okamoto, Y.; Suzuki, K.; Shimamura, J.; Shimizu, K.; Sato, G. P. *Chem. Lett.* **1994**, 1317.
33. Endo, A.; Tagami, U.; Wada, Y.; Saito, M.; Shimizu, K.; Sato, G. P. *Chem. Lett.* **1996**, 243.
34. Campbell, K.; McDonald, R.; Branda, N. R.; Tykwinski, R. R. *Org. Lett.* **2001**, *3*, 1045.
35. Hunter, C. A.; Meah, M. N.; Sanders, J. K. M. *J. Am. Chem. Soc.* **1990**, *112*, 5773.
36. Anderson, H. L. *Inorg. Chem.* **1994**, *33*, 972.
37. Taylor, P. N.; Anderson, H. L. *J. Am. Chem. Soc.* **1999**, *121*, 11538.
38. Gomila, R. M.; Quinonero, D.; Frontera, A.; Ballester, P.; Deya, P. M. *J. Mol. Struct. (Theochem)* **2000**, *531*, 381.
39. Chichak, K.; Branda, N. R. *Chem. Commun.* **199**, 523.
40. Chichak, K.; Branda, N. R. *Chem. Commun.* **2000**, 1211.
41. Anderson, S.; Anderson, H. L.; Sanders, J. K. M. *Acc. Chem. Res.* **1993**, *26*, 469.
42. Anderson, S.; Anderson, H. L.; Sanders, J. K. M. *J. Chem. Soc., Perkin Trans. 1* **1995**, 2255.
43. McCallien, D. W. J.; Sanders, J. K. M. *J. Am. Chem. Soc.* **1995**, *117*, 6611.

44. Marvaud, V.; VidalFerran, A.; Webb, S. J.; Sanders, J. K. M. *J. Chem. Soc., Dalton Trans.* **1997**, 985.
45. Anderson, S.; Anderson, H. L.; Sanders, J. K. M. *Angew. Chem., Int. Ed. Engl.* **1992**, *31*, 907.
46. Kuroda, Y.; Kato, Y.; Ogoshi, H. *Chem. Commun.* **1997**, 469.
47. Simanek, E. E.; Isaacs, L.; Li, X. H.; Wang, C. C. C.; Whitesides, G. M. *J. Org. Chem.* **1997**, *62*, 8994.
48. Gunter, M. J.; Bampos, N.; Johnstone, K. D.; Sanders, J. K. M. *New J. Chem.* **2001**, *25*, 166.
49. Chichak, K.; Walsh, M. C.; Branda, N. R. *Chem. Commun.* **2000**, 847.
50. Balch, A. L.; LatosGrazynski, L.; Noll, B. C.; Olmstead, M. M.; Zovinka, E. P. *Inorg. Chem.* **1992**, *31*, 2248.
51. Balch, A. L.; Noll, B. C.; Reid, S. M.; Zovinka, E. P. *Inorg. Chem.* **1993**, *32*, 2610.
52. Balch, A. L.; LatosGrazynski, L.; Claire, T. N. S. *Inorg. Chem.* **1995**, *34*, 1395.
53. Balch, A. L.; Noll, B. C.; Olmstead, M. M.; Reid, S. M. *J. Chem. Soc., Chem. Commun.* **1993**, 1088.
54. Goff, H. M.; Shimomura, E. T.; Lee, Y. J.; Scheidt, W. R. *Inorg. Chem.* **1984**, *23*, 315.
55. Godziela, G. M.; Tilotta, D.; Goff, H. M. *Inorg. Chem.* **1986**, *25*, 2142.
56. Kobuke, Y.; Miyaji, H. *Bull. Chem. Soc. Jpn.* **1996**, *69*, 3563.
57. Stibrany, R. T.; Vasudevan, J.; Knapp, S.; Potenza, J. A.; Emge, T.; Schugar, H. J. *J. Am. Chem. Soc.* **1996**, *118*, 3980.
58. Gerasimchuk, N. N.; Mokhir, A. A.; Rodgers, K. R. *Inorg. Chem.* **1998**, *37*, 5641.
59. Aoyama, Y.; Kamohara, T.; Yamagishi, A.; Toi, H.; Ogoshi, H. *Tetrahedron Lett.* **1987**, *28*, 2143.
60. Gardner, M.; Guerin, A. J.; Hunter, C. A.; Michelsen, U.; Rotger, C. *New J. Chem.* **1999**, *23*, 309.
61. Knapp, S.; Vasudevan, J.; Emge, T. J.; Arison, B. H.; Potenza, J. A.; Schugar, H. J. *Angew. Chem. Int. Ed.* **1998**, *37*, 2368.
62. Hunter, C. A.; Sarson, L. D. *Angew. Chem., Int. Ed. Engl.* **1994**, *33*, 2313.
63. Bied-Charreton, C.; Mérienne, C.; Gaudemer, A. *New J. Chem.* **1987**, *11*, 633.
64. Salmon, L.; Biedcharreton, C.; Gaudemer, A.; Moisy, P.; Bedioui, F.; Devynck, J. *Inorg. Chem.* **1990**, *29*, 2734.
65. Sarson, L. D.; Ueda, K.; Takeuchi, R.; Shinkai, S. *Chem. Commun.* **1996**, 619.
66. Burrell, A. K.; Officer, D. L.; Reid, D. C. W.; Wild, K. Y. *Angew. Chem., Int. Ed.* **1998**, *37*, 114.
67. Wojaczynski, J.; LatosGrazynski, L. *Inorg. Chem.* **1995**, *34*, 1054.
68. Wojaczynski, J.; LatosGrazynski, L. *Inorg. Chem.* **1995**, *34*, 1044.
69. Wojaczynski, J.; LatosGrazynski, L. *Inorg. Chem.* **1996**, *35*, 4812.
70. Wojaczynski, J.; LatosGrazynski, L.; Olmstead, M. M.; Balch, A. L. *Inorg. Chem.* **1997**, *36*, 4548.
71. Chi, X. L.; Guerin, A. J.; Haycock, R. A.; Hunter, C. A.; Sarson, L. D. *J. Chem. Soc., Chem. Commun.* **1995**, 2567.
72. Funatsu, K.; Kimura, A.; Imamura, T.; Sasaki, Y. *Chem. Lett.* **1995**, 765.
73. Funatsu, K.; Imamura, T.; Ichimura, A.; Sasaki, Y. *Inorg. Chem.* **1998**, *37*, 1798.
74. Okumura, A.; Funatsu, K.; Sasaki, Y.; Imamura, T. *Chem. Lett.* **1999**, 779.
75. Rempel, U.; Vonmaltzan, B.; von Borczyskowski, C. *J. Lumin.* **1992**, *53*, 175.
76. Rempel, U.; Vonmaltzan, B.; von Borczyskowski, C. *Pure Appl. Chem.* **1993**, *65*, 1681.
77. Chernook, A. V.; Shulga, A. M.; Zenkevich, E. I.; Rempel, U.; von Borczyskowski, C. *J. Phys. Chem.* **1996**, *100*, 1918.

78. Zenkevich, E. I.; Shulga, A. M.; Bachilo, S. M.; Rempel, U.; von Richthofen, J.; von Borczyskowski, C. *J. Lumin.* **1998**, *76–77*, 354.
79. Chernook, A. V.; Rempel, U.; von Borczyskowski, C.; Shulga, A. M.; Zenkevich, E. I. *Chem. Phys. Lett.* **1996**, *254*, 229.
80. Johnston, M. R.; Gunter, M. J.; Warrener, R. N. *Chem. Commun.* **1998**, 2739.
81. Haycock, R. A.; Yartsev, A.; Michelsen, U.; Sundstrom, V.; Hunter, C. A. *Angew. Chem. Int. Ed.* **2000**, *39*, 3616.
82. Hunter, C. A.; Hyde, R. K. *Angew. Chem., Int. Ed. Engl.* **1996**, *35*, 1936.
83. Kim, H. J.; Bampos, N.; Sanders, J. K. M. *J. Am. Chem. Soc.* **1999**, *121*, 8120.
84. Anderson, H. L.; Hunter, C. A.; Sanders, J. K. M. *J. Chem. Soc., Chem. Commun.* **1989**, 226.
85. Anderson, S.; Anderson, H. L.; Bashall, A.; McPartlin, M.; Sanders, J. K. M. *Angew. Chem., Int. Ed. Engl.* **1995**, *34*, 1096.
86. Ambroise, A.; Li, J. Z.; Yu, L. H.; Lindsey, J. S. *Org. Lett.* **2000**, *2*, 2563.
87. Slone, R. V.; Hupp, J. T. *Inorg. Chem.* **1997**, *36*, 5422.
88. Wilson, G. S.; Anderson, H. L. *Chem. Commun.* **1999**, 1539.
89. Reek, J. N. H.; Schenning, A. P. H. J.; Bosman, A. W.; Maijer, E. W.; Crossley, M. J. *Chem. Commun.* **1998**, 11.
90. Shachter, A. M.; Fleischer, E. B.; Haltiwanger, R. C. *J. Chem. Soc., Chem. Commun.* **1988**, 960.
91. Senge, M. O.; Smith, K. M. *J. Chem. Soc., Chem. Commun.* **1994**, 923.
92. Marvaud, V.; Launay, J. P. *Inorg. Chem.* **1993**, *32*, 1376.
93. Ikonen, M.; Guez, D.; Marvaud, V.; Markovitsi, D. *Chem. Phys. Lett.* **1994**, *231*, 93.
94. Landrum, J. T.; Reed, C. A.; Hatano, K.; Scheidt, W. R. *J. Am. Chem. Soc.* **1978**, *100*, 3232.
95. Landrum, J. T.; Hatano, K.; Scheidt, W. R.; Reed, C. A. *J. Am. Chem. Soc.* **1980**, *102*, 6729.
96. Maldotti, A.; Varani, G.; Amadelli, R.; Bartocci, C.; Ferri, A. *New J. Chem.* **1988**, *12*, 819.
97. Bartocci, C.; Amadelli, R.; Maldotti, A.; Carassiti, V. *Polyhedron* **1986**, *5*, 1297.
98. Collman, J. P.; McDevitt, J. T.; Yee, G. T.; Leidner, C. R.; McCullough, L. G.; Little, W. A.; Torrance, J. B. *Proc. Natl. Acad. Sci. USA* **1986**, *83*, 4581.
99. Collman, J. P.; McDevitt, J. T.; Yee, G. T.; Zisk, M. B.; Torrance, J. B.; Little, W. A. *Synth. Met.* **1986**, *15*, 129.
100. Collman, J. P.; McDevitt, J. T.; Leidner, C. R.; Yee, G. T.; Torrance, J. B.; Little, W. A. *J. Am. Chem. Soc.* **1987**, *109*, 4606.
101. Saito, M.; Endo, A.; Shimizu, K.; Sato, G. P. *Chem. Lett.* **1995**, 1079.
102. Hanack, M.; Deger, S.; Lange, A. *Coord. Chem. Rev.* **1988**, *83*, 115.
103. Miyaji, H.; Kobuke, Y.; Kondo, J. *Chem. Lett.* **1996**, 497.
104. Haycock, R. A.; Hunter, C. A.; James, D. A.; Michelsen, U.; Sutton, L. R. *Org. Lett.* **2000**, *2*, 2435.

SUBJECT INDEX

D

E

F

G

N

O

P

Q

R

S

T

CONTENTS OF PREVIOUS VOLUMES

PUBLISHER'S NOTE

The present volume marks the last in the series to be edited by Professor A.G. Sykes FRS in whose capable hands it has been since he took up the position of Editor in 1985 with responsibility for Volume 32. Prior to this, he edited four volumes of the Academic Press series *Advances in Inorganic and Bioinorganic Mechanisms* 1982–1986. The acclaim for the *Advances in Inorganic Chemistry* series and the large number of citations it has received are reflected in the high standards he set and the quality of the authors he was able to enlist to write reviews on topics of interest to inorganic and bioinorganic chemists.

The series began as *Advances in Inorganic Chemistry and Radiochemistry* in 1959, and the first 31 volumes were edited by the Cambridge team of H. Emeléus and A.G. Sharpe. With Vol. 31, the title was changed to *Advances in Inorganic Chemistry.* Professor Sykes extended the area of interest to include Bioinorganic studies. The first three contributors Taube, Fischer and Lipscomb, became Nobel Laureates, and since its inception most leading inorganic chemists have contributed to the series. With an impact factor of 11.5 for the year 2000 – the frequency with which the average article is cited in that particular year (ISI Journal Citation Reports 2000) – the series leads the field of 38 inorganic and nuclear chemistry publications covered.

Professor Sykes has had a long and interesting career since obtaining his PhD at the University of Manchester under the supervision of Professor Bill Higginson in 1958. He spent 20 years at Leeds University before taking up his current post at the University of Newcastle. During this time he has had Visiting Positions in the USA, Germany, Austria, Japan, Kuwait, Australia, Canada, the West Indies, Switzerland, South Africa, Spain, Hong Kong and Denmark. His group has been host to large numbers of post-doctoral fellows and visitors (over 40 different nationalities!), and has produced 53 PhDs. Some 470

publications are attributed to the group. His contribution to the field has recently been honoured in a special volume of *Inorganica Chimica Acta* 331 (2002). The international connections have no doubt been of great benefit in his work as Editor of the series.

We would like to acknowledge the significant contribution of Professor Sykes to the success of the series, and to thank him for all the time and effort he has put in to establish its position as the leading reference work in the field. We wish him all the best for his retirement. At the same time we welcome Professor Rudi van Eldik, from the Institute for Inorganic Chemistry at the University of Erlangen-Nürnberg, who has taken up the Editor's baton. With his research interests in inorganic and bioinorganic mechanisms, Professor van Eldik is the ideal person to develop this series further.

Advances in
INORGANIC CHEMISTRY

Including Bioinorganic Studies

EDITED BY

A. G. Sykes

Department of Chemistry
The University of Newcastle
Newcastle upon Tyne
United Kingdom

VOLUME 53

ACADEMIC PRESS

An imprint of Elsevier Science

Amsterdam Boston London New York Oxford Paris
San Diego San Francisco Singapore Sydney Tokyo